NASA TN D-1376

TECHNICAL NOTE

D-1376

INFLUENCE OF TIRE TREAD PATTERN AND RUNWAY SURFACE CONDITION ON BRAKING FRICTION AND ROLLING RESISTANCE OF A MODERN AIRCRAFT TIRE

By Walter B. Horne and Trafford J. W. Leland

Langley Research Center
Langley Station, Hampton, Va.

NATIONAL AERONAUTICS AND SPACE ADMINISTRATION
WASHINGTON
September 1962

TABLE OF CONTENTS

NATIONAL AERONAUTICS AND SPACE ADMINISTRATION

TECHNICAL NOTE D-1376

INFLUENCE OF TIRE TREAD PATTERN AND RUNWAY SURFACE CONDITION ON BRAKING FRICTION AND ROLLING RESISTANCE OF A MODERN AIRCRAFT TIRE

By Walter B. Horne and Trafford J. W. Leland

SUMMARY

A series of taxiing tests was conducted at the Langley landing-loads track with both braked and unbraked (freely rolling) single and tandem wheels equipped with 32x8.8 type VII aircraft tires of different tread designs to obtain data on tire and braking characteristics during operation on dry and on contaminated concrete and asphalt runways. Contaminants used were water, slush, JP-4 jet fuel, and organic and detergent fire-extinguishing foams. Forward velocities for the tests ranged from approximately 13 to 104 knots. Vertical loads of approximately 9,000 to 22,000 pounds and tire inflation pressures of 85 to 350 pounds per square inch were used.

Results indicated that the unbraked tire rolling resistance increased with increasing forward velocity on dry and on contaminated runway surfaces. Peak tire-ground friction coefficients developed during wheel braking decreased rapidly with increasing velocity on contaminated runways but remained relatively unchanged on dry runways as the forward velocity was increased. Dry-runway friction coefficients were found to be relatively insensitive to tire tread pattern. However, the magnitude of the friction coefficients developed by tires on contaminated runways was extremely sensitive to the tire tread pattern used, with circumferential-groove treads developing the highest values of friction coefficient, and smooth and dimple treads the lowest values for the tread patterns and runway conditions investigated.

INTRODUCTION

It has been recognized for many years that the presence of contaminating fluids such as slush, water, and oil on airport runways tends to impair landing and take-off performance of aircraft. Previous NASA work on tire performance under adverse runway conditions is reported in references 1 to 7. British work on this subject, in which a full-scale

jet-fighter airplane was used, is reported in references 8 and 9. This degradation in performance due to contamination has been tolerated with propeller-type aircraft because only rarely are operations made unsafe by the presence of these contaminants. Operations of military jet aircraft and of the recently introduced jet-powered commercial transport aircraft, on the other hand, have proved to be much more affected by runway contaminants than operations of the propeller-type aircraft. Several factors are responsible for the difference in the effect of contaminated runways on the ground performance of the two types of aircraft. The main factors are the higher landing and take-off velocities required of the jets, and their generally lower acceleration and deceleration characteristics while on the ground.

Operation on fluid-contaminated runways affects aircraft performance in several ways. First, the retardation forces developed by aircraft wheels when taking off from slush- or water-covered runways increase the take-off distance required by the airplane and under certain conditions would prevent the airplane from obtaining the required take-off velocity (ref. 2). Second, the high-velocity spray of slush or water originating from the airplane wheels can be damaging to the surfaces of the airplane that are under spray impingement. Third, under certain conditions of vertical load, tire-inflation pressure, and forward velocity, airplane tires on slush- or water-covered runways reach a condition called hydroplaning during which the hydrodynamic lift force developed between the tire footprint and the fluid-covered runway surface equals or exceeds the vertical reaction of the airplane mass acting on the tire. During hydroplaning the tire loses contact with the runway surface and thus loses its directional stability and braking effectiveness. Fourth, at subhydroplaning velocities the friction coefficients developed between aircraft tires and the ground during braking on fluid-contaminated runways are considerably reduced from values obtained on dry runways.

Many investigations under various test conditions have been made of the effects of water or other runway contaminants on the performance of tires. In some of these investigations small tires were used, some of the investigations were confined to low speeds, and in some investigations in which full-scale airplanes were used, difficulty was experienced in maintaining test conditions constant. The presently described investigation extends the range of controlled tests to a higher speed and weight combination. This investigation under controlled conditions was performed at the Langley landing-loads track (track described in ref. 10) to determine the effect of forward velocity; type of runway surface; tire-tread material, pattern, and wear; and type of runway contaminant on the braked and unbraked rolling characteristics of aircraft tires on single and tandem wheels. Some of the preliminary experimental data obtained from this investigation were used in references 1 and 2 to demonstrate the degrading effects of runway slush and water on the take-off and landing performance of several typical jet aircraft.

It is the purpose of this paper to describe the investigation in more detail than was done in references 1 and 2 so that the degradation of braking effectiveness on contaminated runway surfaces may be more fully understood. It will be demonstrated that tread designs or patterns used on tires have little effect on tire and braking performance on dry runways but have a very substantial effect on contaminated runways.

SYMBOLS

A_g	gross footprint area of tire, sq in.
A_n	net footprint area of tire, sq in.
C_L	hydrodynamic lift coefficient (dimensionless)
C_D	hydrodynamic drag coefficient (dimensionless)
C_z	tire constant; 0.02 for type I tires and 0.03 for type III and VII tires (obtained from ref. 12)
d_1	depth of contaminant on runway surface, in.
F_x	instantaneous horizontal (drag) force at wheel axle, lb
$F_{x,g}$	instantaneous horizontal (drag) force acting on tire at ground, $F_{x,g,r} + F_{x,g,b} + F_{x,g,f}$, lb
$F_{x,g,b}$	braking drag (portion of $F_{x,g}$ contributed by forcing tire to roll at values of $s_1 > 0$ either by wheel braking or by other means), lb
$F_{x,g,f}$	fluid-displacement drag (portion of $F_{x,g}$ contributed by horizontal component of hydrodynamic force due to runway contaminant), lb
$F_{x,g,r}$	rolling resistance (drag forces developed on unbraked wheel due to tire hysteresis and inertia effects), lb
F_z	instantaneous vertical force at wheel axle, lb
$F_{z,g}$	instantaneous vertical force acting on tire at ground, lb

$F_{z,L}$	vertical component of hydrodynamic force due to runway contaminant, lb
I	moment of inertia of rotating wheel and tire parts, slug-ft^2
p	unloaded tire inflation pressure, lb/sq in.
p_B	hydraulic-fluid pressure acting on wheel brake, lb/sq in.
$p_{B,1}$	back pressure in return line of brake system, lb/sq in.
p_g	average gross footprint pressure, $F_{z,g}/A_g$, lb/sq in.
p_n	average tire-ground bearing pressure, $F_{z,g}/A_n$, lb/sq in.
p_r	rated tire inflation pressure (one-fourth tire bursting pressure), lb/sq in.
r_o	unloaded tire radius, in.
s_1	slip ratio (dimensionless)
T	net spin-up or spin-down torque acting on wheel, lb-in.
T_B	instantaneous retarding torque developed on wheel by wheel brake, lb-in.
t	time, sec
V_H	carriage forward velocity, knots or ft/sec as noted
V_p	tire hydroplaning velocity (occurs when $F_{z,g} = F_{z,L}$), knots or ft/sec as noted
w	unloaded maximum tire width, in.
$\ddot{x}$	horizontal axle acceleration, ft/sec^2
x_c	instantaneous movement of vertical-load center of pressure, in.
α	angular acceleration of wheel, radians/sec^2
δ	vertical tire deflection, in.

μ instantaneous tire-ground friction coefficient, $F_{x,g}/F_{z,g}$ (dimensionless)

μ_{av} average value of μ developed between slip ratios of 0.1 and 0.5

μ_{max} maximum value of μ developed between slip ratios of 0 and 1

μ_{skid} value of μ developed at slip ratio of 1

ρ mass density of runway contaminant, slugs/cu ft

ω wheel angular velocity, radians/sec

APPARATUS AND PROCEDURE

The present investigation was carried out by making test runs at the Langley landing-loads track (track described in ref. 10). The main carriage (fig. 1) of this facility weighs approximately 100,000 pounds and travels at speeds up to 130 knots on steel rails which are located on each side of a 2,200-foot-long concrete runway. The investigation consisted of a series of braked and unbraked runs conducted at different forward velocities with a type VII tire at inflation pressures ranging from 85 to 350 pounds per square inch. The forward velocities varied from approximately 13 to 104 knots. The vertical load per tire varied from approximately 9,000 to 22,000 pounds. Runway surfaces investigated were concrete, smooth asphalt (sand finish), and rough asphalt (aggregate finish). Runway-surface contaminants investigated were water, slush, JP-4 jet-engine fuel, and fire-extinguishing foam (both detergent and organic types). Both single and tandem wheel arrangements were investigated.

TEST FIXTURE

The tire under test was mounted on a main-landing-gear wheel from a century-series fighter airplane. This wheel was in turn mounted within an instrumented test fixture (fig. 2) suspended from the vertical drop carriage of the main carriage. Most of the tests were conducted with a single wheel. Some tests were made with the tandem arrangement shown in figure 3, where an unbraked wheel was added forward of the instrumented wheel contained in the test fixture. The fixture could be positioned to allow the tire to run 25 inches to either side of the track center line.

TIRES

The tires used in the investigation were 32x8.8, 22 ply rating, type VII (extra high pressure). Through the cooperation of several aircraft tire manufacturers, a number of tires with different tread designs and tread materials were investigated. The tread designs for these tires, along with their footprints for a vertical-loading condition of $F_{z,g} \approx 10,000$ pounds and $p = 260$ lb/sq in., are shown in figure 4. Tire cross sections shown in figure 5 illustrate the two different tread materials investigated, rubber and fabric-reinforced rubber. Several of the fabric-reinforced tires were provided with an extra thickness of rubber at the tire surface so that during test, braking would occur only on a rubber surface. A description of the tires mentioned in this paper, their code designations, and some inflated tire dimensions are given in table I. Tires having the code designation S were made especially for this investigation, and in all cases were molded to full tread depth but with no tread pattern. Before testing, the desired tread patterns were cut into the tire to a depth of approximately one-quarter of an inch by means of an electrically heated knife.

WHEEL BRAKE

The wheel brake used in this investigation was the main-landing-gear disk brake of a century-series jet fighter and consisted of an assembly of 5 rotor and 6 stator brake disks. The braking system for most of the braking runs was equipped with an "on-off" type of automatic braking device that dumped brake pressure p_B whenever the wheel deceleration during braking exceeded 45 to 60 radians/sec^2. A recovery signal was generated, recocking the automatic braking device, when, after brake release, the wheel angular velocity became equal to the angular velocity of an inertia-type flywheel mounted in the device. During the free-roll or unbraked taxiing runs, the brake hydraulic system was vented to atmosphere to minimize brake torque. For most of the wheel-braking test runs, the brake system, with antiskid unit operating, was set up to represent a pilot continuously riding brakes during the landing roll. Thus, 20 to 30 braking cycles occurred for a test run at low forward velocity and 5 to 8 braking cycles for a run at high forward velocity. A few wheel-braking runs were made without automatic braking. For these runs, the brake was cycled once each run at specified locations on the track runway by means of a track-mounted knife edge which actuated solenoid valves.

RUNWAY TROUGHS AND SURFACES

A cross section of the test runway surfaces is shown in figure 6. The concrete dikes located along the edges of both the asphalt and concrete runways formed troughs into which runway contaminants such as water, slush, foam, and JP-4 jet-engine fuel could be deposited to the desired depth. The concrete runway test surface shown at the right in figure 6 is similar to actual portland-cement concrete surfaces in current use for airport runways. The asphalt runway shown at the left in figure 6 was rolled in two adjoining sections (fig. 7). The initial 400-foot section had a smooth sand-finish surface, while the remaining portion of the asphalt runway had a rough aggregate surface. Photographs of the asphalt runway surfaces are shown in figure 8. The sand particles used for the smooth asphalt would pass through a 1/10-inch sieve. The rough-asphalt aggregate conformed to a standard highway specification wherein 100 percent of the aggregate could pass through a 1-inch sieve, 95 to 100 percent through a 3/4-inch sieve, 60 to 80 percent through a 3/8-inch sieve, 40 to 60 percent through a 1/4-inch sieve, 20 to 40 percent through a 1/10-inch sieve, and 3 to 10 percent through a 1/80-inch sieve.

RUNWAY WETNESS

The elevation characteristics of the concrete runway within the confines of the trough shown in figure 7 were such that with just the high spots of the runway showing through the water surface, the water depth in the trough varied between 0 and 0.3 inch. This degree of wetness corresponds to conditions measured on an actual runway during a heavy rain shower. Figure 9 is a photograph of the concrete runway for this condition of wetness.

The asphalt runway surfaces under similar wetness conditions (high spots showing through water surface) showed a variation in water depth of 0 to 0.5 inch. The larger variation in water depth for the asphalt runway surface is felt to be the result of the method used in rolling the asphalt during its installation on the track runway, and may be representative of actual runway surfaces. Most of the wheel-braking runs of this investigation were made with the wetness conditions just described (concrete, d_1 = 0 to 0.3 inch; asphalt, d_1 = 0 to 0.5 inch). For the unbraked rolling runs (performed on the concrete runway only), the water depth varied from 0.25 to 1.75 inches.

OTHER RUNWAY CONTAMINANTS

Both braked and unbraked rolling runs were made on slush-covered runways with slush depths ranging from 0.5 to 2.0 inches. A detailed description of the slush, slush trough, and method of determining slush density is given in reference 1.

One braked rolling run was performed on the asphalt runway after the surface had been covered with JP-4 jet-engine fuel. For this run, a strip of the asphalt runway 1 to 2 feet wide and approximately 600 feet long was coated as uniformly as possible with 12 gallons of JP-4 fuel. The fuel was allowed to stand on the runway for about an hour, at which time most of the puddles of fuel had disappeared either by evaporation or penetration into the asphalt surface. The runway was then lightly sprayed with water to simulate the beginning of a rain shower, and the test run was made as soon as the entire surface was wetted.

One braked rolling run was performed on the concrete runway after the surface had been covered with 2 to 5 inches of fire-extinguishing foam such as might be used to cover airport runways during emergency landing of airplanes. Two types of foam were used, organic (protein-base solution, Joint Army-Navy Specification JAN-C-266) and detergent (Unox No. 3 wetting-agent foam). Figure 10 shows the foam being applied to the runway surface. The foam issuing from the nozzle in figure 10 is of the organic type. The detergent foam was placed on the runway farther down the track.

In addition to the purposely applied contaminants, the tires themselves contaminated the runway surfaces by depositing abraded and molten rubber on the runway surface during braked rolling. The abraded rubber (deposited only at very low taxiing speeds) did not stick to the runway surface and was readily removed. The molten rubber (deposited at the higher taxiing speeds) solidified in the irregularly shaped voids of the runway surface and was extremely difficult to remove. A stiff steel brush was used to remove as much as possible of the molten rubber deposits on the runway before the start of most of the wheel-braking runs.

INSTRUMENTATION

Instrumentation was provided to obtain the vertical and drag forces developed between the single tire or rear tandem tire and the runway. (See figs. 2 and 3.) Also obtained were the vertical and drag accelerations of the wheel axle; brake torque; wheel angular acceleration, velocity, and displacement; forward velocity of the carriage; brake pressure; vertical displacement of the test fixture (tire deflection); and time.

A 16-channel oscillograph was used to record the outputs of this instrumentation during a test run. A more detailed discussion of the instrumentation is given in reference 1. In addition, high-speed (200 frames per second) 16-mm motion pictures were taken from three different positions around the tire during each braked and unbraked rolling run.

GENERAL CONSIDERATIONS

DEFINITION OF TERMS

A discussion of various parameters that affect the unbraked and braked rolling of aircraft tires is included here as a basis for the presentation of the data to follow. Consider the external forces and moments acting on the rolling tire shown in figure 11. The net torques or moments acting on the wheel must equal the acceleration of the wheel (neglecting wheel-bearing frictional torque):

$$\alpha = \frac{T_B + F_{z,g} x_c - F_{x,g}(r_o - \delta)}{I} \qquad (1)$$

For the notation used, positive α denotes wheel spin-down and negative α denotes wheel spin-up. Some of the parameters involved in this equation, as well as other tire parameters, will now be discussed.

Instantaneous Drag Force

An airplane tire during landing or take-off can be subjected to at least three distinct types of drag loading. The first type of loading is called rolling resistance $F_{x,g,r}$ and arises from wheel-bearing friction, tire hysteresis, and inertia effects. The second type of drag loading $F_{x,g,f}$ occurs only on fluid-covered runways and is created by the aircraft tire displacing the fluid, for example slush or water, from the wheel path on the runway. Finally, the drag force $F_{x,g,b}$ is created on a tire during changes in wheel rotational velocity and during locked-wheel skidding. The magnitudes of $F_{x,g,f}$ and $F_{x,g,b}$ depend upon the vertical load acting on the tire and the friction coefficients developed between the tire and the ground. The instantaneous drag force acting on the tire is the sum of these three types of drag force:

$$F_{x,g} = F_{x,g,r} + F_{x,g,f} + F_{x,g,b}$$

Vertical Ground Force

The vertical ground force $F_{z,g}$ is defined as the instantaneous ground force acting on the tire. It should be noted that this vertical ground force is practically never constant during take-off and landing because of runway roughness and changes in the airplane attitude on the runway.

Brake Torque

The brake torque T_B is the wheel spin-down torque created by mechanically braking a rolling aircraft tire through use of wheel brakes. It is a resistive torque and its magnitude must equal the sum of the other torques acting on the wheel at any instant during braking.

Deflected Tire Radius

The difference between the unloaded tire radius r_o and the vertical tire deflection δ defines the length of the arm $(r_o - \delta)$ through which the drag force $F_{x,g}$ acts in spinning up a tire.

Movement of Vertical-Load Center of Pressure

Because of tire elasticity, inertia, and hydrodynamic (wet runways only) effects, the center of pressure of the vertical load on a rolling tire will be displaced from its static position beneath the wheel-axle center line. Positive values of x_c in equation (1) denote a shift of the center of pressure in the direction of motion, negative values the opposite.

Footprint Area

The tire contacts the ground in a finite area whose shape is illustrated in figure 4 for a number of tires. For tires with a tread pattern, this area consists of alternate spaces where the tire contacts the ground and where it does not contact the ground. The total area, including the spaces that do not contact the ground, is designated as the gross footprint area A_g of the tire. The actual ground-contact area, or bearing area, is referred to as the net footprint area A_n.

Wheel Moment of Inertia

The wheel moment of inertia I is defined as the sum of the moments of inertia of all masses rotating about the wheel axle. The rotating masses in this investigation consisted of the wheel, tire, tube, and brake rotors. The moment of inertia was determined experimentally with tire R1 mounted on the wheel, and was found to be 2.73 slug-ft^2. It is assumed that the moment of inertia had the same magnitude when the other tires were mounted on the test wheel.

Slip Ratio

The difference between the peripheral velocity of the tire and the horizontal velocity of the wheel axle is defined as the relative skidding velocity occurring between the tire and the ground. The ratio of this relative skidding velocity to the horizontal velocity of the axle is defined as the slip ratio s_1. Thus for a freely rolling wheel the slip ratio is effectively zero while for a completely braked wheel (full skid) the slip ratio equals 1. When the rolling wheel is gaining angular velocity ($-\alpha$) - that is, rolling at decreasing slip ratio - the condition is called spin-up. This condition occurs after touchdown at landing as well as after brake release during wheel braking. A loss in angular velocity ($+\alpha$) - that is, rolling at increasing slip ratio - is called wheel spin-down and occurs, on dry runways, during wheel-brake application only. Wheel spin-down and spin-up can also occur during high-speed unbraked rolling of tires on fluid-covered runways as a result of hydrodynamic effects.

Tire-Ground Friction Coefficient

The ratio of the instantaneous ground drag load $F_{x,g}$ developed by a rolling or nonrolling tire during straight-ahead (0° yaw) translation on a runway surface and the instantaneous vertical ground load $F_{z,g}$ acting on the tire is arbitrarily defined as the tire-ground friction coefficient $\mu = \frac{F_{x,g}}{F_{z,g}}$. For the special case of an unbraked rolling tire undergoing straight-ahead translation on a dry runway, $F_{x,g} = F_{x,g,r}$ and the ratio $F_{x,g,r}/F_{z,g}$ is defined as the coefficient of rolling resistance. During wheel braking, if the braking torque T_B is sufficiently large, the tire will be forced from a freely rolling condition ($s_1 = 0$) to a full-skid condition ($s_1 = 1$) and the tire-ground friction coefficient μ will vary with slip ratio (for a dry runway) in the manner

shown schematically in figure 12. The relationship between friction coefficient μ and slip ratio s_1 has considerable significance with regard to wheel braking. For example, to obtain maximum effectiveness, automatic braking systems must be designed to operate near peak μ (μ_{max} usually occurs at a slip ratio between 0.1 and 0.2). If operation occurs at a slip ratio greater than that required for peak friction, tire tread life is reduced by skidding and braking effectiveness is reduced. Operation at a slip ratio below that required for peak friction simply results in reduced braking action.

Because of the transient nature of the tire-slip phenomenon, operation by the pilot or antiskid unit at μ_{max} is not generally realized without some overshooting or undershooting of the slip ratio for μ_{max}. For this reason, the average friction coefficient μ_{av} developed between slip ratios of 0.1 and 0.5 (see fig. 12), rather than μ_{max}, was arbitrarily chosen in this paper as more nearly representative of the friction coefficient attainable with present-day braking systems. In most of the comparisons made in this paper, μ_{av} is used. The friction coefficient at full skid ($s_1 = 1$) is also of interest and is designated μ_{skid}.

MECHANICS OF THE ROLLING TIRE

For the condition of straight-ahead (unyawed) rolling on a runway surface, equation (1) specifies the angular acceleration a wheel will experience during both braked and free-rolling conditions.

Unbraked Rolling

Dry runways.- For the special case of unbraked rolling at constant V_H (constant ω) on dry runway surfaces, both α and T_B must equal zero and equation (1) reduces to

$$F_{x,g,r}(r_o - \delta) = F_{z,g}x_c \qquad (2)$$

Equation (2) thus specifies that the moment $F_{z,g}x_c$ must be equal and opposite in direction to the wheel spin-up moment $F_{x,g,r}(r_o - \delta)$ created by the tire rolling resistance, which means that for positive rolling resistance x_c must move forward of the axle center line in the direction of motion for a rolling unbraked tire. One possible explanation of this phenomenon is based on the accelerations imparted to radial

elements of the tire when entering and leaving the tire footprint region. (See fig. 13(b).) If constant axle height above the runway (constant vertical load) during the rolling process is assumed, radial elements of the tire are accelerated toward the axle as they pass through the forward half of the tire footprint region, from r_o at the leading edge of the footprint to $r_o - \delta$ directly below the axle center line. As the radial tire elements rotate out of the rear half of the footprint region they are accelerated away from the axle by the internal tire pressure, from $r_o - \delta$ beneath the axle to r_o where exit from the footprint occurs. These accelerations, and associated tire hysteresis effects, create forces which are thought to change the vertical-load distribution within the footprint from the symmetrical distribution of a standing tire (fig. 13(a)) to a distribution such as that schematically indicated in figure 13(b), with the resulting center of pressure of the vertical load moved forward of the wheel-axle center line in the direction of horizontal axle motion. Since the accelerations of the tire within the footprint are a function of the tire rotational velocity (accelerations must increase with increasing rotational velocity), it would appear logical for x_c to move increasingly forward as the rotational velocity or forward speed is increased. Such a trend is indicated by the data shown in figure 14(b). According to Kamm (see ref. 11), this effect may result in loss of adhesion over the last third of the contact surface at high rolling speeds.

Wet runways.- Consider the case of a freely rolling unbraked tire accelerating on a fluid-covered runway as in airplane take-off. As the moving tire contacts and displaces the stationary runway fluid the resulting change in momentum of the fluid creates hydrodynamic pressures that react on the runway and tire surfaces. The tire engages the runway fluid at a definite angle of attack that is determined by the intersection of the tire equator and the ground plane. (See fig. 13(c).) As the forward speed is increased, a wedge of water penetrates farther and farther into the tire footprint region until at some high forward speed, complete separation between the tire and runway occurs. This speed is referred to as the tire hydroplaning velocity. At this speed, the tire loses practically all of its directional stability because of the inability of a fluid to develop large shear forces. Experimental measurements of vertical-load center of pressure obtained from the present investigation indicate that the hydrodynamic pressure generated at the front of the tire footprint by the wedge of water distorts the vertical-load distribution within the tire footprint region so that x_c moves farther forward of the axle than for the case of a tire rolling at the same forward velocity on a dry runway (shown schematically in fig. 13(c)). In addition, the horizontal component of the hydrodynamic force adds to the tire rolling resistance to produce a larger wheel spin-up moment.

As in the case of the braked tire (eq. (1)), the net torques and moments acting on the unbraked tire must equal the acceleration of the wheel. Including hydrodynamic effects, this can be expressed approximately as

$$\alpha = \frac{F_{z,g}x_c - \left[F_{x,g,r} + F_{x,g,f} + \left(F_{z,g} - F_{z,L}\right)\mu\right](r_o - \delta)}{I} \tag{3}$$

When the vertical component of the hydrodynamic force $F_{z,L}$ equals the vertical ground force $F_{z,g}$ in equation (3), the tire-ground frictional spin-up moment vanishes and since the tire is entirely supported by the runway fluid for this condition, tire hydroplaning then exists. If $F_{z,L}$ is assumed to be proportional to V_H^2 and directly proportional to tire-ground gross contact area A_g and fluid density ρ, and if all other effects such as those due to tire tread design and fluid viscosity are ignored, the following approximate expression for tire hydroplaning velocity V_p may be obtained:

$$F_{z,g} = F_{z,L} = \frac{1}{2} C_L \rho A_g V_p^2 \tag{4}$$

Rearranging terms gives

$$V_p = \sqrt{\frac{F_{z,g}}{A_g}\frac{2}{C_L\rho}} \tag{5}$$

The term $F_{z,g}/A_g$ is actually the gross footprint pressure p_g exerted by the tire on the ground. From reference 12, this pressure may be represented (for modern airplane tires) by

$$p_g = \frac{F_{z,g}}{A_g} = \left[1.05 - C_z\left(\frac{\delta}{w}\right)^{-1}\right]\left(p + 0.08p_r\right) \tag{6}$$

Thus the tire hydroplaning velocity may be approximately expressed for modern aircraft tires by the equation

$$V_p = \sqrt{\frac{2\left[1.05 - C_z\left(\frac{\delta}{w}\right)^{-1}\right]\left(p + 0.08p_r\right)}{C_L\rho}} \tag{7}$$

The data shown in figure 15 indicate that reasonable agreement between calculated and experimental tire hydroplaning velocities occurs when $C_L = 0.7$ is used in equations (5) and (7). Equation (5), rather than equation (7), was used to calculate V_p for the nonaircraft tires shown in figure 15 because the effects of carcass stiffness on p_g for these particular tires is not known.

Experimental data obtained from the present tests and reference 6 indicate that when tire hydroplaning velocity is approached or exceeded by an unbraked rolling tire, tire spin-down or even tire stopping ($\omega = 0$) can occur. Figure 16 shows data obtained on the buffed dimple tire D5M1 when it entered a wet runway unbraked at a forward speed of 113 knots. The predicted hydroplaning velocity (from eq. (7)) for the test tire pressure of 90 lb/sq in. was 85 knots. It will be noticed in this figure that the tire started slowing down immediately upon entering the wet runway and stopped rotating at approximately 102 knots, which is 17 knots above the predicted hydroplaning velocity. These data support the conclusion reached from the treadmill tests (ref. 5) that a hydroplaning tire is stable about $\omega = 0$ for forward velocities in excess of the hydroplaning velocity V_p and for moderate fluid depths. The data in figure 16 also show that tire D5M1 did not spin up on the wet runway until the forward velocity had decreased to 72 knots, a speed which is 13 knots below the predicted hydroplaning velocity. This result indicates a hysteresis effect which was noticed in the investigation of reference 5 but not reported. Because of this effect, the forward velocity required for a tire to spin down and stop under increasing forward velocity conditions is always greater than the forward velocity required to spin up the tire (after hydroplaning) under decreasing forward velocity conditions.

It is of interest to note that a similar test was performed at the same forward velocity on the rib-tread tire R4 for a tire pressure of 85 lb/sq in. rather than the 90 lb/sq in. which was used for tire D5M1. Tire R4 never stopped rotating, but did suffer a 20-percent loss in angular velocity while in the water trough, which was covered with water to a depth of 0.1 to 0.4 inch. From equation (7), the hydroplaning velocity for rib-tread tire R4 should be slightly lower than that for smooth-tread tire D5M1 because the inflation pressure for tire R4 was 5 lb/sq in. less; yet tire R4 showed less tire spin-down than tire D5M1. The tread depth of tire R4 at the time of the test was approximately 0.2 inch. The test results thus indicate a tread effect on tire hydroplaning even when the water depth is somewhat greater on the average than the tread depth.

Braked Rolling

In order to develop drag forces for stopping aircraft on runways or for directional control, a resistive torque opposing tire rotation is applied to an aircraft wheel by means of wheel brakes. Rearranging equation (1) gives an expression for this resistive torque T_B in terms of all the other torques or moments acting about the wheel axle at any instant. A typical variation of T_B with time is shown in figure 17 for tire R2 undergoing braked rolling on a wet runway at high forward speed (V_H = 96 to 93.5 knots). Also shown in this figure are time histories of ω, α, p_B, μ, and the net spin-up moment $F_{x,g}(r_o - \delta) - F_{z,g}x_c$ under these test conditions.

The mechanics involved in braking a rolling tire can be treated best by discussing figure 17 in detail. Just before time zero in this figure, the tire is unbraked and rolling at a velocity of 130 radians/sec. At time zero, a valve is opened to allow hydraulic fluid to flow from an accumulator through a micrometer needle valve and into the brake, where the pressure p_B builds up to the accumulator pressure. This pressure acts on pistons positioned around the wheel which force brake stators (splined to the wheel axle) against brake rotors (rotating with the wheel). The stator and rotor rubbing surfaces (brake pucks) generate a resistive torque T_B which opposes tire rotation. The torque T_B is a function of the pressure p_B supplied to the brake, the friction coefficient developed between the rubbing surfaces, and the distance between the axle and brake-puck center lines. It will be noticed in figure 17 that the initial rise of p_B after time zero does not create a corresponding rise in T_B until p_B exceeds approximately 100 lb/sq in. This lag is explained by the fact that the brake pistons must first overcome return spring forces before the stators will start sliding along the axle toward the rotors. The small constant value of T_B before stator motion starts is believed to be due to light contact between the stators and rotors while unloaded.

As p_B increases further, there is a corresponding rise in the curves for both T_B and $F_{x,g}(r_o - \delta) - F_{z,g}x_c$ until the slip ratio for μ_{max} is exceeded. At this point the wheel decelerates rapidly as a result of the net torque impulse (area between curves for T_B and $F_{x,g}(r_o - \delta) - F_{z,g}x_c$). The change in momentum imparted to the wheel by the brakes must exactly equal this net torque impulse. This comparison is shown in figure 17 for both spin-down and spin-up conditions. The agreement shown is typical for the instrumentation used in this investigation.

Continuing along the time history of the braking cycle in figure 17, a point is reached where the wheel comes to a complete stop. At this point α and $F_{x,g,r}$ equal zero and T_B equals $\left(F_{x,g,f} + F_{z,g}\mu_{skid}\right)(r_o - \delta) - F_{z,g}x_c$. The symbol μ_{skid} is the friction coefficient for the tire under full-skid $\left(s_1 = 1\right)$ conditions, and is considerably lower than μ_{max} for the wet-runway test conditions of figure 17. At time 0.63 second in figure 17, the brakes are released by dumping the pressure p_B. Almost immediately, the net spin-up moment increases above T_B and the resulting net torque impulse spins up the wheel to the angular velocity required for free rolling. It is interesting to note that considerable T_B exists after p_B has been reduced to near zero values. This effect is attributed to grabbing of the brakes (stators and rotors do not disengage at zero p_B) due to dynamic conditions in the brake. The residual T_B after release of p_B was a variable in the current tests. Some runs developed larger residual T_B values than others without establishing any identifiable pattern. This residual torque can seriously affect wheel spin-up characteristics when tire treads with low friction coefficients are used at high forward speeds on wet runways, as is shown in figure 18.

AUTOMATIC BRAKING DEVICES

This section of the paper will discuss how the deterioration of wheel angular acceleration with increasing forward velocity on wet runways impairs the performance of the antiskid unit used in this investigation.

The operation of many antiskid units in use on aircraft at the present time is based on changes in wheel angular acceleration. The antiskid unit used in the present investigation is such a device. Depressing the pilot's brake pedal releases pressure from an accumulator to the wheel brake. This hydraulic pressure forces the brake stators against the brake rotors (for a disk brake), creating an increasing resistive torque T_B that opposes wheel rotation in the direction of motion. A point will soon be reached where the slip ratio required for maximum tire-ground friction coefficient will be exceeded and the tire will suddenly decelerate. The test antiskid unit was set to dump brake pressure (by means of a solenoid-operated valve) when this angular deceleration exceeded 45 to 60 radians/sec^2. In the test antiskid unit, an inertia-type flywheel disengages from the main wheel when the main wheel starts to decelerate. This inertia flywheel then coasts, continuously losing its angular velocity because of bearing frictional torque and possibly clutch drag.

After brake-pressure release, the resistive torque T_B decays to zero and the drag-load spin-up moment accelerates the main wheel back up to runway speed. When the angular velocity of the wheel equals the rotational velocity of the antiskid inertia flywheel, which has now slowed below its value at brake release, a signal is generated to close the pressure dump valve and open a valve located between the accumulator and the brake, allowing pressure to be applied to the brake again, and another braking cycle commences.

For dry runways, spin-up accelerations are large enough so that the inertia flywheel loses little velocity during the recovery portion of the braking cycle, and successive braking cycles always start with the tire rotating at or near the tangential velocity required for the airplane's forward speed along the runway ($s_1 = 0$). Such is not the case under certain braking conditions on wet runways, as is shown in figures 19 to 21. These figures show sample oscillograph tracings obtained during wet-runway braking tests at different forward speeds with several tires having different tread patterns. Figure 19 shows tracings obtained for the rib-tread tire S2M2 at low and high forward speeds. This figure illustrates satisfactory antiskid operation on a wet runway, with the tire recovering the necessary tangential velocity before each new braking cycle.

Figure 20 shows sample oscillograph tracings obtained during wet-runway braking tests at approximately the same test forward velocities for a less skid-resistant tire, smooth all-rubber-tread tire S1. Notice that the developed drag loads and spin-up accelerations in figure 20 are much less than those shown in figure 19 for the rib-tread tire S2M2. Figure 20(b) illustrates a characteristic of the test antiskid unit in that reapplication of brake pressure initiates another braking cycle before complete wheel spin-up has been attained.

The end result of this antiskid characteristic is illustrated in figure 21, where tracings of oscillograph records obtained during wet-runway tests at high forward speeds are shown for tire D1 at $p = 260$ lb/sq in. and tire S1 at $p = 120$ lb/sq in. The initial braking cycle for tire D1 (fig. 21(a)) started on dry concrete. Note that for both tires D1 and S1, the initial angular velocity of the wheel was never completely regained before the next braking cycle commenced, resulting in completely locked wheels (wheels at full skid) at the end of 3 or 4 braking cycles.

The test antiskid unit had a lockout feature for low-speed taxiing (below 4 or 5 mph) so that the pilot could arbitrarily brake each wheel up to full skid without operation of the antiskid unit. This feature is illustrated in figure 21(b), where after the last braking cycle the

brake pressure p_B is seen to be increasing rapidly. (Brake pressure p_B went to full system pressure in subsequent portions of the oscillograph records of fig. 21.) Inadvertent operation of the antiskid lockout feature also occurred during the first wet braking run with a new and unused test tire (tracings not shown). Conditions for this test were: $F_{z,g}$ = 10,000 pounds, p = 260 lb/sq in., and V_H = 100 knots. The wheel developed a full-skid condition on the wet concrete in a manner similar to that shown in figure 21 and then skidded onto a portion of the concrete runway that was dry. The tire failed (see fig. 22) after sliding (locked wheel) approximately 60 feet on the dry runway surface. It is obvious that the combination of this antiskid lockout feature and a pilot continuously riding the brakes can be hazardous to airplane operation on runways which are intermittently wet and dry.

In summary, it is apparent that the relatively long spin-up times, due to low spin-up accelerations, developed by some tires during braking at high speeds on wet runways can seriously impair the performance of antiskid units that utilize an inertia flywheel for reference angular velocity. The antiskid-unit lockout feature used in some airplane braking systems to permit differential braking by the pilot at low taxiing speeds with antiskid on, can lead to tire failure under certain braking conditions on wet runways at high forward speeds.

Examination of equation (1) shows that highest wheel spin-up acceleration on wet runways will result when (a) the forward shift of x_c is a minimum, (b) the drag moment $F_{x,g}(r_o - \delta)$ is as large as possible, and (c) the brake torque T_B drops to zero immediately after brake-pressure release. The test results indicate that for wet conditions (a) and (b) are functions of tire tread and runway design while (c) is a function of the braking system (hydraulic resistance and brake grab).

DISCUSSION OF PARAMETERS

ROLLING RESISTANCE

The variation of the steady-state unbraked-rolling resistance force $F_{x,g,r}$ with forward velocity is shown in figure 14(a) in terms of the ratio $F_{x,g}/F_{z,g}$. The data shown in this figure were obtained from the unbraked-rolling tests under essentially constant conditions of vertical ground load $F_{z,g}$ and tire pressure p on a dry concrete runway. The scatter of the test data in this figure is such that no

discernible tendency of the rolling resistance to increase with decreasing tire pressure (at constant vertical load) is evident. Such a trend would be expected from tire hysteresis and inertia considerations because of the larger deformations of the carcass experienced by tires rolling at reduced tire pressures. The tendency of rolling resistance to increase with increasing forward velocity shown in figure 14(a) is in agreement with the findings of reference 11. The rolling-resistance values obtained from the present tests are, however, somewhat higher than those reported in reference 11 for airplane tires on hard surfaces. It is felt that brake grab (discussed in an earlier section of this paper) is mainly responsible for this disagreement in that drag forces produced by the unloaded wheel-brake rubbing surfaces add to the actual rolling-resistance values to produce larger effective rolling resistance values for the tire being tested. The possibility that modern aircraft tires, such as those used in the present tests, might develop larger rolling-resistance values than the older and smaller aircraft tires discussed in reference 11 should, however, not be entirely ruled out as a factor contributing to this difference.

FLUID-DISPLACEMENT DRAG

Single or Leading Tandem Wheels

When an unbraked rolling tire encounters a fluid of finite depth on a runway surface, the drag force acting on the rolling tire will increase in the manner shown in figures 16 and 23. In reference 1, where the initial results obtained from the unbraked-rolling portion of this investigation were used, it was determined for the velocity range covered that this increase in tire rolling resistance due to fluid displacement drag $F_{x,g,f}$ could be represented with reasonable accuracy by the equation

$$F_{x,g,f} = C_D \rho w d_1 V_H^2 \left[\left(\frac{\delta + d_1}{w} \right) - \left(\frac{\delta + d_1}{w} \right)^2 \right]^{1/2} \tag{8}$$

In words, equation (8) states that $F_{x,g,f}$ for a single wheel or a front-mounted tandem wheel varies approximately linearly with fluid density, fluid depth, tire cross-sectional width at the fluid surface on the runway, and forward velocity squared. The comparison of the predictions of equation (8) and experimental data from unbraked-rolling runs on a water-covered concrete runway made later in the test program (not included in ref. 1) is shown in figure 24. The scatter of the data in figure 24 is attributed mainly to wind effects, which produced water-depth gradients in the water trough when the wind was blowing during

test runs, and to the elevation characteristics of the concrete runway, which produced water-depth variations of as much as 0.3 inch in the test trough. (See section entitled "Runway Troughs and Surfaces.")

Rear Tandem Wheels

It was observed in reference 1 that when a single wheel passed through the slush trough, most of the slush in the wheel path was completely removed or thrown from the slush trough. Reference 1 also states that the slush residue remaining in the trough in the path of the wheel did not exceed 0.1 inch. This observation on the path-clearing effectiveness of the front wheel is confirmed by the data shown in figure 25. The solid curve in this figure is the slush-displacement drag acting on a single wheel for the slush conditions noted, calculated from equation (8), while the single data point shows the slush-displacement drag developed on a rear tandem wheel at the same forward velocity (approximately 92 knots) for the same runway slush conditions. With a slush depth of 1.75 inches on the runway, the drag force developed on the rear wheel of the tandem gear was the same as a single wheel would experience in approximately 0.1 to 0.2 inch of slush. These data indicate that for the test conditions noted, the fluid-displacement drag developed on rear tandem wheels is only 0.1 the magnitude of the drag force developed on a single wheel or front-mounted tandem wheel.

BRAKING DRAG

When relative motion exists between the tire footprint (the part of the tire in contact with a runway surface) and the runway surface, a drag force $F_{x,g,b}$ is created which is equal to the product of the vertical load acting on the tire and the friction coefficient μ developed between the tire and runway surfaces. (See section entitled "Definition of Terms.") No further treatment of $F_{x,g,b}$ will be given in this paper since a knowledge of the variation of μ and the vertical load automatically defines the variation of $F_{x,g,b}$. The coefficient μ is discussed in detail in a subsequent section.

MOVEMENT OF VERTICAL-LOAD CENTER OF PRESSURE

The ground-pressure distribution within the footprint of a tire undergoing translation along the ground can be distorted by different ground-load conditions so that the vertical-load center of pressure of

the tire may shift either ahead of or behind the wheel-axle center line. Tire fore-and-aft elastic effects displace the tire footprint in the direction of the applied ground-drag loads and cause x_c to move toward the rear of the footprint. Tire hysteresis and inertia, and runway hydrodynamic effects, distort the pressure distribution within the footprint in such a way that x_c must move toward the front.

For the condition of unbraked rolling on a dry runway, tire elastic effects are small and tire hysteresis and inertia effects predominate, so that x_c is always a small distance forward of the axle center line. Figure 14(b) illustrates this condition and also shows that x_c tends to move farther forward as the rolling velocity or forward velocity is increased. For the condition of unbraked rolling on fluid-covered runways, the hydrodynamic effects predominate, expecially at the higher forward speeds and greater fluid depths, and x_c moves farther forward of the axle center line than for the equivalent dry-runway conditions. These effects are shown in figures 16, 23, and 26. It is interesting to note in figure 16 that just before the unbraked hydroplaning tire encounters the greater water depth on the runway and after tire spin-down to a stop, x_c decreases in magnitude. Apparently the decrease in x_c at this point is caused by tire hysteresis and inertia effects dropping to zero when the tire stops rotating.

On a dry runway during wheel braking, tire elastic effects predominate and x_c moves toward the rear of the tire footprint at the larger values of ground-drag load during both wheel spin-down and spin-up, as is shown in figure 27 for tire R2. During wheel braking on wet runways, hydrodynamic effects become increasingly larger as the forward velocity is increased and tend to reduce or eliminate the rearward movement of x_c shown for dry runways. This trend was evident for all tires investigated but especially for the less skid-resistant tread designs; for example, see figure 28 for the smooth-tread tire S1.

WHEEL SPIN-UP AND SPIN-DOWN

Satisfactory operation of most antiskid devices in use on airplanes today is dependent upon quick recovery of wheel rotational velocity by the braked wheel upon release of the wheel brakes. (See section entitled "Automatic Braking Devices.") Test results indicate that the degree of runway wetness, tire-tread design, tire inflation pressure, and the location of the tire (in tandem-wheel landing-gear arrangements) can influence wheel spin-down and spin-up characteristics markedly.

The test data indicate that for braking on dry runway surfaces, tread design has little effect on wheel spin-up characteristics. For

example, compare the solid curves in figure 29 for the rib-tread tire R1 and the dimple-tread tire D1. All of the tire-tread designs investigated show a degradation in wheel spin-up performance during braking on wet runways, especially at the higher forward velocities of the investigation. For the velocity range covered, multirib-tread tires such as tires R1 and S2M2 showed considerably less decrease in spin-up performance than did the other tire tread types. For example, compare the dashed curves in figure 29 for the multirib-tread tires R1 and S2M2 with the dashed curves obtained for tires D1 and S3.

The test data also indicate that wheel spin-up performance on wet runways will be further impaired for the less skid-resistant tires by reducing the tire inflation pressure while keeping the vertical load on the tire constant (see fig. 30), which increases the length of the contact region between the tire and the ground. The multirib-tread tire S2M2 under the same test conditions (see fig. 30) showed little loss in spin-up performance.

Wheel spin-up performance on wet runways for the less skid-resistant tires may be improved by mounting these tires on the rear wheels of tandem landing gears, thus utilizing the path-clearing ability of the front or leading tandem wheel. (See discussion of fluid-displacement drag $F_{x,g,f}$.) The curves in figure 31 indicate that no large improvement in wheel spin-up performance is experienced by the more skid-resistant tires (represented in fig. 31 by tire S2M2) when they are mounted on the rear wheel of a tandem landing gear.

INSTANTANEOUS TIRE-GROUND FRICTION COEFFICIENT

Time histories illustrating the variation of the instantaneous tire-ground friction coefficient μ developed during braking test runs on wet concrete runways for a tire with good skid resistance (tire R2) and a tire with poor skid resistance (tire D1) are shown in figures 17 and 18, respectively. The variation of μ with slip ratio is shown in the appendix for most of the skid cycles obtained during braking tests of a single wheel on wet concrete runways for the different tires investigated.

MAXIMUM TIRE-GROUND FRICTION COEFFICIENT

Dry Runways

For dry concrete runways, the curves of μ as a function of slip ratio for the different tires investigated usually displayed a very

prominant peak μ_{max} between slip ratios of 0.1 and 0.2 (see appendix). The data shown in figure 32 indicate that μ_{max} is practically independent of forward velocity, with most of the tire tread designs indicating little or no decrease in the magnitude of μ_{max} over the forward velocity range investigated.

The magnitude of μ_{max} is, however, dependent upon the average tire-ground bearing pressure p_n, as shown in figure 33, where μ_{max} decreases in magnitude with increasing values of p_n. This is the trend reported in reference 12 for μ_{max} values obtained at very low forward speeds ($0.009 < V_H < 2$ knots). It is interesting to note that the equation $\mu_{max} = 0.93 - 0.0011p_n$, which was empirically derived on the basis of low-speed data (ref. 12), also fits the high-speed data of this investigation with fair accuracy. This agreement also supports the conclusion that μ_{max} is relatively independent of forward speed for a dry concrete runway surface.

Contaminated Runways

The data from this investigation and other available experimental data (refs. 4 to 9) indicate that μ_{max} decreases with increasing forward velocity on fluid-covered or contaminated runways. The test data indicate that μ_{max} follows the trends observed for μ_{av} but at somewhat higher values of μ.

FULL-SKID TIRE-GROUND FRICTION COEFFICIENT

Dry Runways

The variations of μ_{skid} with forward velocity on a dry concrete runway for several of the tire designs investigated are shown in figure 32. It is seen that μ_{skid} decreases as the forward velocity increases for the velocity range investigated. This trend is more clearly shown in figure 34, where the ratio μ_{skid}/μ_{max} is plotted against forward velocity for a number of tires used in this and other investigations. The data in figure 34 indicate very small differences between μ_{skid} and μ_{max} at low forward velocities and very large differences $\left(\frac{\mu_{skid}}{\mu_{max}} \approx 0.32\right)$ at the higher forward velocities. The substantial difference in tire behavior at low and high forward velocities

is attributed to tire heating effects. For example, at the low velocities of references 13 to 15, the rubber deposited on the runway by the sliding tires consisted of small solid particles that were evidently sheared or abraded from the tire surface by the asperities of the runway surface. At the conclusion of each of these low-speed runs, the rubber tread in the ground-contact region was warm to the touch but showed no evidence of being subjected to high heat. In contrast, in the present investigation, inspection of the skid marks after high-speed skids on a dry concrete runway revealed that the rubber apparently was deposited in the liquid state since the concrete surface gave the appearance of having been painted with rubber. At the conclusion of each high-speed braking run, the rubber or rubber-fabric tread of the ground-contact region of the tire was hot and sticky to the touch. In fact, when the brake was released after a high-speed skid, this sticky contact area of the tire would stamp the runway at each succeeding revolution of the wheel and leave a clear imprint on the runway surface. As a point of interest, these stampings looked exactly like the tire footprints shown in figure 4.

Correlation of the movie films taken on each braking run with the corresponding oscillograph records showed that the puff of smoke (oxidized rubber) emanating from the tire footprint region during a braking cycle at high speed occurred at slip ratios ranging from 1.0 (full skid) to as low as 0.15. The reduced values of μ_{skid}/μ_{max} obtained on tires at the higher forward velocities are probably caused by the molten rubber in the tire footprint region acting as a lubricant between the tire and the ground. Prolonged skids of a tire at or near μ_{skid} can cause rapid erosion of the tire tread and carcass and result in failure of the tire. Figure 22 is a photograph of a tire that failed after a full skid of only 60 feet on a dry concrete runway. No tests were conducted on dry asphalt runways during this investigation.

Water-Covered Runways

Figure 35 shows the variation of μ_{skid} with forward velocity for several different rib-tread aircraft tires on water-covered concrete and asphalt runway surfaces. For comparison purposes, this figure includes British flight-test data (refs. 8 and 9) that were obtained under similar runway wetness conditions. Both British flight tests and NASA track tests indicate that μ_{skid} decreases with increasing forward velocity for wet concrete and asphalt runways, although the British values of μ_{skid} are generally lower than the track values over the velocity range investigated. Both British and NASA track data indicate that the wet asphalt-runway surfaces investigated gave higher μ_{skid} values than did the wet concrete surfaces at the higher forward velocities.

AVERAGE TIRE-GROUND FRICTION COEFFICIENT

Dry Runways

In figure 12, μ_{av} is defined as the average value of the tire-ground friction coefficient μ obtained between slip ratios of 0.1 and 0.5. For tires on a dry concrete runway, the data shown in figure 36 indicate that μ_{av} is approximately 10 percent lower in magnitude than μ_{max} over the forward-velocity range investigated. Figure 36 also indicates that μ_{av} (as was found earlier for μ_{max}) appears to be independent of forward velocity over the range of conditions investigated, on a dry concrete runway.

Contaminated Runways

In contrast to the dry-runway results, which showed little or no forward-velocity effect on μ_{av}, the experimental data obtained during braking runs on contaminated runway surfaces disclosed that μ_{av} decreases markedly with increasing forward velocity. The magnitude of the decrease in μ_{av} was found to depend upon such parameters as:

Runway composition and surface

Type and depth of contaminant on runway

Vertical ground load acting on tire

Tire inflation pressure

Tire position in tandem wheel arrangements

Tire tread material

Tire tread pattern

It is the purpose of this section to show how these parameters affect the magnitude of μ_{av} developed on contaminated runway surfaces.

Runway composition and surface.- The effect on μ_{av} of braking a single wheel on water-covered runways of different composition and surface texture is shown in figure 37. These data indicate that the values of μ_{av} developed on asphalt surfaces with both the smooth sand finish

and the rough aggregate finish were higher than those developed on the concrete surface for the low and medium forward velocities investigated. At the higher forward velocities, μ_{av} values developed on the test runway surfaces were approximately equal. Figure 37 also shows that the surface texture of the asphalt runways investigated apparently had little effect on μ_{av}, since both the smooth and rough asphalt surfaces gave rise to approximately the same values of μ_{av} for the range of conditions investigated.

Type and depth of contaminant on runway.- Figure 38 shows faired μ_{av} data obtained during single-wheel braking runs on both slush-covered and water-covered runways for tires D2 and S2M2. By comparing curves A (water) and curves B (slush) of this figure, it may be seen that curves B increase at the higher forward velocities whereas curves A continue to decrease. This rising trend of the slush data at the higher velocities is believed to be due to the depth of slush on the runways during the tests. The fluid-displacement drag forces due to slush for the test conditions were calculated by means of equation (8), and these calculations in terms of an effective μ_{av} are shown as curves C of figure 38. The same calculations were made for the water-covered runway at a forward speed of 100 knots, and an effective μ_{av} equal to approximately 0.014 was obtained. This low value is due to the small average water depth $(d_1 = 0.15 \text{ inch})$ used in the tests. The differences between curves B and C are curves D of figure 38, the contribution to μ_{av} of tire braking friction and tire rolling resistance. Curves D decrease with forward velocity in a manner similar to data for the water-covered runway (curves A), which contain a negligible amount of water-displacement drag as just indicated. Comparison of curves A and D indicates that lower values of μ_{av} are generated during braking on slush-covered runway surfaces than on water-covered surfaces.

Test results indicate that the presence of measurable fluid depths on a runway surface are not a necessary requirement for low braking friction on contaminated runways. Values of μ_{av} that are considerably reduced from dry-runway values can also be obtained during braking runs on runways that are only damp, that is, moistened with just enough water or other fluids to create a film on the runway surface, but not sufficient to form puddles. This effect is shown in figure 39 for tire S1M3 on a concrete runway and for tire S2M2 on an asphalt runway. The data in figure 39 indicate that μ_{av} values developed on both the damp (with water) asphalt and concrete runways are only slightly higher than the values obtained for the water-covered $(d_1 = 0 \text{ to } 0.3 \text{ inch})$ runways. The data shown in figure 39(b) for an asphalt runway contaminated with JP-4 fuel and water indicate that this form of runway contamination

results in an even greater decrease of μ_{av} than was obtained for the asphalt runway dampened with water only. No tests were made with the concrete runway contaminated with JP-4 fuel.

The data obtained during braked rolling on a concrete runway covered with two types of fire-extinguishing foam (organic and detergent) are shown in figure 40. For the velocity range investigated these data indicate that μ_{av} values developed on the foam-covered runway were approximately equal to those developed on a water-covered concrete runway. The large depths of foam indicated for this particular braking run can be discounted, since both types of foam were of very low density and foam-displacement drag forces would be negligible.

The results of the braking runs on runways damp with water, damp with JP-4 fuel and water, slush-covered, and foam-covered tend to indicate that the reduction of μ_{av} developed on these surfaces may depend less on depth and density and more on lubrication or other properties of the particular contaminant, especially at subhydroplaning velocities.

Most airport runway surfaces are contaminated to some extent by rubber from aircraft tires that is deposited on the runway surface during wheel spin-up at initial airplane touchdown, and during wheel braking in the landing roll. The data shown in figure 41 indicate that the tire-ground friction coefficient is reduced from the values for uncontaminated dry runways when wheel braking occurs on a rubber-contaminated surface. These data indicate that μ_{av} decreases from about 0.64 for the dry uncontaminated concrete surface to about 0.48 for the dry rubber-contaminated concrete surface under the conditions of the investigation.

Vertical ground load acting on tire.- Increasing the vertical ground load on tire S2M2 (fig. 4(n)) while keeping the tire inflation pressure constant during single-wheel braking tests on a wet runway affects μ_{av} as shown in figure 42. The data in figure 42 indicate that for this particular tread design, an increase in the tire vertical load from 10,000 pounds to 22,000 pounds decreases the magnitude of μ_{av} throughout the forward-velocity range investigated. Apparently this result is a tread effect rather than a load effect, since for this particular tire the higher load condition results in a larger footprint area and consequently a larger region near the outside of the footprint without grooves to furnish escape paths for the water trapped between the footprint and the ground.

It is interesting to note that while an increase in the vertical load at constant tire pressure reduces μ_{av}, this load condition also increases the average wheel spin-up acceleration acting on tire S2M2

after brake release, as is shown in figure 42(b). This result points out the fact that it is the product of $F_{z,g}$ and μ, rather than μ alone, that determines the wheel spin-up acceleration. For this reason, better wheel spin-up acceleration will probably result if wing lift is dumped as quickly as possible after touchdown during landing, so that the full weight of the airplane will act on the tires.

Tire inflation pressure.- Decreasing the tire inflation pressure while keeping the vertical ground load on a tire constant affects the tire-ground contact region in two ways. First, the tire footprint length and width is increased, and second, the tire-ground bearing pressure is reduced. The data shown in figure 43 indicate that lowering the tire pressure from 260 to 120 lb/sq in. at $F_{z,g} \approx 10{,}000$ pounds produces little change in μ_{av} for tires S1, S2, and S2M2 on a wet concrete runway. These data do, however, show some tendency for the low-pressure μ_{av} values to be higher at low forward speeds than the high-pressure μ_{av} values. The reverse is true at the higher forward speeds. These trends are best illustrated in figure 43(a) for data obtained for tire S2M2 on the wet asphalt runway. The same trends are shown in figure 43(b) where average spin-up acceleration is plotted against forward speed for the same tires and test conditions (on the concrete runway) as those of figure 43(a). For the condition of constant vertical load, average wheel spin-up acceleration reflects the magnitude of the tire-ground friction coefficient that is developed during wheel spin-up.

Tire position in tandem wheel arrangements.- As pointed out in reference 1, the forward or leading wheel of a tandem-wheel landing-gear arrangement tends to clear the path for the rear wheel of the tandem gear during unbraked rolling on a fluid-covered runway. This observation was confirmed by the data shown in figure 25. The data shown in figure 44(a) indicate that this path-clearing ability of the forward wheel can also raise the level of μ_{av} developed during braking on wet runways by tires with poor skid resistance when these tires are used on rear tandem wheels. These data also indicate that for the conditions investigated, position of the tire in a tandem gear had little or no effect on μ_{av} values developed by the skid-resistant rib-tread tire S2M2. The same trend is indicated in figure 44(b), where the average wheel spin-up accelerations developed under the test conditions of figure 44(a) are plotted against forward velocity. The path-clearing effect of the leading wheel in a tandem arrangement is even more pronounced when braking occurs on slush-covered runways, as illustrated in figure 44(c).

Tire tread material.- Until the advent of jet aircraft, tire designers used rubber alone as tread material with very satisfactory

results. The much higher landing and take-off velocities required of most jet aircraft as compared with propeller-type aircraft, however, compelled designers to reinforce the rubber tread by means of fabric laminations in order to meet the new high-speed design requirements concerning tread wear and tread integrity. Typical all-rubber and fabric-reinforced tire-tread sections are shown in figure 5. The data in figure 45 indicate that the effect of tread material on the magnitude of μ_{av} is largely insignificant over most of the forward-velocity range investigated. At the higher forward velocities, however, the fabric-reinforced treads tend to develop slightly higher μ_{av} values on wet concrete runways than do all-rubber treads. In fact, the buffed dimple tire D5M1 (fig. 4(d)), which had all of the tread removed so that the carcass cords were exposed, developed the highest μ_{av} values at the higher forward velocities of all the tires investigated for this effect. In summary, reinforcing rubber tire treads by means of fabric laminations in the tread does not impair the braking effectiveness of tires on wet concrete runways.

Tire tread pattern.- The variations in average tire-ground friction coefficient μ_{av} with forward velocity obtained for the 20 different tread patterns (see fig. 4) investigated during single-wheel braking tests on a wet concrete runway are shown in figure 46. The μ_{av} values shown in this figure were determined from wheel spin-down data given in the appendix. The tread-pattern comparisons to follow make use of the faired lines drawn through the data of figure 46.

Smooth and dimple treads: Tires with smooth and dimple treads developed the lowest μ_{av} values of all the different tires investigated on wet runway surfaces. The variations of μ_{av} with forward velocity for these tire treads were similar in shape and magnitude, as is shown in figure 47. For the conditions investigated, the smooth and dimple-tread tires developed values of μ_{av} ranging from 0.14 to 0.175 at 50 knots and 0.060 to 0.085 at 100 knots forward velocity.

The path of the braked wheel through the water-covered runway was examined after each braking run. This examination revealed that at the higher forward velocities, the smooth- and dimple-tread tires investigated did not deposit rubber on the wet concrete surface as did the rib-tread tires R1 and S2M2. The only visual evidence on the runway that the smooth- and dimple-tread tires had been subjected to braking action was that the path of the tire was much cleaner and whiter than the surrounding concrete surface. The inference follows that most of the footprint was supported by a water film at the higher velocities, or else penetration to the concrete surface would have occurred and rubber would have been deposited on the runway surface.

Circumferential rib treads: Tire designers have known for many years that cutting grooved patterns into tire treads can substantially increase the braking coefficients of tires on wet surfaces. This effect is shown in figure 48, where μ_{av} values obtained for the smooth-tread tires S1 and S2 are compared with values obtained for the identical tires after circumferential grooves were cut into the treads. Also shown in figure 48 are the comparisons between μ_{av} values obtained for the dimple-tread tire D2 and values obtained for the similar dimple-tread tires D6M1 and D8M1 which were modified before the test by cutting five and two circumferential grooves, respectively, into the tread. In every case shown in figure 48, cutting circumferential grooves into the smooth and dimple tire treads resulted in large increases in braking friction, especially at the higher test velocities. The curves in this figure also indicate that increasing the number of grooves cut into a tread increases the braking friction for the tires shown. In fact, tire R1 (see figs. 4(s) and 46(w)), which has nine circumferential grooves, developed the highest values of μ_{av} at most forward speeds of all the tires investigated. It should be noted, however, that other design considerations, such as tread wear, tread integrity, and reinforcing of the tread for high-speed operation, act to limit the number of grooves that can be incorporated in a tread. As an example, this same tire R1 which produces such good braking friction on wet runways is not qualified for use on high-speed aircraft because of the excessive tread wear and tread chunking that occurs for this tire during high-speed operation.

The test data also indicate that the width of the circumferential groove cut into a tire tread is of utmost importance with regard to developing high braking coefficients on wet runways. For example, increasing the width of the single groove from 1/2 inch for tire S1M1 (fig. 4(j)) to 3/4 inch for tire S1M2 (fig. 4(k)) tended to decrease μ_{av}, as is shown in figure 46(k). Removing the zigzag rib between the grooves of tire D8M1 (fig. 4(g)), thus increasing greatly the width of the groove for tire D8M2 (fig. 4(h)), resulted in lower μ_{av} values for tire D8M2 over the forward-velocity range shown in figure 46(h). On the other hand, the addition of a narrow groove to tire S2M1 (fig. 4(m)) resulted in higher values of μ_{av} for tire S2M2 (fig. 4(n)) than for tire S2M1, as is shown in figure 48(b).

As previously mentioned, close scrutiny of the wet concrete runway surface after braking runs in which circumferential-groove-tread tires were used disclosed that these tire treads deposited rubber on the concrete surface during braking cycles at the higher forward velocities, whereas smooth- and dimple-tread tires did not. The implication is that at least a portion of the footprint area of these tires must have been in intimate contact with the runway surface during the braking process on water-covered runways. In some instances, deposited rubber was found

on the runway for the circumferential-groove-tread tires where the water depth on the runway was as much as 1/2 inch.

Other treads: In addition to the tire treads already discussed, studies were made of tire treads having lateral grooves (fig. 4(f)), large diamond patterns (fig. 4(p)), and small diamond patterns (fig. 4(q)). In figure 49, faired μ_{av} data obtained for these treads are compared with faired μ_{av} data obtained for the circumferential-groove-tread tires R1 and S2M2. It should be mentioned that all the tires in figure 49 had approximately the same value of A_n/A_g (see table I) and therefore exerted approximately equal pressures on the runway surface. The curves for the two diamond-tread tires shown in this figure indicate that the small-diamond tread (more grooves) developed larger μ_{av} values than did the large-diamond tread. This result is in agreement with the results shown for the circumferential groove tires in that increasing the number of grooves increases the value of μ_{av}. The curves of figure 49 also indicate that the lateral-groove and diamond treads are not as efficient as the circumferential-groove treads in increasing the braking effectiveness of tires rolling at zero yaw angle on a wet concrete runway.

TIRE TREAD WEAR

Tire tread wear produces a marked degradation in the braking effectiveness of grooved tires on contaminated runway surfaces, a fact clearly illustrated by figure 48 if it is assumed that the smooth tires S1 and S2 before modification represent tires with the tread worn off completely. This assumption is substantiated by the data in figure 50 (taken from ref. 2), which show that on wet concrete, when tire R2 was 80 to 90 percent worn it developed values of μ_{max} only about half as good as those it developed when 0 to 50 percent worn. As tire wear progresses past the point where the tread is worn off completely, the tire footprint will undergo little change until the tire carcass cords are exposed, when its appearance is radically altered. For example, compare the unworn dimple-tread tires D2 and D3 shown in figures 4(a) and 4(b) with the buffed dimple tire D5M1, figure 4(d). Tire D5M1 was buffed down mechanically until the tread was completely removed and the tire carcass cords exposed. The curves shown in figures 45, 46(b), 46(c), and 46(e) indicate that at the higher forward velocities on a water-covered runway, the tire with the exposed carcass cords (D5M1) develops slightly higher μ_{av} values than do the less-worn tires. Thus it is apparent that as a grooved-tread tire becomes progressively worn, braking effectiveness on wet runways will suffer greatly as the tire approaches the smooth-tread condition, recovering only a small part of its original effectiveness after the carcass cords are exposed.

SUMMARY OF RESULTS

An investigation was made with 32×8.8 type VII aircraft tires of different tread designs mounted on a single wheel and on tandem wheels to examine the effects of dry and contaminated runway surfaces on the unbraked and braked rolling characteristics of the tires. The principal results found for the range of conditions investigated were:

1. The unbraked rolling resistance of an aircraft tire increases with increasing forward velocity on dry and contaminated runway surfaces. For contaminated surfaces, the rolling resistance increases parabolically with increasing forward velocity and approximately linearly with depth and density of the contaminating fluid.

2. The center of pressure of the vertical load on the tire moves progressively forward of the axle center line (in the direction of motion) as the forward velocity is increased during unbraked rolling on both dry and contaminated runway surfaces.

3. Automatic braking devices that use an inertia flywheel for reference angular velocity tend to become deficient in operation at high forward velocities on runways contaminated with slush and water because of the longer time required for wheel spin-up and consequent greater reference-flywheel spin-down. Chiefly responsible for this effect are low tire-ground friction coefficients, forward movements of the vertical-load center of pressure of the tire, and unloaded-wheel brake drag that develop under certain contaminated-runway conditions and combine to produce extremely low wheel spin-up accelerations.

4. Peak tire-ground friction coefficients developed during braking on contaminated runway surfaces tend to decrease rapidly with increasing forward velocity. In contrast, peak friction coefficients obtained on dry runway surfaces appear to be relatively insensitive to changes in forward velocity.

5. The magnitude of tire-ground friction coefficients developed on contaminated runway surfaces is extremely sensitive to tire tread design; of the various tread patterns tested, the circumferential-groove treads exhibited the least degradation of friction coefficient, and smooth and dimple treads the greatest degradation, for the contaminated-runway conditions investigated.

6. The magnitude of tire-ground friction coefficients developed by tire treads with poor skid resistance was increased on contaminated runway surfaces by mounting tires having these treads on the rear wheel of a tandem-wheel landing gear.

Langley Research Center,
National Aeronautics and Space Administration,
Langley Station, Hampton, Va., May 16, 1962.

APPENDIX

For those who may desire more detailed information, figures 51 to 79 contain plots of instantaneous tire-ground friction coefficient as a function of slip ratio for all tires and tire tread designs used in this investigation. All test runs utilized single-wheel braking only, with the vertical load $F_{Z,g}$ on the tire approximately equal to 10,000 pounds. As explained in the body of this report, the test runs in which the automatic braking device was used consisted of from 3 to 22 braking cycles, depending on forward velocity. In those instances where automatic braking was not used, brakes were applied by a knife-edge-activated solenoid valve, and only one braking cycle per test run was obtained. The brake hydraulic system was modified for some of the test runs and incorporated some residual back pressure $p_{B,1}$ into the system. These runs are so indicated, all other runs having zero back pressure.

All test runs in figures 51 to 79 were intended to investigate braking effectiveness on water-covered concrete surfaces only. In some instances, however, braking action was initiated before the wet test section was reached, with the result that in some runs part or all of a particular braking cycle occurred on dry concrete. Braking cycles that occurred entirely on dry surfaces are indicated in the pertinent figures by the words "Dry runway." In those cases where braking started on dry concrete and ended on wet concrete the transition point is indicated by a vertical line marked "A." This should be interpreted to mean that spin-down values to the left of the line occurred on dry concrete, while spin-down values to the right of the line, and all spin-up values, were on wet concrete. The depth of the water on the surface varied from damp (no puddles, $d_1 \approx 0$) to wet (high spots showing, $d_1 = 0$ to 0.3 inch) to flooded (runway completely covered, $d_1 = 0.2$ to 0.5 inch), and these depth variations are indicated in each figure.

Figures 51 to 79 are arranged in the same manner as table I, that is, data for dimple treads and modified dimple treads are presented first, then data for smooth and modified smooth treads, and finally data for grooved or rib treads. The runs for each tire are arranged in order of increasing forward velocity, except in figure 79. The decrease in forward velocity from cycle to cycle in a particular run is due to wind and rolling resistance that acts to decelerate the main carriage upon termination of the catapult stroke.

In figure 79, the runs are arranged chronologically rather than in order of increasing velocity. Braking tests on tire R3 started with the new tire, as did the braking tests on each of the other tires. At

the conclusion of run 3, however, the tire was considerably worn by heavy braking action on dry concrete (see run 3, fig. 79). Two more runs were made on this tire to demonstrate the effect of excessive tread wear, and upon conclusion of the last run the tire was judged to be approximately 90 percent worn.

REFERENCES

1. Horne, Walter B., Joyner, Upshur T., and Leland, Trafford J. W.: Studies of the Retardation Force Developed on an Aircraft Tire Rolling in Slush or Water. NASA TN D-552, 1960.

2. Horne, Walter B., and Joyner, Upshur T.: Some Effects of Runway Slush and Water on the Operation of Airplanes, With Particular Reference to Jet Transports. Preprint No. 275A, Soc. Automotive Eng., Jan. 1961.

3. Trant, James P., Jr.: NACA Research on Friction Measurements. Proc. First Int. Skid Prevention Conf., Pt. I, Virginia Council of Highway Invest. and Res. (Charlottesville), Aug. 1959, pp. 297-308.

4. Sawyer, Richard H., and Kolnick, Joseph J.: Tire-to-Surface Friction-Coefficient Measurements With a C-123B Airplane on Various Runway Surfaces. NASA TR R-20, 1959.

5. Harrin, Eziaslav N.: Low Tire Friction and Cornering Forces on a Wet Surface. NACA TN 4406, 1958.

6. Harrin, Eziaslav N.: Investigation of Tandem-Wheel and Air-Jet Arrangements for Improving Braking Friction on Wet Surfaces. NASA TN D-405, 1960.

7. Sawyer, Richard H., Batterson, Sidney A., and Harrin, Eziaslav N.: Tire-to-Surface Friction Especially Under Wet Conditions. NASA MEMO. 2-23-59L, 1959.

8. Anon.: Flight Tests to Determine the Coefficients of Friction Between an Aircraft Tyre and Various Wet Runway Surfaces. Part II - Trials on a Brushed Concrete Runway at R.R.E. Pershore. S & T Memo 5/60, British Ministry of Aviation, Apr. 1960.

9. Anon.: Flight Tests to Determine the Coefficients of Friction Between an Aircraft Tyre and Various Wet Runway Surfaces. Part I - Preliminary Instrumentation-Proving Trials at Wisley Airfield. S & T Memo 15/59, British Ministry of Aviation, Sept. 1959.

10. Batterson, Sidney A.: Investigation of the Maximum Spin-Up Coefficients of Friction Obtained During Tests of a Landing Gear Having a Static-Load Rating of 20,000 Pounds. NASA MEMO 12-20-58L, 1959.

11. Hadekel, R.: The Mechanical Characteristics of Pneumatic Tyres - A Digest of Present Knowledge. S & T Memo. No. 10/52, British Ministry of Supply, TPA $3/T_IB$, Nov. 1952.

12. Smiley, Robert F., and Horne, Walter B.: Mechanical Properties of Pneumatic Tires With Special Reference to Modern Aircraft Tires. NASA TR R-64, 1960. (Supersedes NACA TN 4110.)

13. Horne, Walter B., Stephenson, Bertrand H., and Smiley, Robert F.: Low-Speed Yawed-Rolling and Some Other Elastic Characteristics of Two 56-Inch-Diameter, 24-Ply-Rating Aircraft Tires. NACA TN 3235, 1954.

14. Horne, Walter B., Smiley, Robert F., and Stephenson, Bertrand H.: Low-Speed Yawed-Rolling Characteristics and Other Elastic Properties of a Pair of 26-Inch-Diameter, 12-Ply-Rating, Type VII Aircraft Tires. NACA TN 3604, 1956.

15. Horne, Walter B., and Smiley, Robert F.: Low-Speed Yawed-Rolling Characteristics and Other Elastic Properties of a Pair of 40-Inch-Diameter, 14-Ply-Rating, Type VII Aircraft Tires. NACA TN 4109, 1958.

TABLE I.- CHARACTERISTICS OF 32×8.8 TYPE VII TIRES OF THE INVESTIGATION

Tire	Description	Inflated dimensions (p = 260 lb/sq in.)		
		Diameter, in.	Tread radius, in.	Area ratio, $\frac{A_n}{A_g}$
D1	Dimple, fabric-reinforced tread, fabric surface	(a)	(a)	(a)
D2	Dimple, fabric-reinforced tread, fabric surface	30.3	6.5	0.87
D3	Dimple, fabric-reinforced tread, rubber surface	30.4	6.0	0.87
D4	Dimple, fabric-reinforced tread (ice grip)	30.5	6.0	0.86
D5M1	Dimple, fabric-reinforced tread modified by buffing to remove the dimples	(a)	(a)	1.00
D6M1	Dimple, fabric-reinforced tread modified by 5 circumferential grooves	30.2	6.2	0.59
D7M1	Dimple, fabric-reinforced tread modified by 37 lateral grooves	30.6	6.0	0.75
D8M1	Dimple, fabric-reinforced tread modified by 2 zigzag circumferential grooves	30.9	(a)	0.75
D8M2	Tire D8M1 modified by removing rib between the 2 zigzag grooves	(a)	(a)	0.60
S1	Smooth, all-rubber tread	30.8	6.6	1.00
S1M1	Tire S1 modified by 1/2-inch-wide circumferential groove	(a)	6.6	0.91
S1M2	Tire S1 modified by 3/4-inch-wide circumferential groove	(a)	6.6	0.86
S1M3	Tire S1M2 modified by adding two 3/8-inch-wide circumferential grooves	(a)	6.6	0.78
S2	Smooth, fabric-reinforced tread, rubber surface	30.9	(a)	1.00
S2M1	Tire S2 modified by 4 circumferential grooves	30.9	(a)	0.79
S2M2	Tire S2M1 modified by adding 1 narrow circumferential groove at center line	31.1	(a)	0.78
S3	Smooth, fabric-reinforced tread, fabric surface	30.9	(a)	1.00
S4M1	Smooth, fabric-reinforced tread, rubber surface, modified by a large diamond pattern	30.9	(a)	0.81
S5M1	Smooth, fabric-reinforced tread, rubber surface, modified by a small diamond pattern	30.8	(a)	0.72
S6M1	Smooth, fabric-reinforced tread, rubber surface, modified by 7 circumferential grooves (sine-wave cross section)	30.9	(a)	0.62
R1	Rib, all-rubber tread, 9 grooves	30.6	5.7	0.77
R2	Rib, all-rubber tread, 9 grooves	(a)	(a)	(a)
R3	Rib, all-rubber tread, 9 grooves	(a)	(a)	(a)
R4	Rib, all-rubber tread, 11 grooves	(a)	(a)	(a)
R5	Rib, fabric-reinforced tread, 3 grooves	30.6	5.7	0.79

[a]Not recorded.

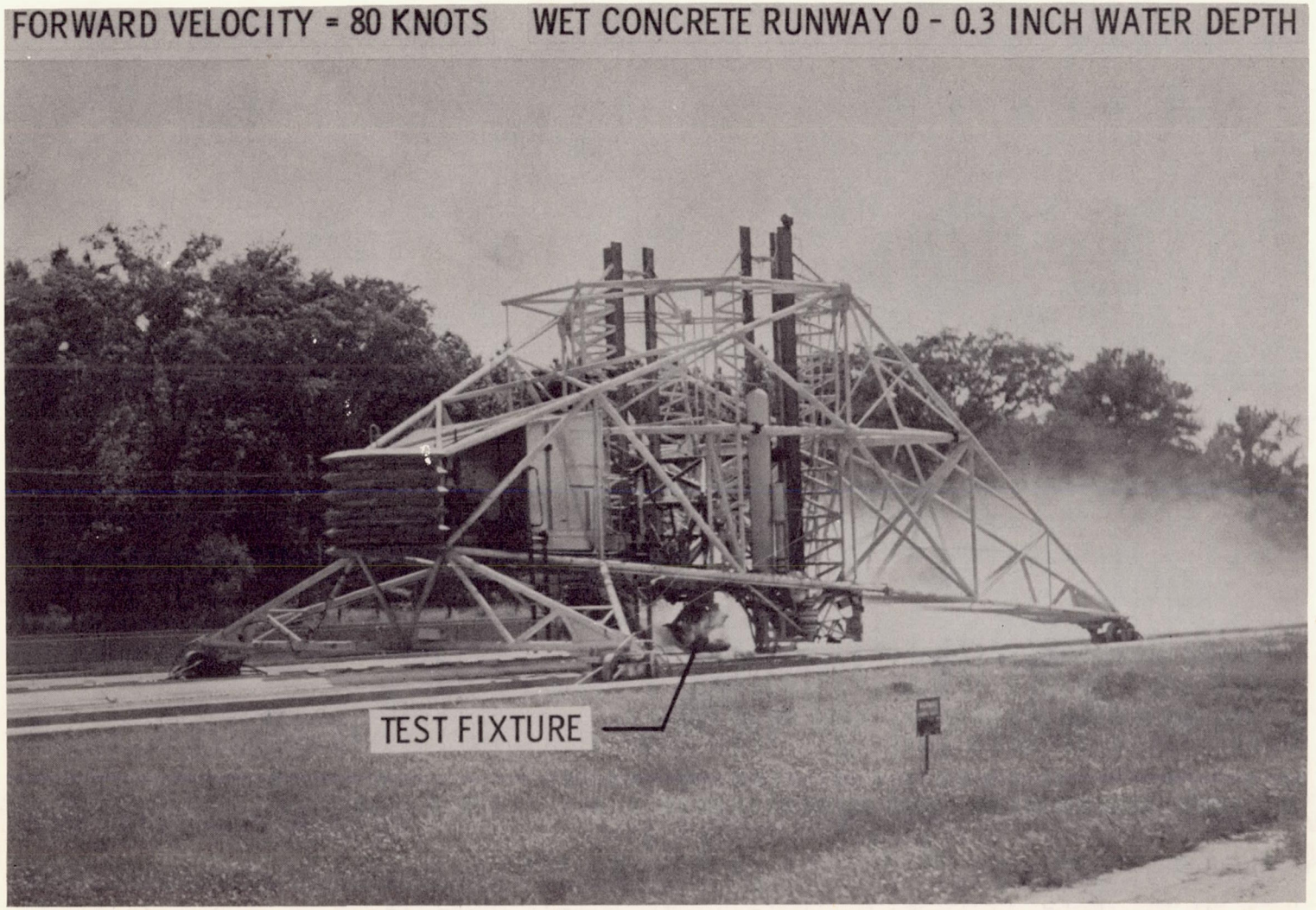

Figure 1.- Main carriage of Langley landing-loads track. L-60-2485.1

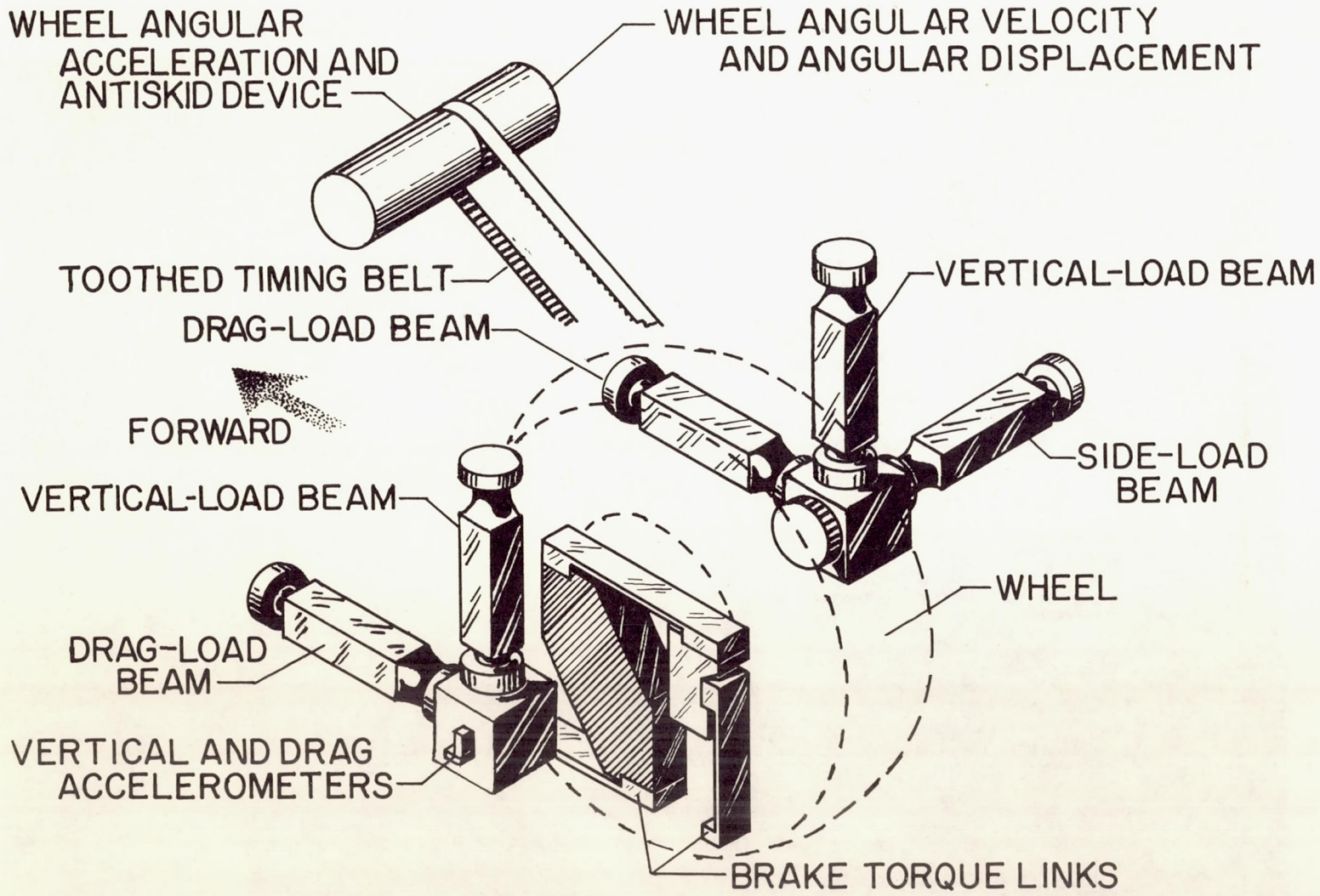

Figure 2.- Test fixture.

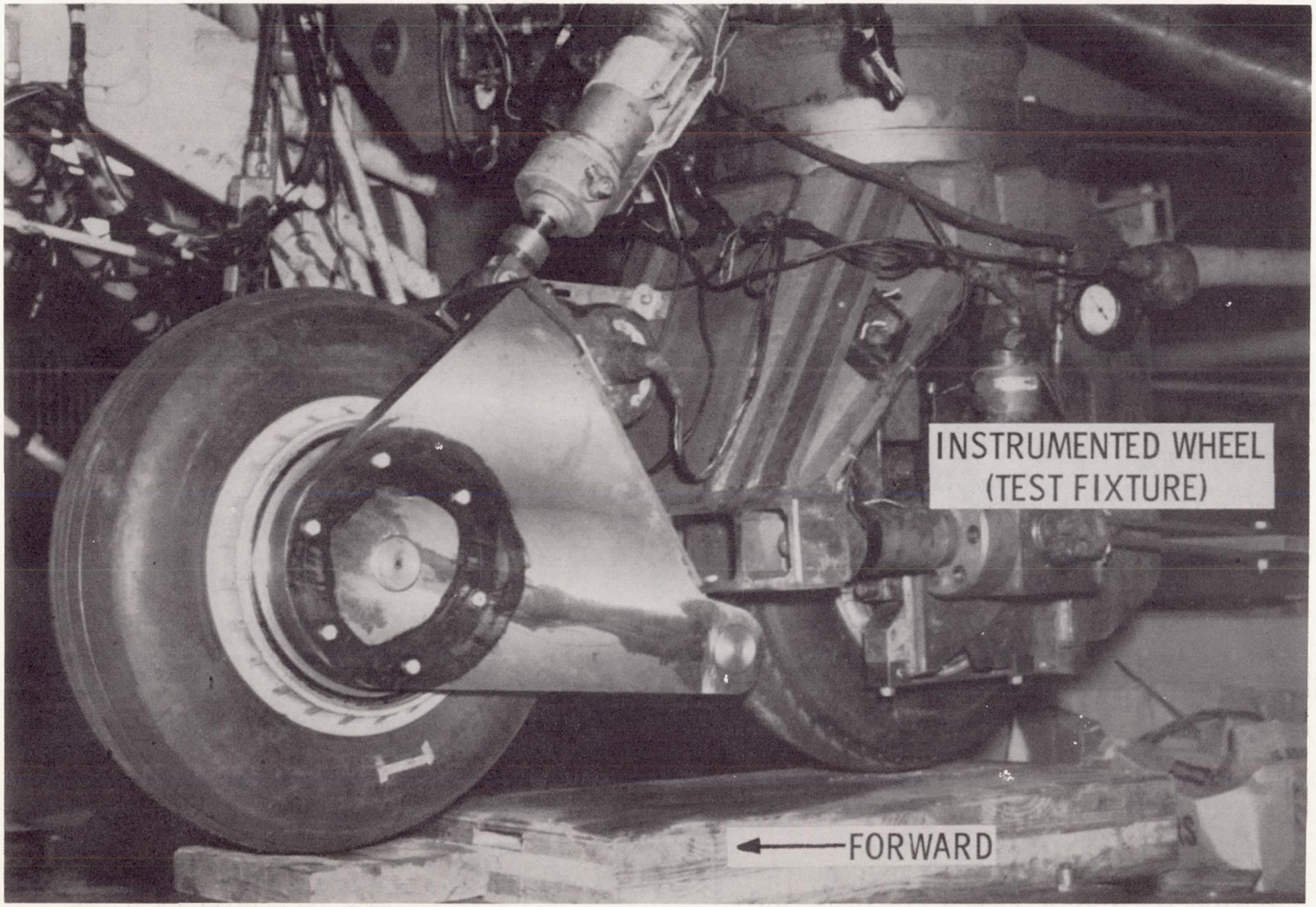

Figure 3.- Tandem wheel setup at Langley landing-loads track. L-60-6948

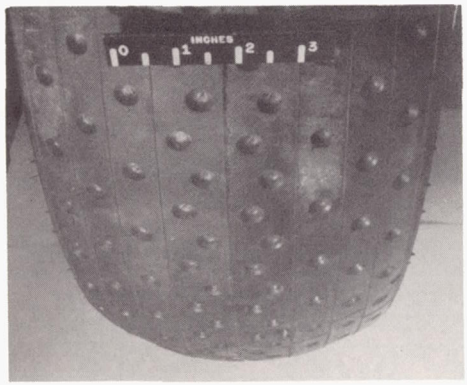

Before test

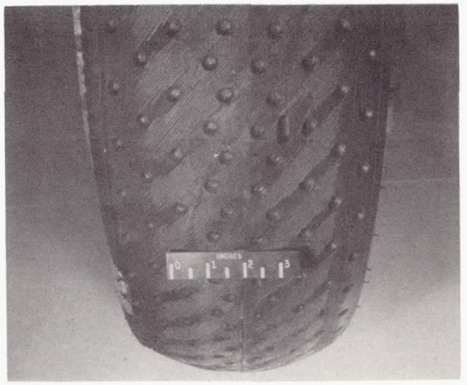

After test

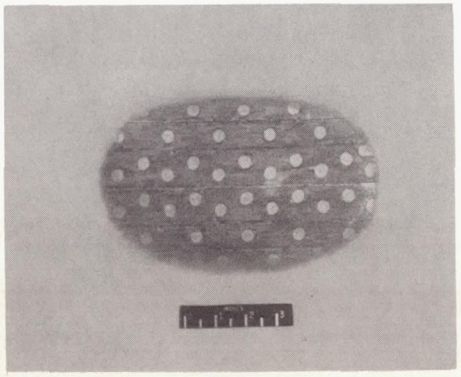

Tire footprint

(a) Tire D2; dimple, fabric-reinforced tread, fabric surface. L-60-6980

Figure 4.- 32×8.8 type VII aircraft tires. Tire footprint conditions: $F_{z,g} \approx 10,000$ pounds; $p = 260$ lb/sq in.

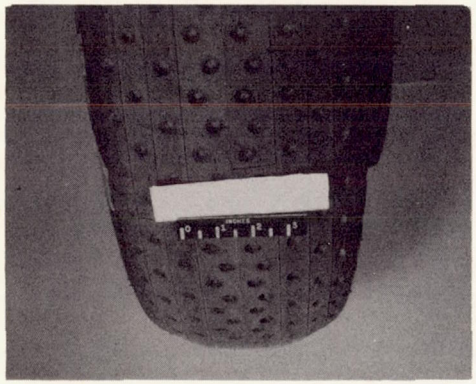

Before test

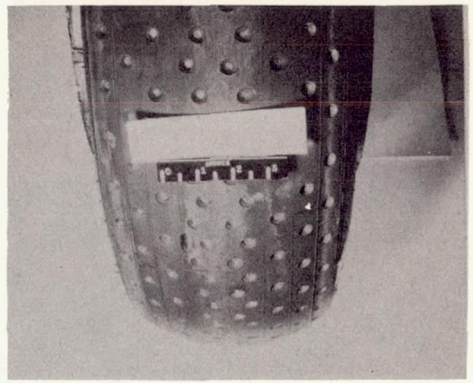

After test

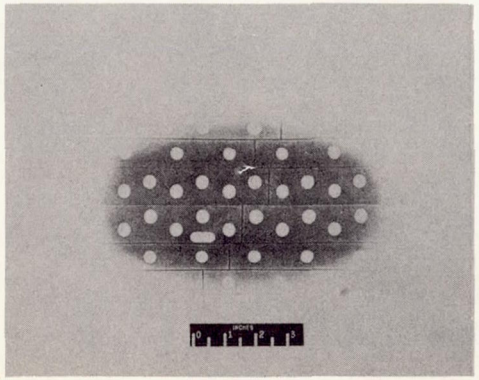

Tire footprint

(b) Tire D3; dimple, fabric-reinforced tread, rubber surface. L-62-2062

Figure 4.- Continued.

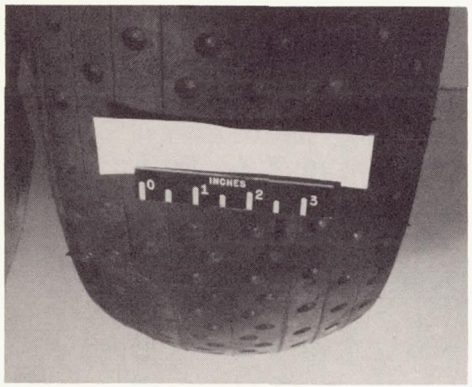

Before test

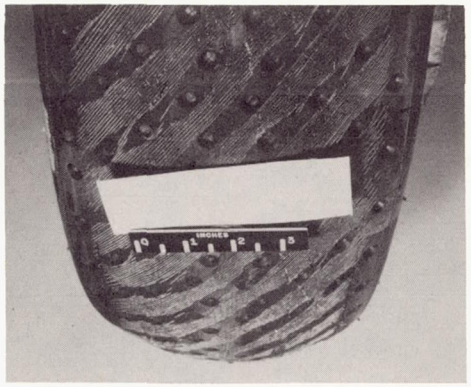

After test

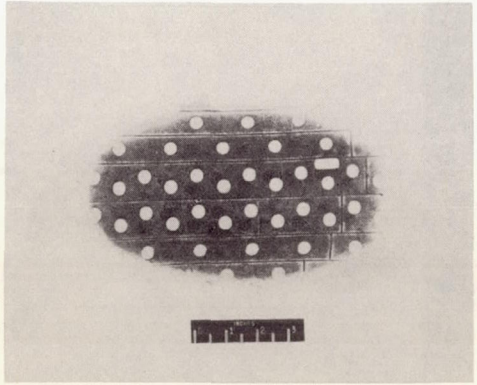

Tire footprint

(c) Tire D4; dimple, fabric-reinforced tread (ice grip). L-62-2063

Figure 4.- Continued.

Before test

After test

No footprint available

L-60-3527

(d) Tire D5M1; dimple, fabric-reinforced tread modified by buffing to remove the dimples.

Figure 4.- Continued.

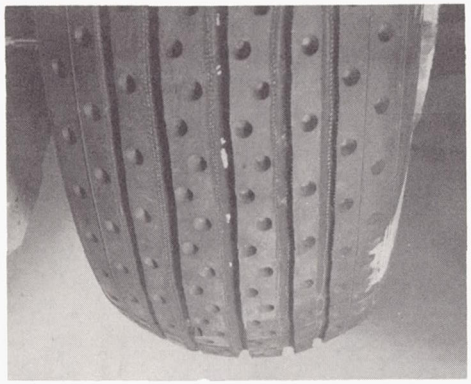

Before test

After test

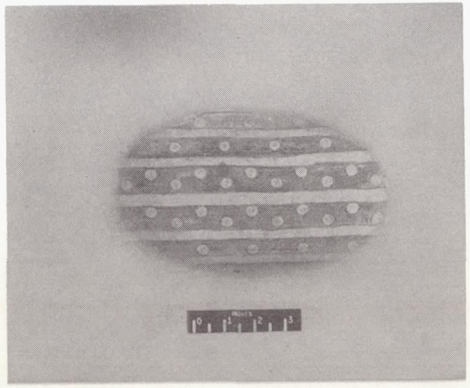

Tire footprint

L-62-2064

(e) Tire D6M1; dimple, fabric-reinforced tread modified by 5 circumferential grooves.

Figure 4.- Continued.

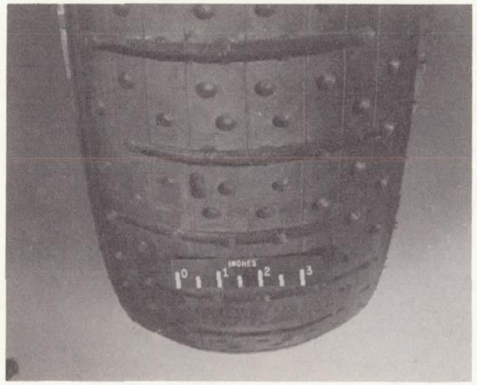

Before test

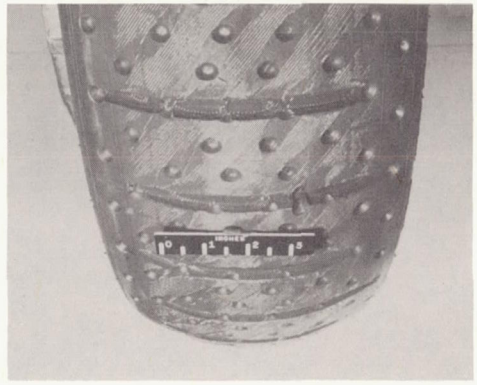

After test

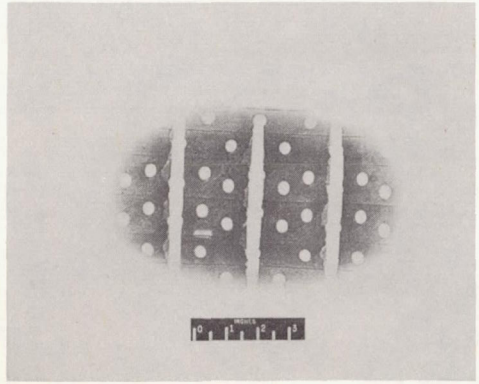

Tire footprint

L-62-2065

(f) Tire D7M1; dimple, fabric-reinforced tread modified by 37 lateral grooves.

Figure 4.- Continued.

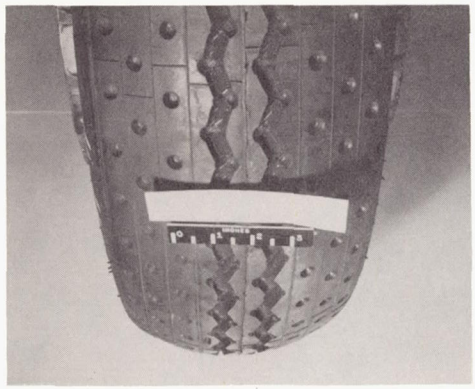

Before test

No photo available

After test

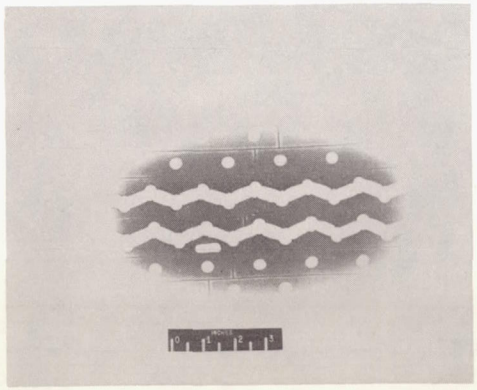

Tire footprint

L-62-2066

(g) Tire D8M1; dimple, fabric-reinforced tread modified by 2 zigzag circumferential grooves.

Figure 4.- Continued.

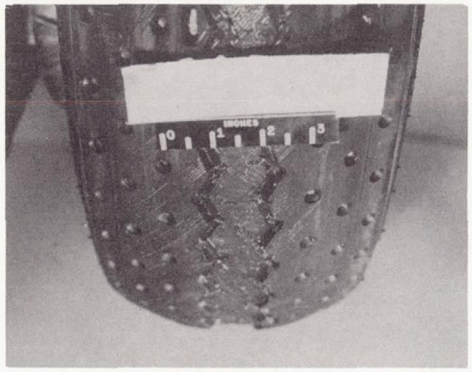

Before test

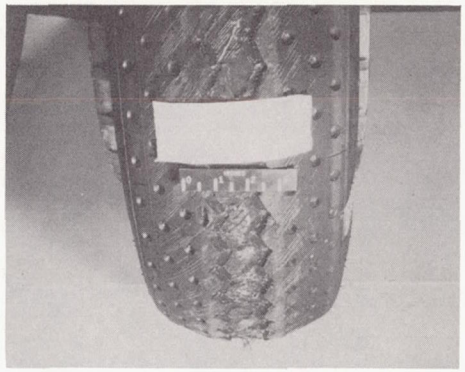

After test

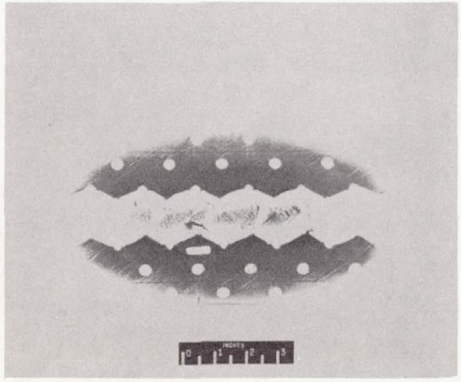

Tire footprint

L-62-2067

(h) Tire D8M2; tire D8M1 modified by removing rib between the 2 zigzag grooves.

Figure 4.- Continued.

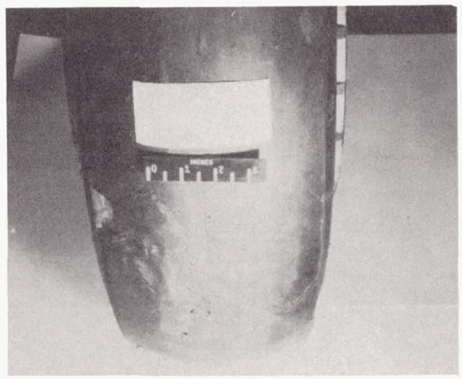

Before test

No photo available

After test

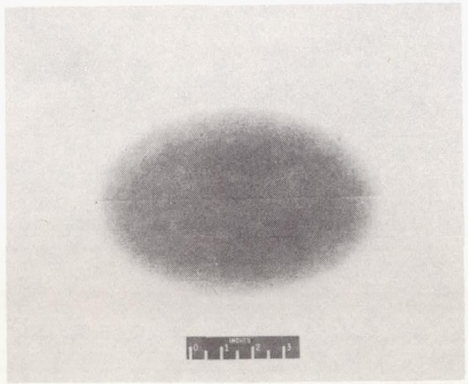

Tire footprint

(i) Tire S1; smooth, all-rubber tread. L-60-6979

Figure 4.- Continued.

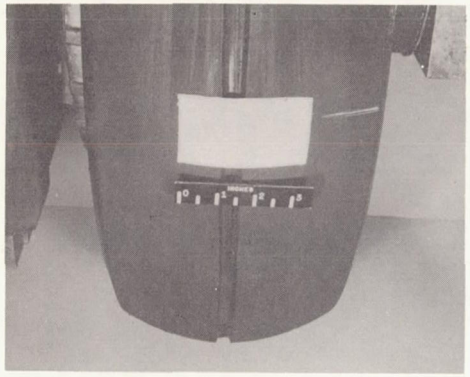

Before test

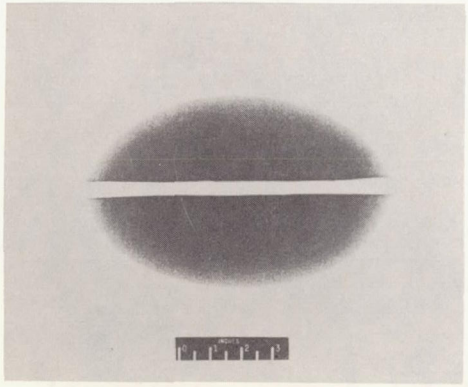

Tire footprint

(j) Tire S1M1; tire S1 modified by 1/2-inch-wide circumferential groove.

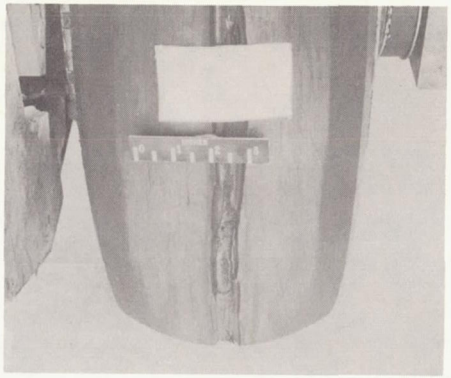

Before test

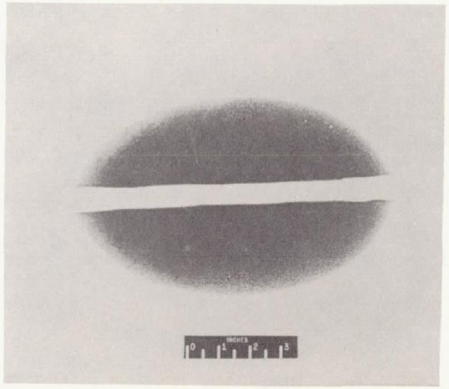

Tire footprint

L-62-2068

(k) Tire S1M2; tire S1 modified by 3/4-inch-wide circumferential groove.

Figure 4.- Continued.

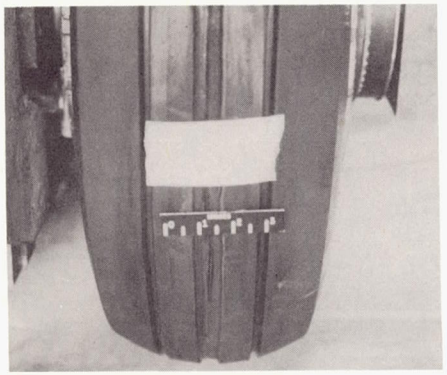

Before test

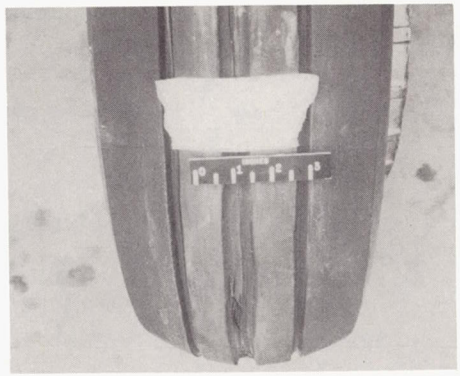

After test

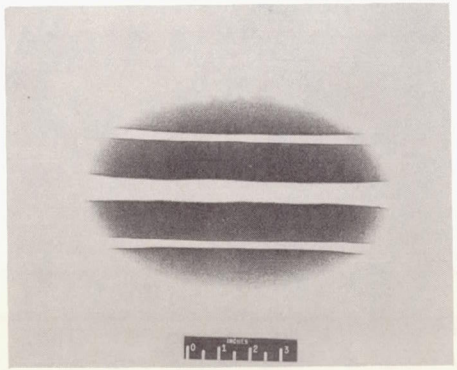

Tire footprint

L-62-2069

(l) Tire S1M3; tire S1M2 modified by adding two 3/8-inch-wide circumferential grooves.

Figure 4.- Continued.

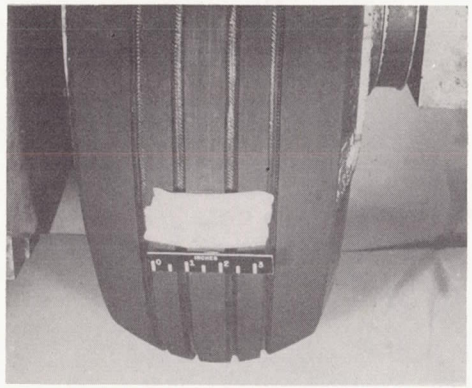

Before test

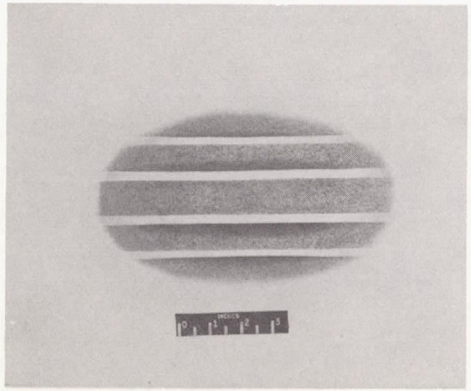

Tire footprint

(m) Tire S2M1; smooth, fabric-reinforced tread, rubber surface, modified by 4 circumferential grooves.

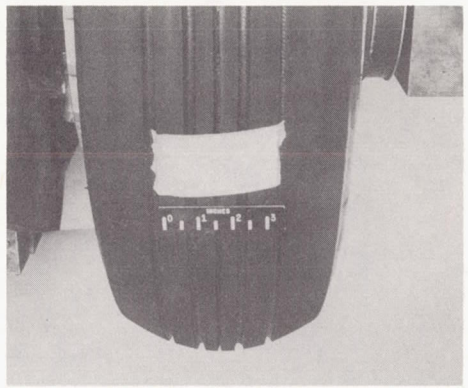

Before test

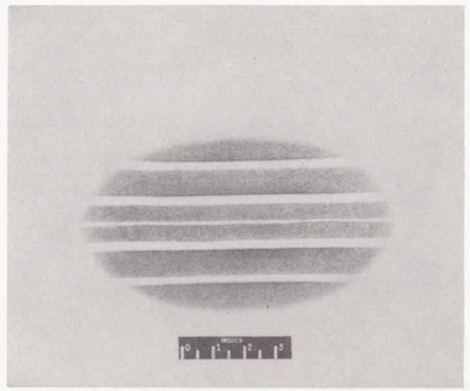

Tire footprint

L-60-6981

(n) Tire S2M2; tire S2M1 modified by adding 1 narrow circumferential groove at center line.

Figure 4.- Continued.

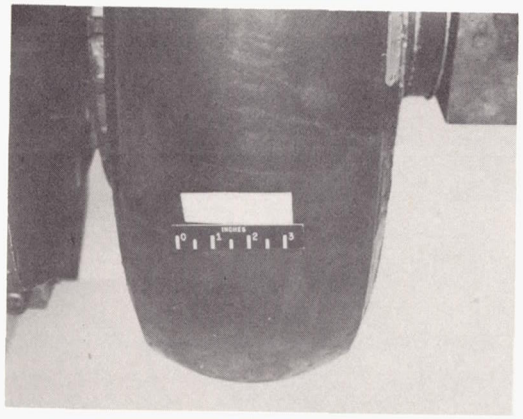

Before test

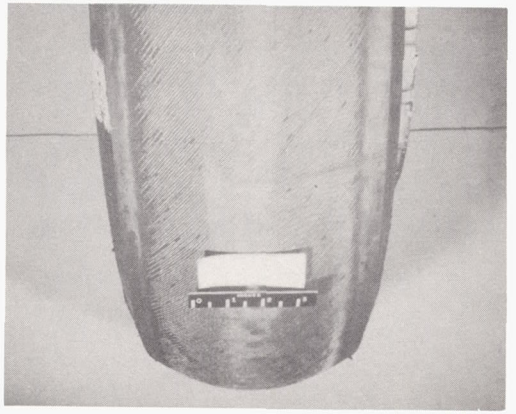

After test

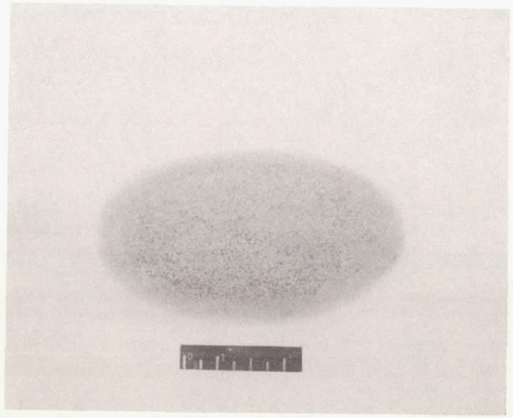

Tire footprint

(o) Tire S3; smooth, fabric-reinforced tread, fabric surface. L-62-2070

Figure 4.- Continued.

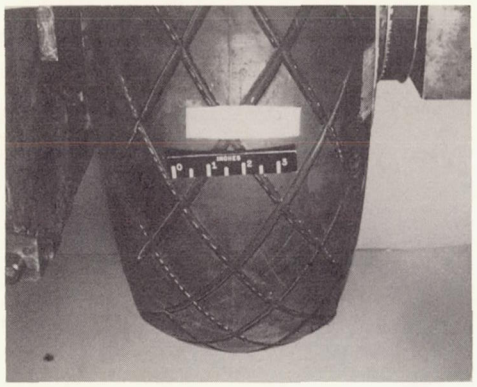

Before test

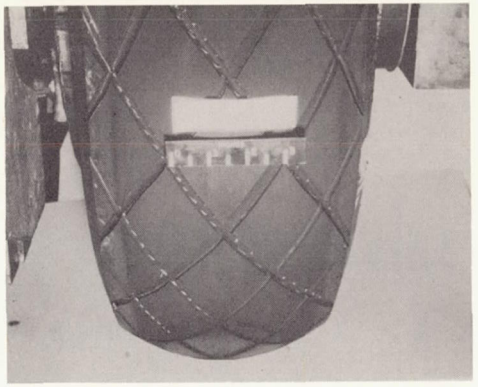

After test

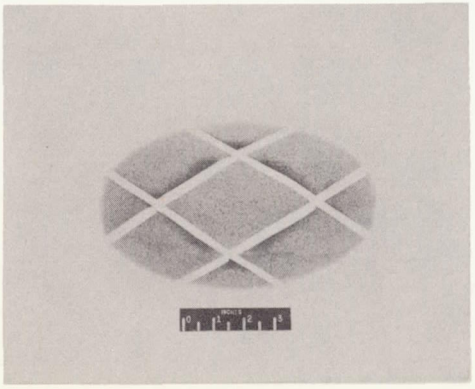

Tire footprint

L-62-2071

(p) Tire S4M1; smooth, fabric-reinforced tread, rubber surface, modified by a large diamond pattern.

Figure 4.- Continued.

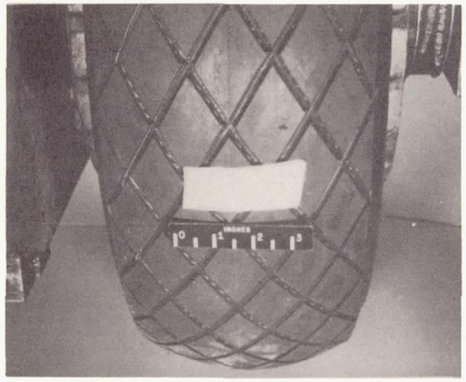

Before test

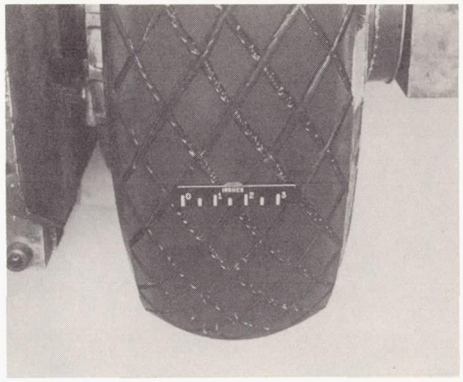

After test

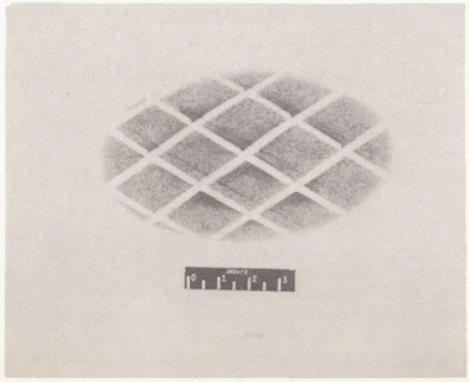

Tire footprint

L-62-2072

(q) Tire S5M1; smooth, fabric-reinforced tread, rubber surface, modified by a small diamond pattern.

Figure 4.- Continued.

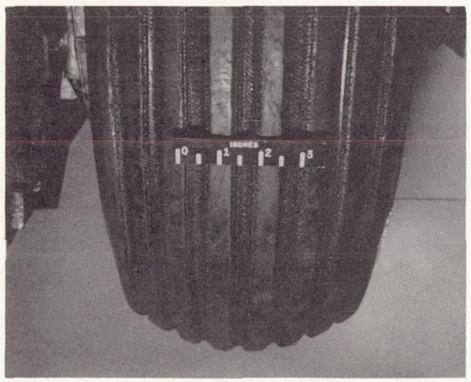

Before test

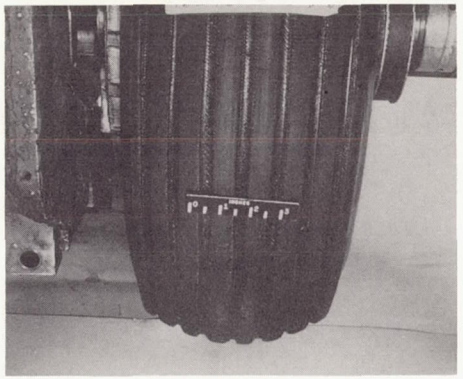

After test

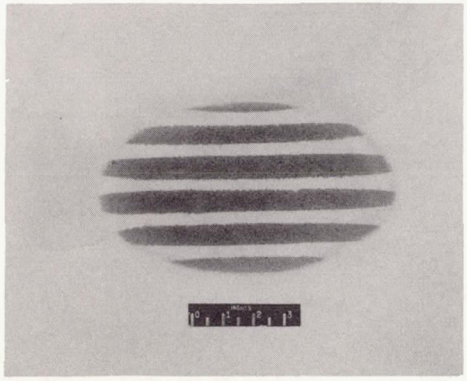

Tire footprint

L-62-2073

(r) Tire S6M1; smooth, fabric-reinforced tread, rubber surface, modified by 7 circumferential grooves (sine-wave cross section).

Figure 4.- Continued.

No photo available

Before test

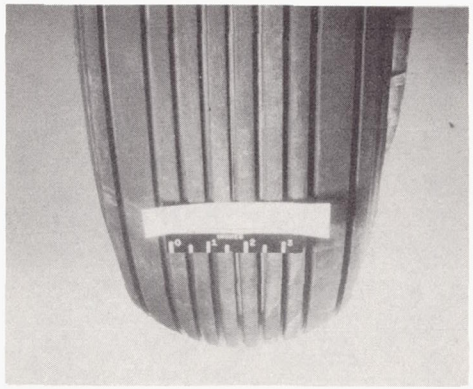

After test

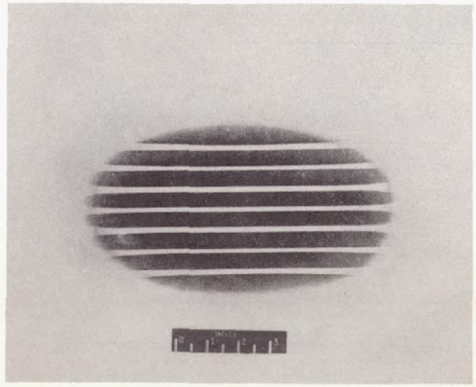

Tire footprint

(s) Tire R1; rib, all-rubber tread, 9 grooves. L-60-6978

Figure 4.- Continued.

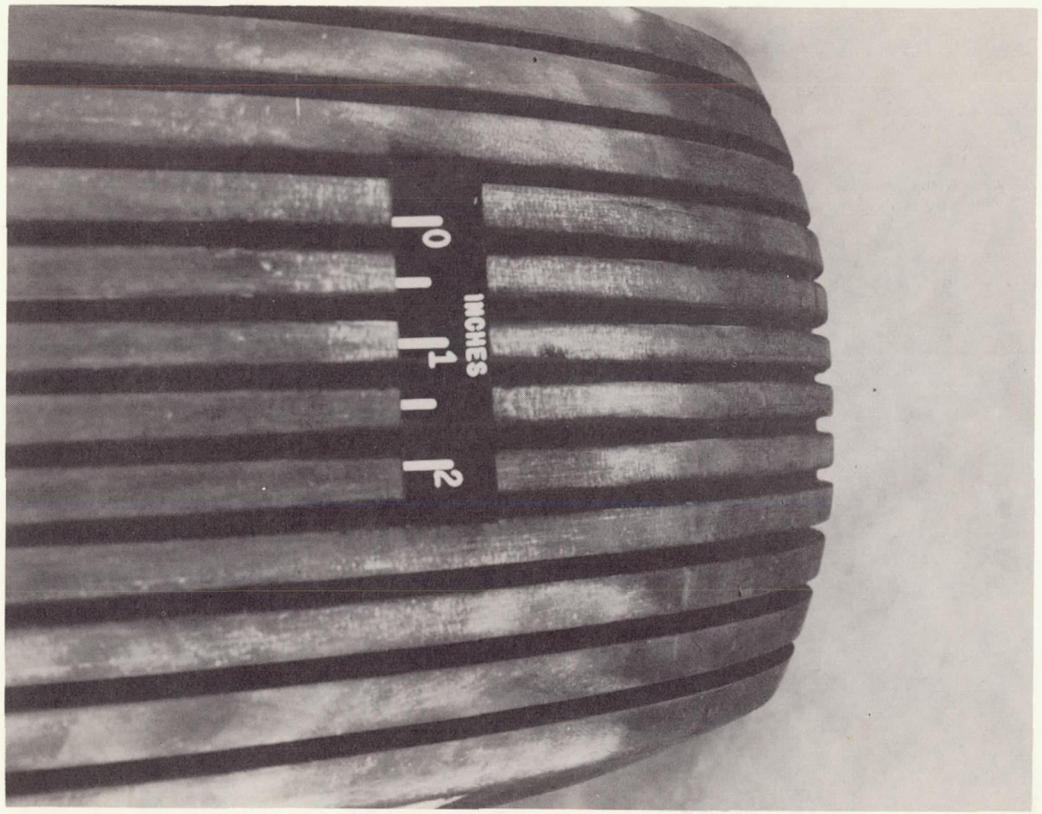

(t) Tire R4; rib, all-rubber tread, 11 grooves (after test). L-60-3426

Figure 4.- Continued.

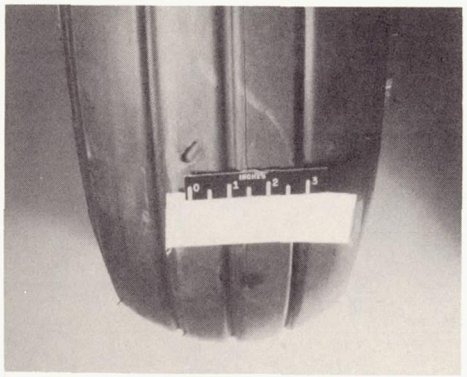

Before test

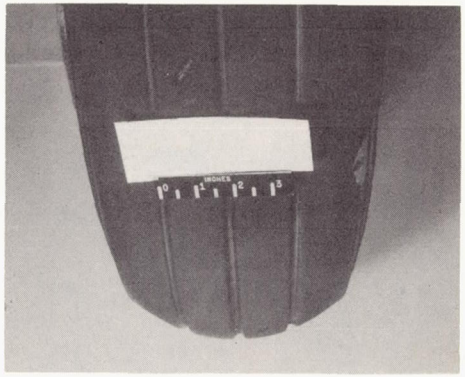

After test

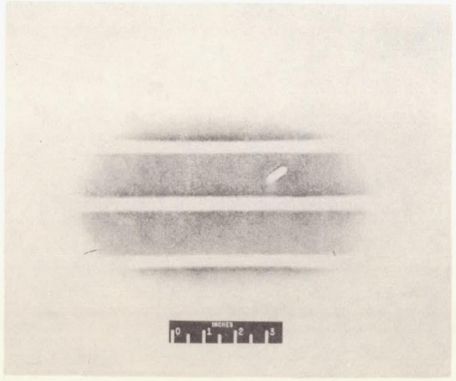

Tire footprint

(u) Tire R5; rib, fabric-reinforced tread, 3 grooves. L-62-2074

Figure 4.- Concluded.

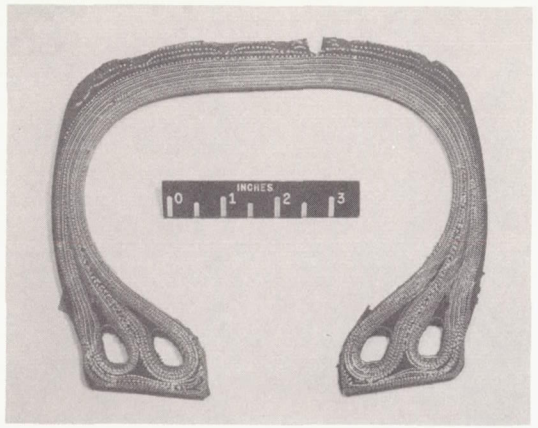

(a) Fabric-reinforced dimple tread (similar to tires D1, D2).

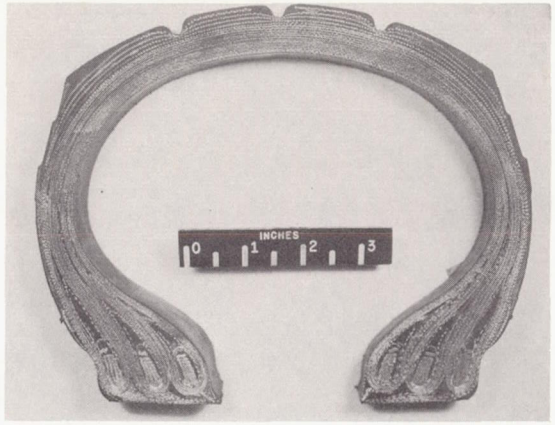

(b) Fabric-reinforced rib tread (similar to tire R5).

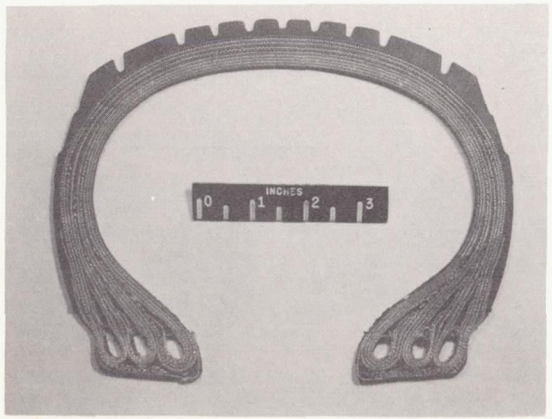

(c) All-rubber rib tread (similar to tires R1, R2, R3).

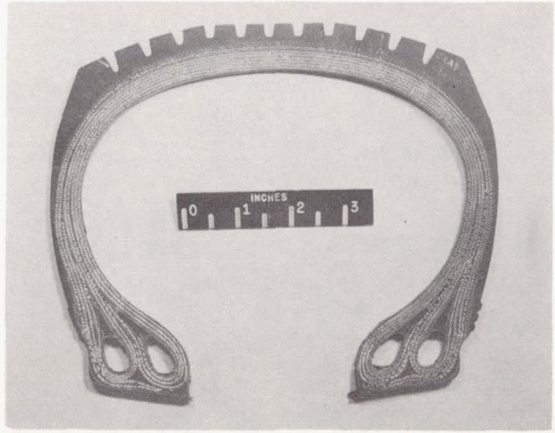

L-62-2075

(d) All-rubber rib tread (similar to tire R4).

Figure 5.- Cross sections obtained from 32x8.8 type VII aircraft tires with fabric-reinforced tread and all-rubber tread.

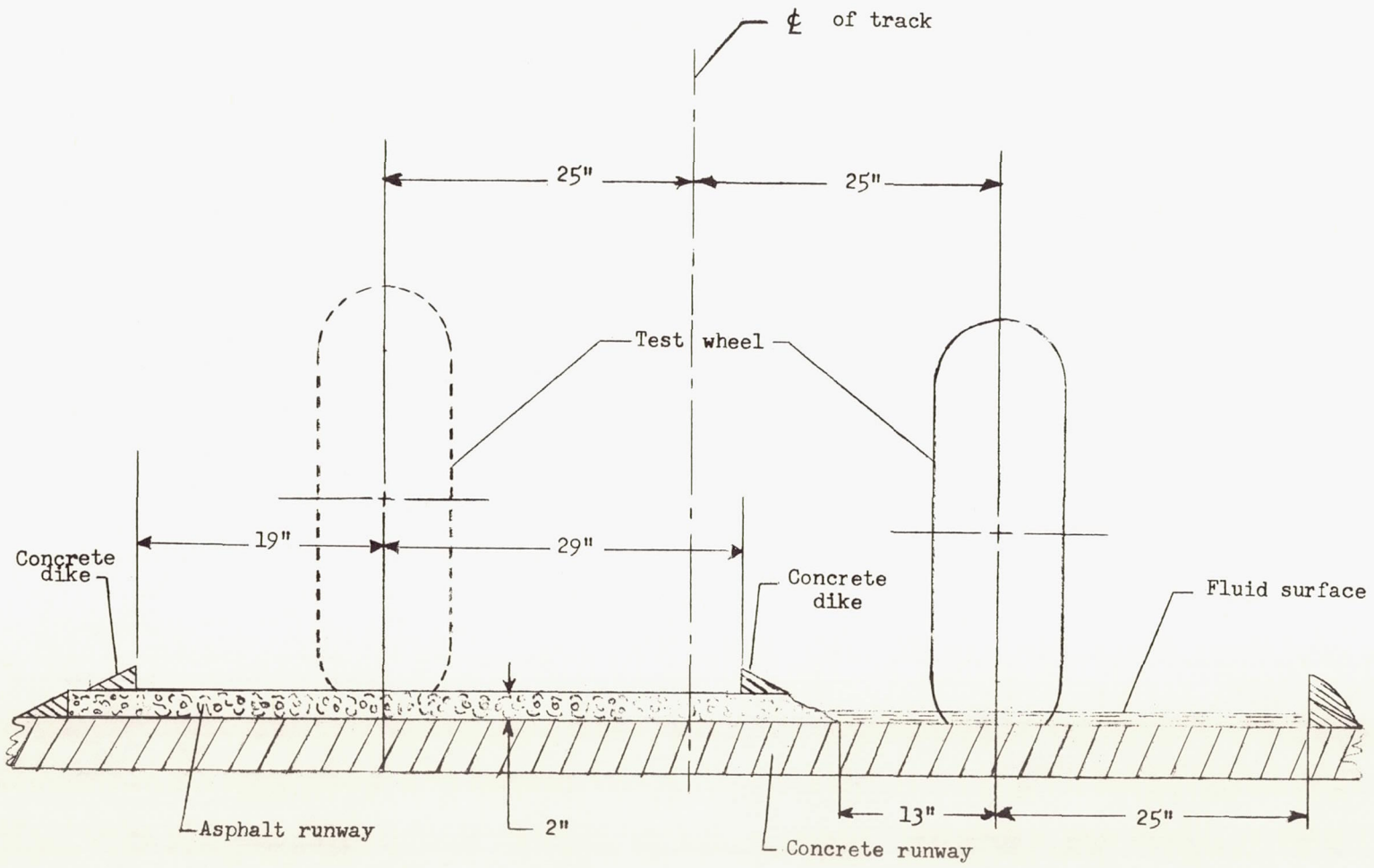

Figure 6.- Cross section of test runway surfaces.

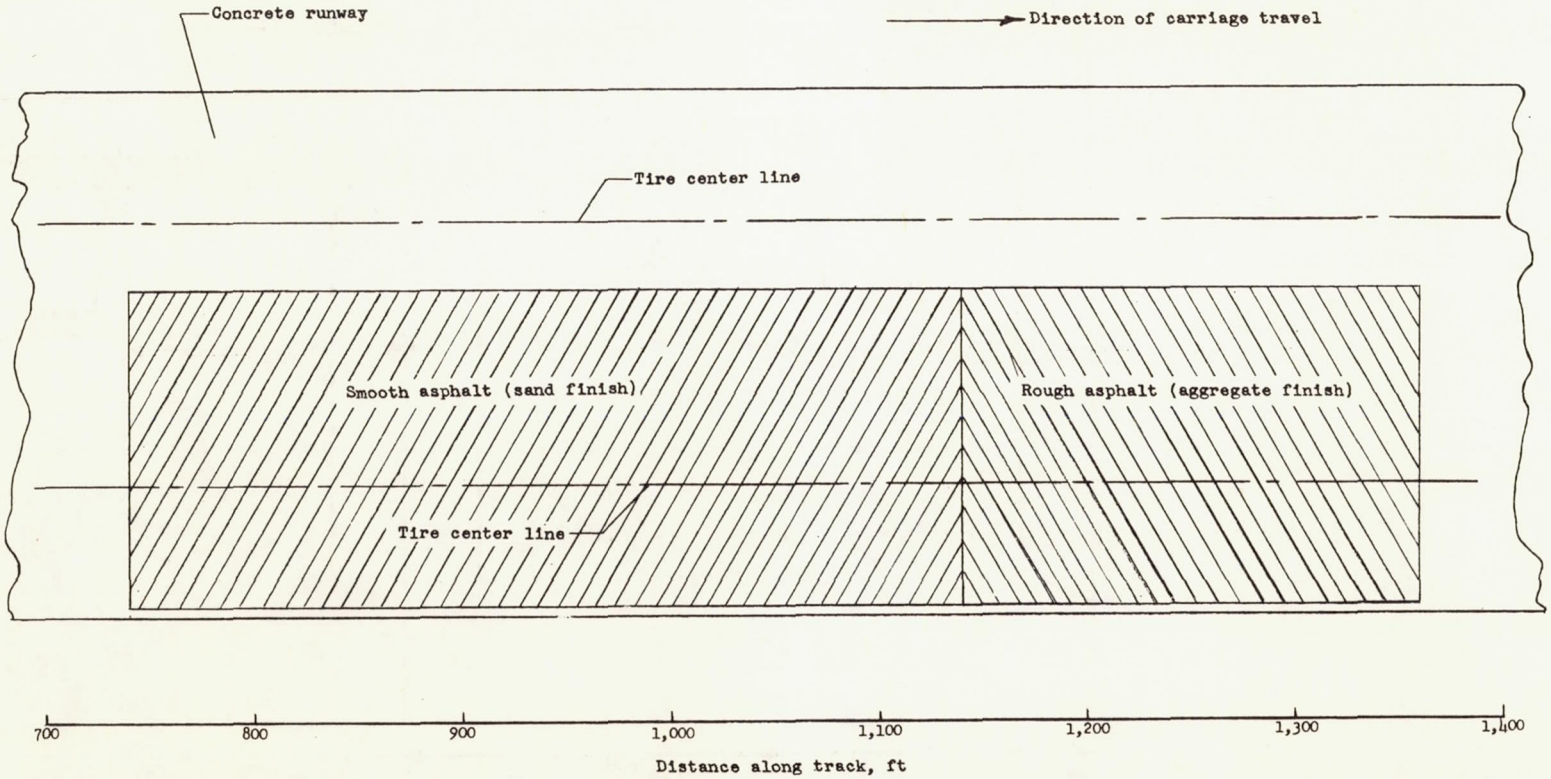

Figure 7.- Schematic diagram showing location of test runways on Langley landing-loads track.

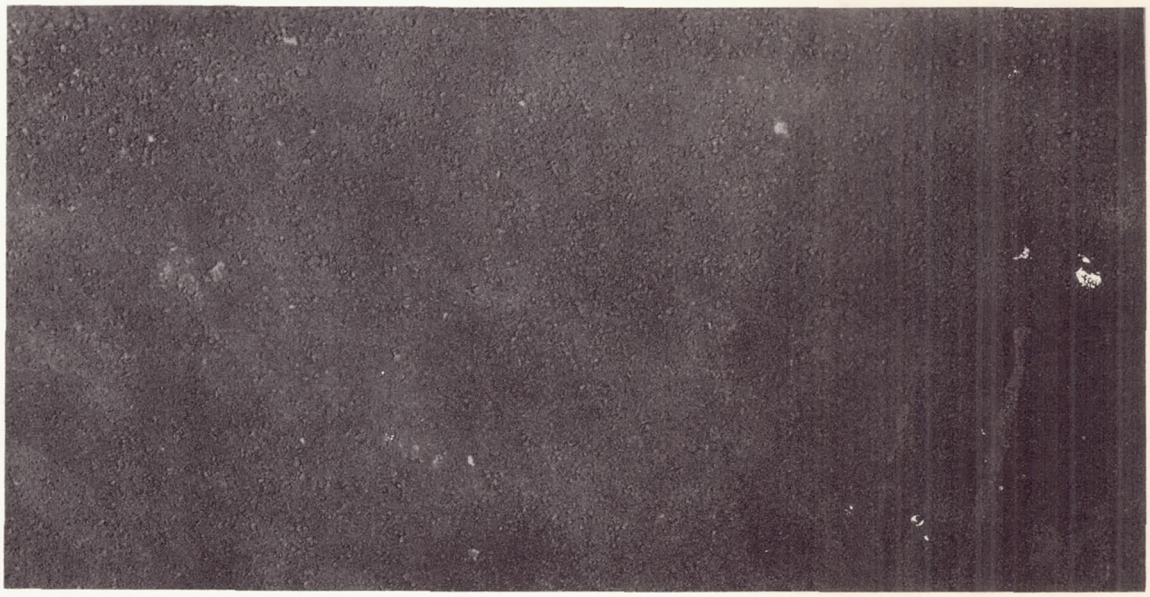

(a) Smooth asphalt runway (sand finish). L-59-7643

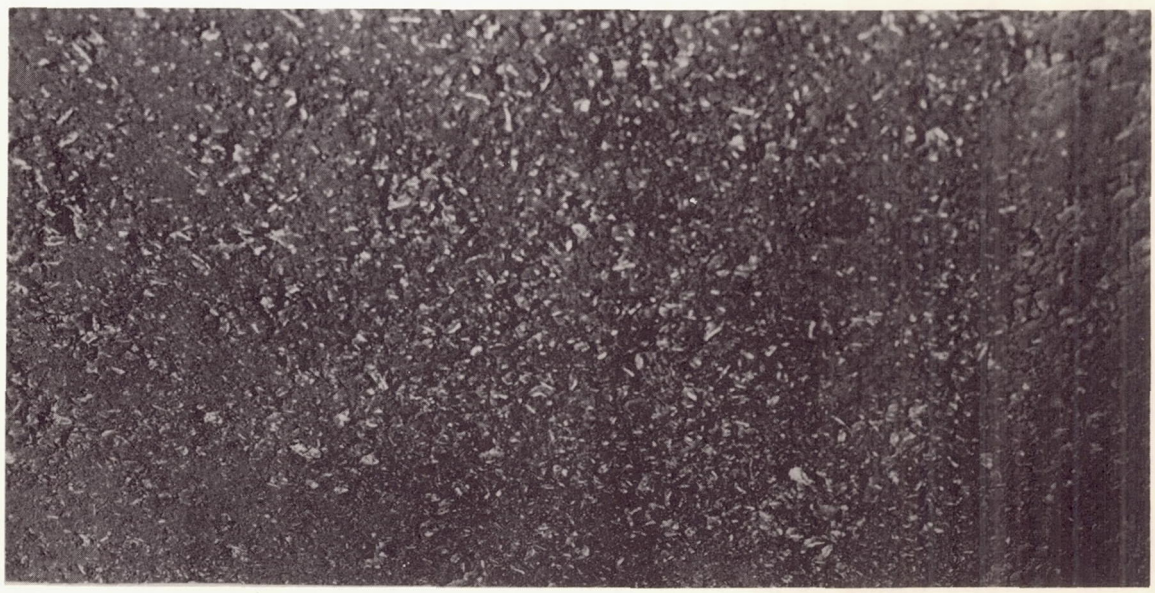

(b) Rough asphalt runway (aggregate finish). L-59-7644

Figure 8.- Asphalt runway surfaces used in investigation.

L-62-2076

Figure 9.- Water-covered concrete runway immediately before wheel-braking run. d_1 = 0 to 0.3 inch.

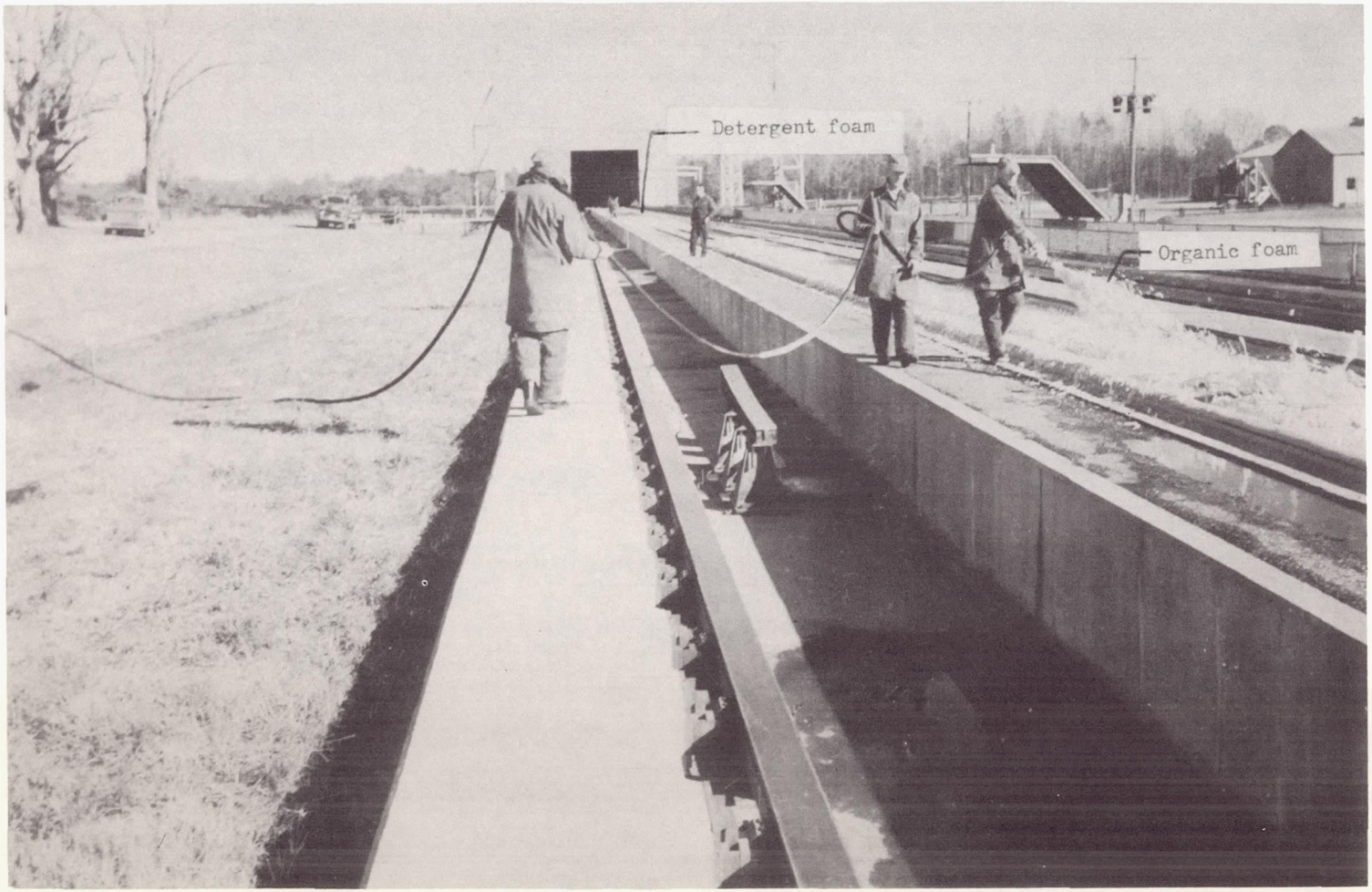

L-62-2077

Figure 10.- Spreading detergent and organic foam on concrete runway just before start of a braked rolling run.

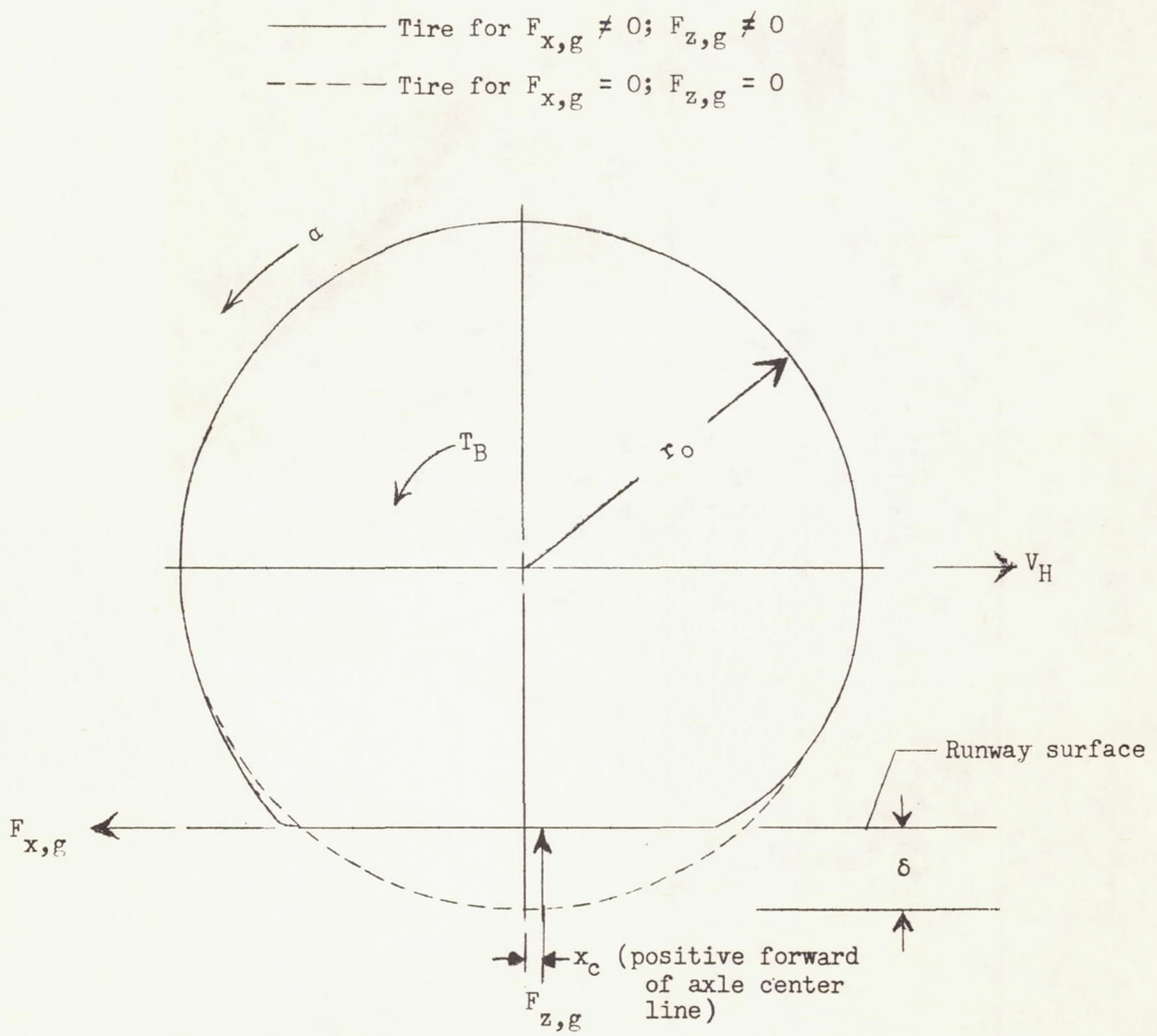

Figure 11.- Moments and torques acting on decelerating tire during braked rolling. (Wheel-bearing frictional torque is disregarded.)

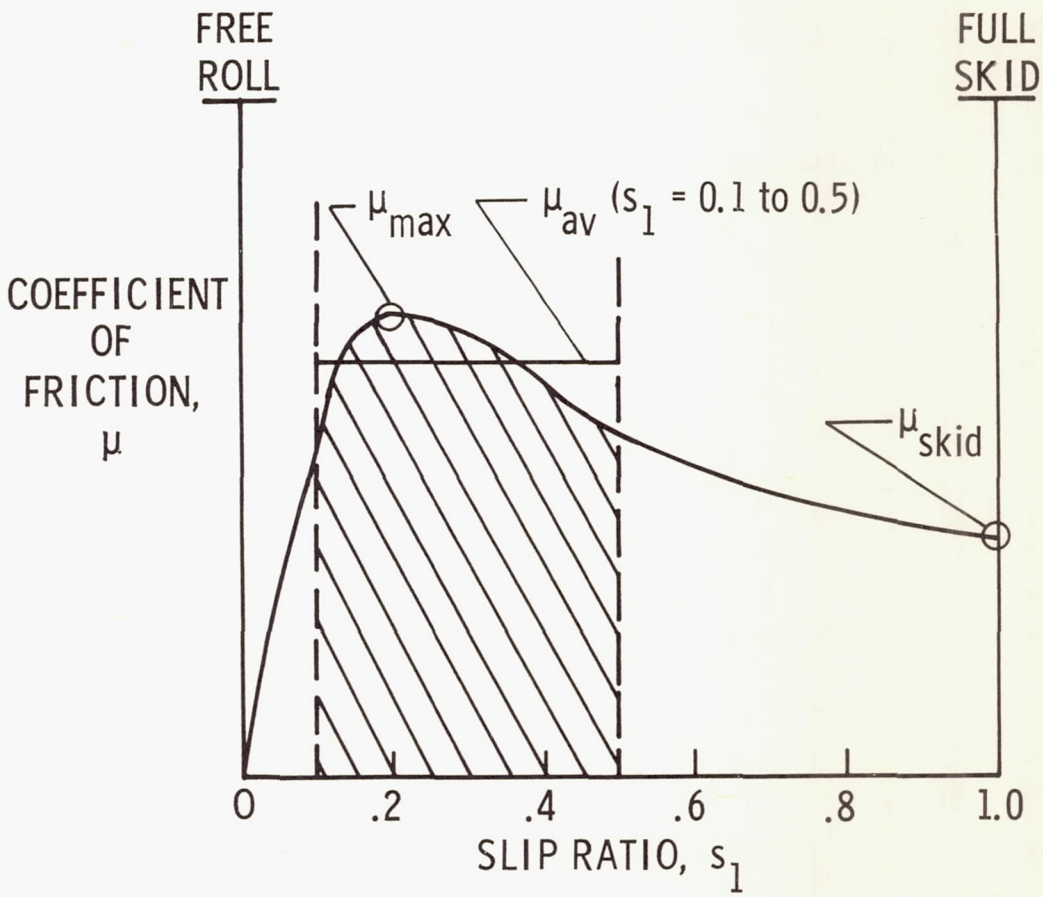

Figure 12.- Determination of μ_{av}.

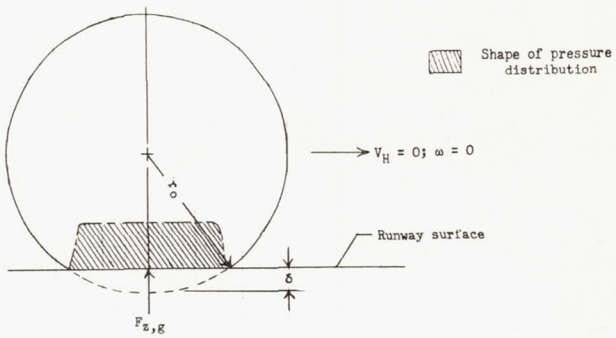

(a) Standing tire under vertical load only.

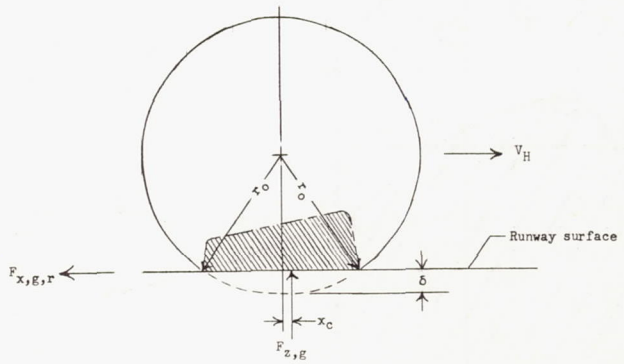

(b) Unbraked tire rolling at constant velocity on dry runway. $\alpha = 0$; $T_B = 0$.

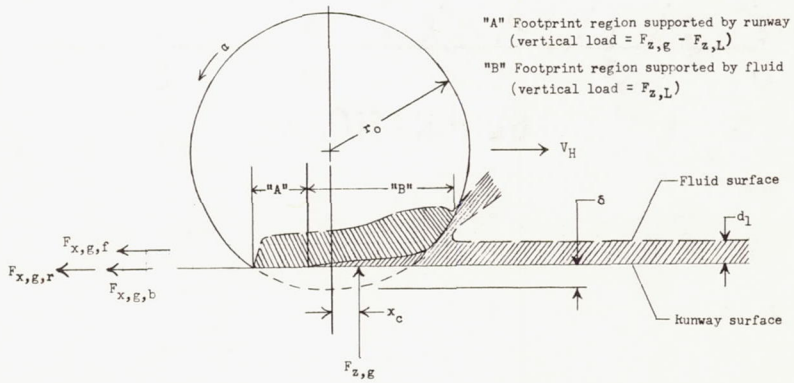

(c) Unbraked rolling tire undergoing spin-down on fluid-covered runway. $\alpha > 0$; $T_B = 0$.

Figure 13.- Schematic representation of pressure distributions developed in footprint region of a loaded tire under various rolling conditions.

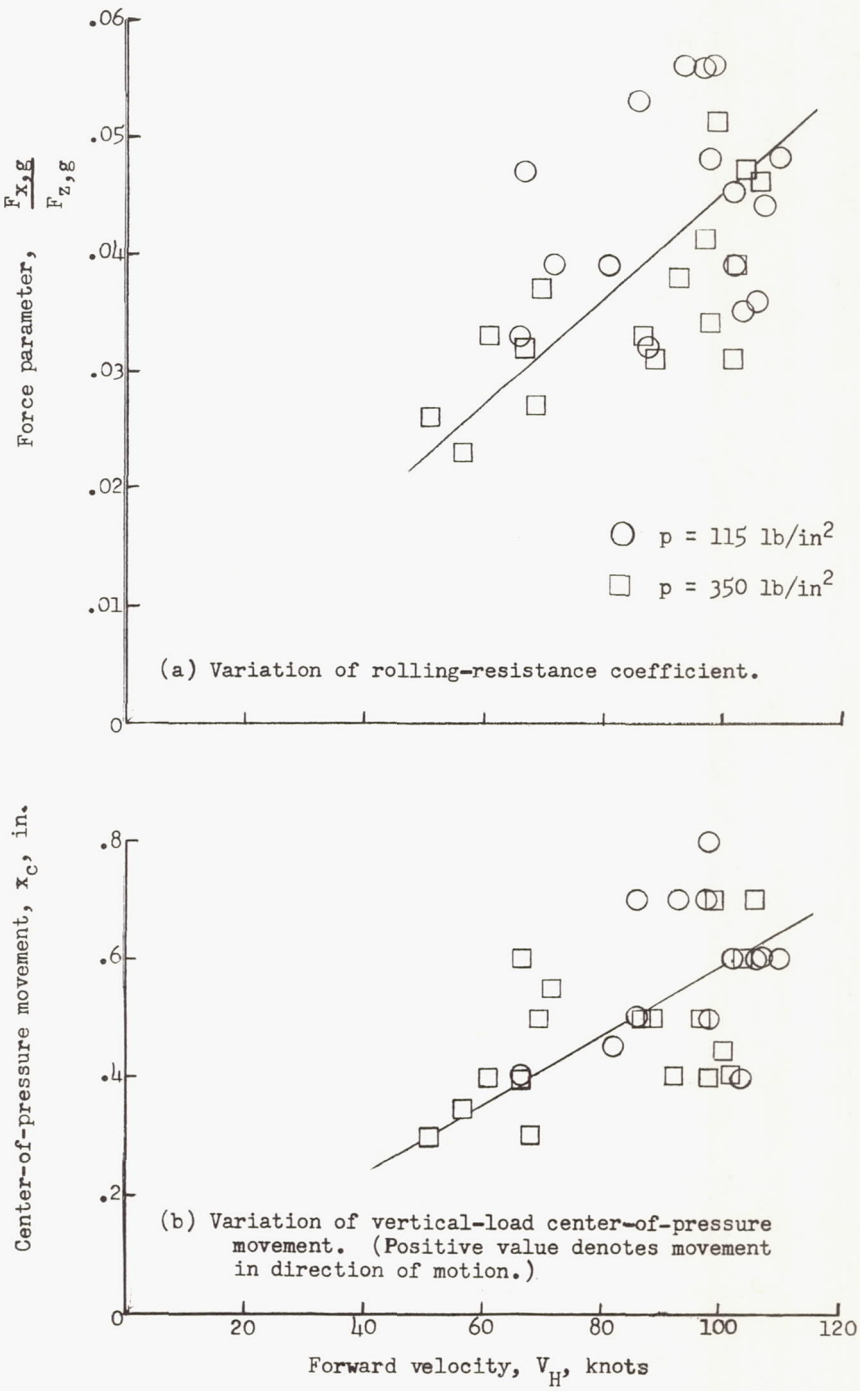

Figure 14.- Variation of rolling-resistance coefficient and vertical-load center-of-pressure movement with forward velocity for an unbraked tire (R2) rolling on a dry concrete runway.

Calculations based on $C_L = 0.7$ in eq. (5)

△ 6.70-15 automobile tire (unpublished data from friction-cart tests; see ref. 3 for description of cart):
$p = 18\text{-}40$ lb/in^2; $F_{z,g} = 1{,}875$ lb; smooth tread; $d_1 \approx 0.3$ inch

▽ 12 inch diameter x 3 inch width tire (ref.5)
$p = 7.5\text{-}28.5$ lb/in^2; $F_{z,g} = 100$ lb; smooth tread; $d_1 \approx 0.05$ inch

Calculations based on $C_L = 0.7$ in eq. (7)

○ 32 x 8.8 type VII aircraft tire (present test):
$p = 115$ lb/in^2; $F_{z,g} = 9{,}400$ lb; rib tread; $d_1 \approx 0.5\text{-}0.8$ inch

□ 44 x 13 type VII aircraft tire (ref.7):
$p = 100\text{-}150$ lb/in^2; $F_{z,g} = 20{,}000$ lb; rib tread; $d_1 \approx 0.1$ inch

◇ 17.00-20 type III aircraft tire (ref.4):
$p = 65$ lb/in^2; $F_{z,g} = 10{,}000$ lb; rib tread; $d_1 \approx 0.4$ inch

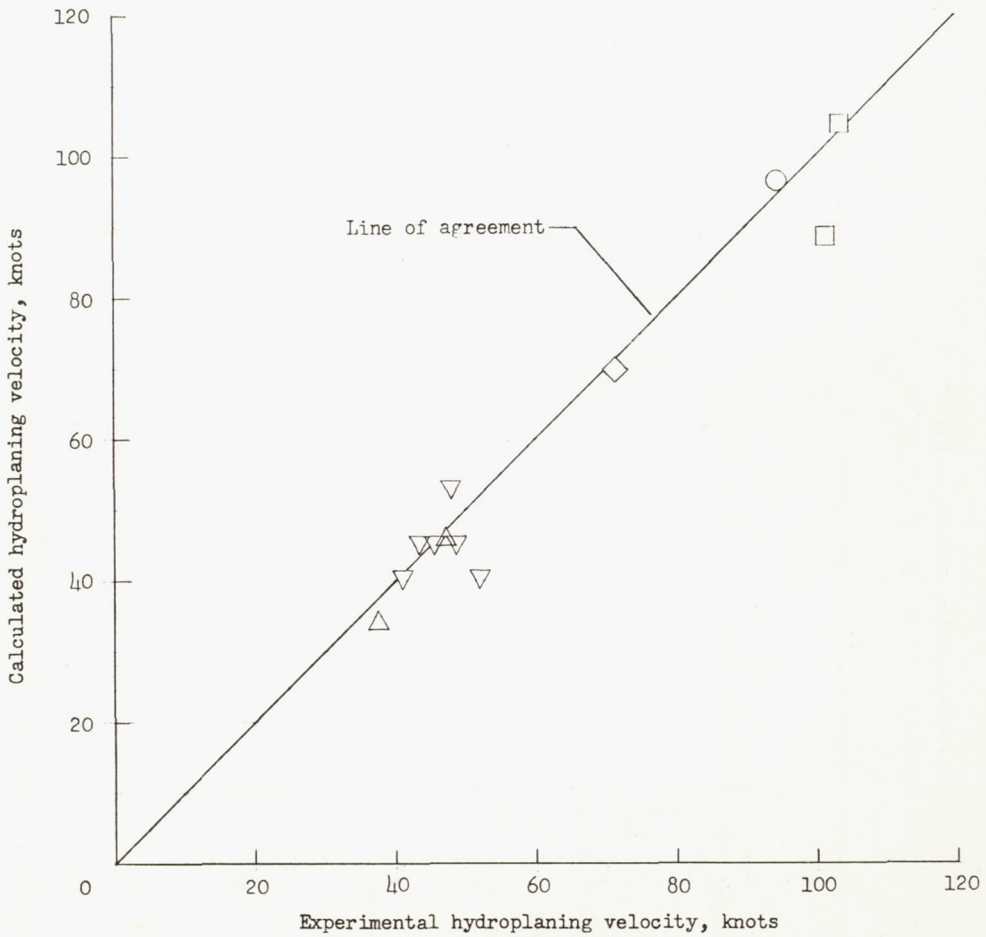

Figure 15.- Comparison of experimental hydroplaning velocities obtained from tests on wet runway surfaces and velocities calculated by using $C_L = 0.7$ in equations (5) and (7).

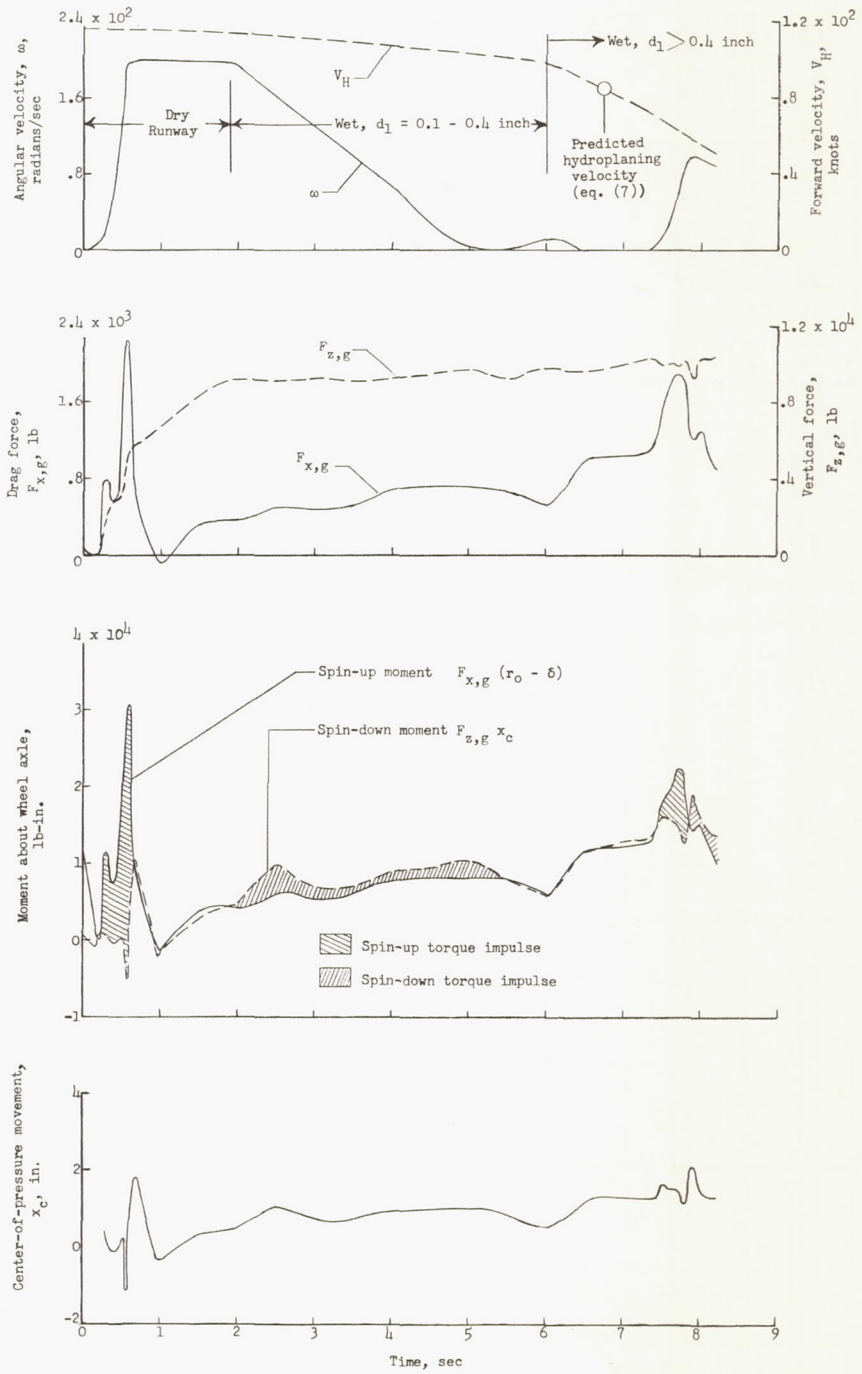

Figure 16.- Unbraked rolling run during which tire hydroplanes and spins down to stop on water-covered concrete runway. Tire D5M1; p = 90 lb/sq in.

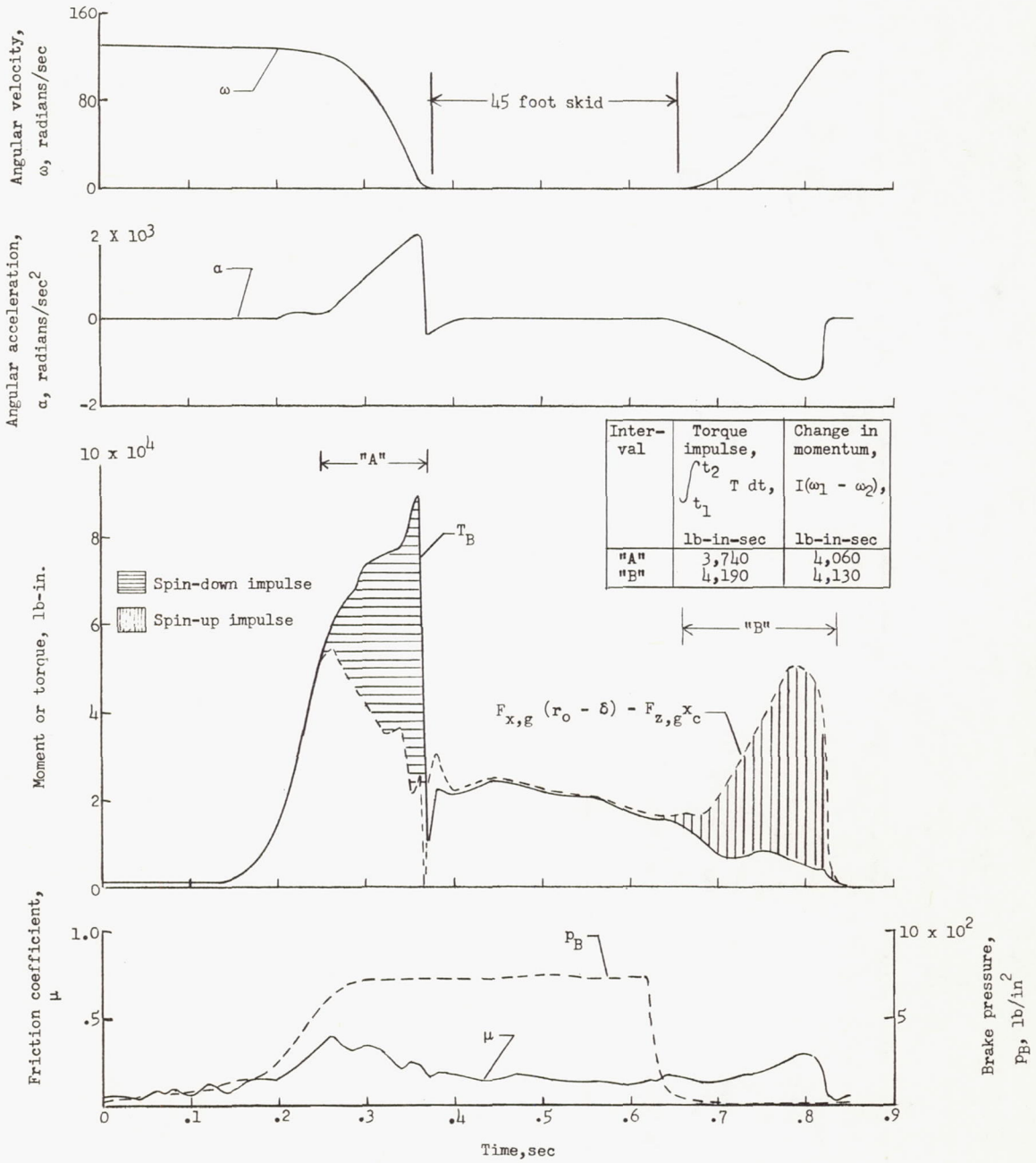

Interval	Torque impulse, $\int_{t_1}^{t_2} T\,dt$, lb-in-sec	Change in momentum, $I(\omega_1 - \omega_2)$, lb-in-sec
"A"	3,740	4,060
"B"	4,190	4,130

Figure 17.- Braking cycle for tire R2 on wet concrete. $F_{z,g} \approx 10{,}000$ pounds; p = 260 lb/sq in.; d_1 = 0.05 to 0.3 inch; V_H = 96 to 93.5 knots; antiskid unit not used. Brake pressure was sequenced by energizing solenoid valves in brake circuit through knife edges positioned on track runway.

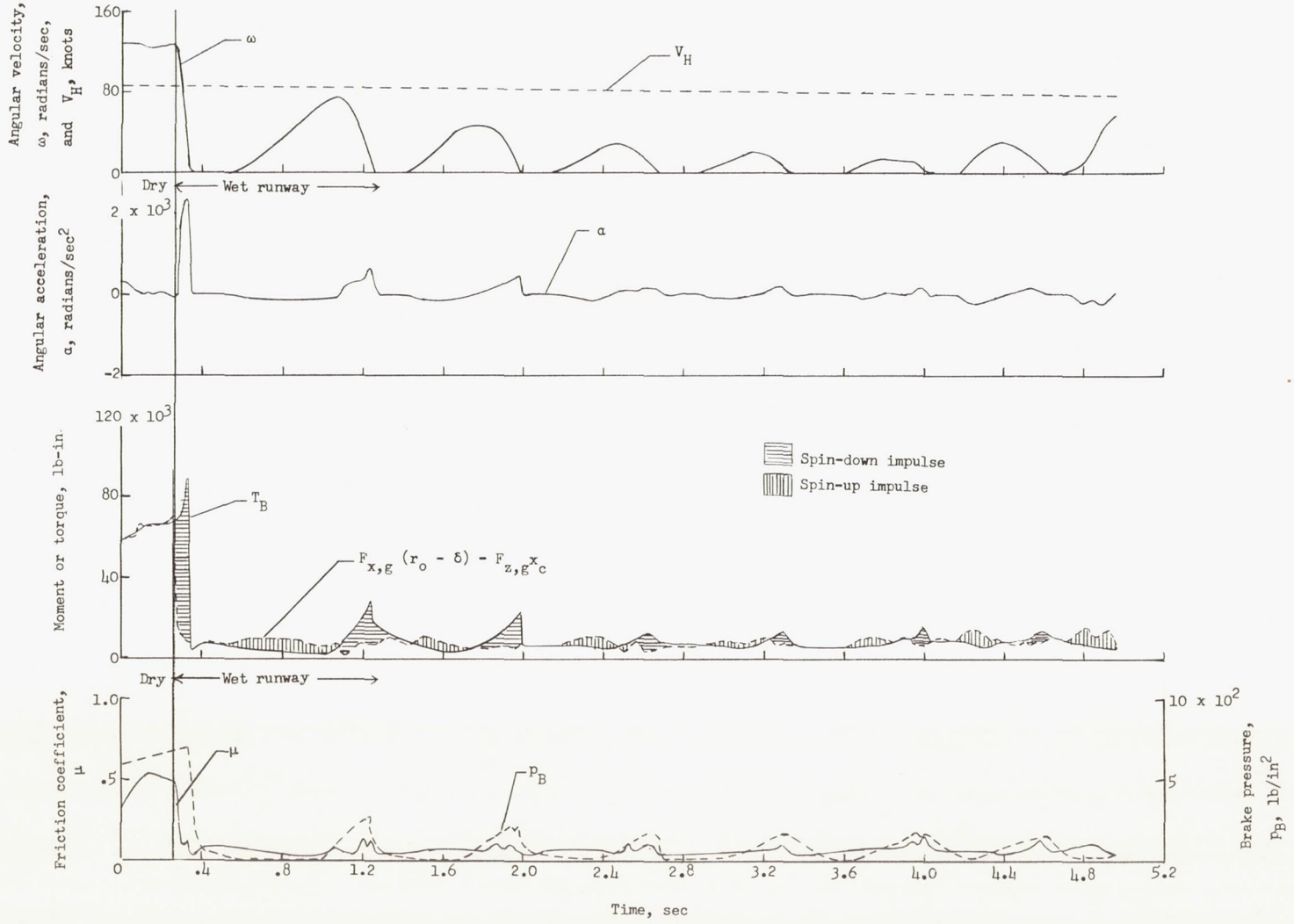

Figure 18.- Braking of tire D1 on wet concrete runway with antiskid unit operating. $F_{Z,g} \approx 10,000$ pounds; p = 260 lb/sq in.; $p_{B,1}$ = 50 lb/sq in.

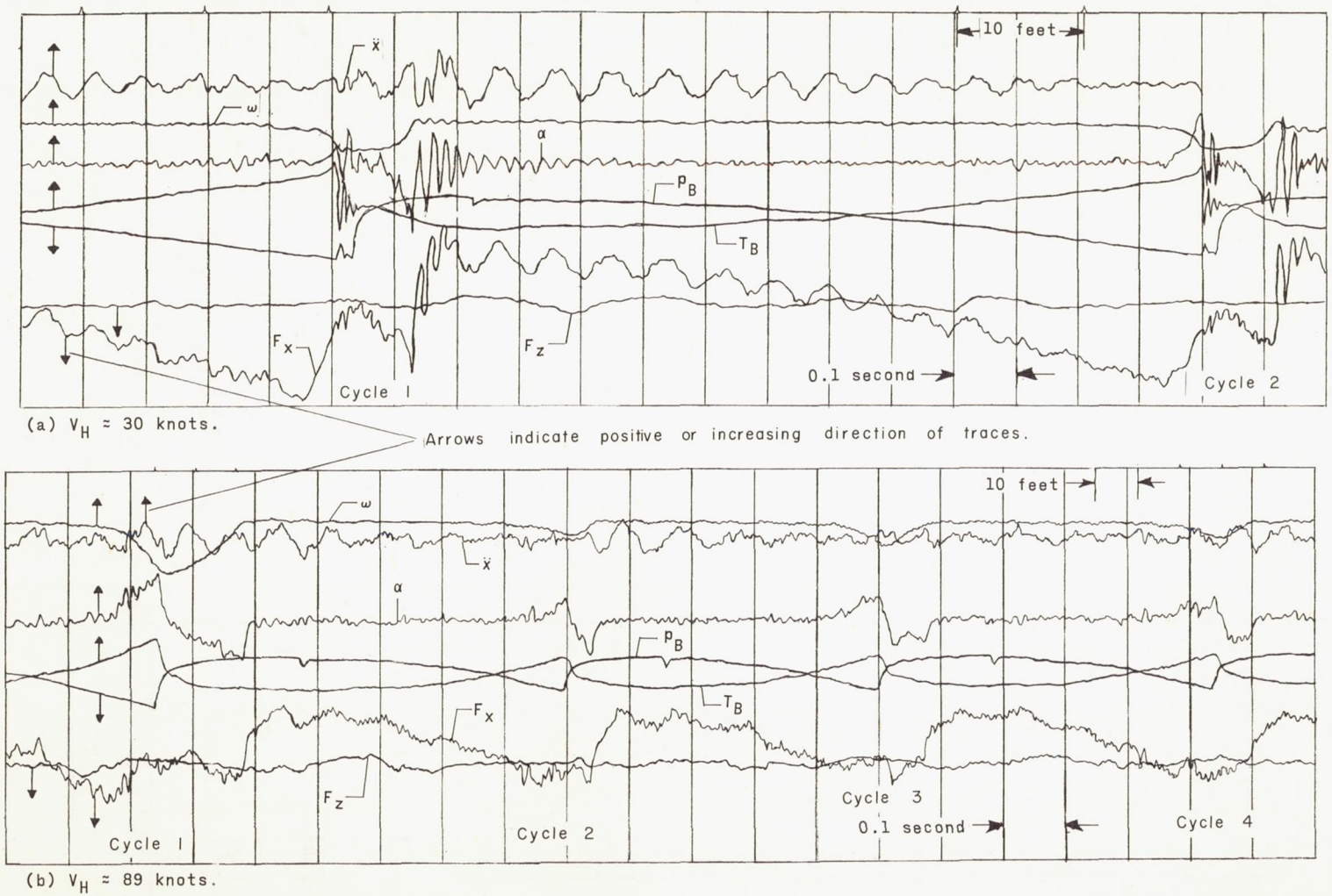

Figure 19.- Typical oscillograph tracings obtained during low-speed and high-speed braking on a wet concrete runway with the fabric-reinforced rib-tread tire S2M2. $F_{Z,g} \approx 10,000$ pounds; $p = 260$ lb/sq in.; $d_1 = 0$ to 0.3 inch.

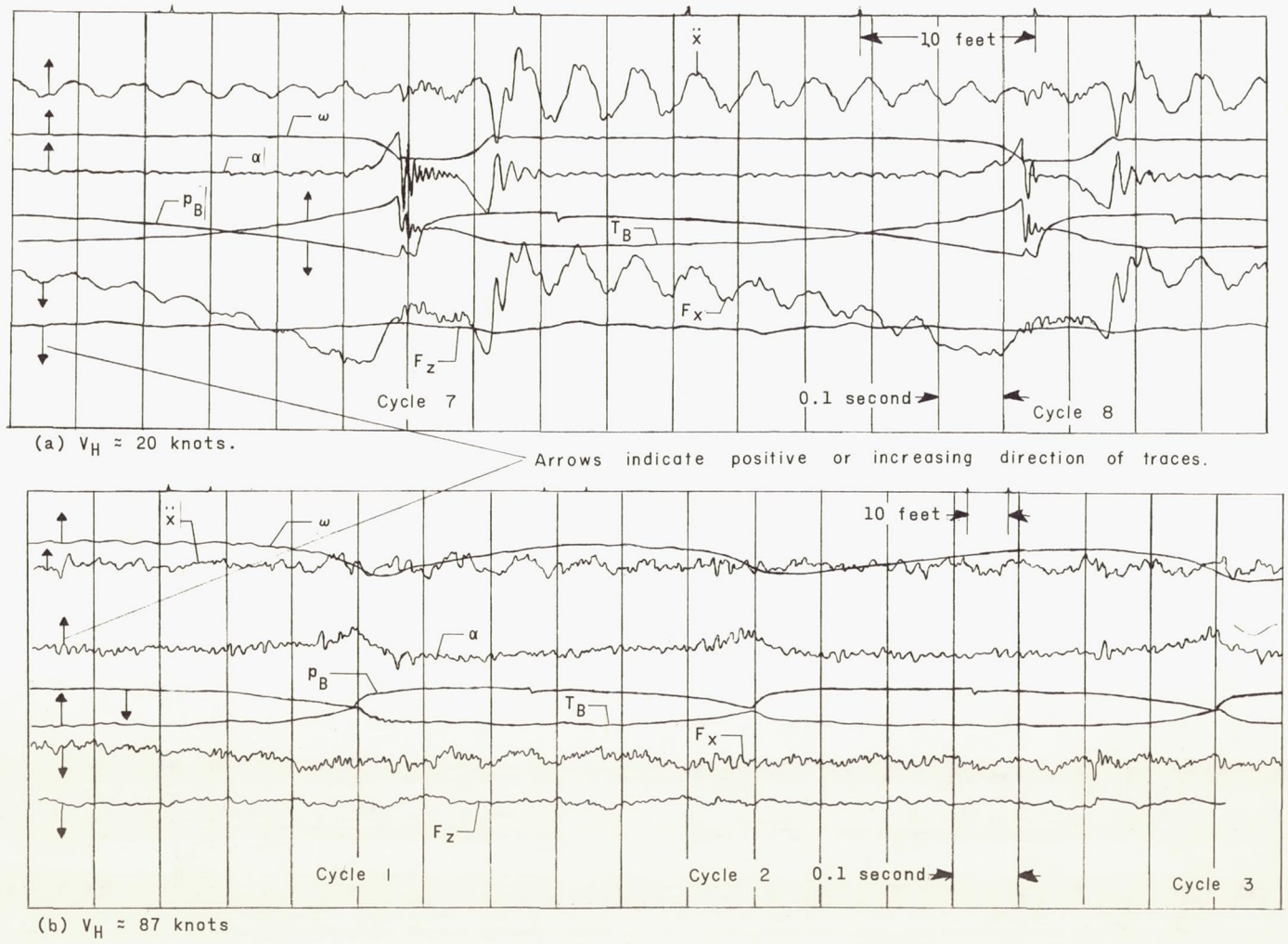

Figure 20.- Typical oscillograph tracings obtained during low-speed and high-speed braking on a wet concrete runway with the all-rubber smooth-tread tire S1. $F_{z,g} \approx 10,000$ pounds; p = 260 lb/sq in.; d_1 = 0 to 0.3 inch.

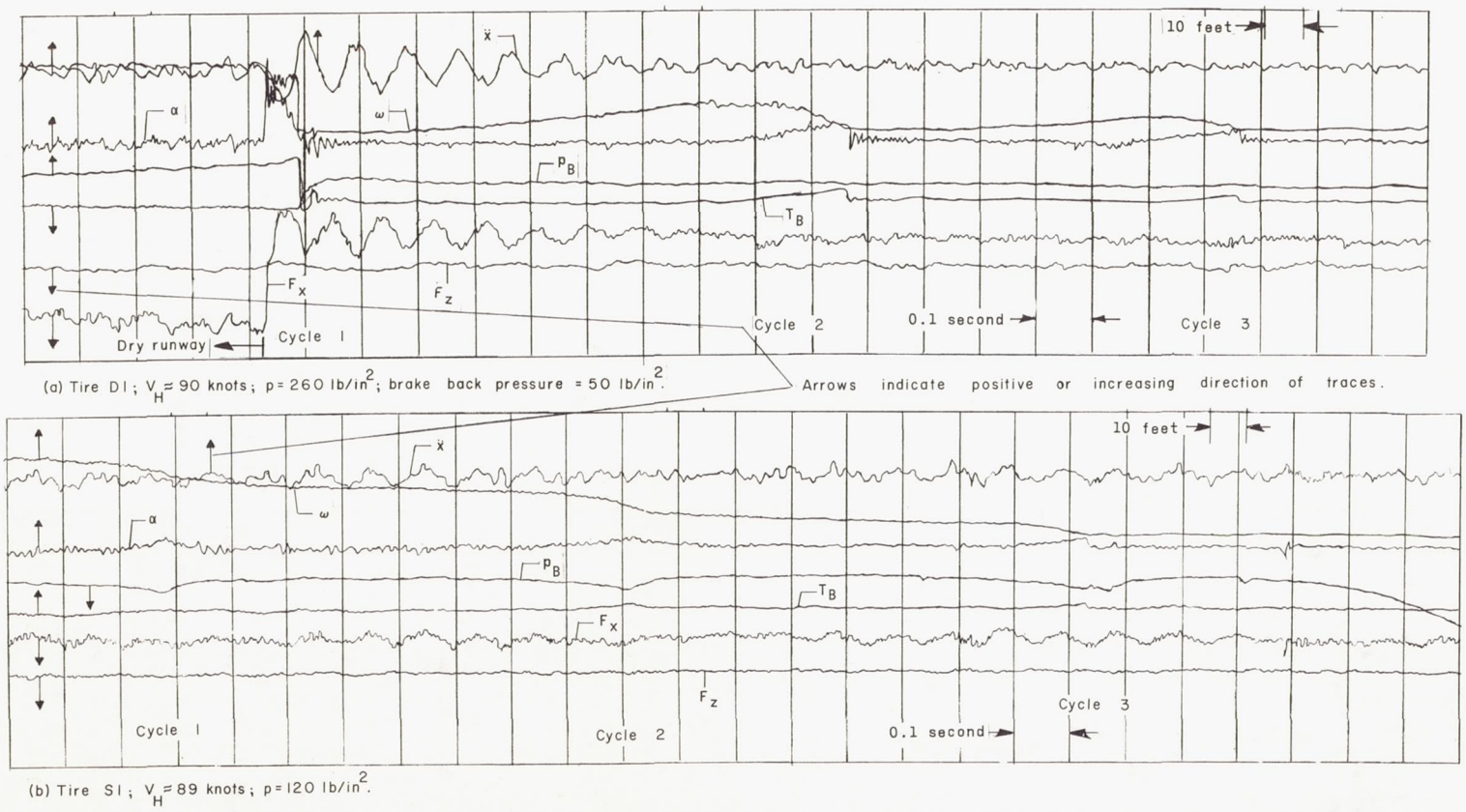

Figure 21.- Typical oscillograph tracings obtained during high-speed braking on a wet concrete runway with the fabric-reinforced dimple-tread tire D1 and the all-rubber smooth-tread tire S1. $F_Z \approx 10,000$ pounds; $d_1 = 0$ to 0.3 inch.

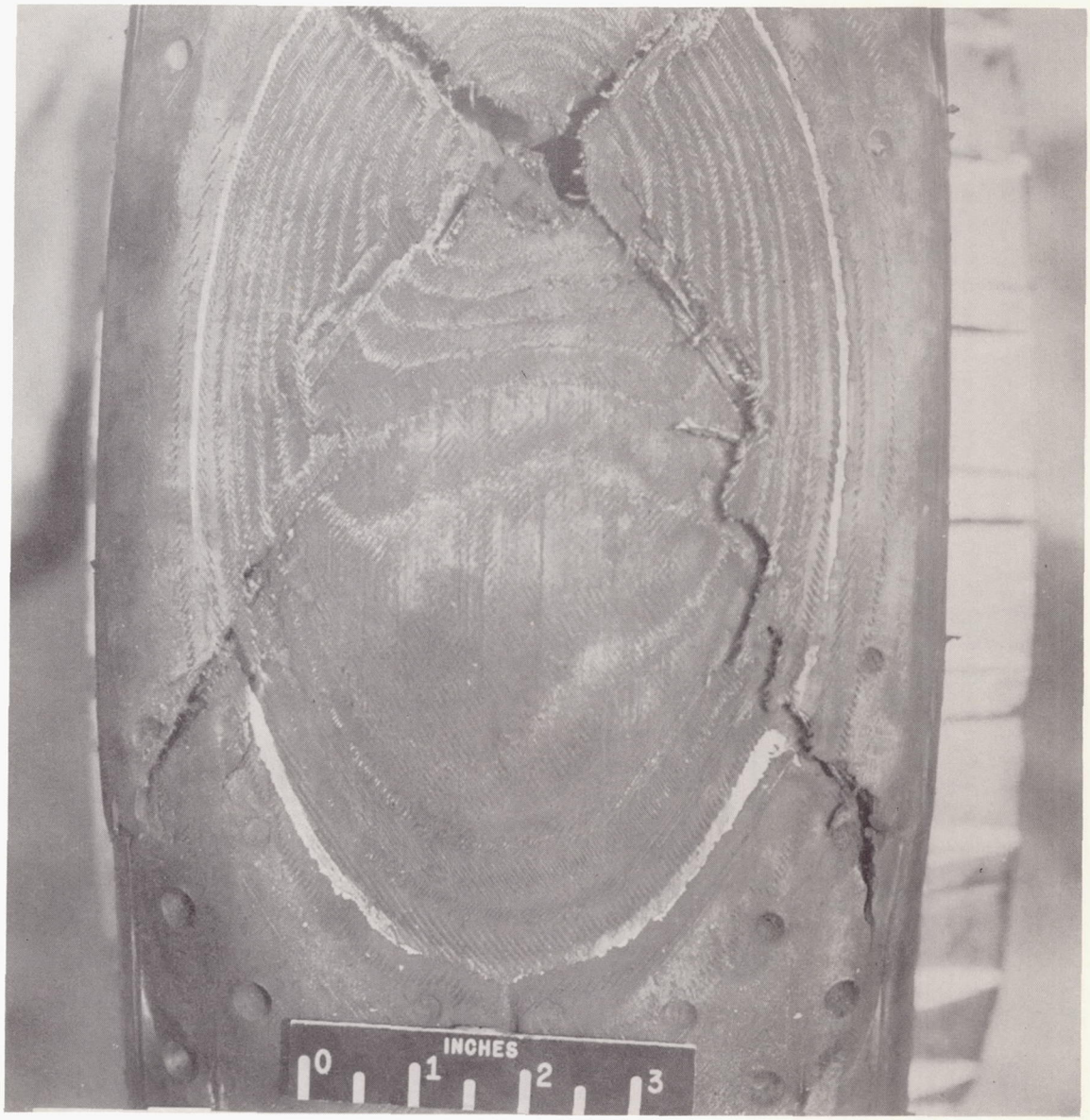

L-62-2078

Figure 22.- Tire appearance after skidding approximately 60 feet on a dry concrete runway.

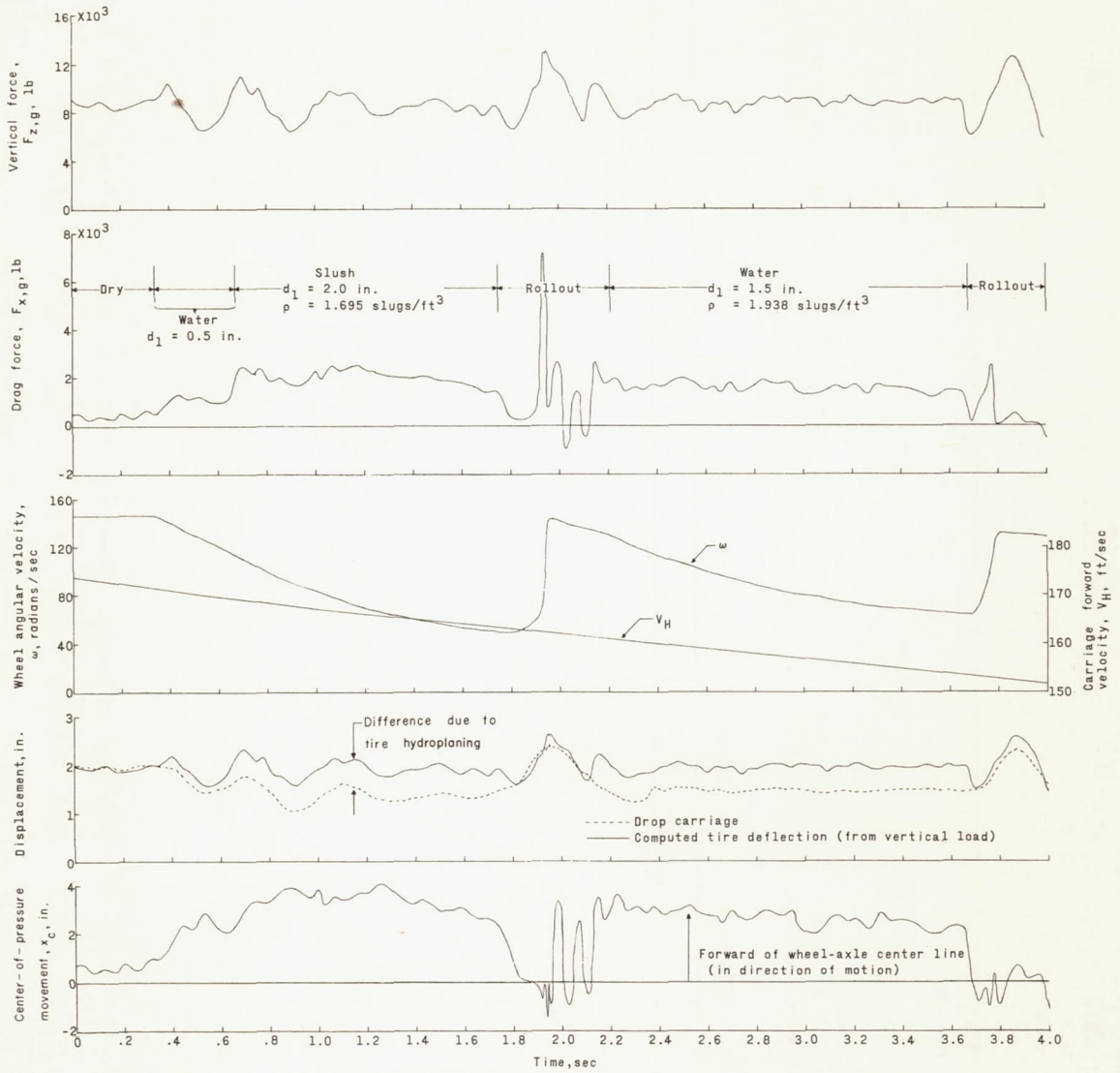

Figure 23.- Typical time history of wheel loads, velocities, and displacement during unbraked rolling through slush and water troughs on a concrete runway. p = 115 lb/sq in.

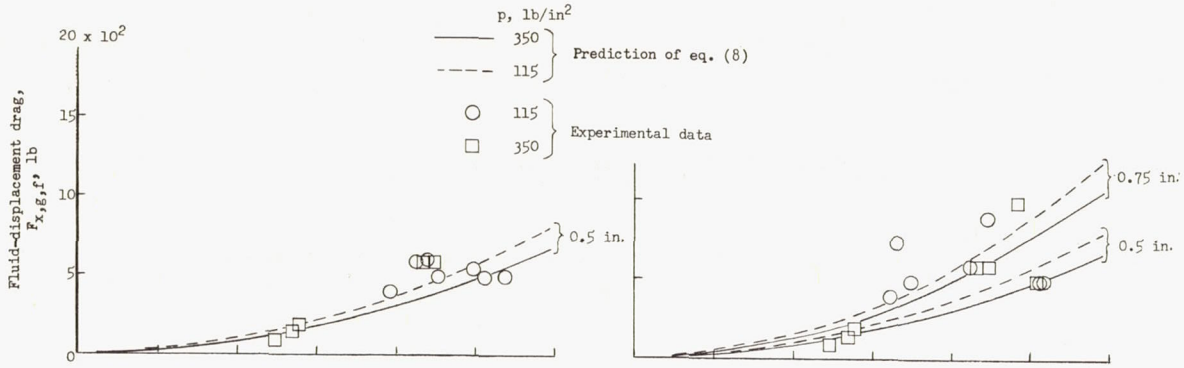

(a) Water depth d_1 = 0 to 0.5 inch. (b) Water depth d_1 = 0.5 to 0.75 inch.

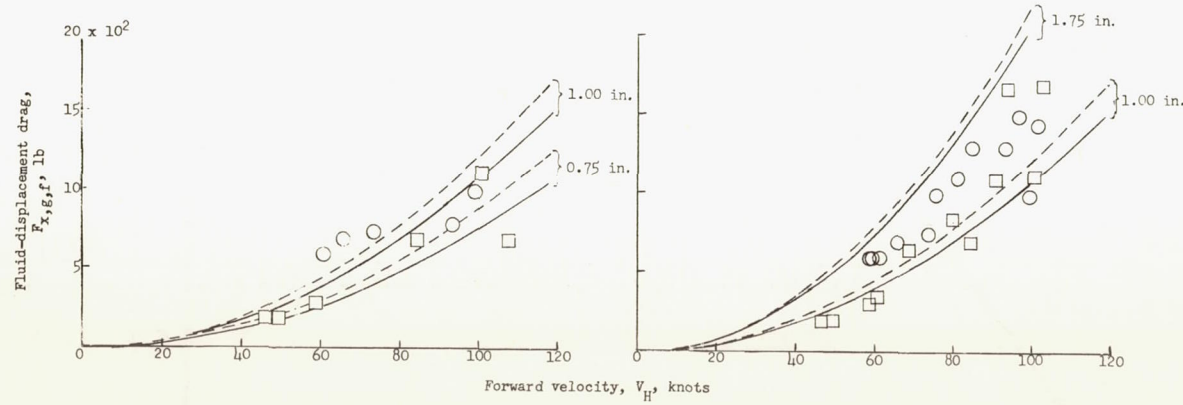

(c) Water depth d_1 = 0.75 to 1.00 inch. (d) Water depth d_1 = 1.00 to 1.75 inches.

Figure 24.- Variation of fluid-displacement drag force with forward velocity and water depth on a concrete runway. Tire R2.

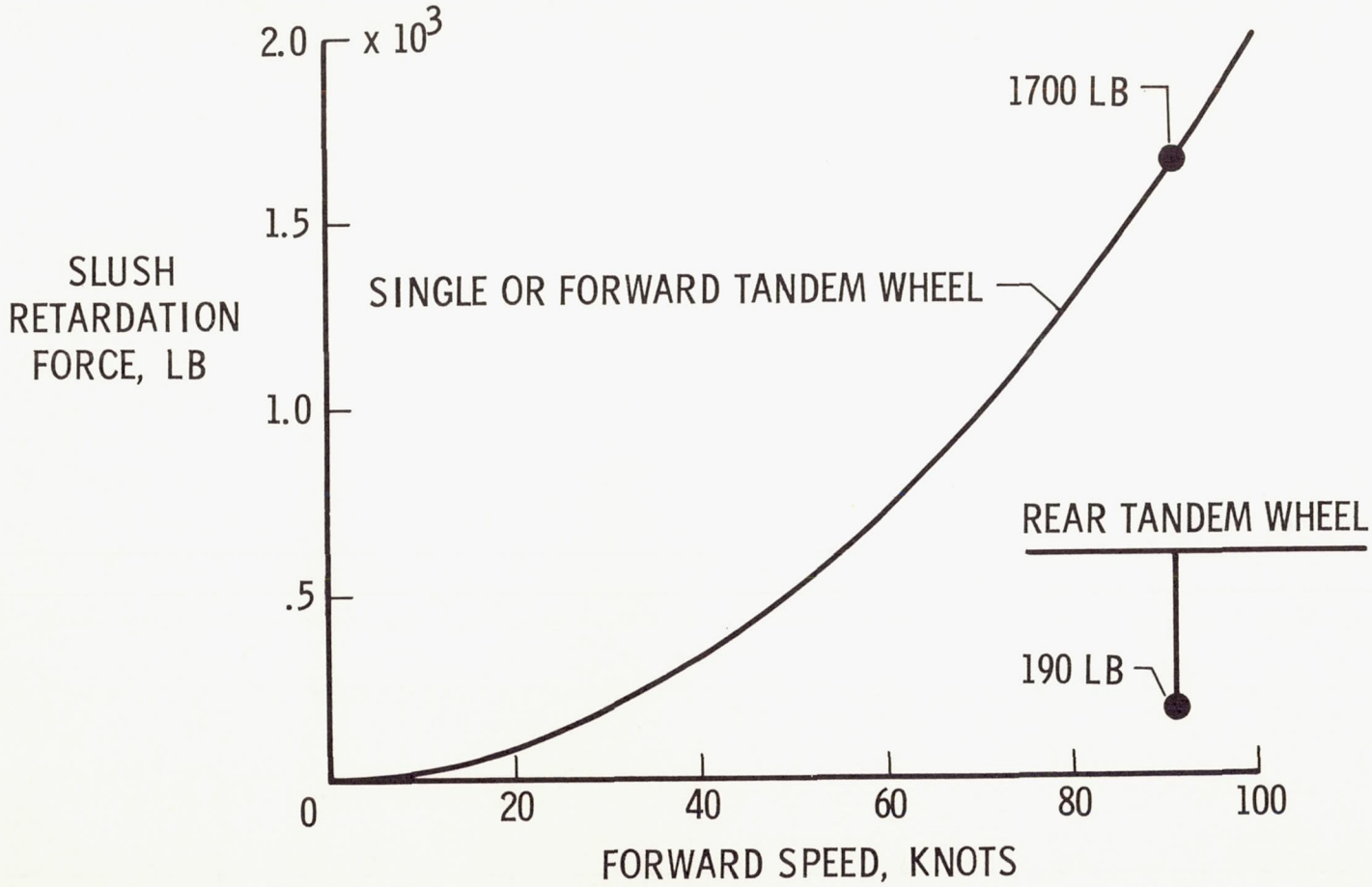

Figure 25.- Forces developed on unbraked tandem wheels in slush. Slush depth, 1.75 inches; slush density, 1.82 slugs/cu ft.

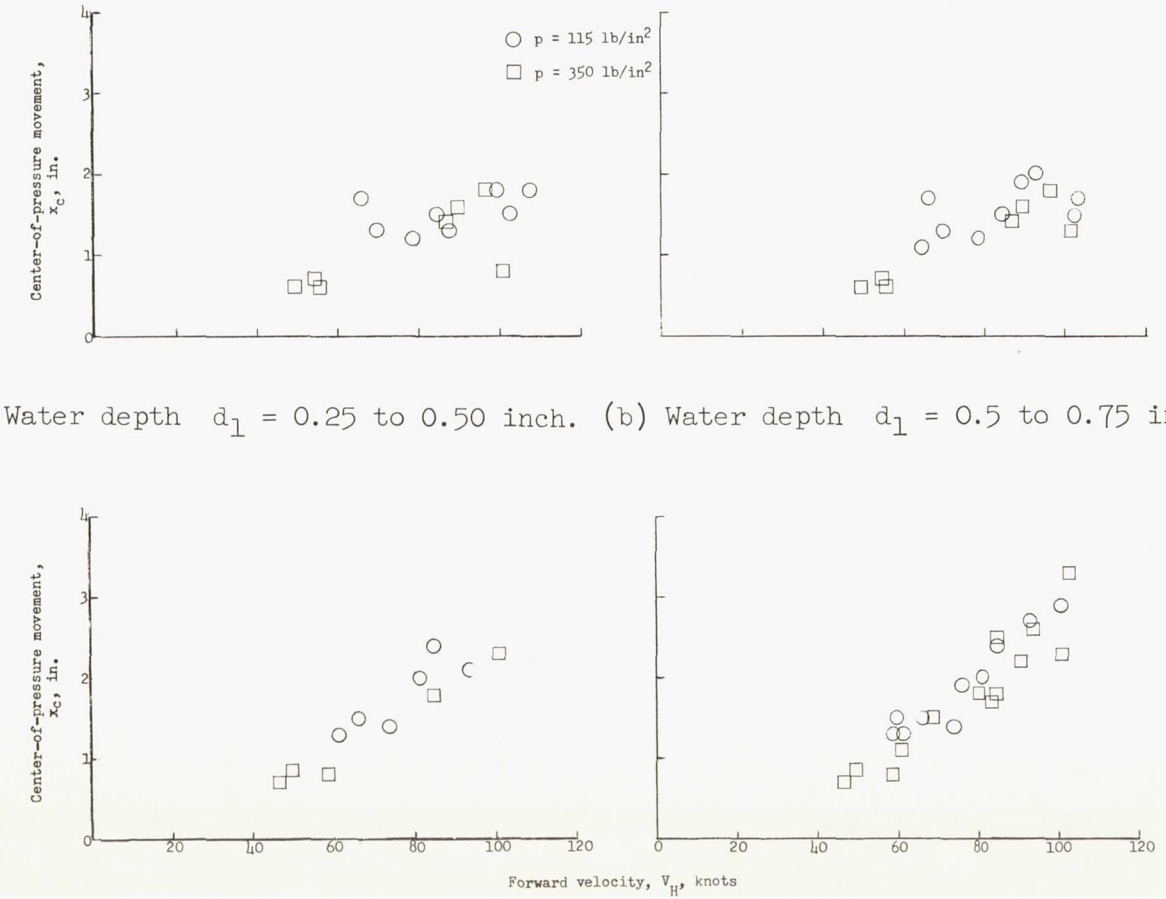

(a) Water depth d_1 = 0.25 to 0.50 inch. (b) Water depth d_1 = 0.5 to 0.75 inch.

(c) Water depth d_1 = 0.75 to 1.00 inch. (d) Water depth d_1 = 1.00 to 1.75 inches.

Figure 26.- Variation of vertical-load center-of-pressure movement x_c with forward velocity and water depth for tire R2.

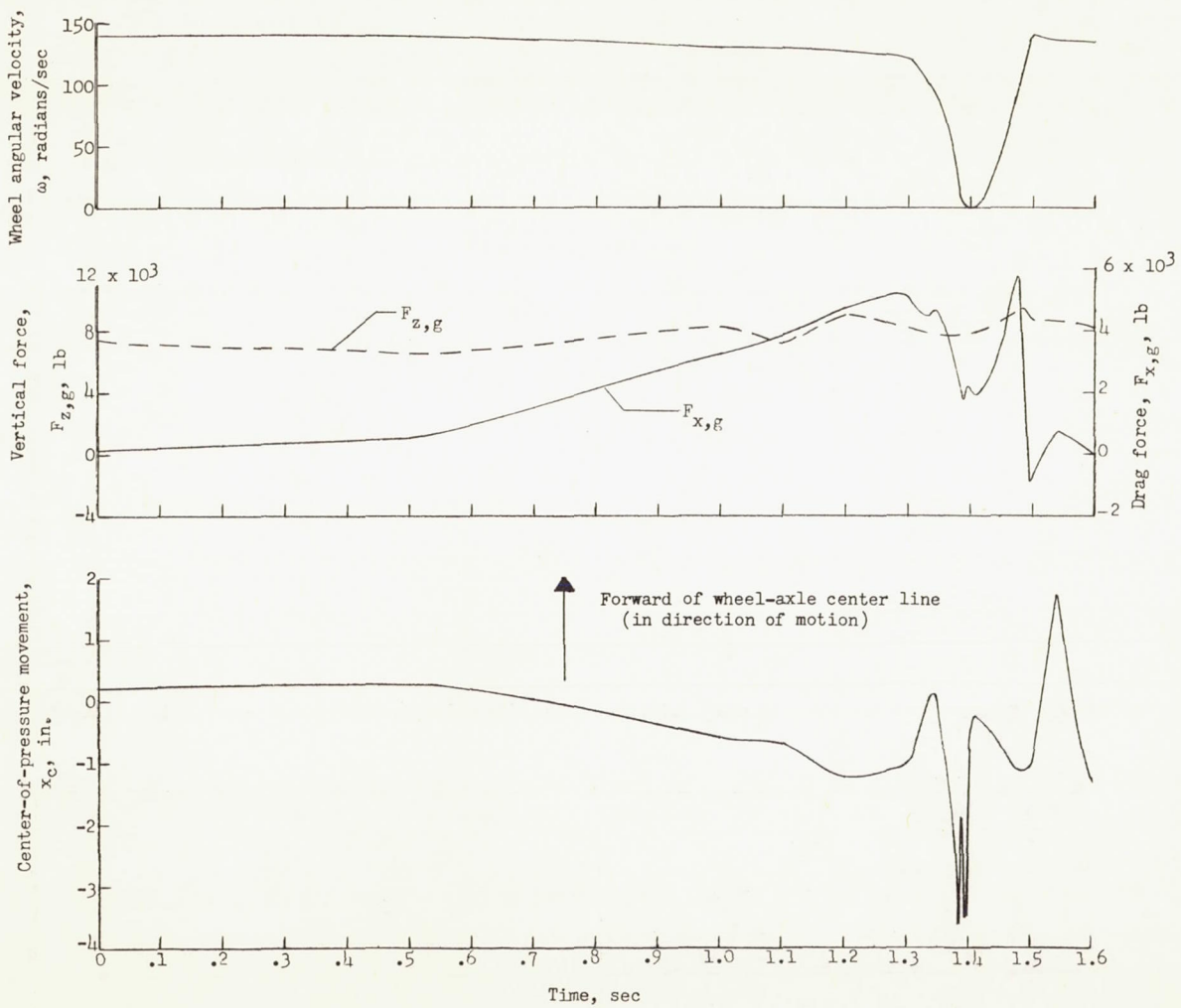

Figure 27.- Variation of wheel angular velocity, vertical force, drag force, and vertical-load center-of-pressure movement during a braking cycle with tire R2 on a dry concrete runway. $V_H \approx 79$ knots.

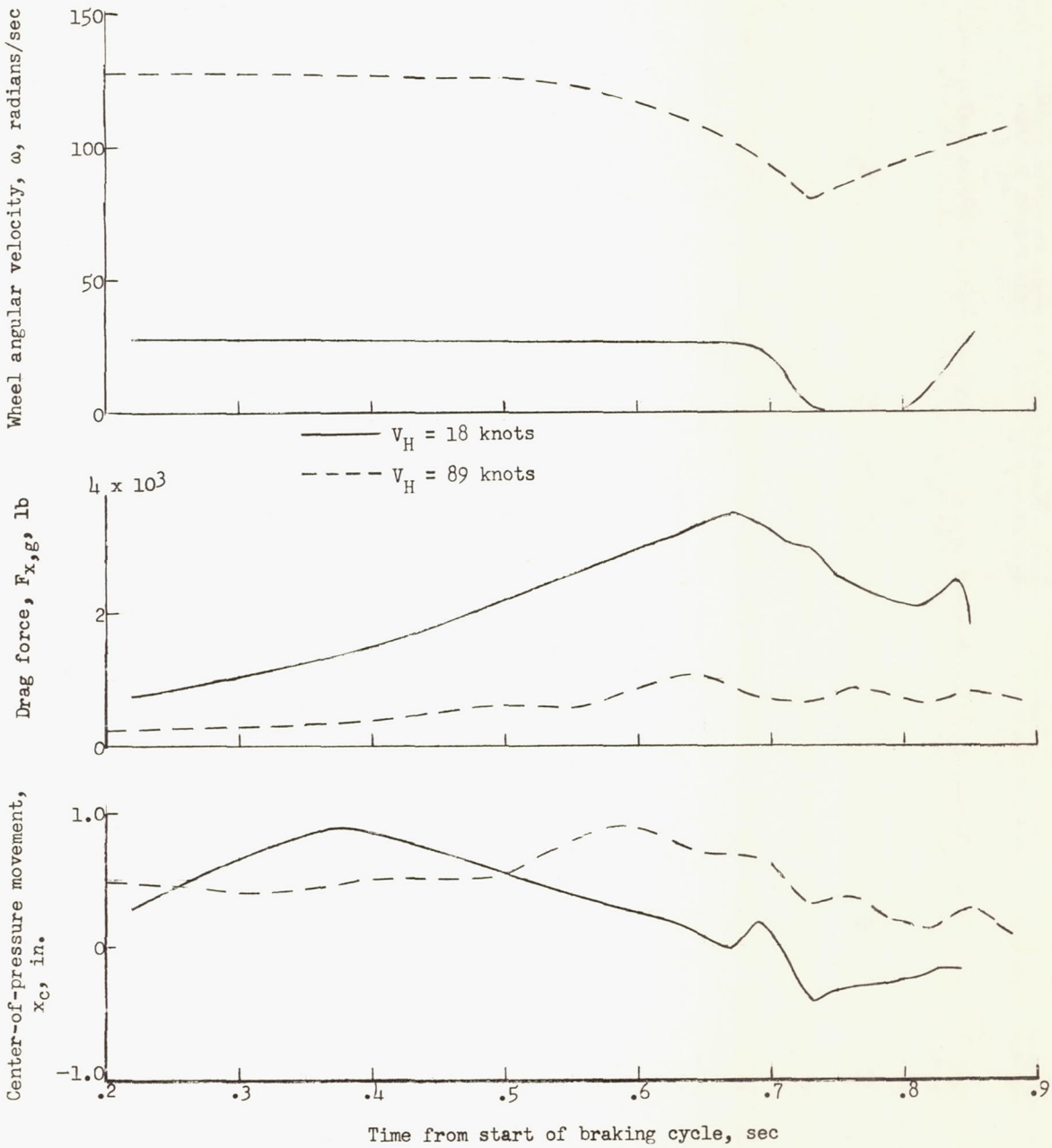

Figure 28.- Variation of wheel angular velocity, drag force, and vertical-load center-of-pressure movement during braking cycles with tire S1 on a wet concrete runway. $F_{Z,g} \approx 10,000$ pounds; p = 260 lb/sq in; d_1 = 0 to 0.3 inch.

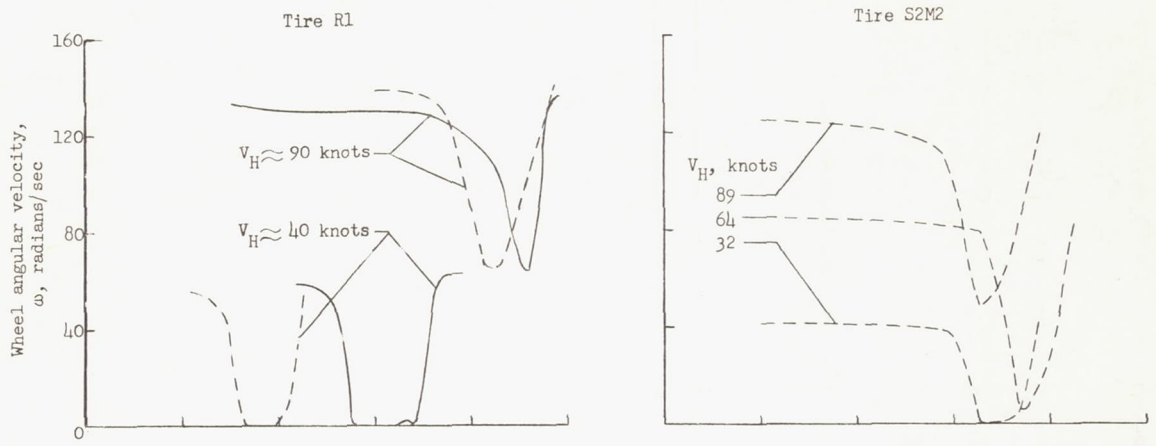

(a) Tires with good skid resistance.

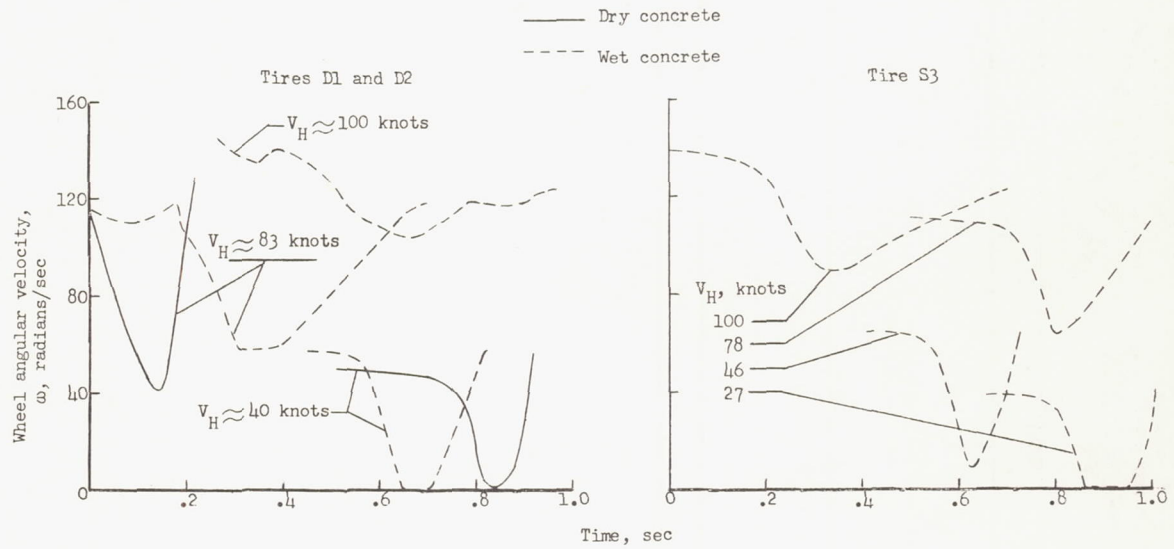

(b) Tires with poor skid resistance.

Figure 29.- Wheel spin-down and spin-up characteristics for tread designs with good and poor skid resistance on dry and wet (with water) concrete runways. Data obtained during braking tests on single wheels. $F_{z,g} \approx 10{,}000$ pounds; p = 260 lb/sq in.; d_1 = 0 to 0.3 inch on wet runways.

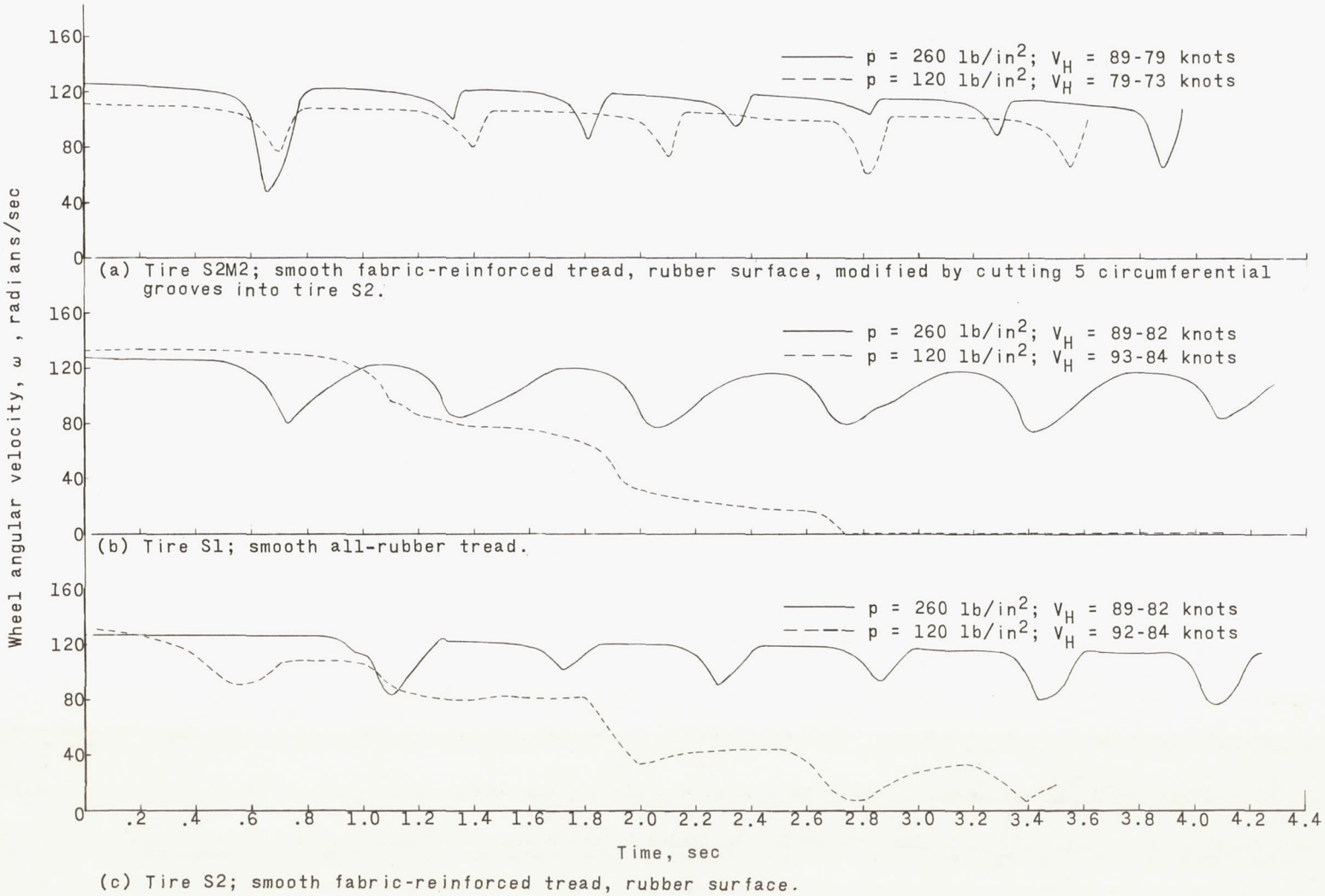

Figure 30.- Effect of tire pressure on the spin-down and spin-up characteristics of tires with smooth and grooved treads. Data were obtained during braking tests of a single wheel on a wet concrete runway. $F_{z,g} \approx 10{,}000$ pounds; $d_1 = 0$ to 0.3 inch.

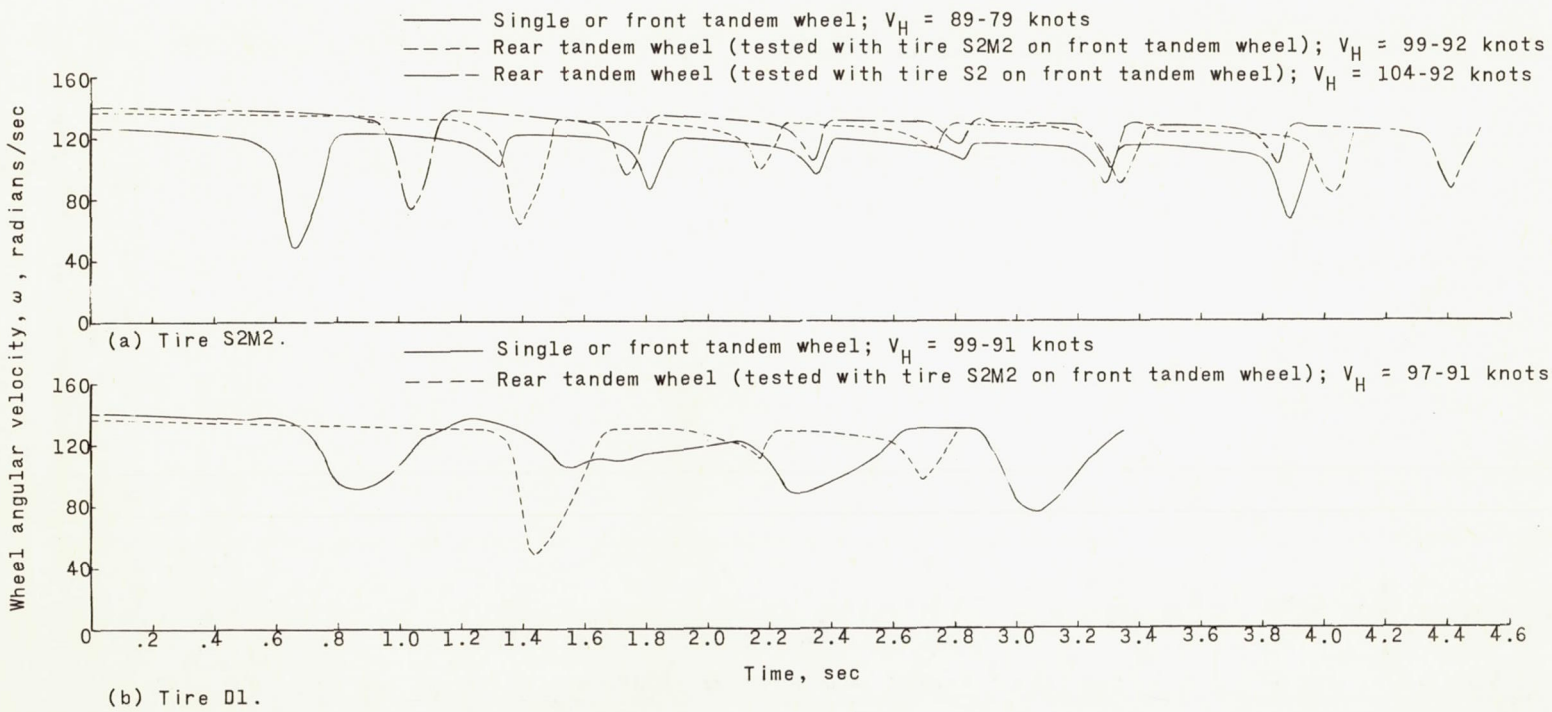

Figure 31.- Effect of tire location on wheel spin-up characteristics in a tandem wheel arrangement. Data were obtained during braking tests on a wet concrete runway. Vertical load per tire ≈ 10,000 pounds; p = 260 lb/sq in.; d_1 = 0 to 0.3 inch.

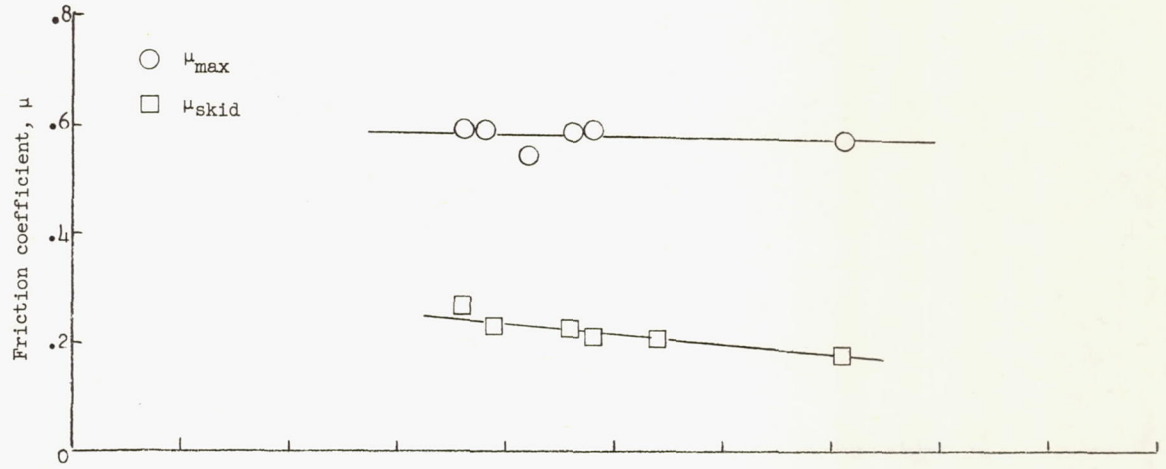

(a) Tire D5M1 (dimple, fabric-reinforced tread; dimples buffed off). $F_{Z,g} \approx 10{,}000$ pounds; p = 260 lb/sq in.

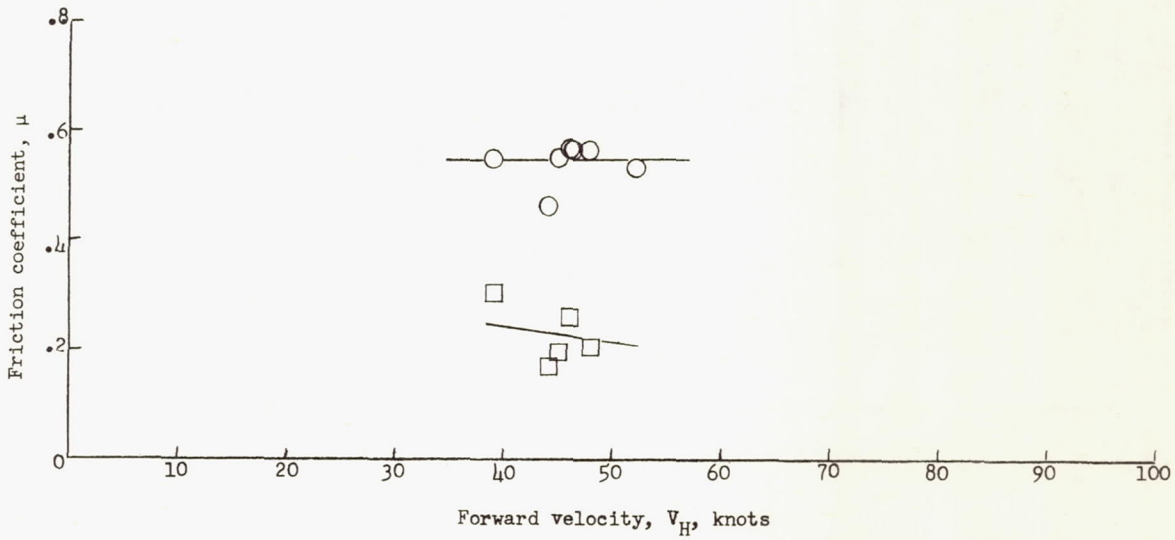

(b) Tire R4 (all-rubber rib tread; 11 circumferential grooves). $F_{Z,g} \approx 10{,}000$ pounds; p = 260 lb/sq in.

Figure 32.- Variation of maximum and full-skid tire-ground friction coefficients with forward velocity for several tire tread designs. Data were obtained during single-wheel braking tests on a dry concrete runway.

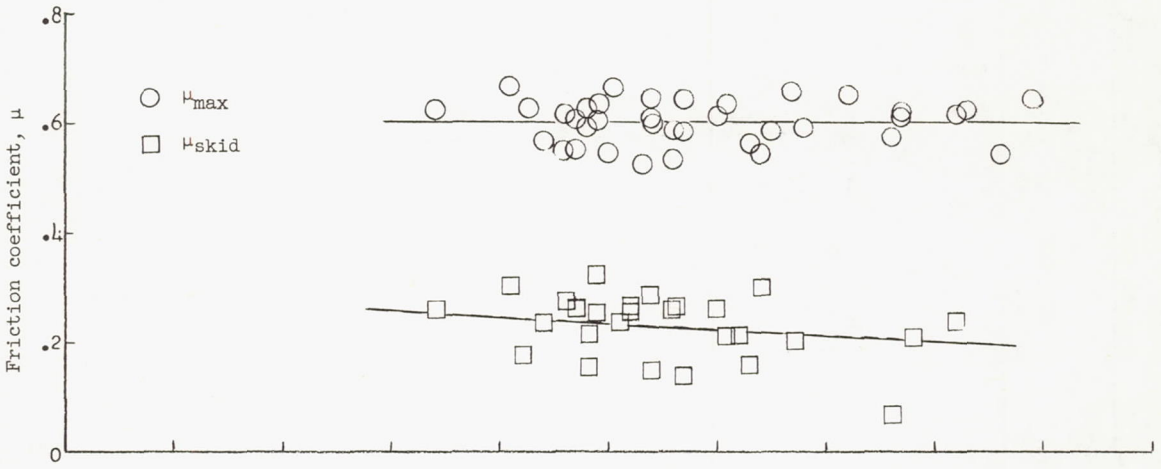

(c) Tires R2 and R3 (all-rubber rib tread; 9 circumferential grooves). $F_{Z,g} \approx 10{,}000$ pounds; p = 260 lb/sq in.

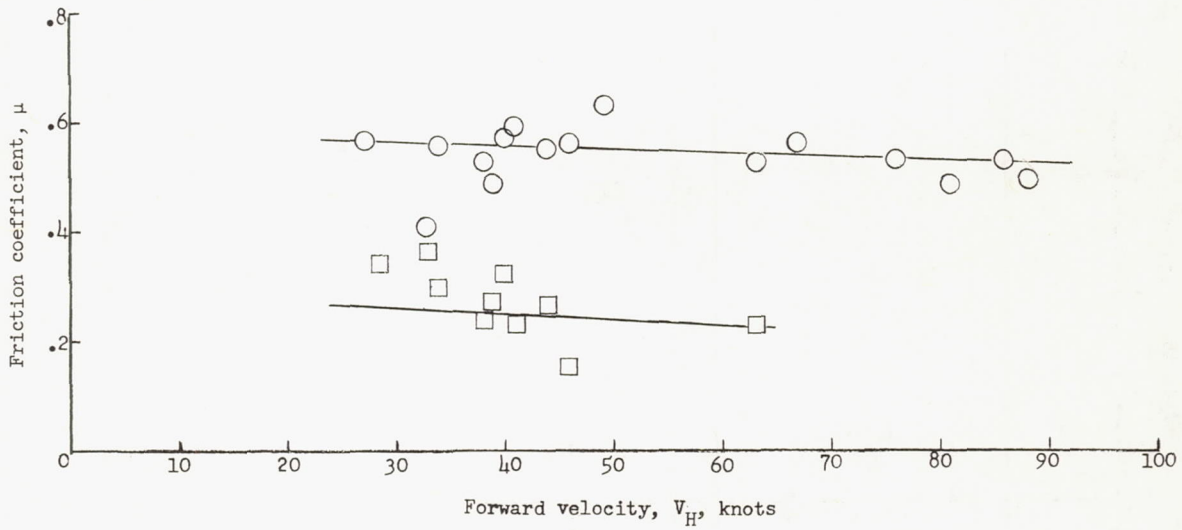

(d) Tire D1 (dimple, fabric-reinforced tread, fabric surface). $F_{Z,g} \approx 10{,}000$ pounds; p = 260 lb/sq in.

Figure 32.- Continued.

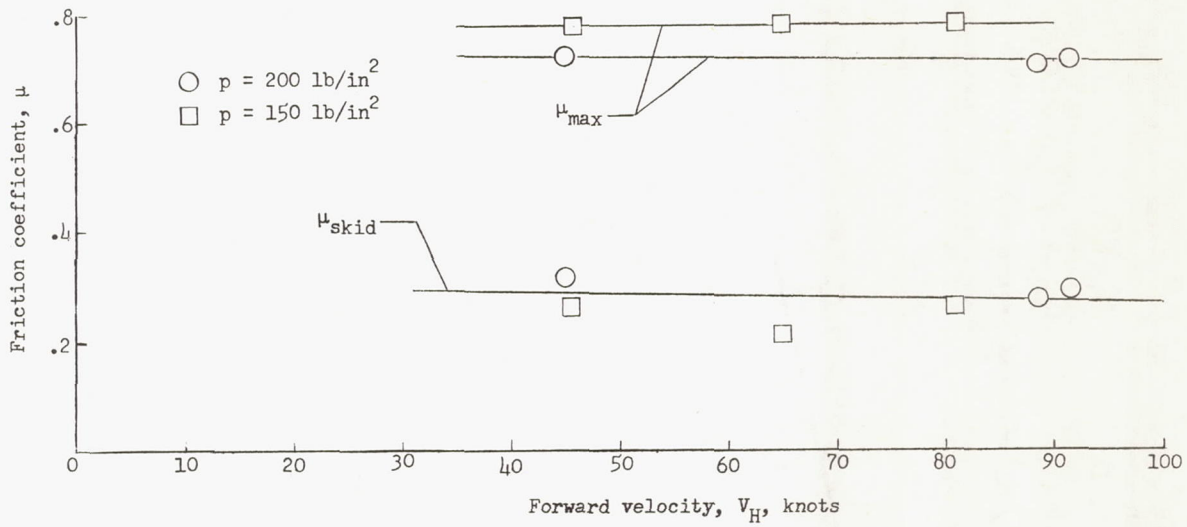

(e) 44x13, type VII, 26-ply-rating tire, all-rubber rib tread, 5 circumferential grooves. Unpublished data from NASA landing-loads track. $F_{Z,g} \approx 20,400$ pounds.

Figure 32.- Concluded.

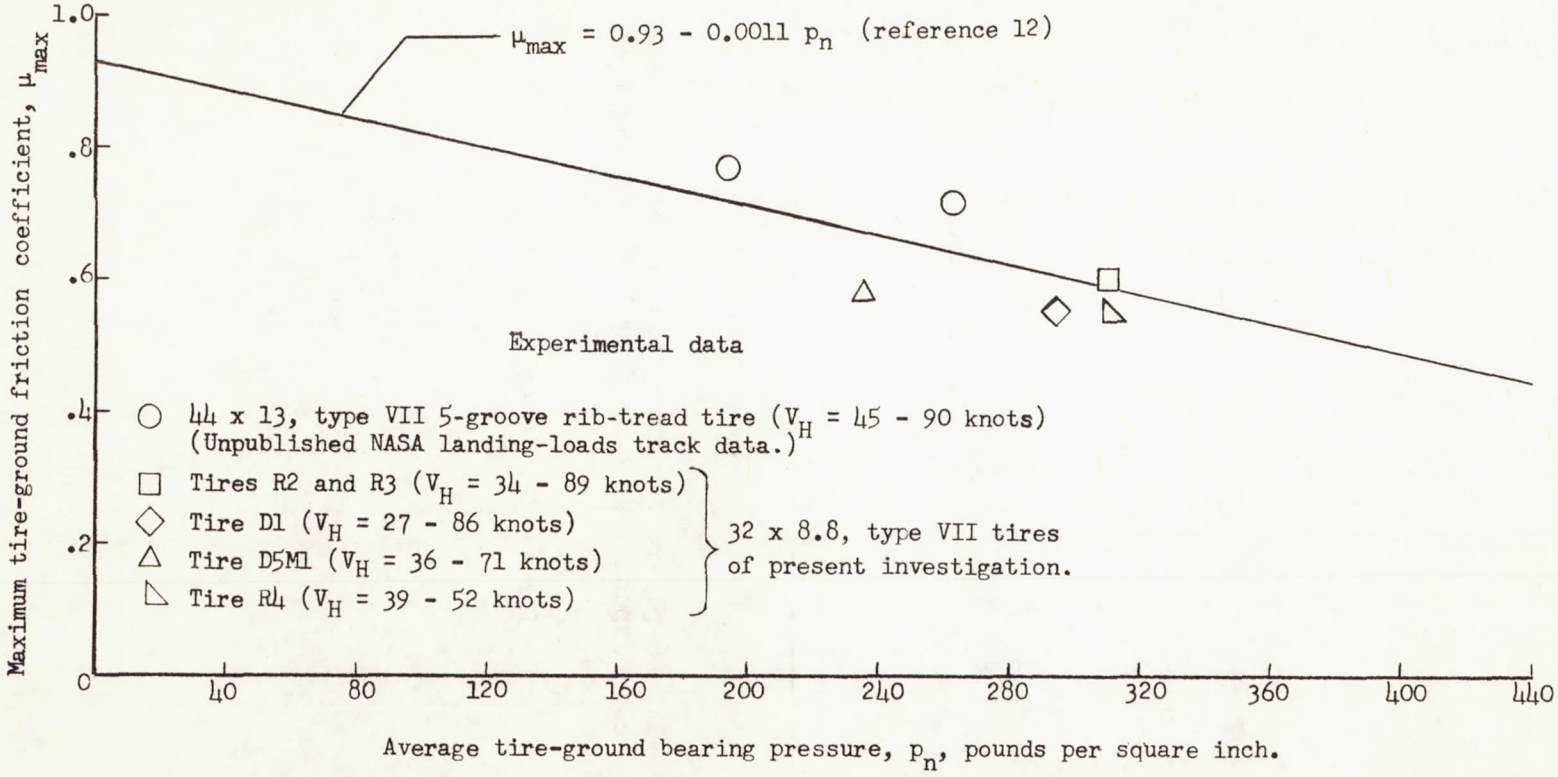

Figure 33.- Variation of maximum tire-ground friction coefficient μ_{max} with average tire-ground bearing pressure p_n for several different tires and tread designs on a dry concrete runway.

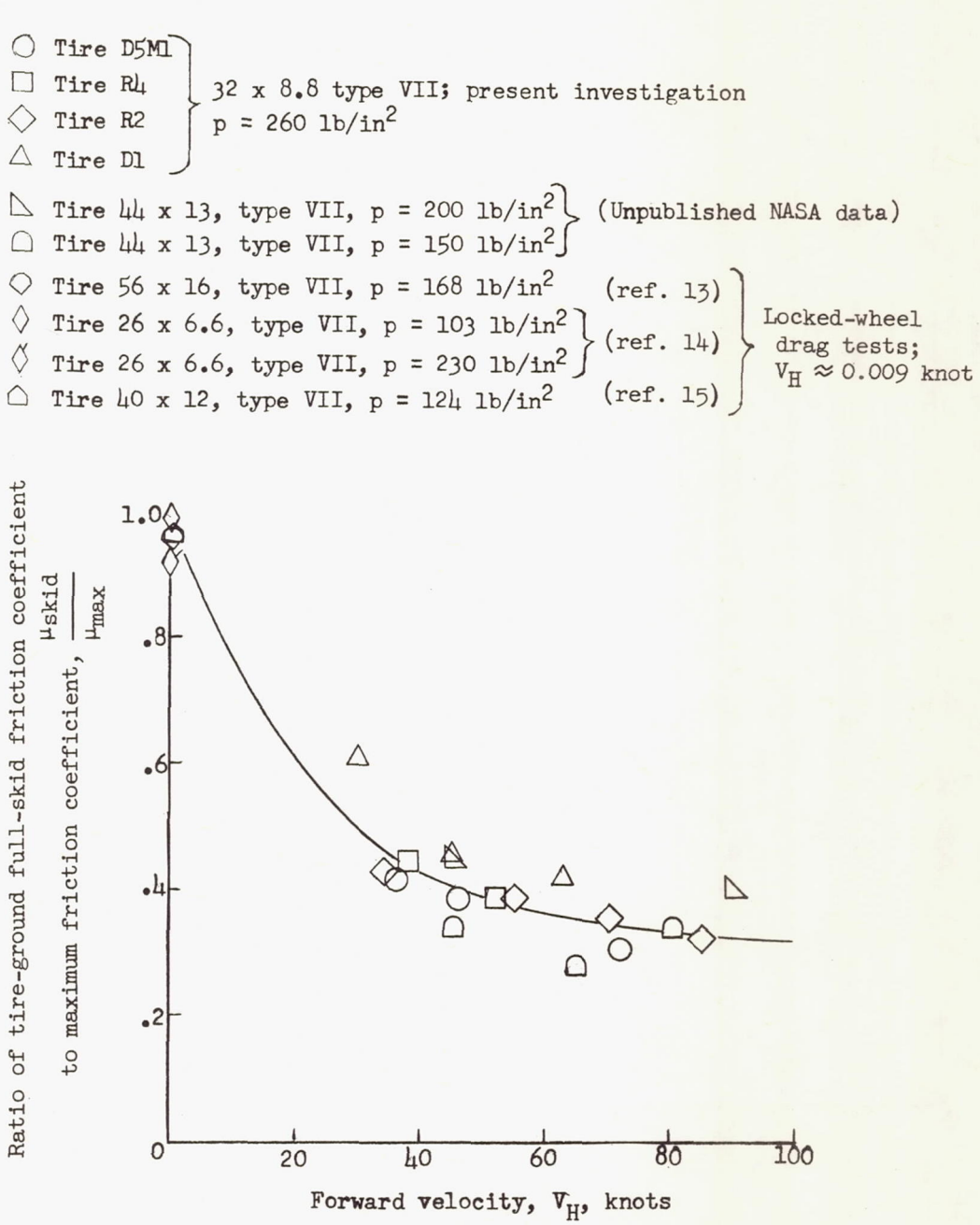

Figure 34.- Effect of forward velocity on the ratio of tire-ground full-skid friction coefficient to maximum friction coefficient $\frac{\mu_{skid}}{\mu_{max}}$. Data obtained on dry concrete runways.

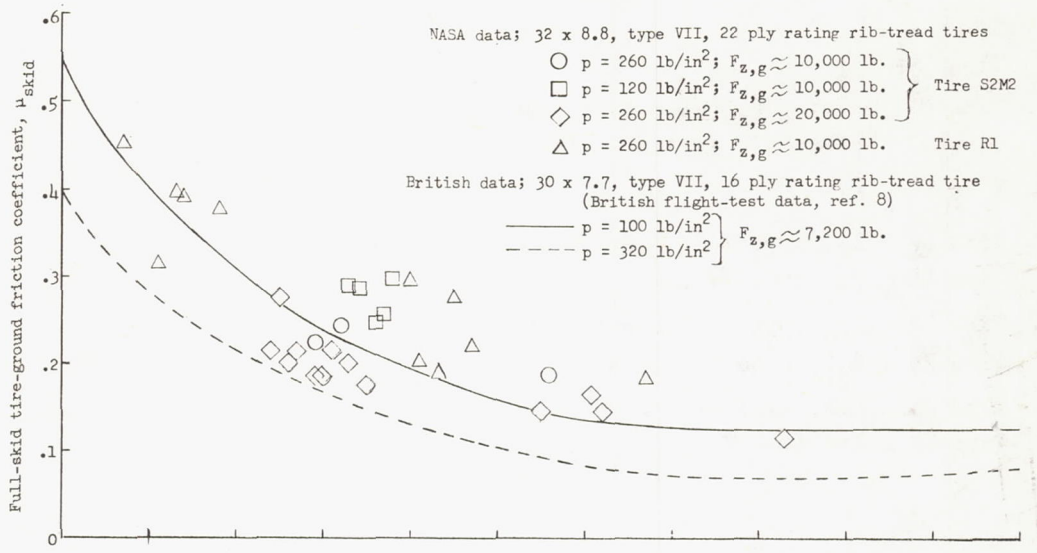

(a) Concrete runways.

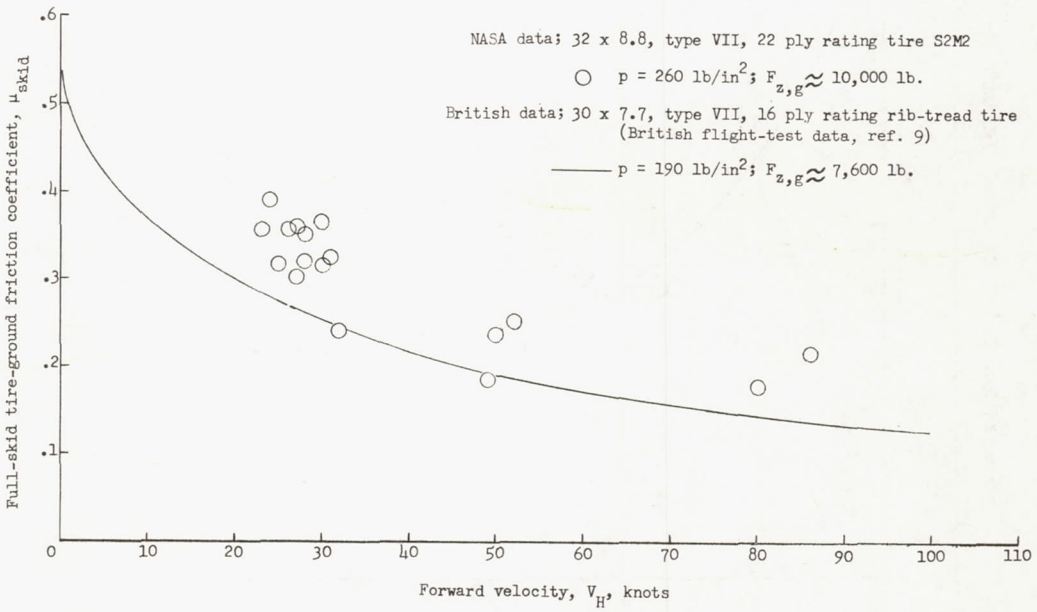

(b) Asphalt runways.

Figure 35.- Variation of full-skid tire-ground friction coefficient with forward velocity for several different rib-tread aircraft tires on water-covered concrete and asphalt runways. For NASA data, d_1 = 0 to 0.3 inch; for British data, $d_1 \approx 0.08$ inch.

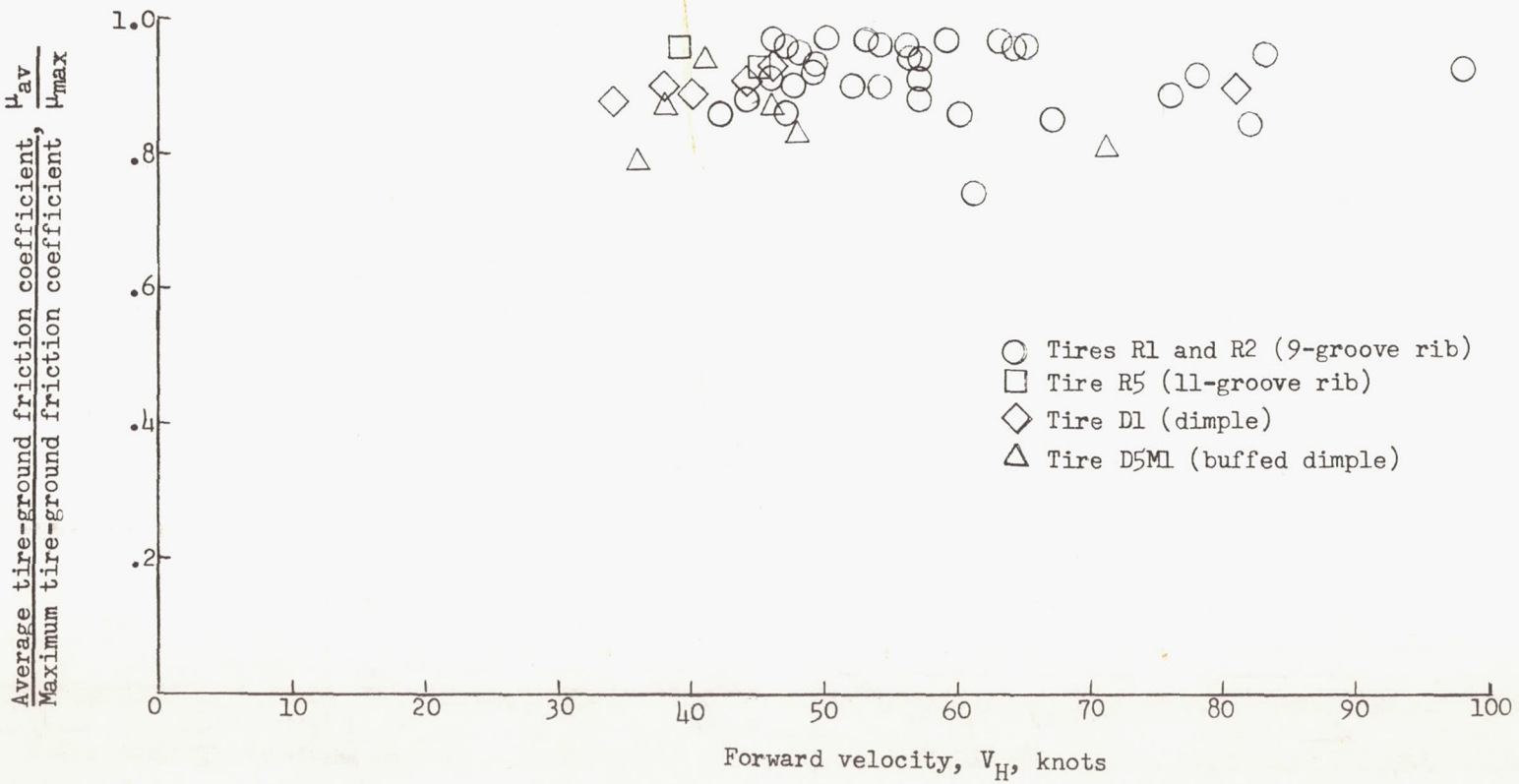

Figure 36.- Variation of the ratio of tire-ground friction coefficient $\frac{\mu_{av}}{\mu_{max}}$ with forward velocity for several tires on a dry concrete runway. $F_{Z,g} \approx 10,000$ pounds; p = 260 lb/sq in.

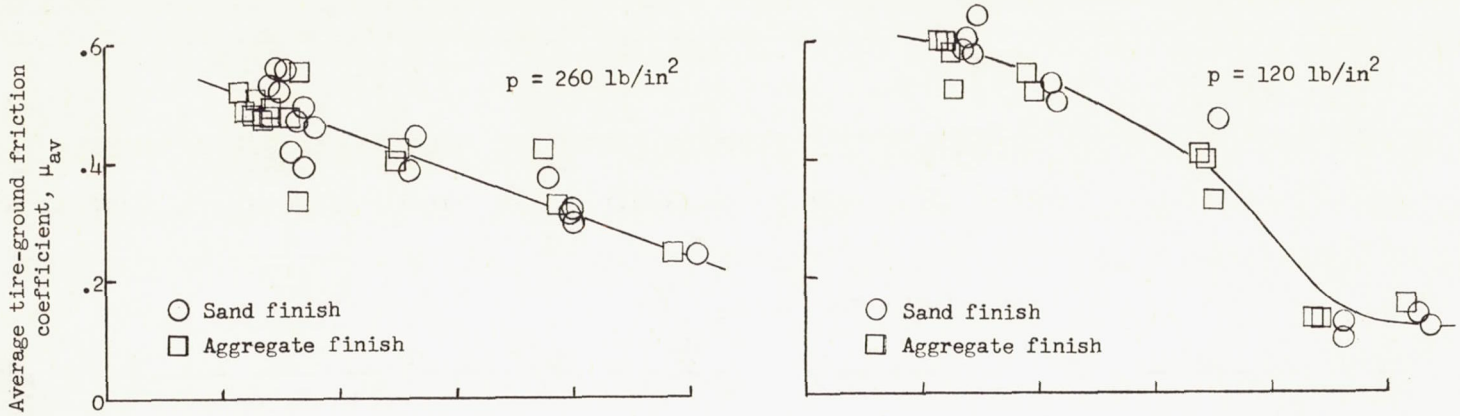

(a) Asphalt runway; d_1 = 0 to 0.5 inch.

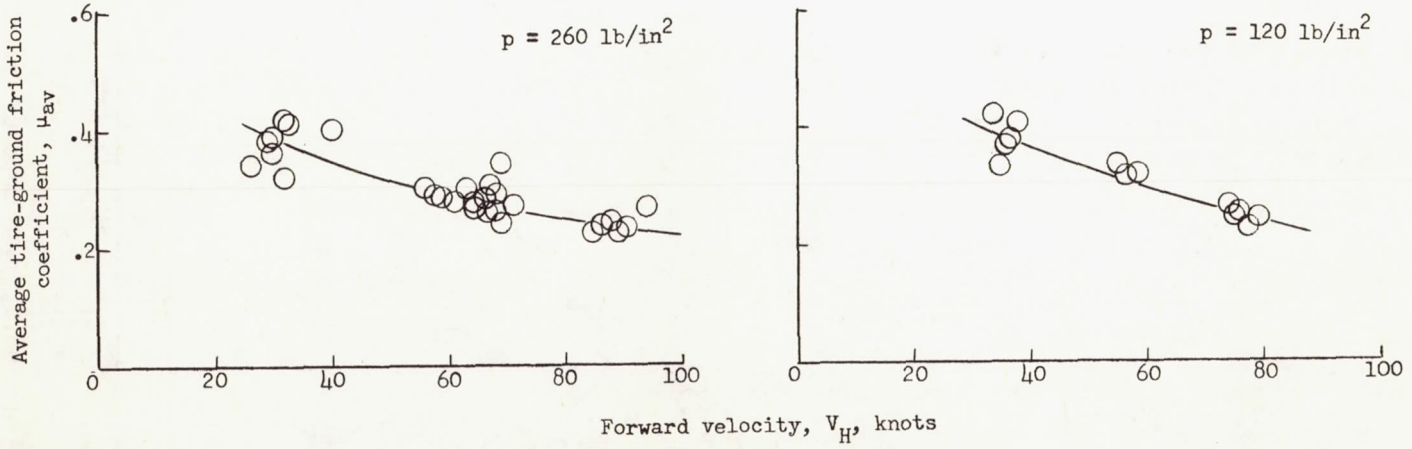

(b) Concrete runway; d_1 = 0 to 0.3 inch.

Figure 37.- Effect of runway surface on the magnitude of μ_{av} developed while braking tire S2M2 on water-covered runways.

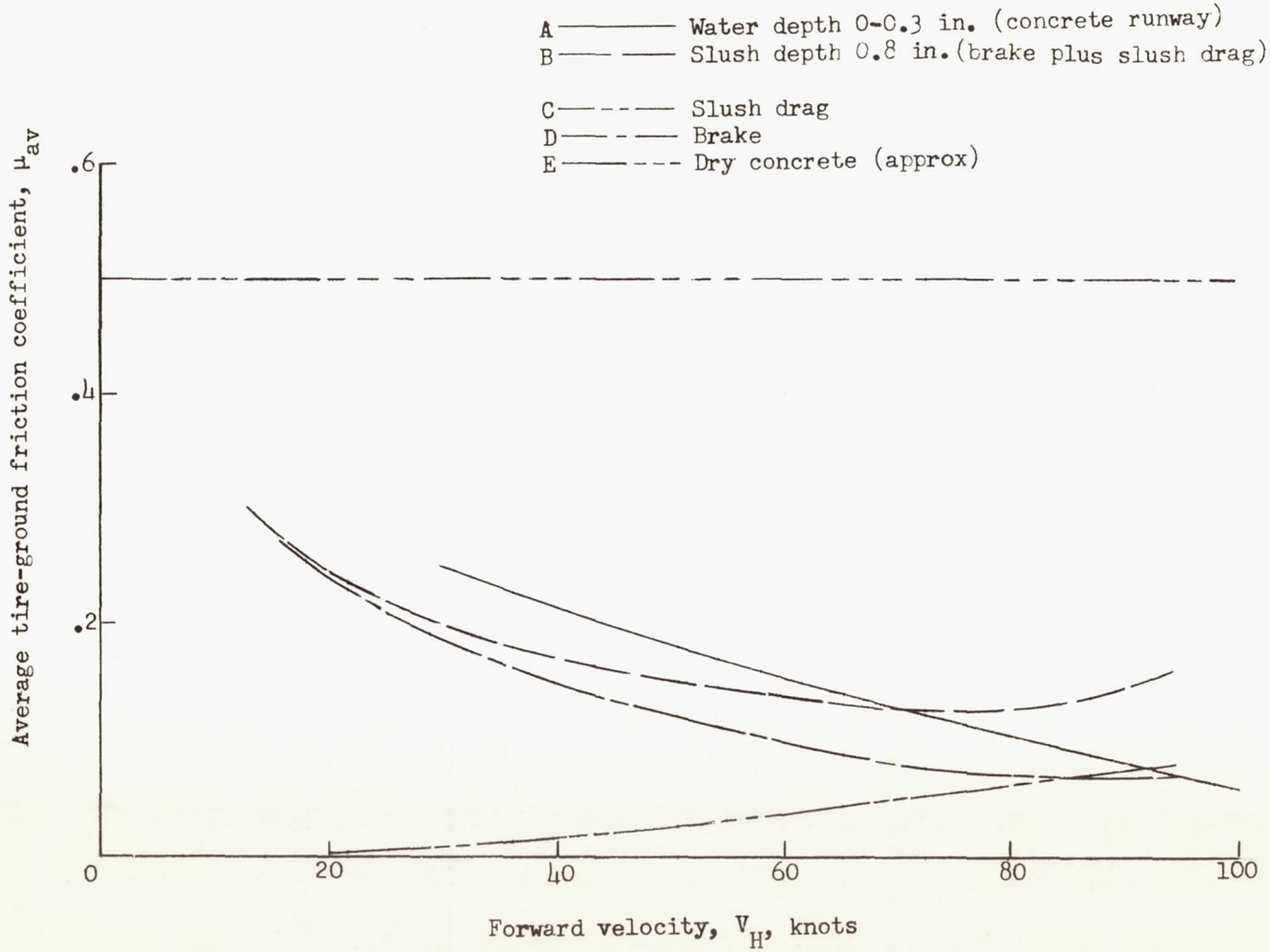

(a) Tire D2; dimple, fabric-reinforced tread, fabric surface.

Figure 38.- Average tire-ground friction coefficient obtained during single-wheel braking runs on slush- and water-covered runway surfaces. $F_{z,g} \approx 10,000$ pounds; p = 260 lb/sq in.

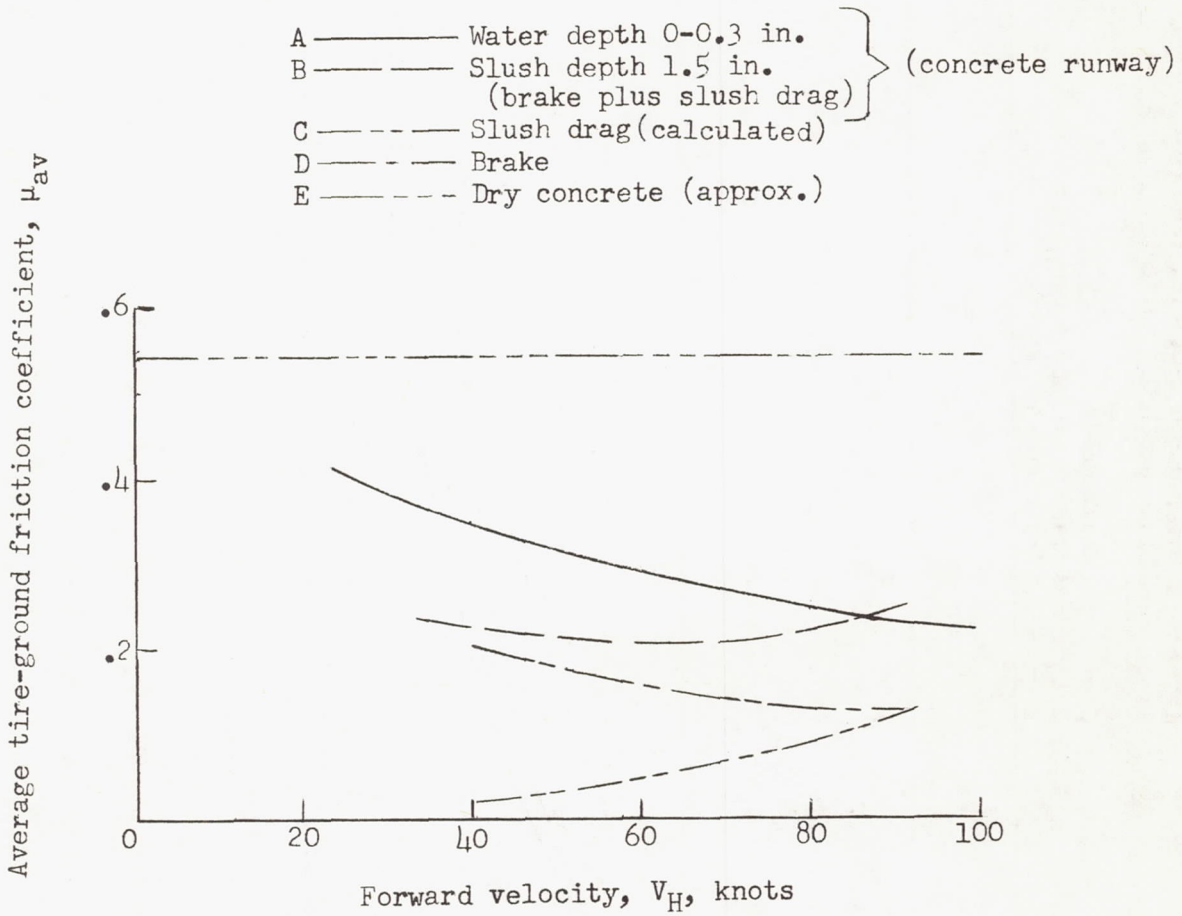

(b) Tire S2M2; fabric-reinforced rib tread, rubber surface.

Figure 38.- Concluded.

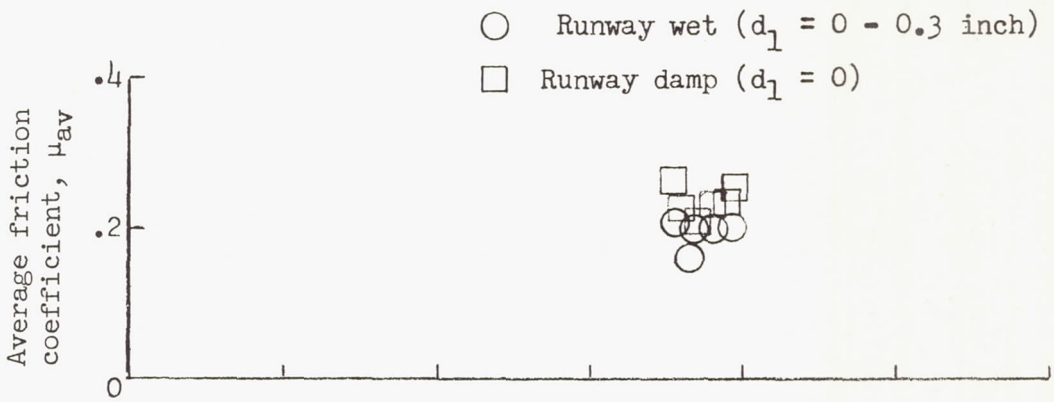

(a) Concrete runway; tire S1M3.

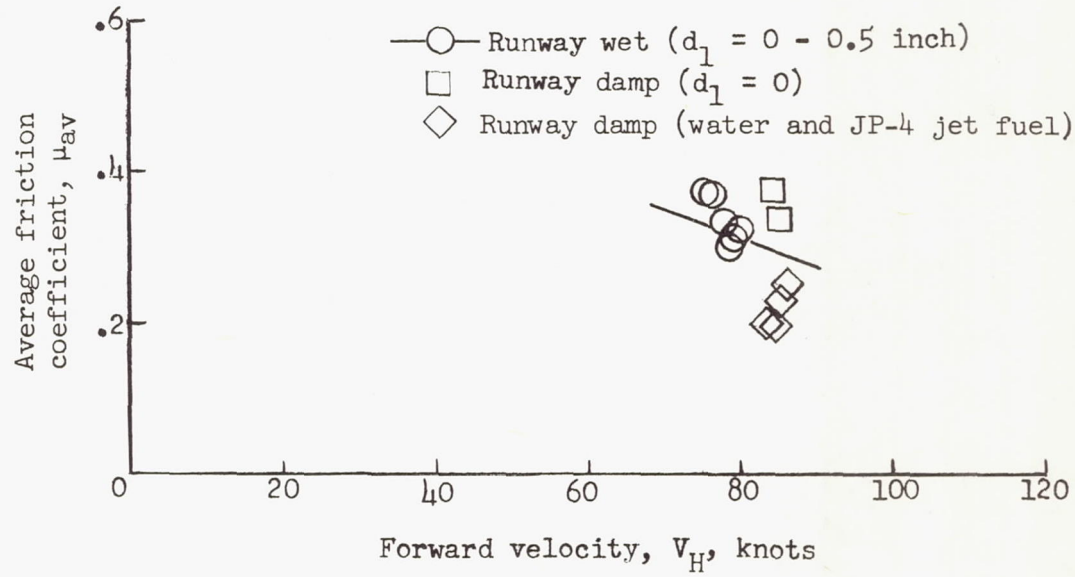

(b) Asphalt runway; tire S2M2.

Figure 39.- Comparison of average tire-ground friction coefficients obtained on water-covered and damp runways. Data obtained during single-wheel braking tests. $F_{z,g} \approx 10,000$ pounds; p = 260 lb/sq in.

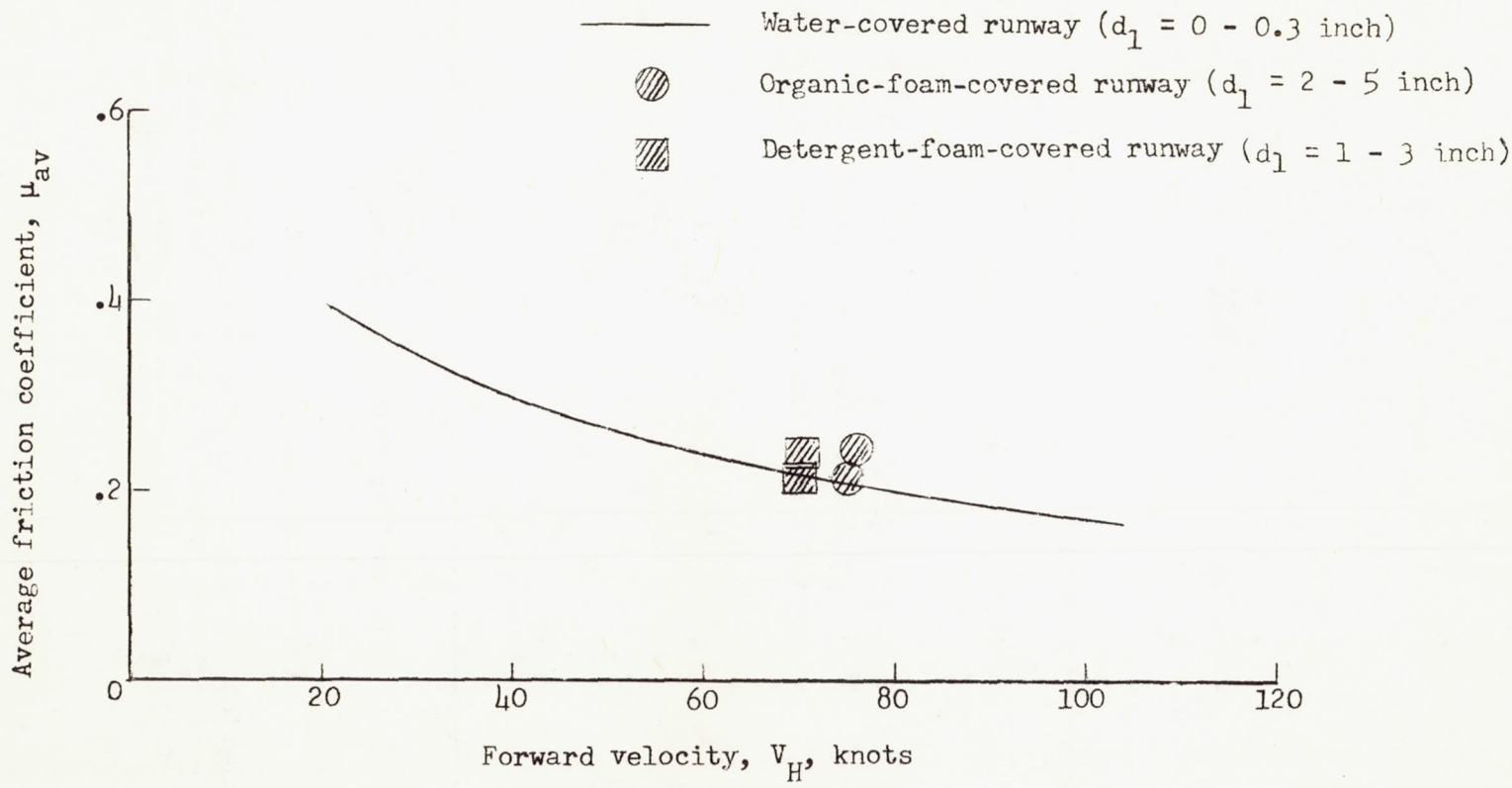

Figure 40.- Comparison of average tire-ground friction-coefficient values obtained during single-wheel braking tests on foam- and water-covered runways for tire S2M2.

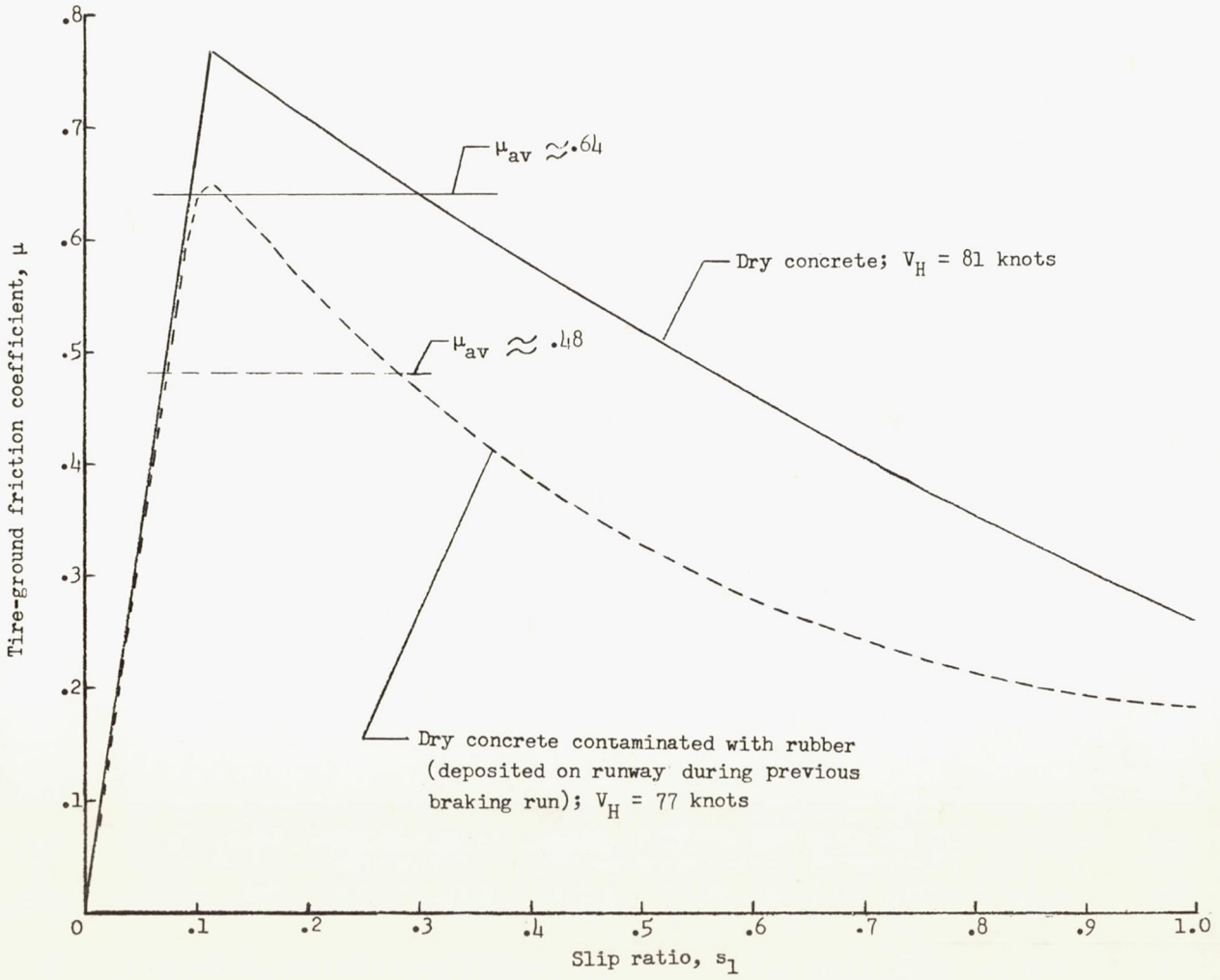

Figure 41.- Effect of rubber contamination of a concrete runway surface on the braking friction developed by a 44x13, type VII, 26-ply-rating aircraft tire. $F_{Z,g} \approx 20,400$ pounds; p = 150 lb/sq in. (Unpublished NASA landing-loads-track data.)

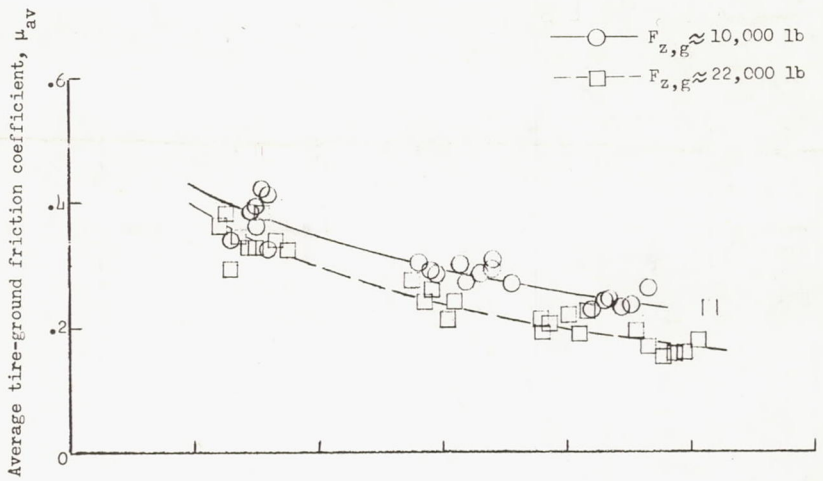

(a) Average tire-ground friction coefficient μ_{av}.

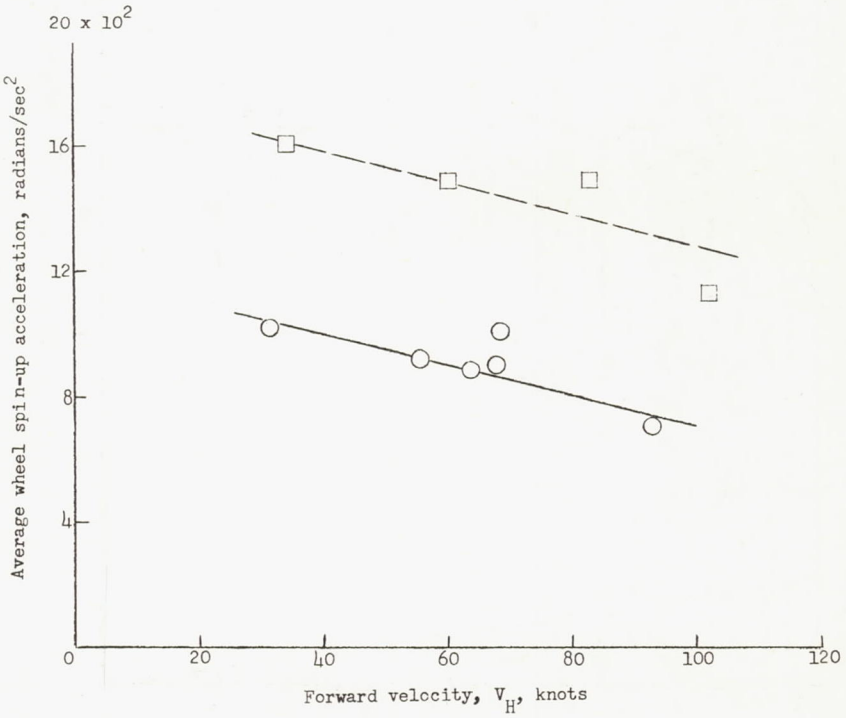

(b) Average wheel spin-up acceleration.

Figure 42.- Average tire-ground friction coefficients and wheel spin-up accelerations obtained during single-wheel braking runs with tire S2M2 at ground vertical loads of approximately 10,000 and 22,000 pounds. Wet concrete runway; d_1 = 0 to 0.3 inch; p = 260 lb/sq in.

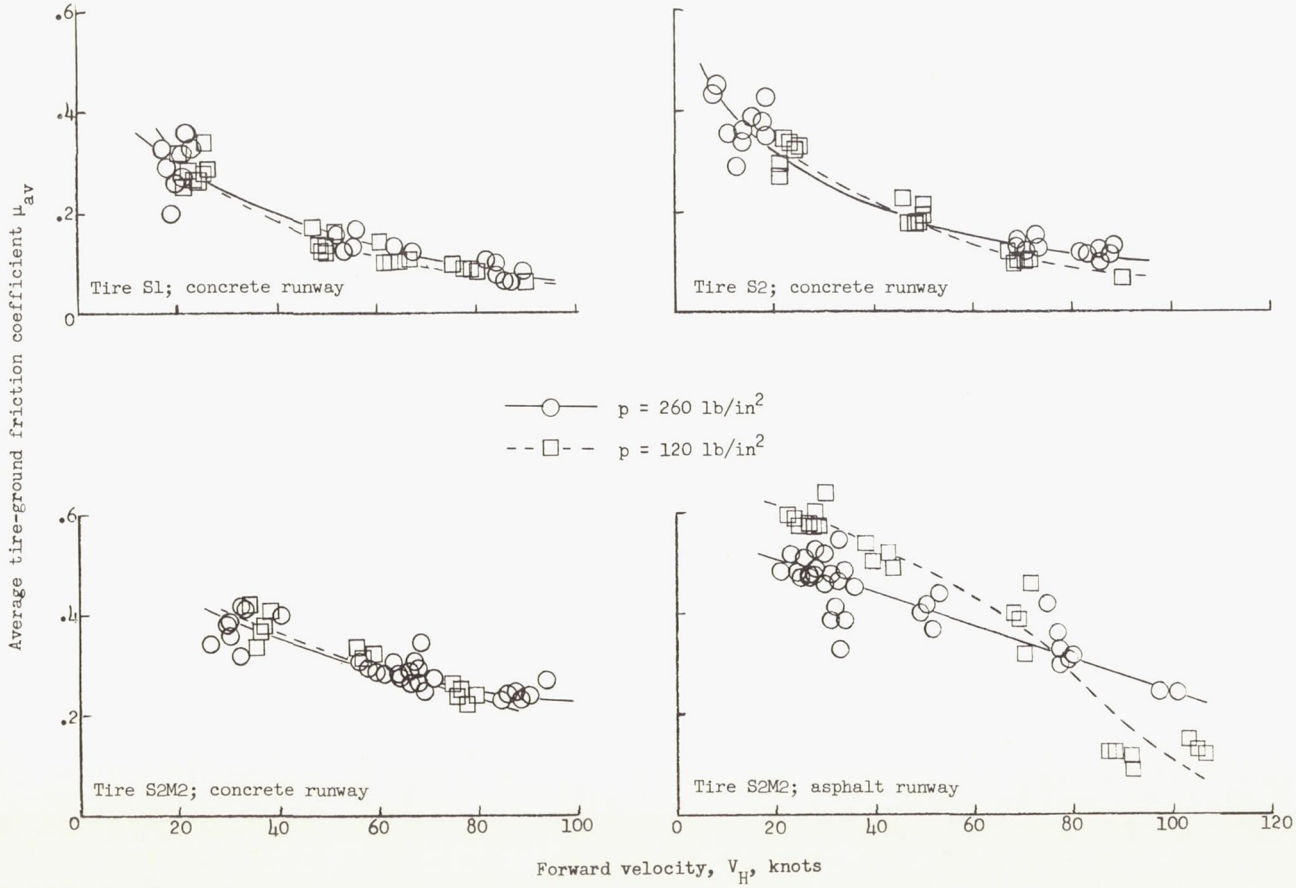

(a) Average tire-ground friction coefficient μ_{av}.

Figure 43.- Effect of tire inflation pressure on average tire-ground friction coefficients and wheel spin-up accelerations. Data were obtained during single-wheel braking tests on wet runways for several different tires. $F_{z,g} \approx 10,000$ pounds; d_1 (asphalt) = 0 to 0.5 inch; d_1 (concrete) = 0 to 0.3 inch.

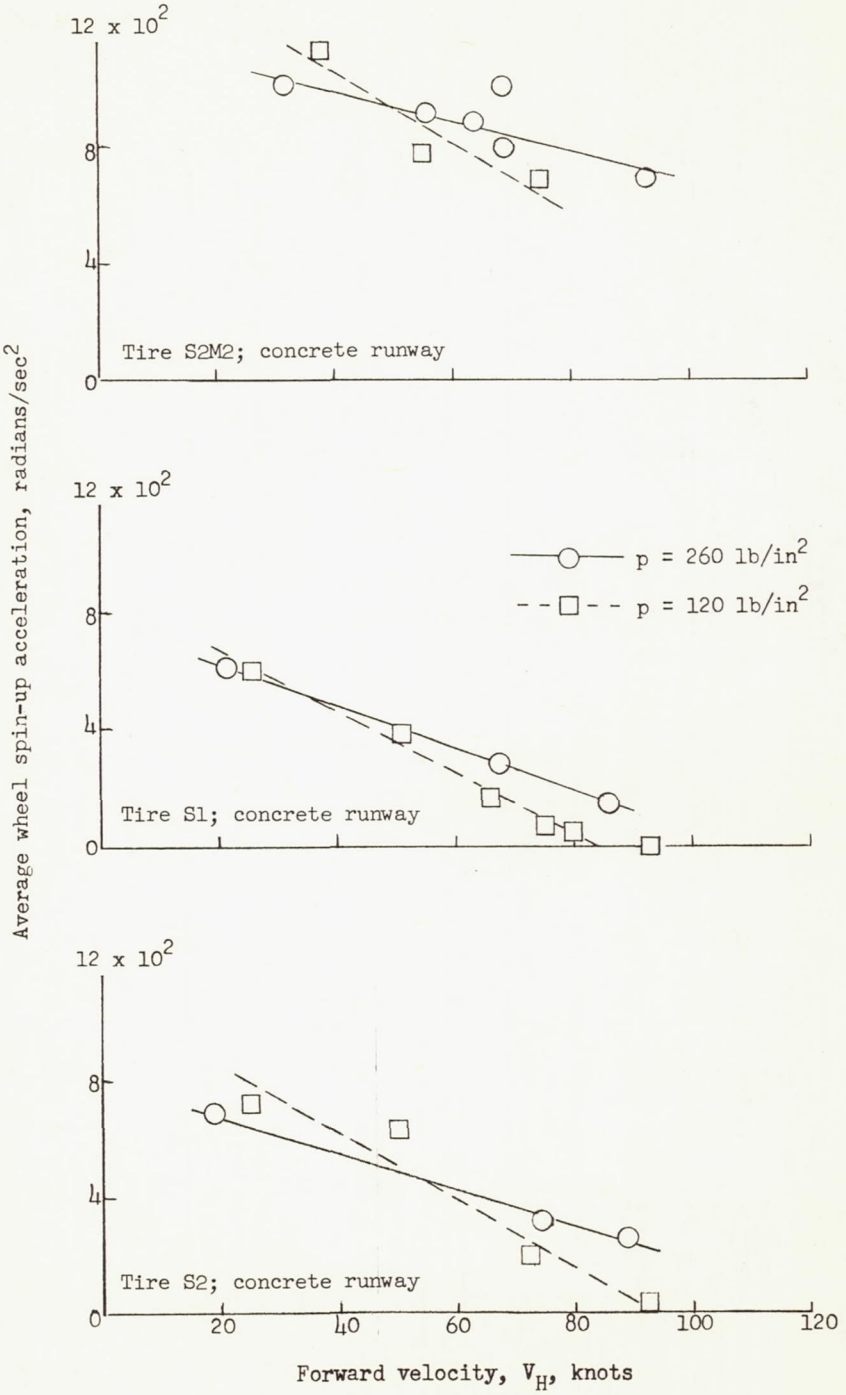

(b) Average wheel spin-up acceleration.

Figure 43.- Concluded.

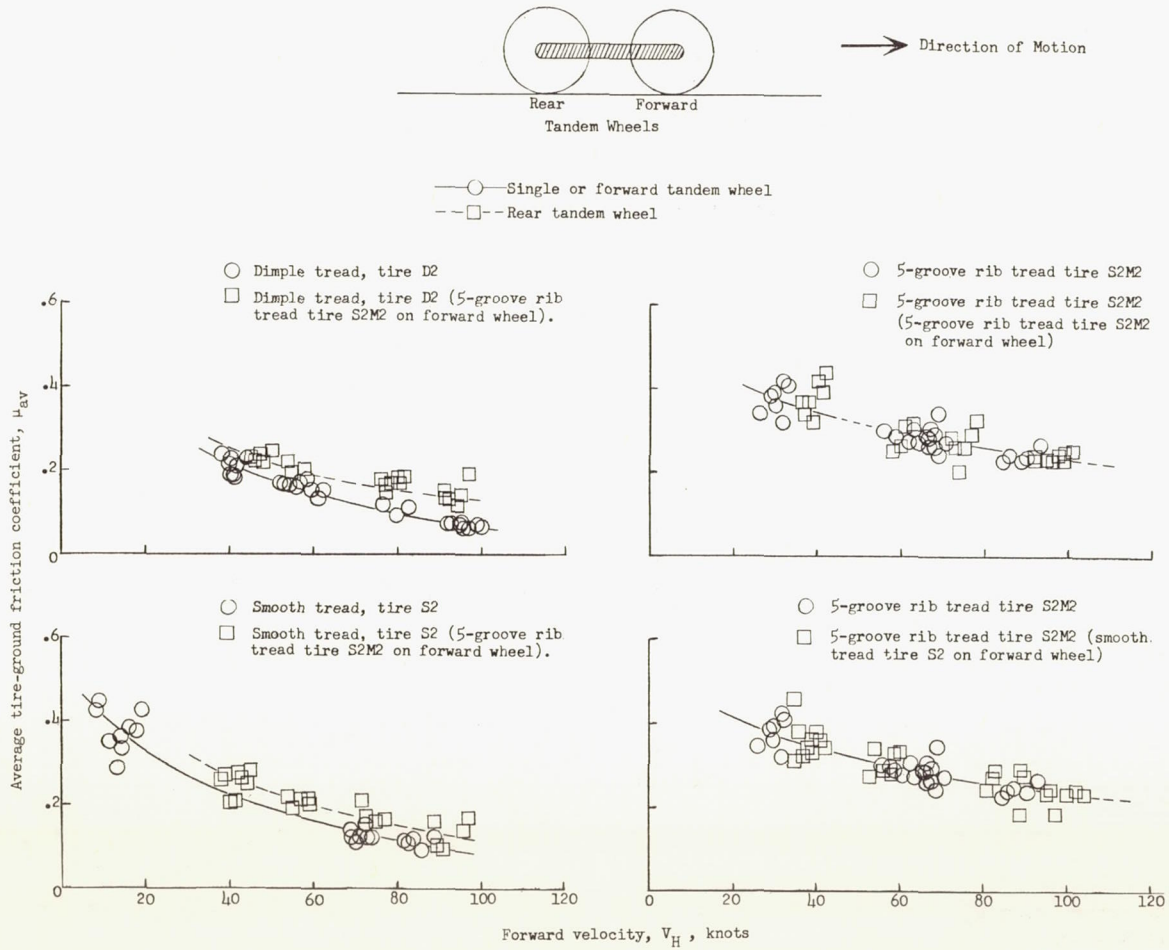

(a) Average tire-ground friction coefficient μ_{av}.

Figure 44.- Effect of tire position in a tandem wheel arrangement on average tire-ground friction coefficients and wheel spin-up accelerations developed during braking tests on wet concrete runways. $F_{z,g} \approx 10{,}000$ pounds per tire; p = 260 lb/sq in.; d_1 = 0 to 0.3 inch.

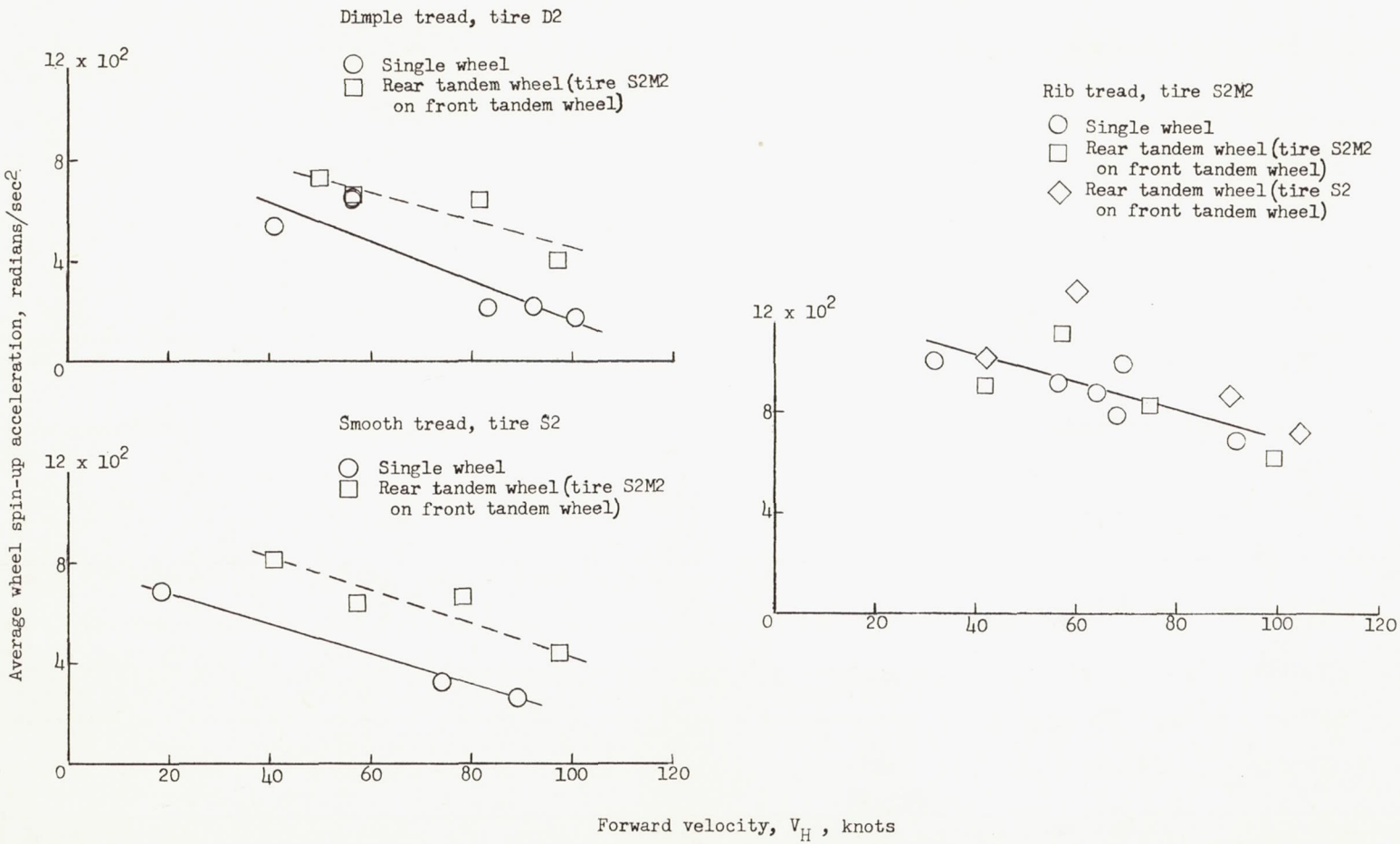

(b) Average wheel spin-up acceleration.

Figure 44.- Continued.

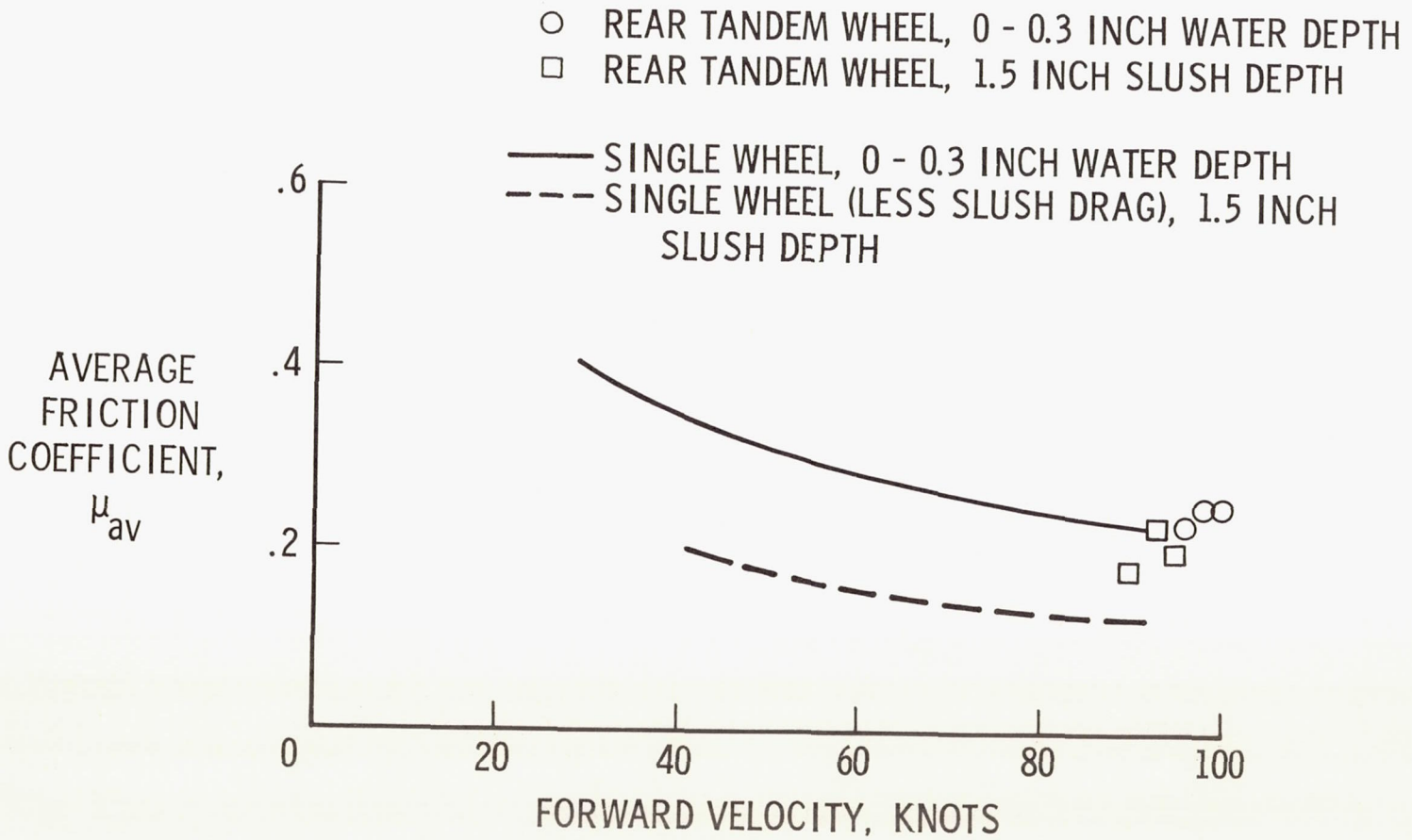

(c) Average tire-ground friction coefficient μ_{av} for tire S2M2 braking in slush and water.

Figure 44.- Concluded.

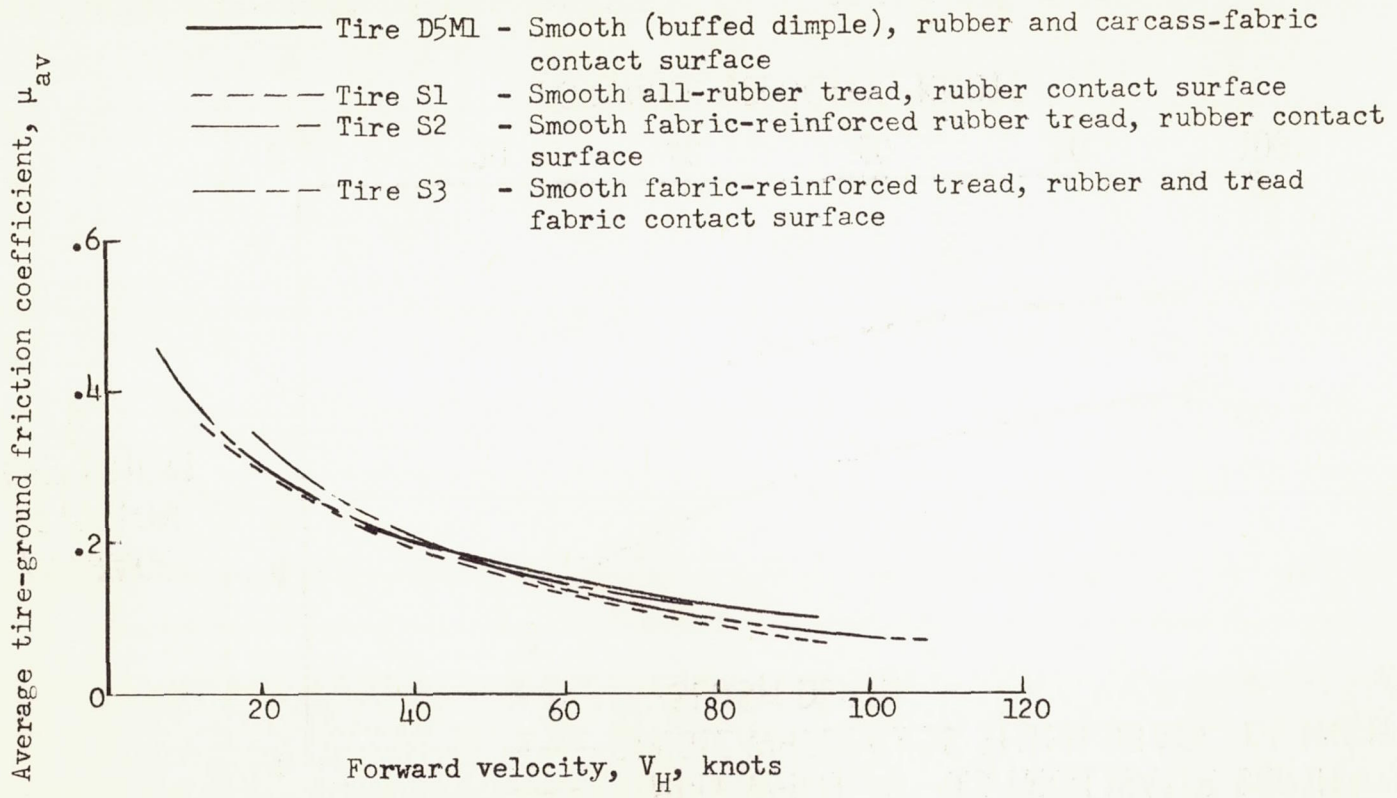

Figure 45.- Effect of tire tread material on the average tire-ground friction coefficients developed during single-wheel braking tests on wet concrete runways. $F_{Z,g} \approx 10,000$ pounds; p = 260 lb/sq in; d_1 = 0 to 0.3 inch.

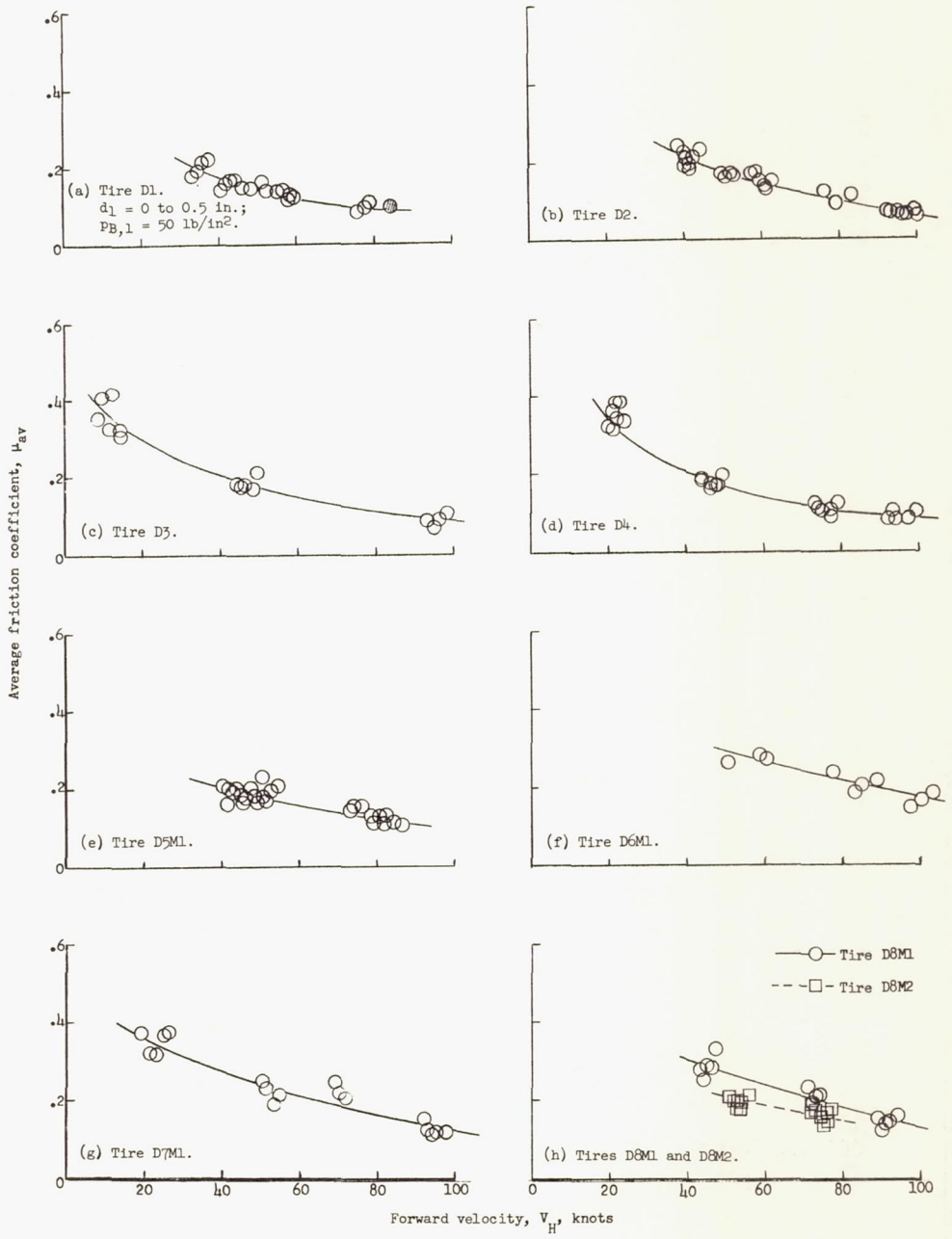

Figure 46.- Variations of average tire-ground friction coefficient with forward velocity for the different tires investigated during single-wheel braking tests on a water-covered concrete runway. Test conditions, except where noted, are $F_{Z,g} \approx 10{,}000$ pounds, $p = 260$ lb/sq in., and $d_1 = 0$ to 0.3 inch. Shaded circle symbols in this figure denote average values over several braking cycles due to inability of tire to spin up after brake release.

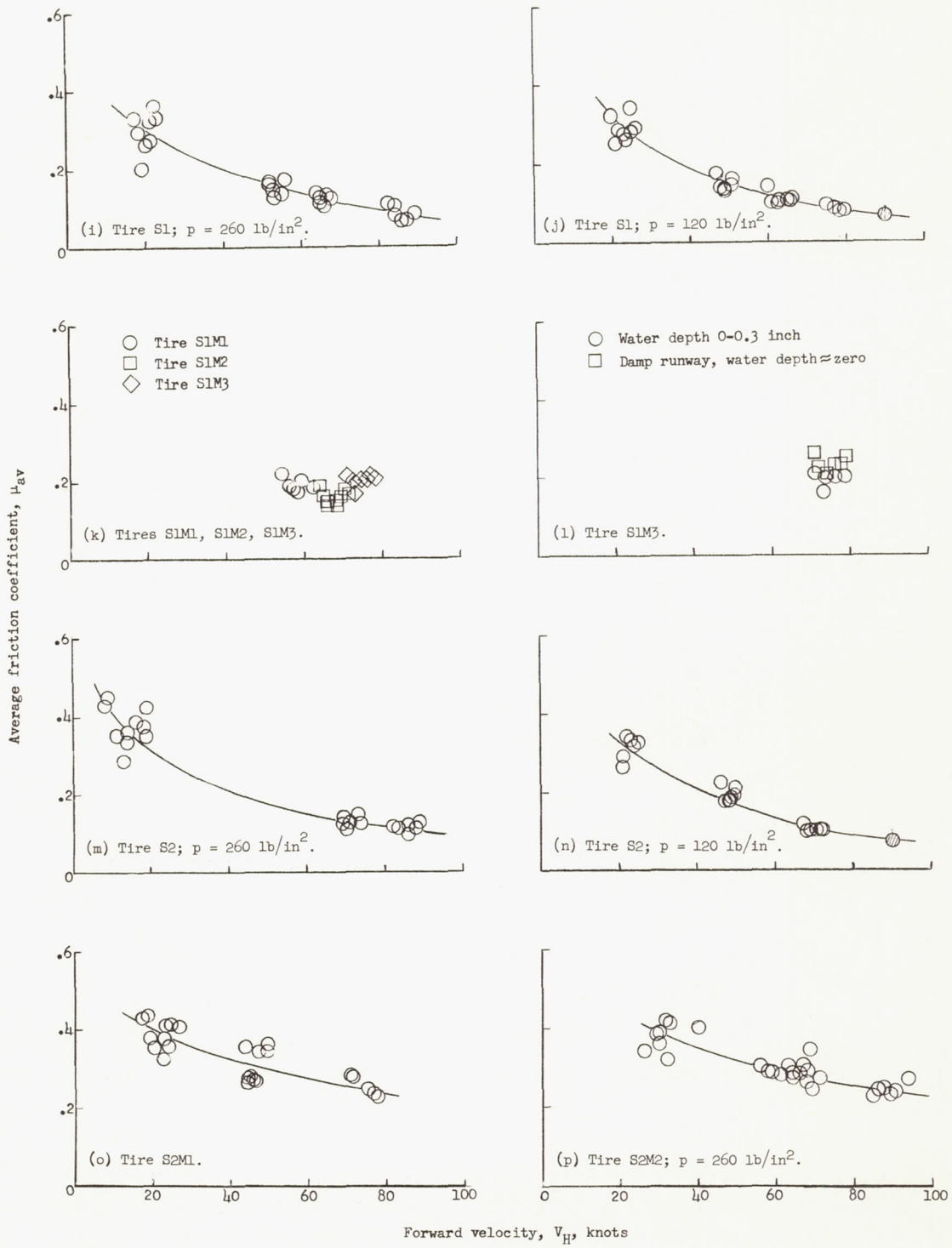

Figure 46.- Continued.

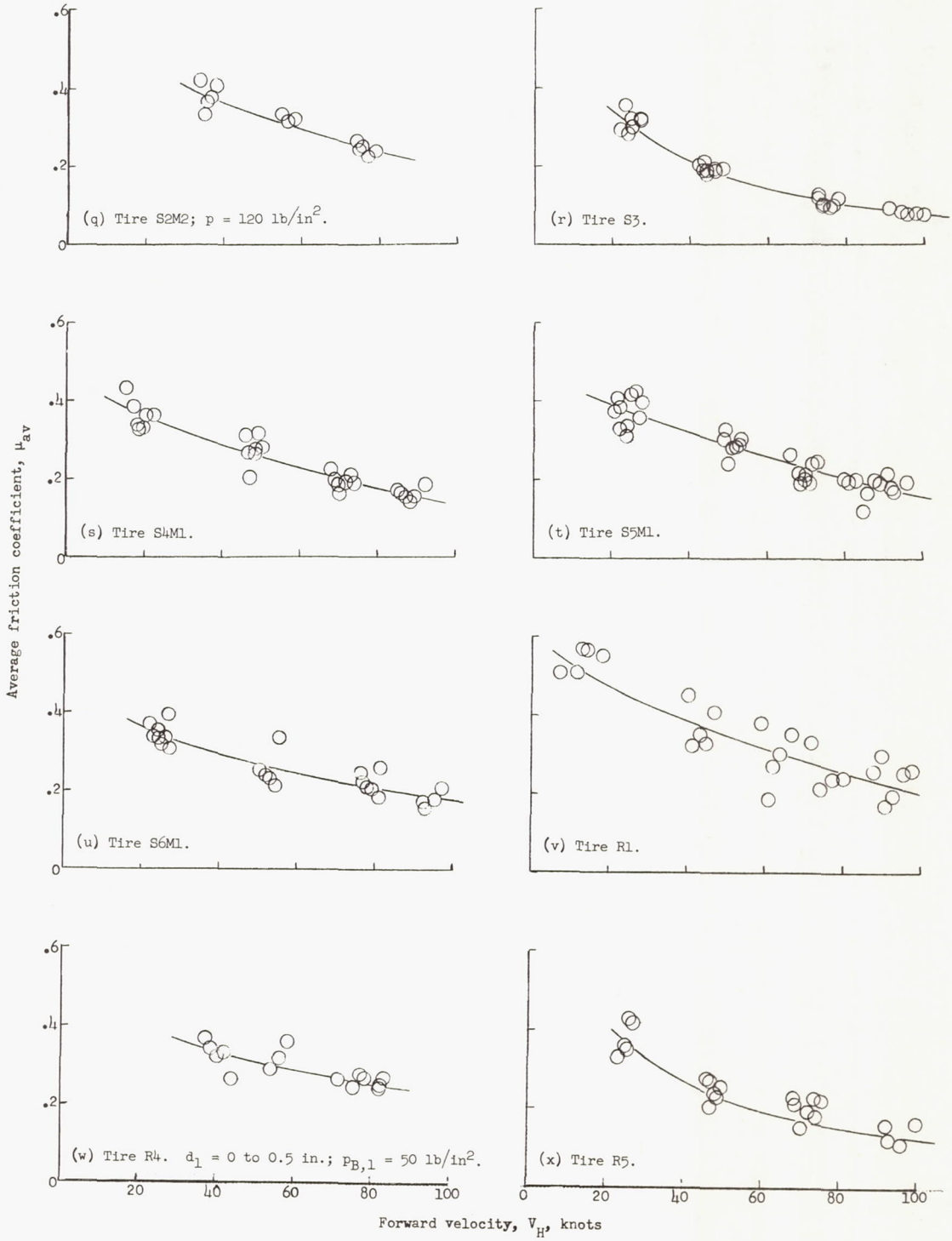

Figure 46.- Concluded.

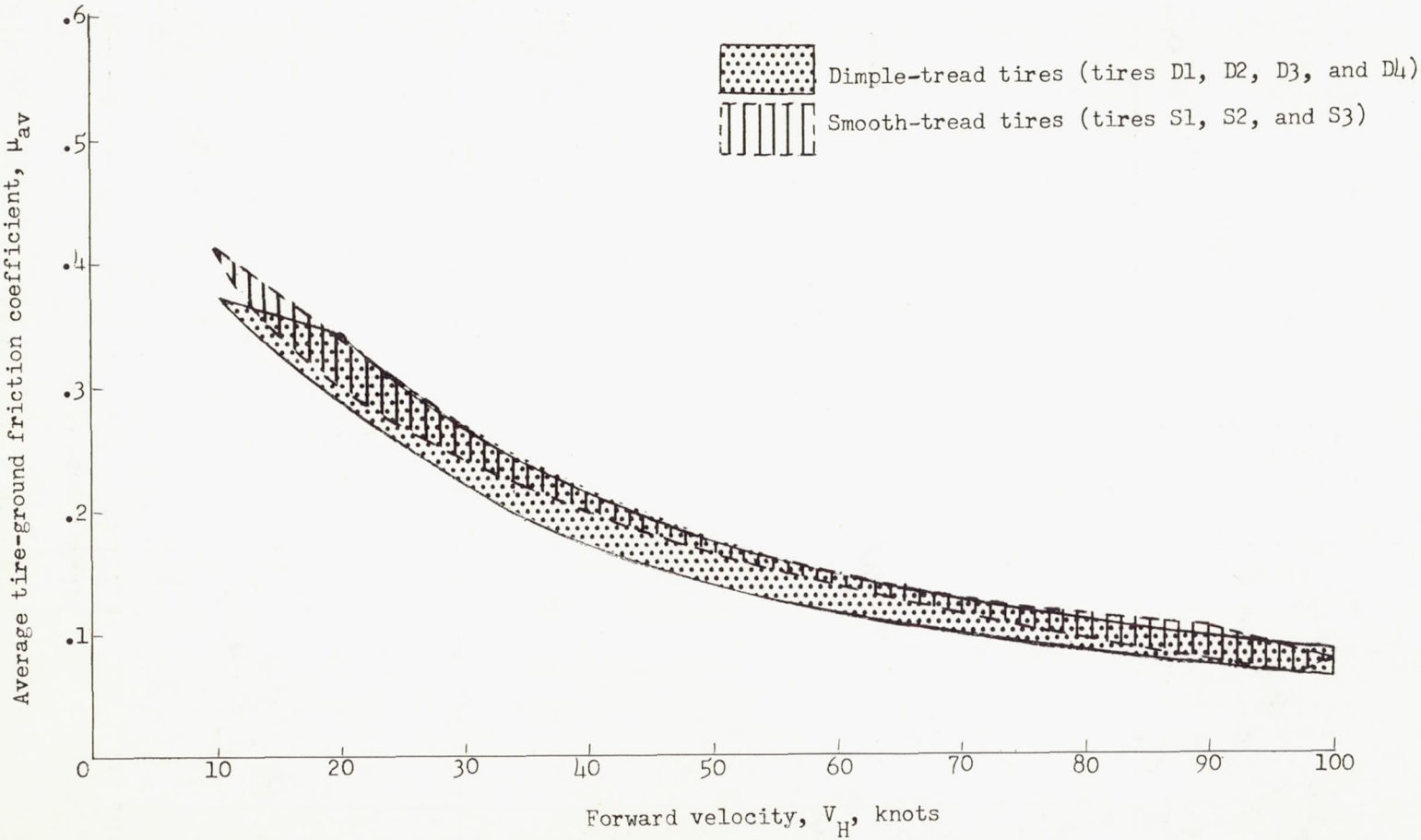

Figure 47.- Average tire-ground friction coefficients obtained with smooth- and dimple-tread tires during braking tests on a water-covered concrete runway. $F_{z,g} \approx 10,000$ pounds; $p = 260$ lb/sq in.; $d_1 = 0$ to 0.3 inch.

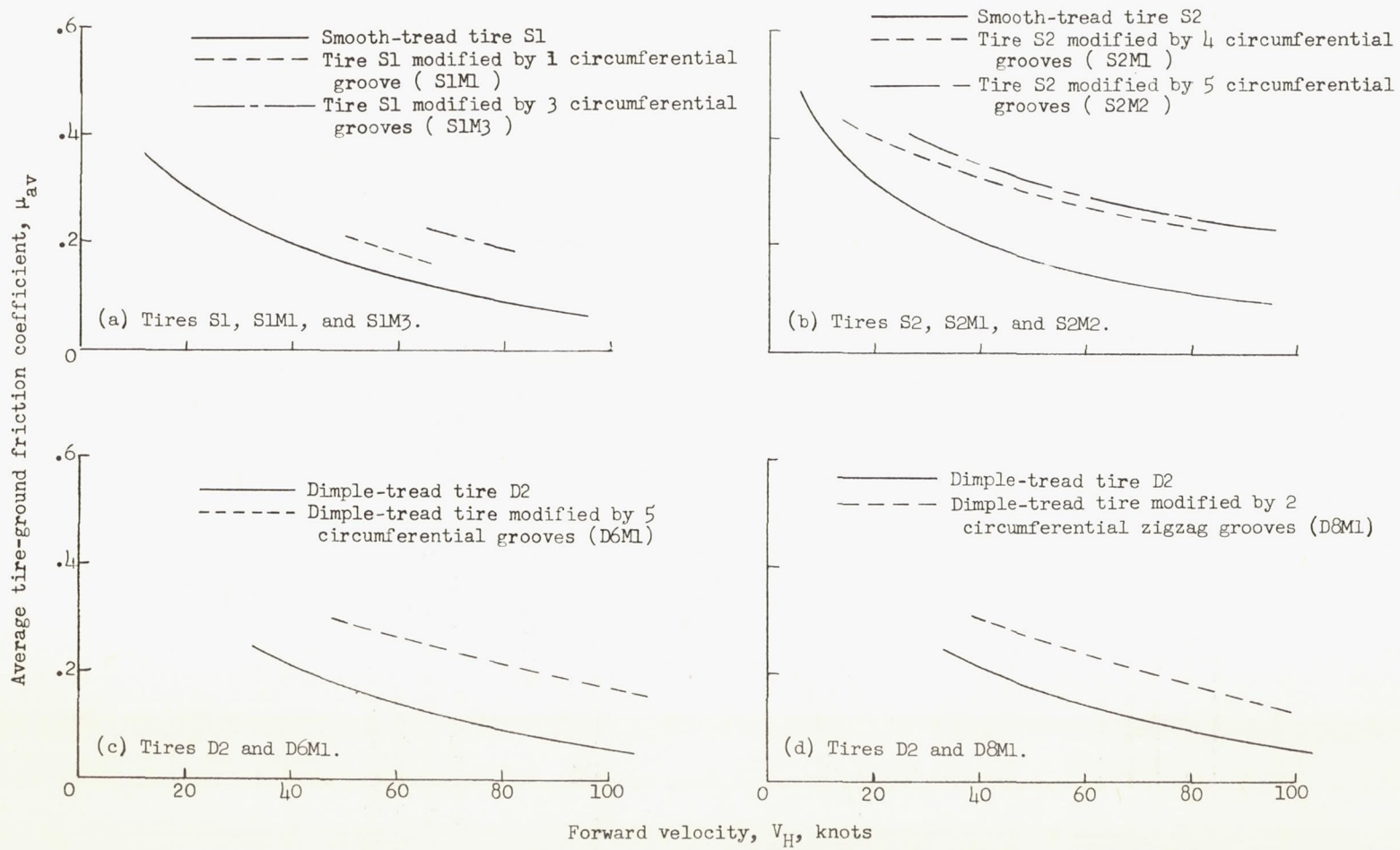

Figure 48.- Braking effectiveness of smooth- and dimple-tread tires on water-covered runways before and after circumferential grooves were cut into tire tread. $F_{z,g} \approx 10,000$ pounds; $p = 260$ lb/sq in.; $d_1 = 0$ to 0.3 inch.

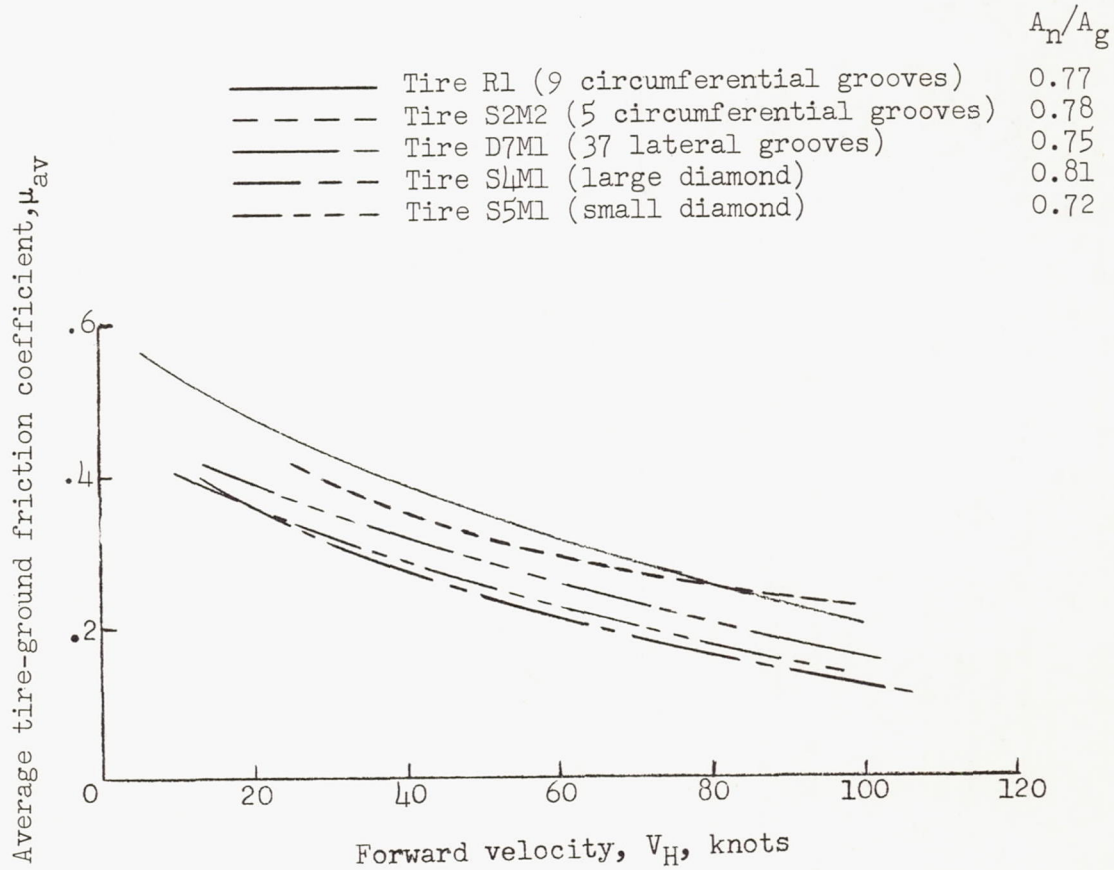

Figure 49.- Wet-runway braking effectiveness of tire treads with lateral grooves, diamond patterns, and circumferential grooves. Data obtained during single-wheel braking tests on a wet concrete runway. $F_{z,g} \approx 10,000$ pounds; $p = 260$ lb/sq in.; $d_1 = 0$ to 0.3 inch.

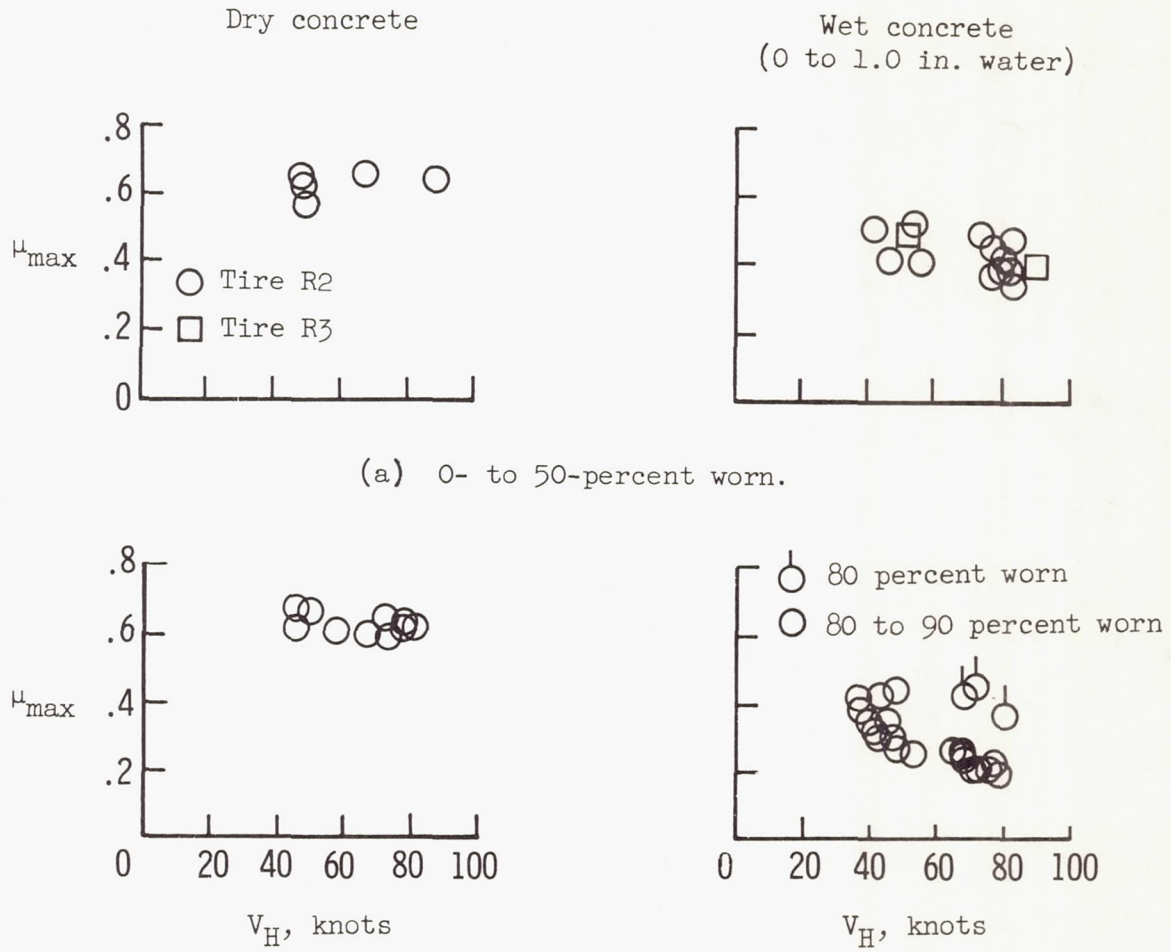

(a) 0- to 50-percent worn.

(b) 50- to 90-percent worn.

Figure 50.- Effect of tread wear on maximum tire-ground friction coefficient μ_{max} for tires R2 and R3 (9 circumferential grooves, all-rubber tread). $F_{z,g} \approx 10{,}000$ pounds; p = 260 lb/sq in.

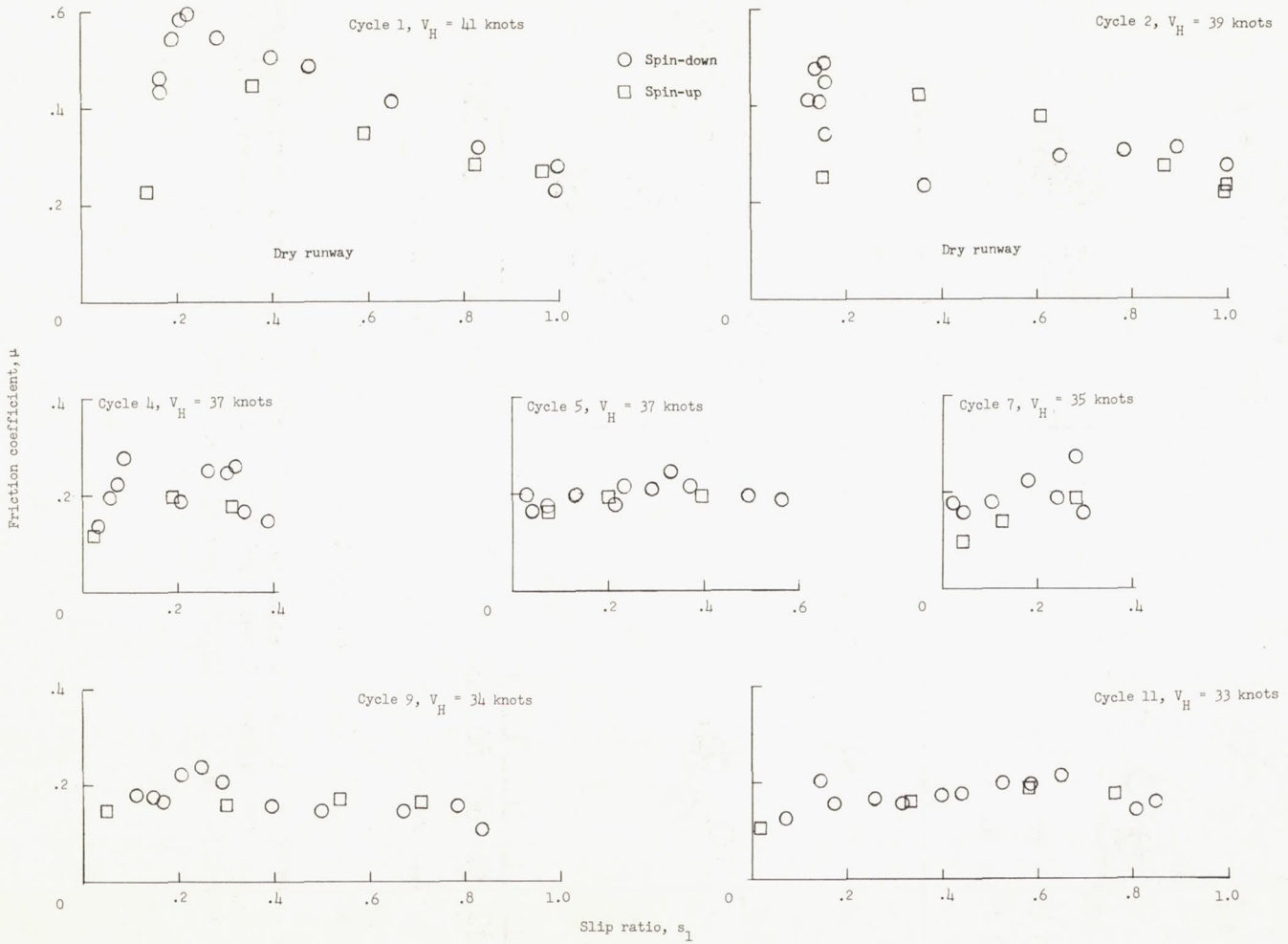

(a) Run 1.

Figure 51.- Tire D1, dimple fabric-reinforced tread, fabric surface. Antiskid unit operating; p = 260 lb/sq in.; d_1 = 0.2 to 0.5 inch (except where noted); $p_{B,1}$ = 50 lb/sq in.

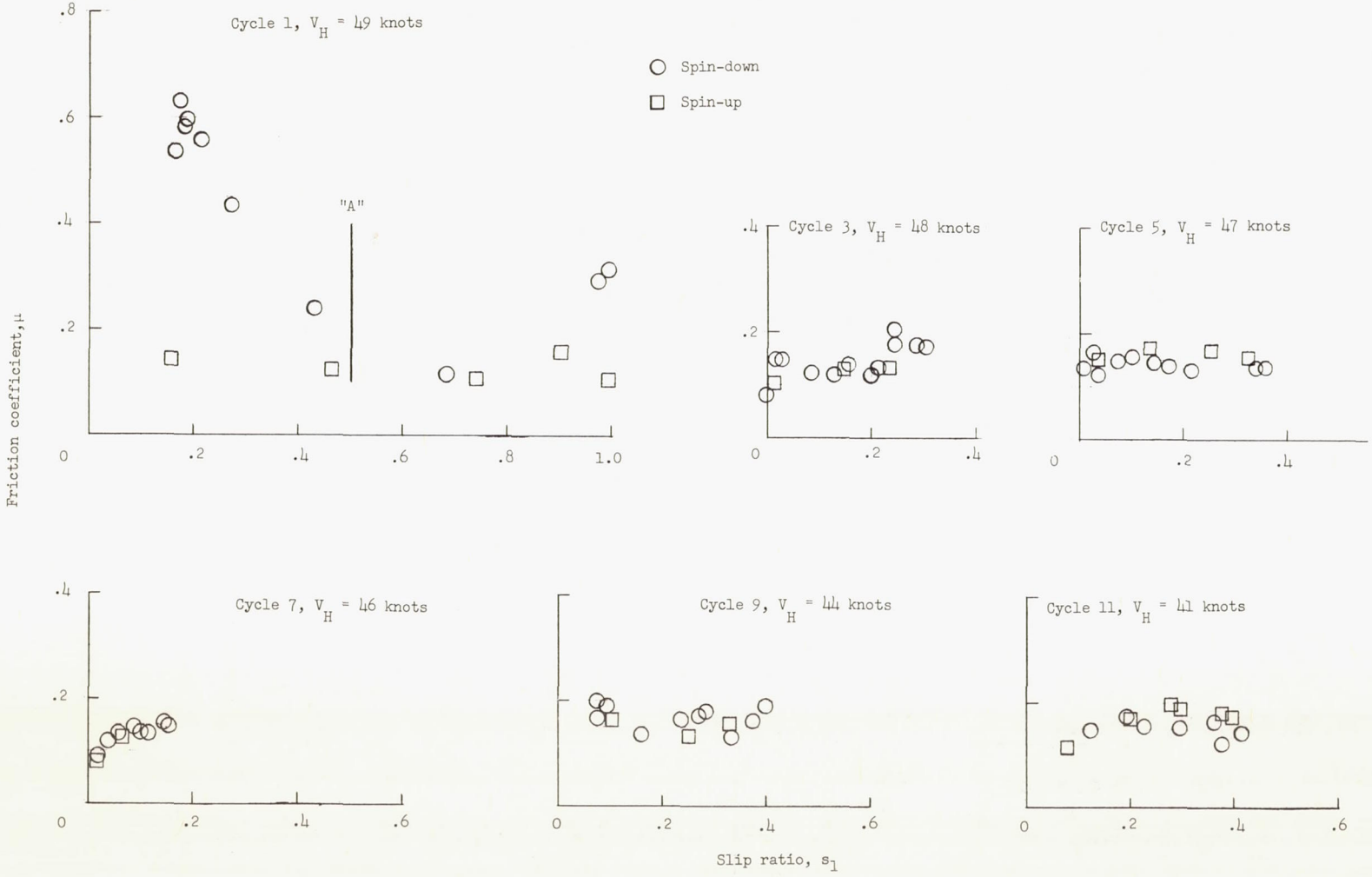

(b) Run 2.

Figure 51.- Continued.

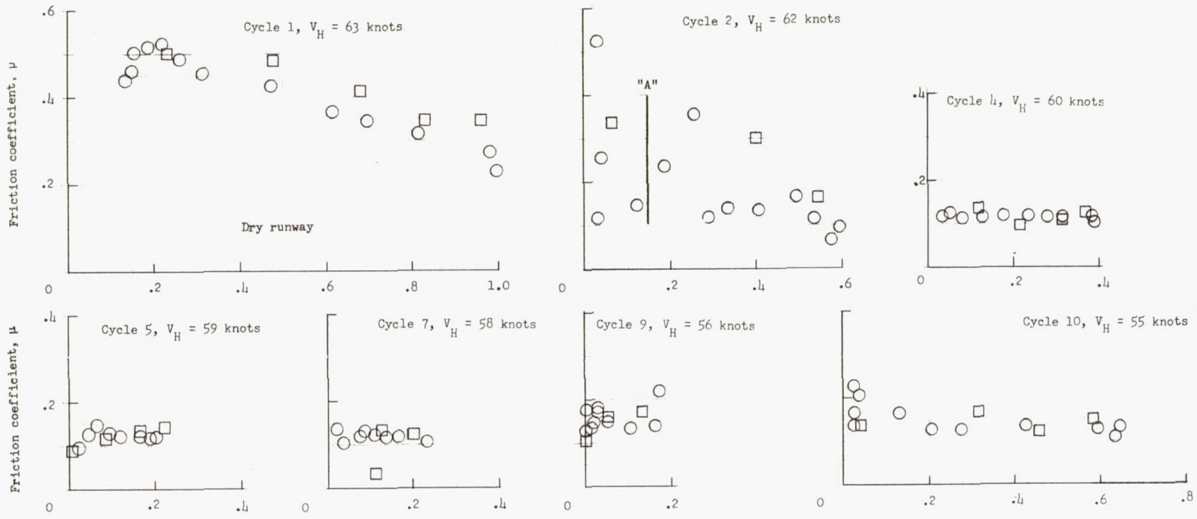

(c) Run 3.

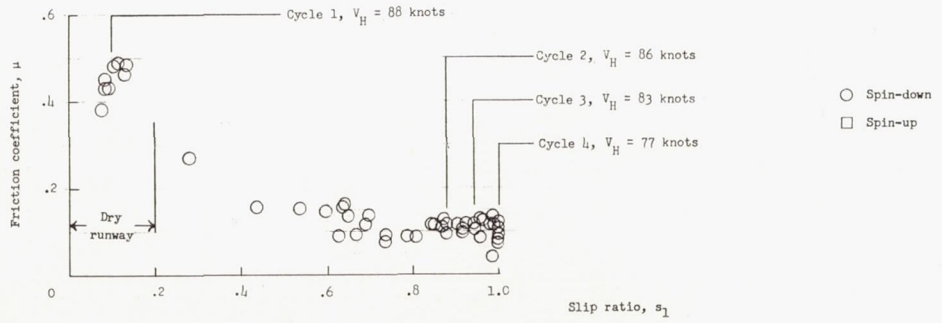

(d) Run 4.

Figure 51.- Concluded.

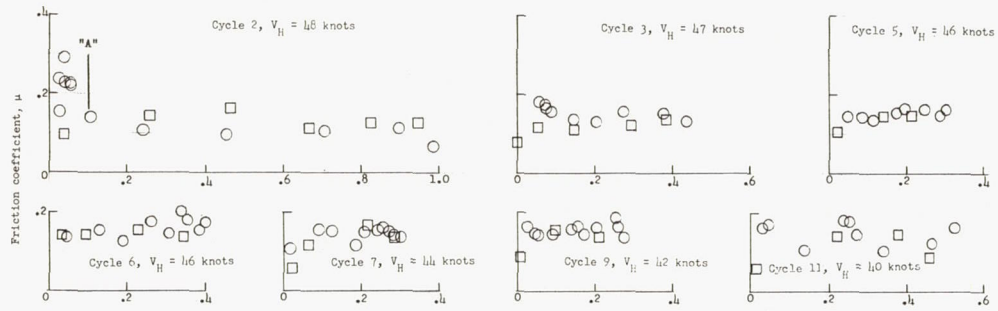

(a) Run 1.

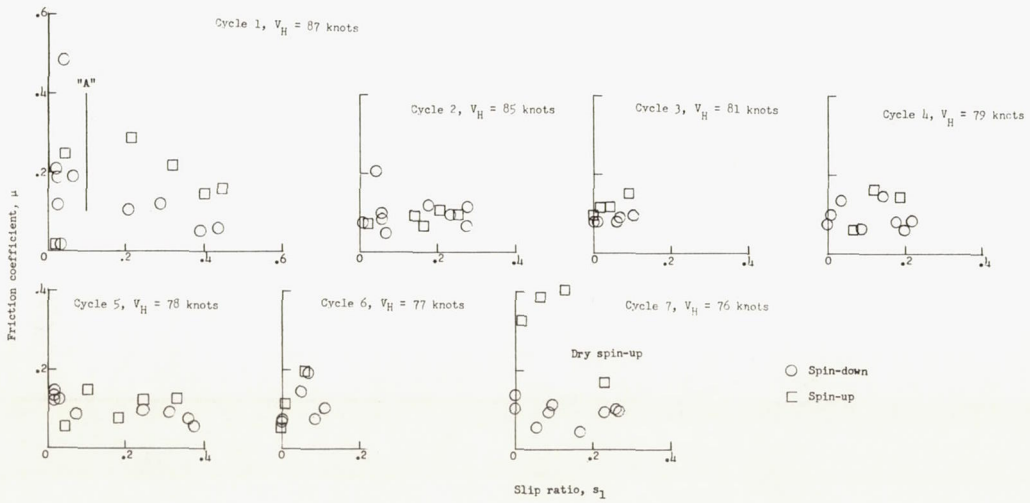

(b) Run 2.

Figure 52.- Tire D1, dimple fabric-reinforced tread, fabric surface. Antiskid unit operating; p = 260 lb/sq in.; d_1 = 0 to 0.3 inch (except where noted); $p_{B,1}$ = 50 lb/sq in.

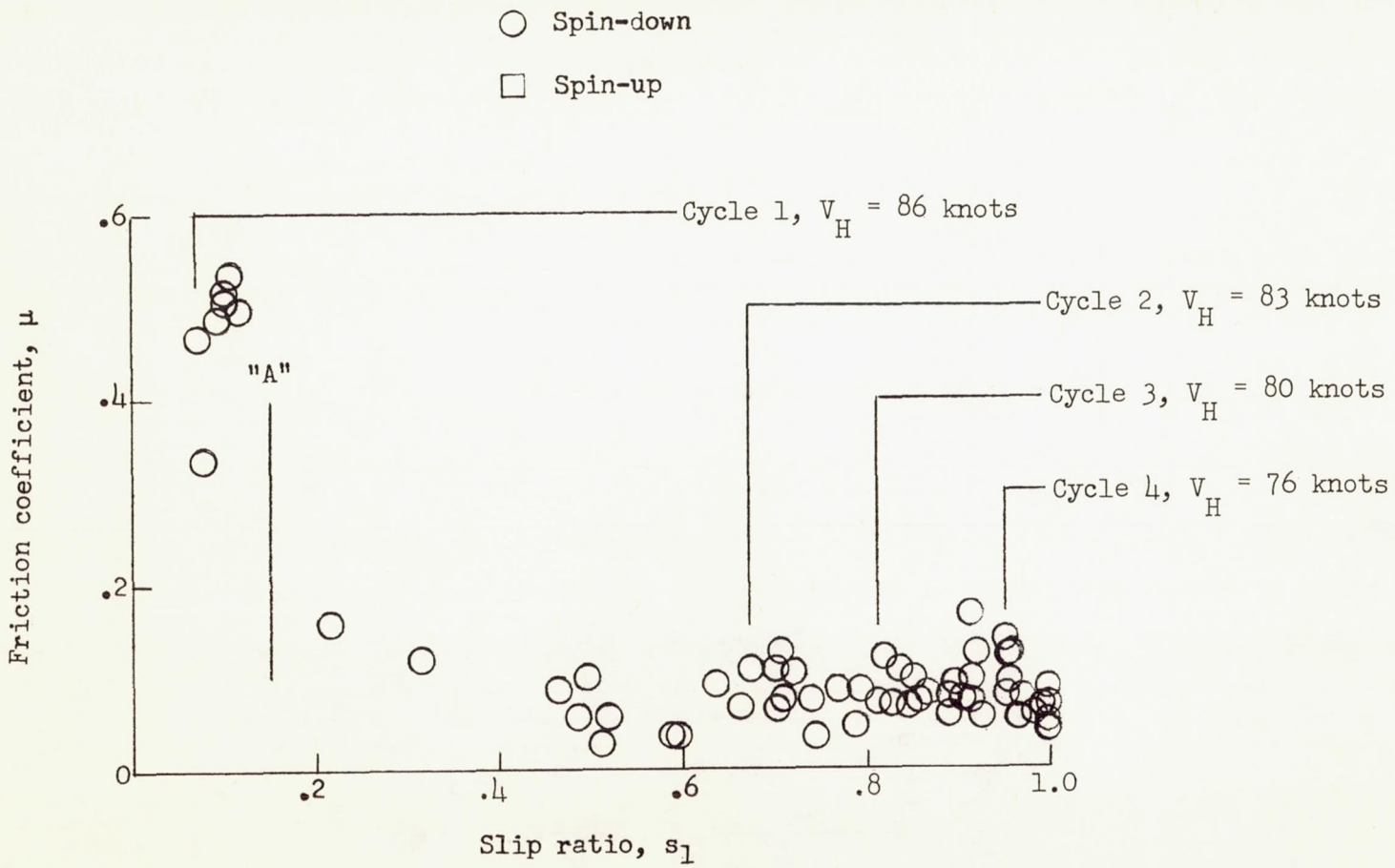

(c) Run 3.

Figure 52.- Concluded.

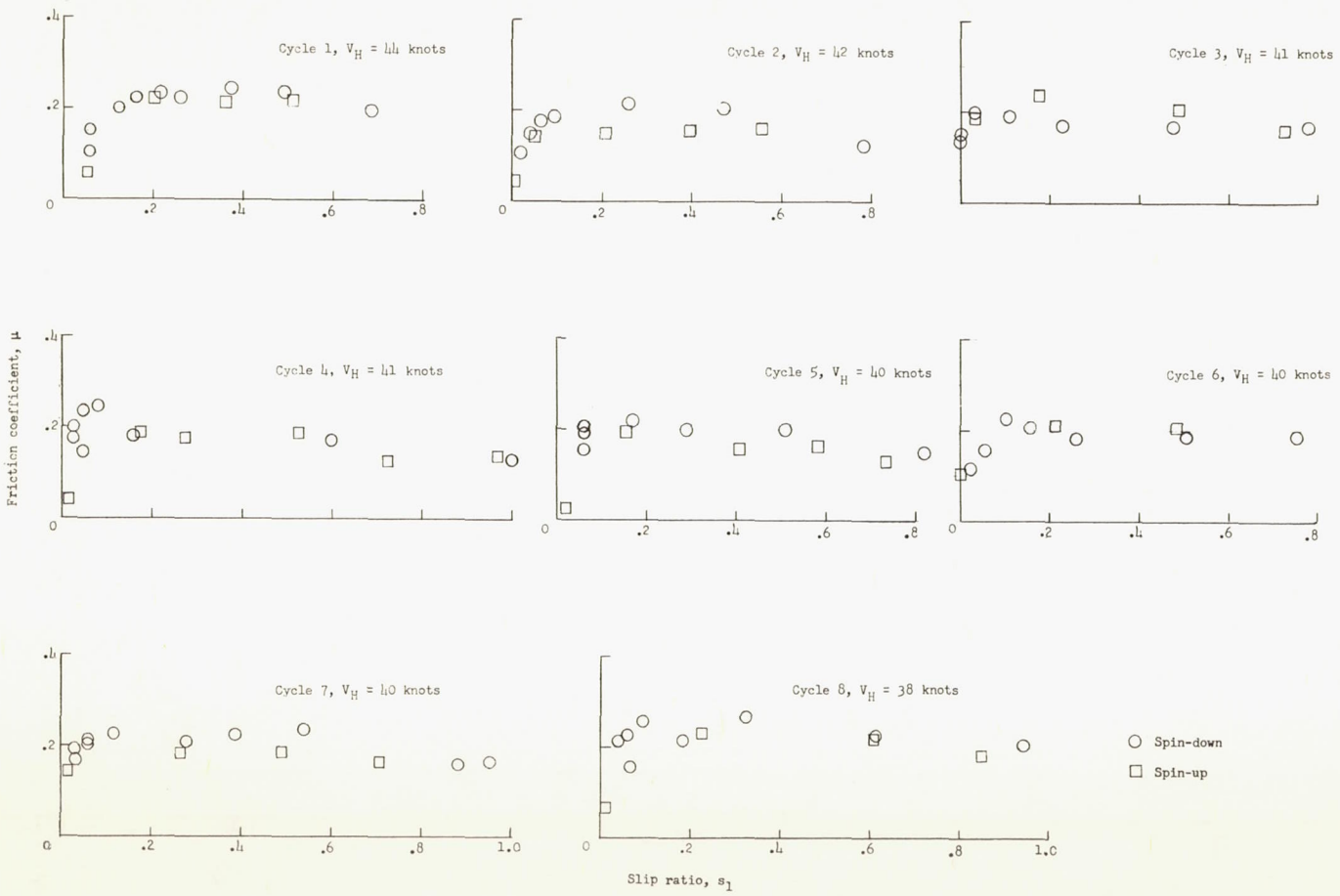

(a) Run 1.

Figure 53.- Tire D2, dimple fabric-reinforced tread, fabric surface. Antiskid unit operating; p = 260 lb/sq in.; d_1 = 0 to 0.3 inch.

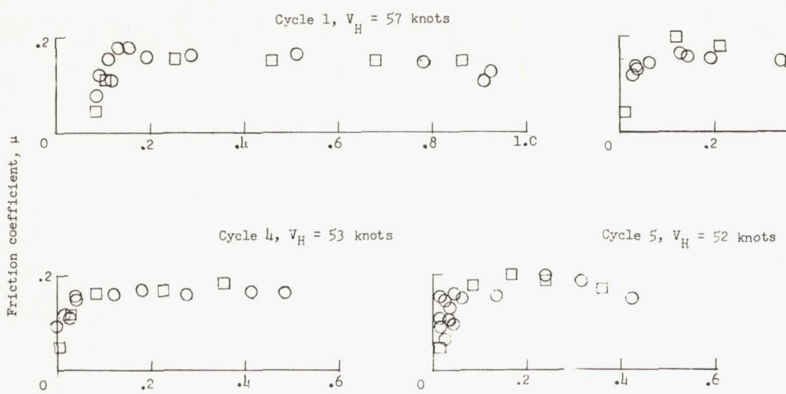

(b) Run 2.

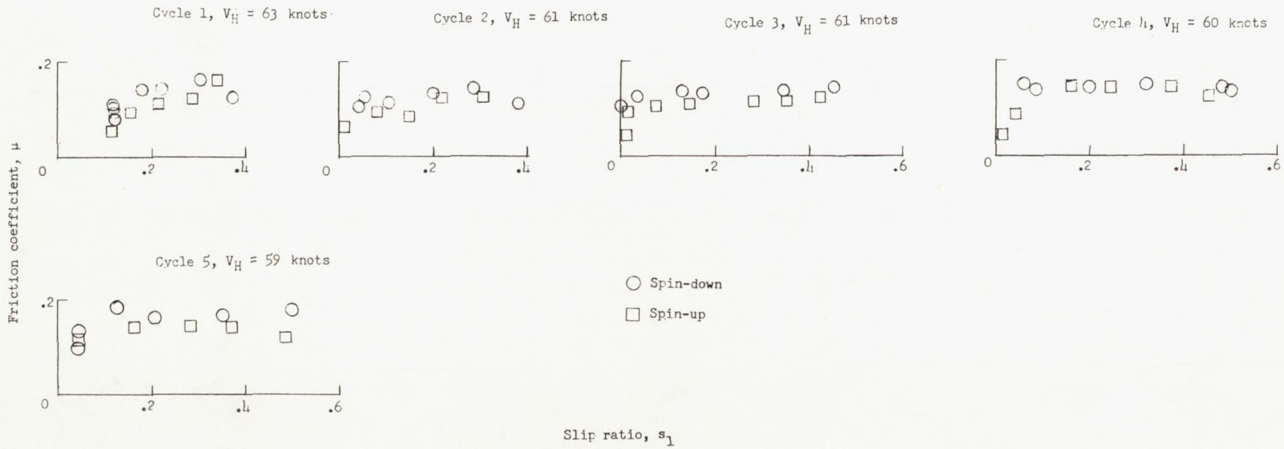

(c) Run 3.

Figure 53.- Continued.

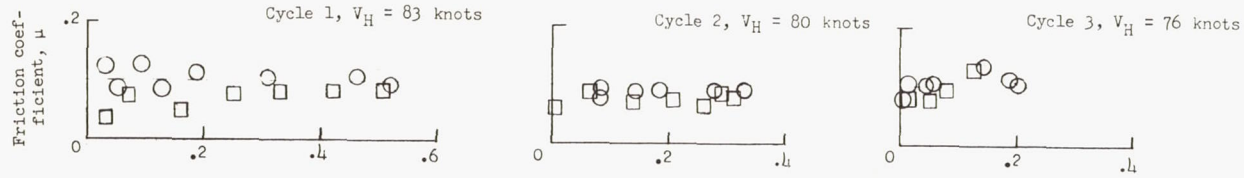

(d) Run 4.

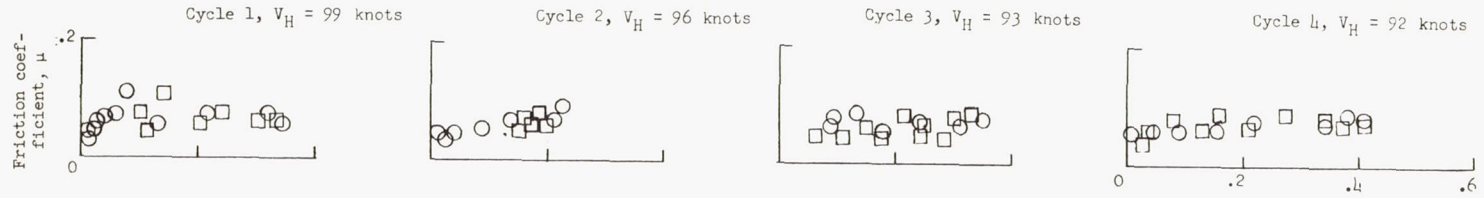

(e) Run 5.

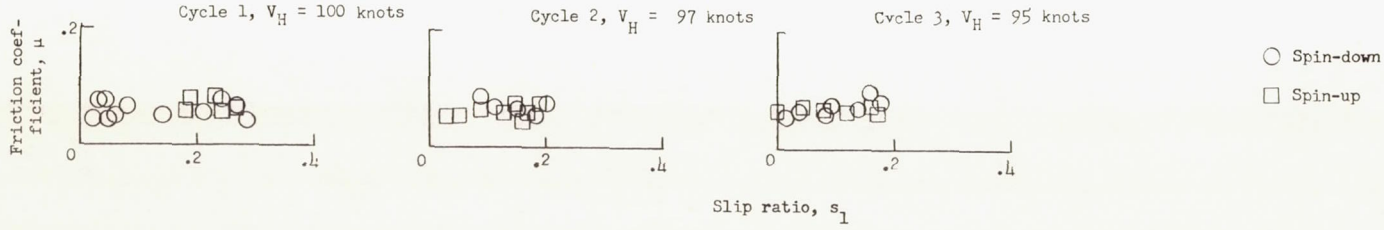

(f) Run 6.

Figure 53.- Concluded.

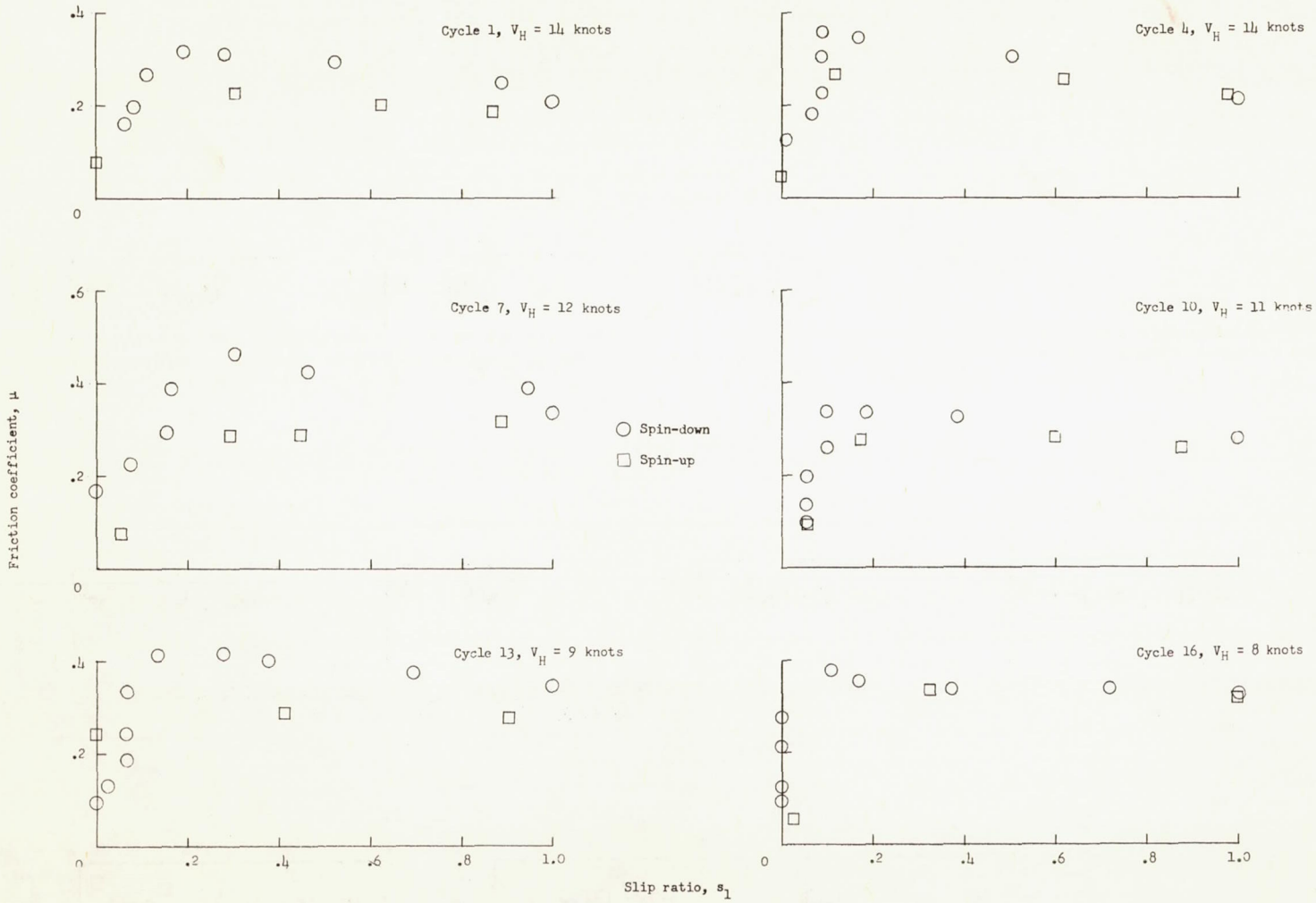

(a) Run 1.

Figure 54.- Tire D3, dimple fabric-reinforced tread, rubber surface. Antiskid unit operating; p = 260 lb/sq in.; d_1 = 0 to 0.3 inch.

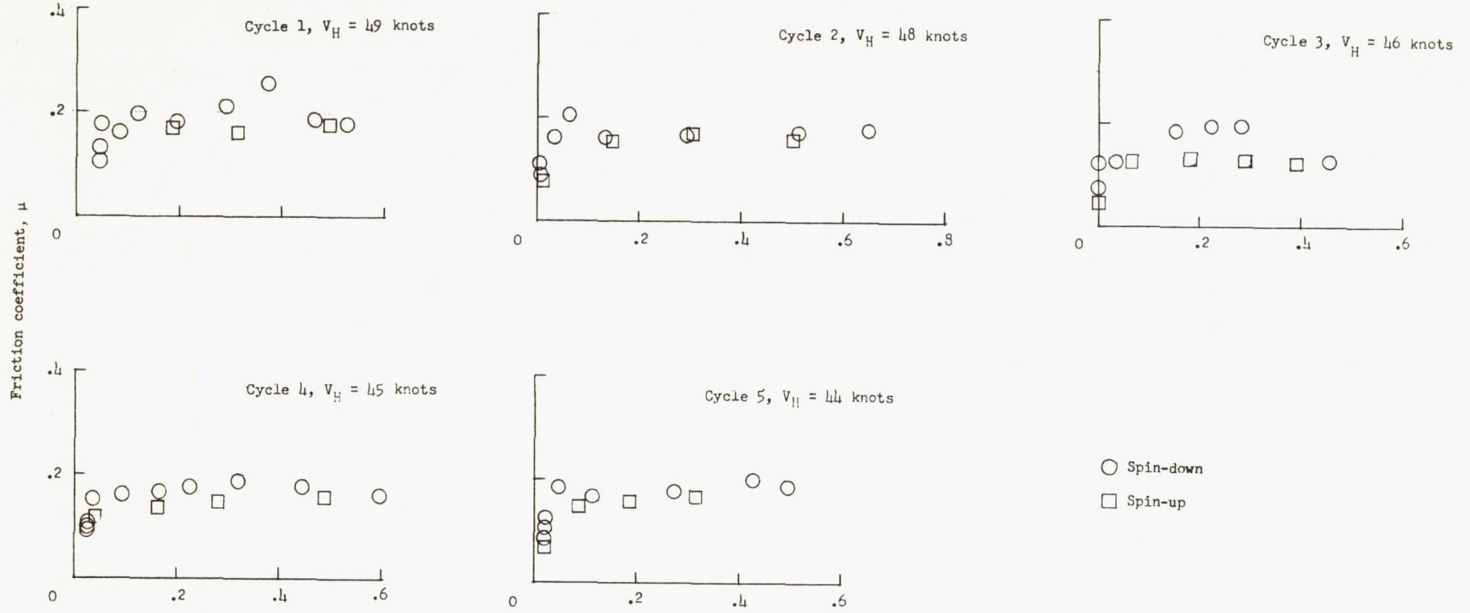

(b) Run 2.

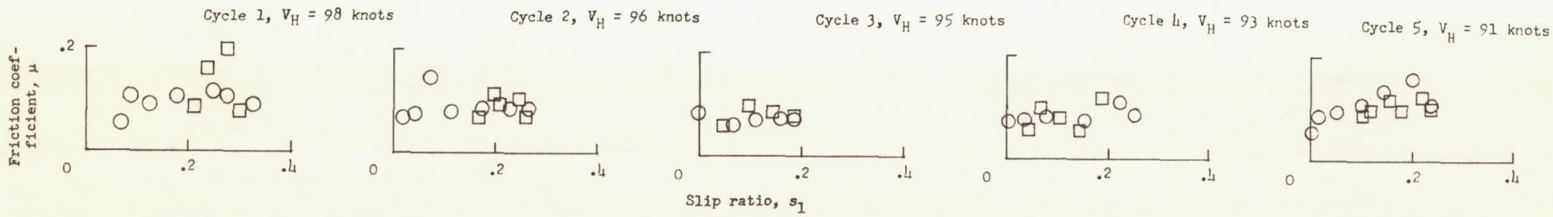

(c) Run 3.

Figure 54.- Concluded.

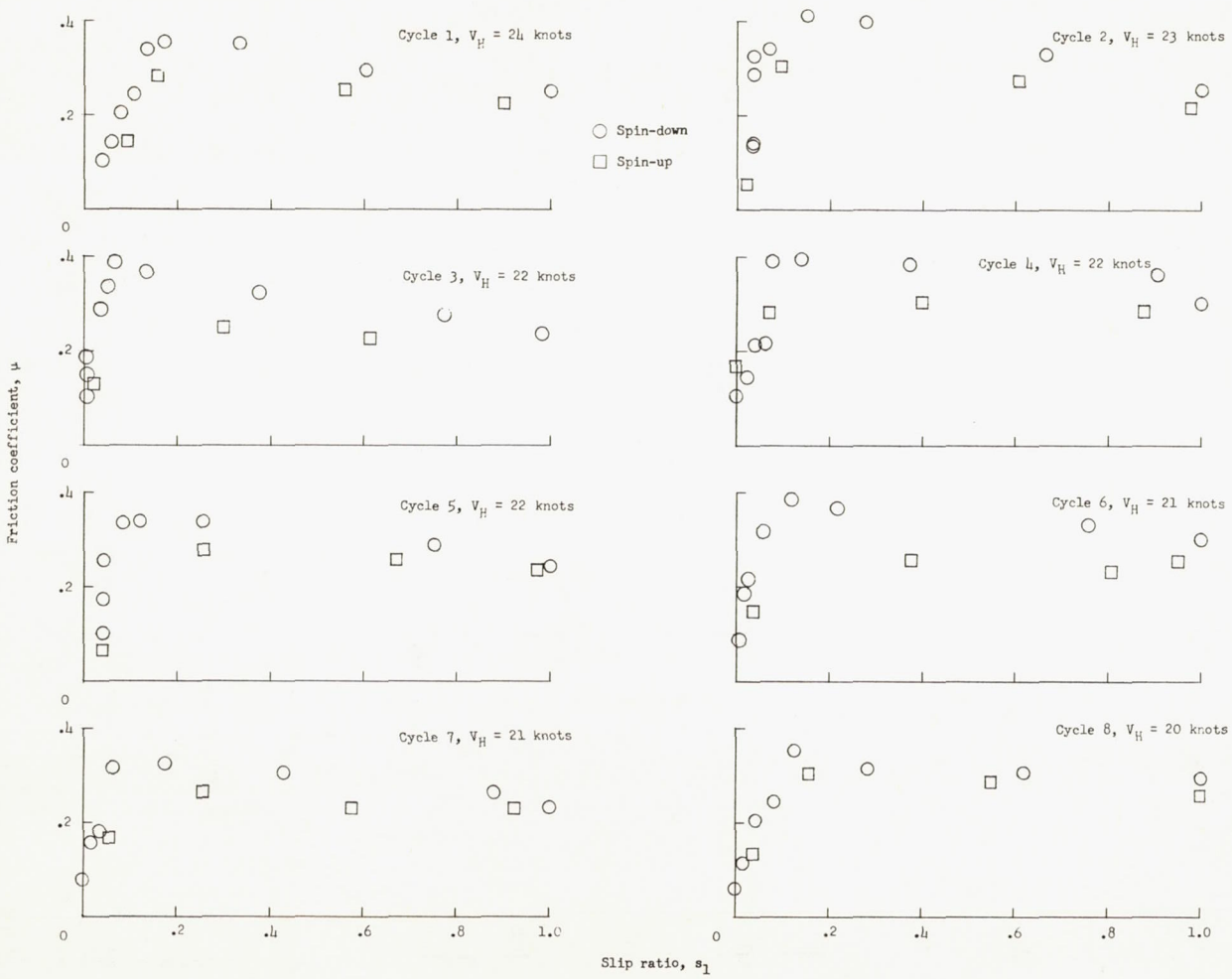

(a) Run 1.

Figure 55.- Tire D4, dimple fabric-reinforced tread (ice grip). Antiskid unit operating; p = 260 lb/sq in.; d_1 = 0 to 0.3 inch.

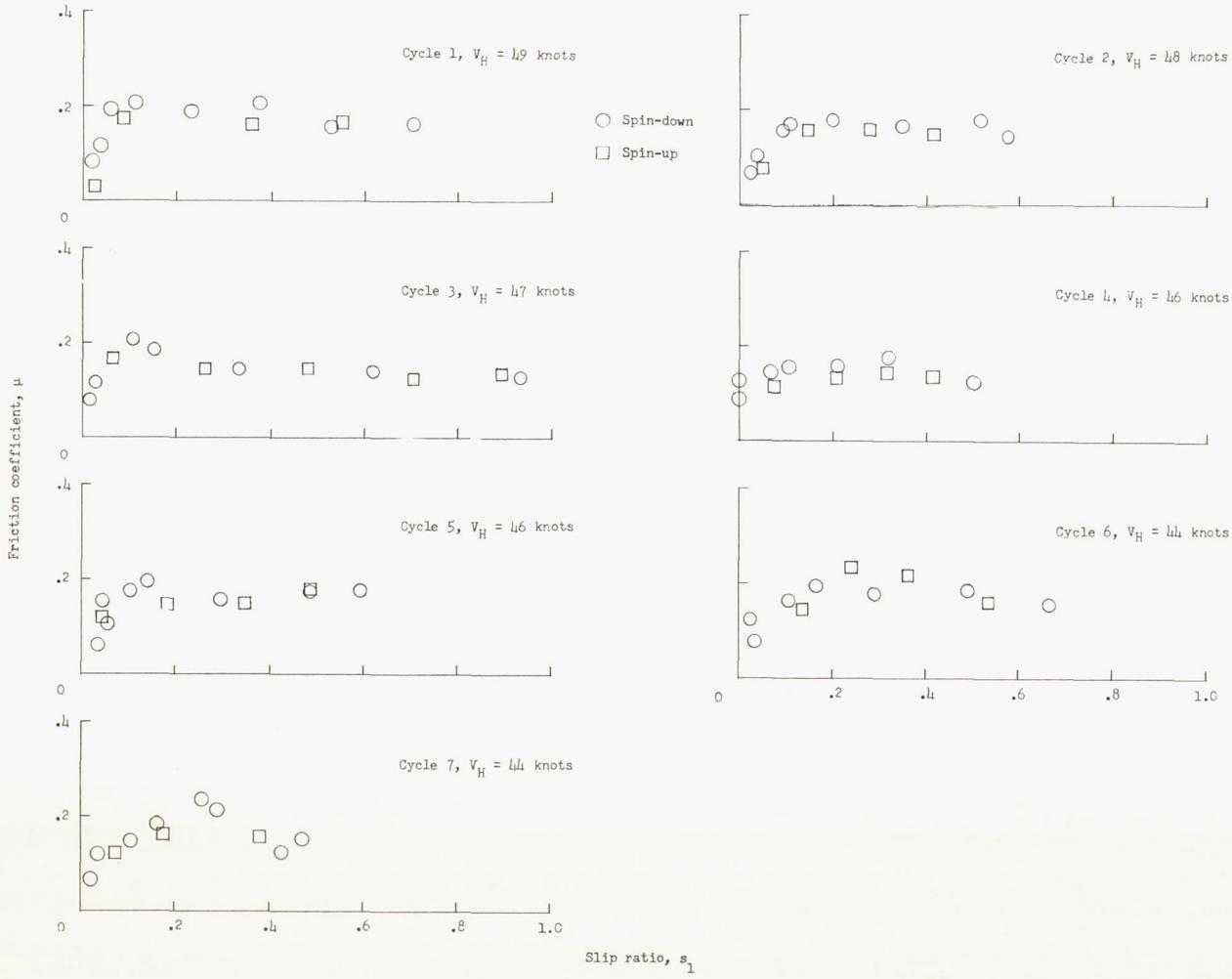

(b) Run 2.

Figure 55.- Continued.

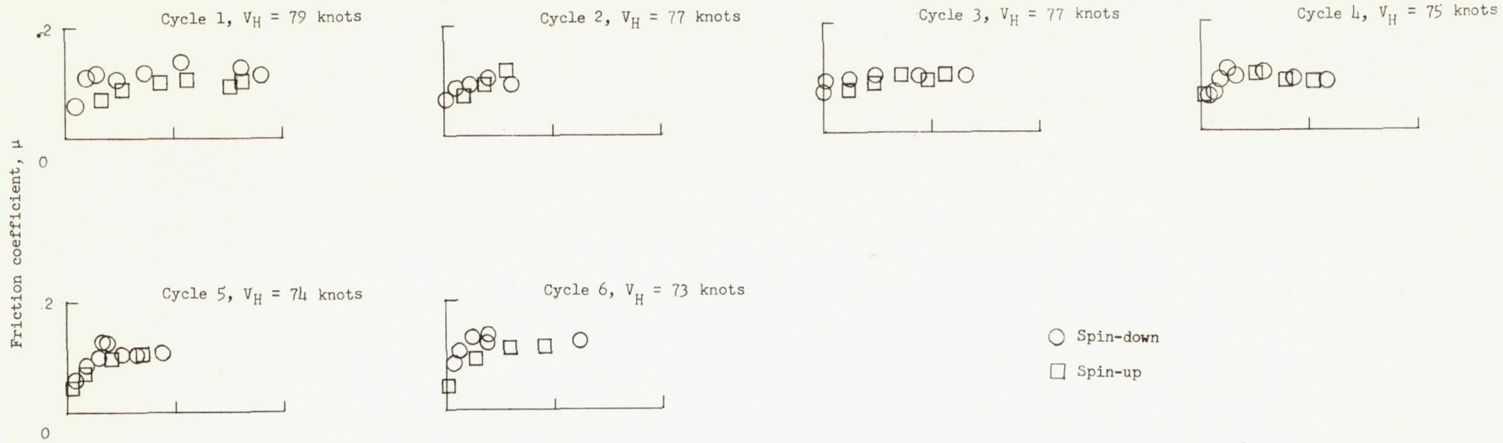

(c) Run 3.

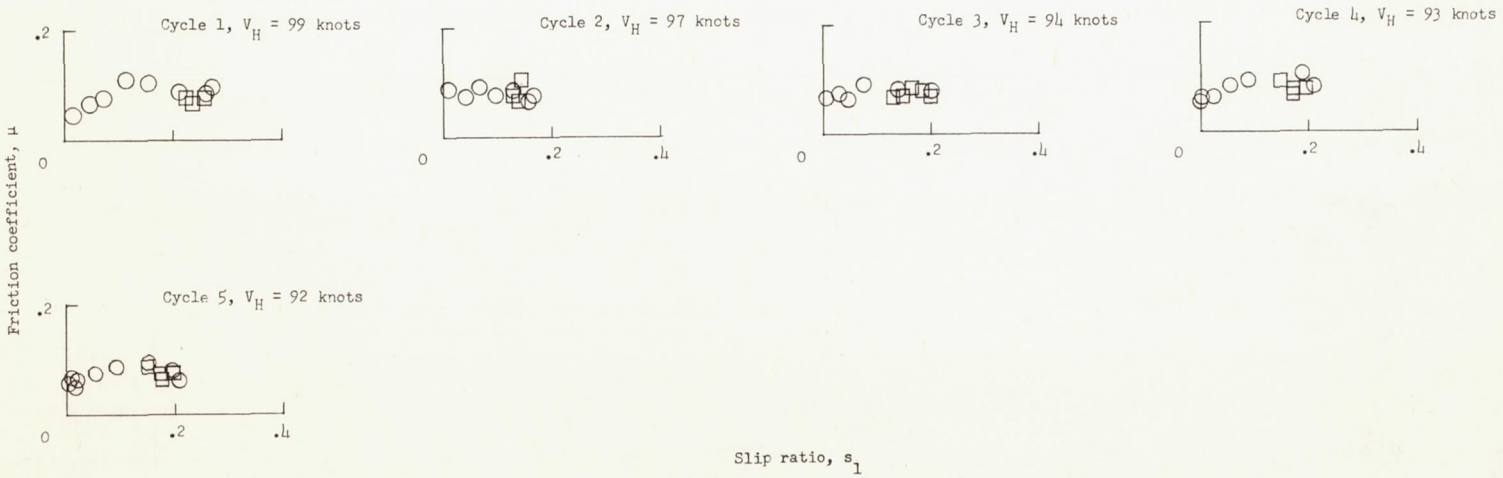

(d) Run 4.

Figure 55.- Concluded.

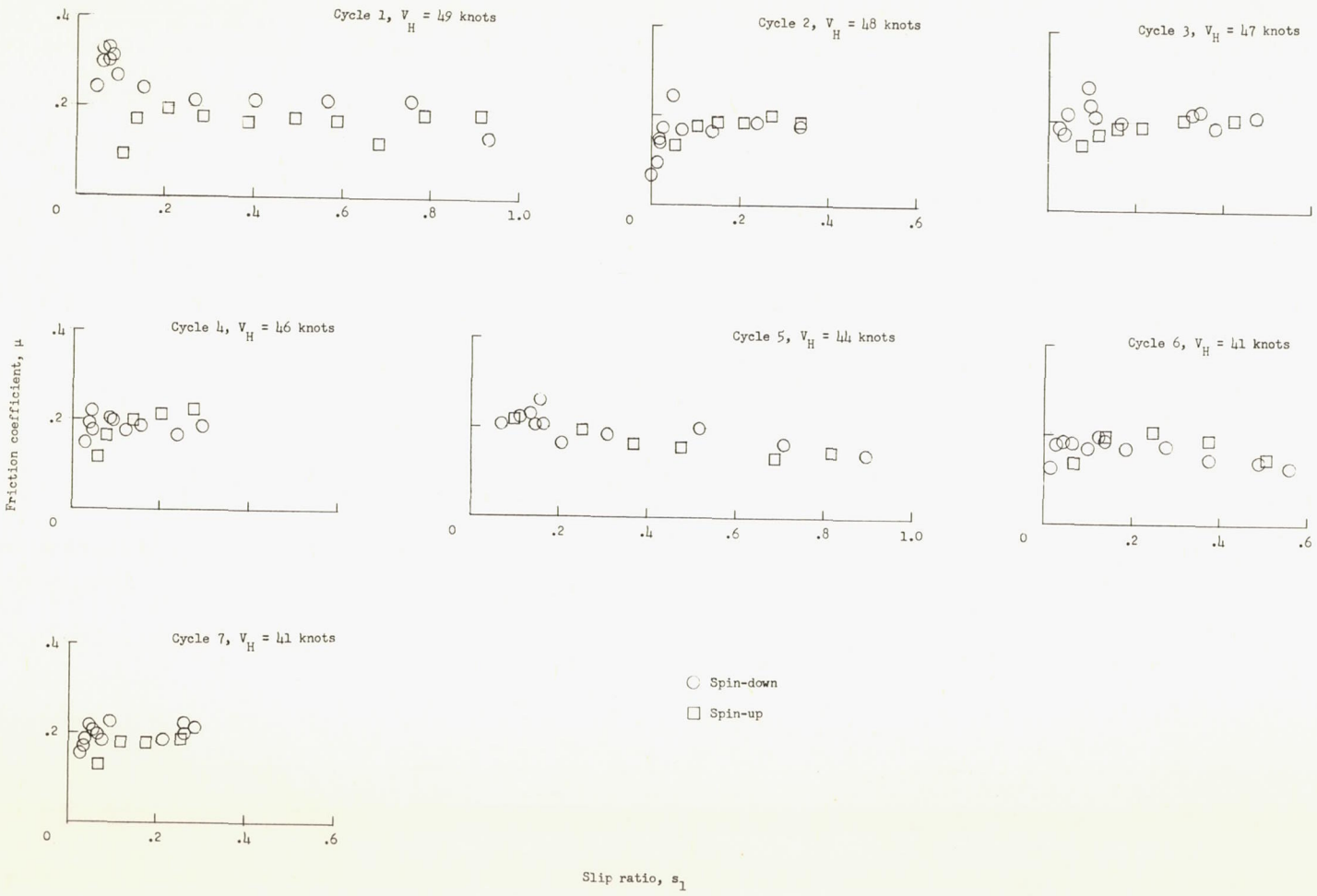

(a) Run 1.

Figure 56.- Tire D5M1, dimple fabric-reinforced tread modified by buffing the tire to remove the dimples. Antiskid unit operating; p = 260 lb/sq in.; d_1 = 0.2 to 0.5 inch (except where noted); $p_{B,1}$ = 50 lb/sq in.

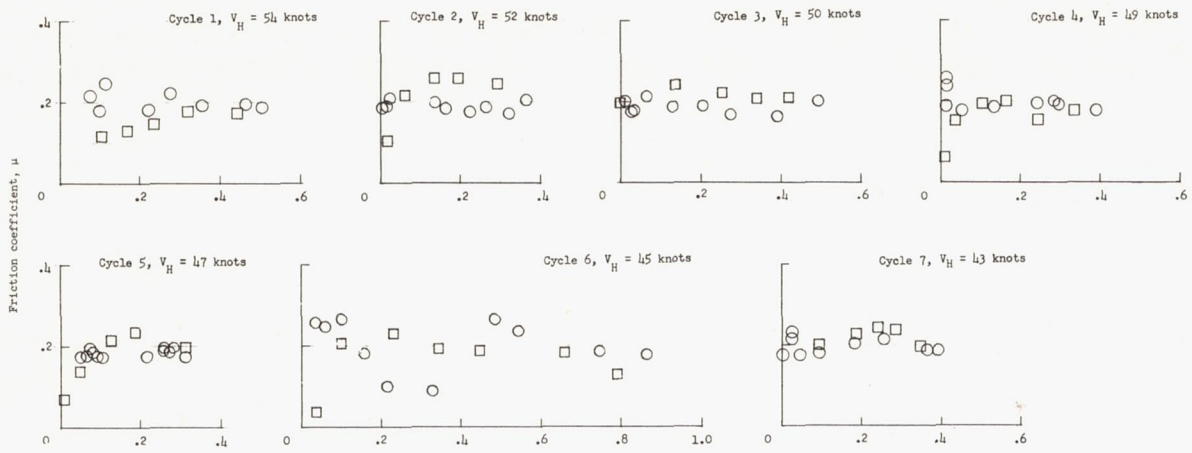

(b) Run 2.

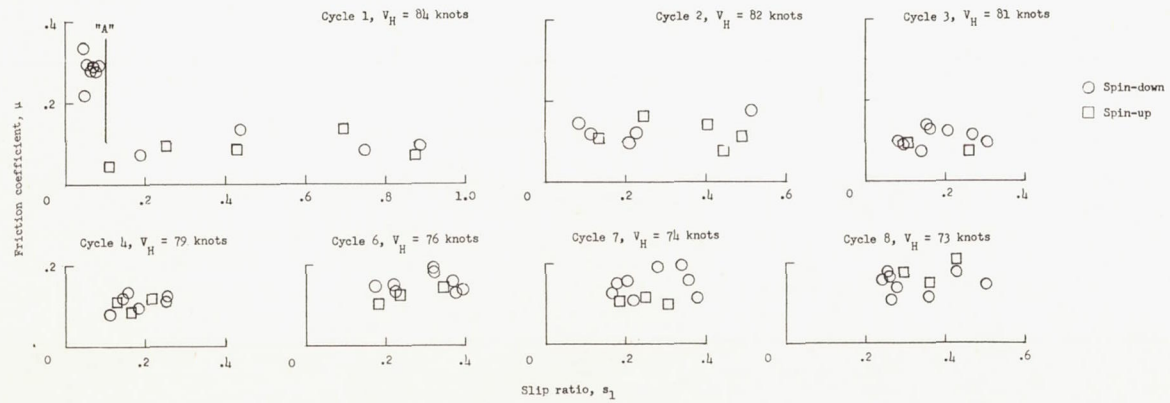

(c) Run 3.

Figure 56.- Concluded.

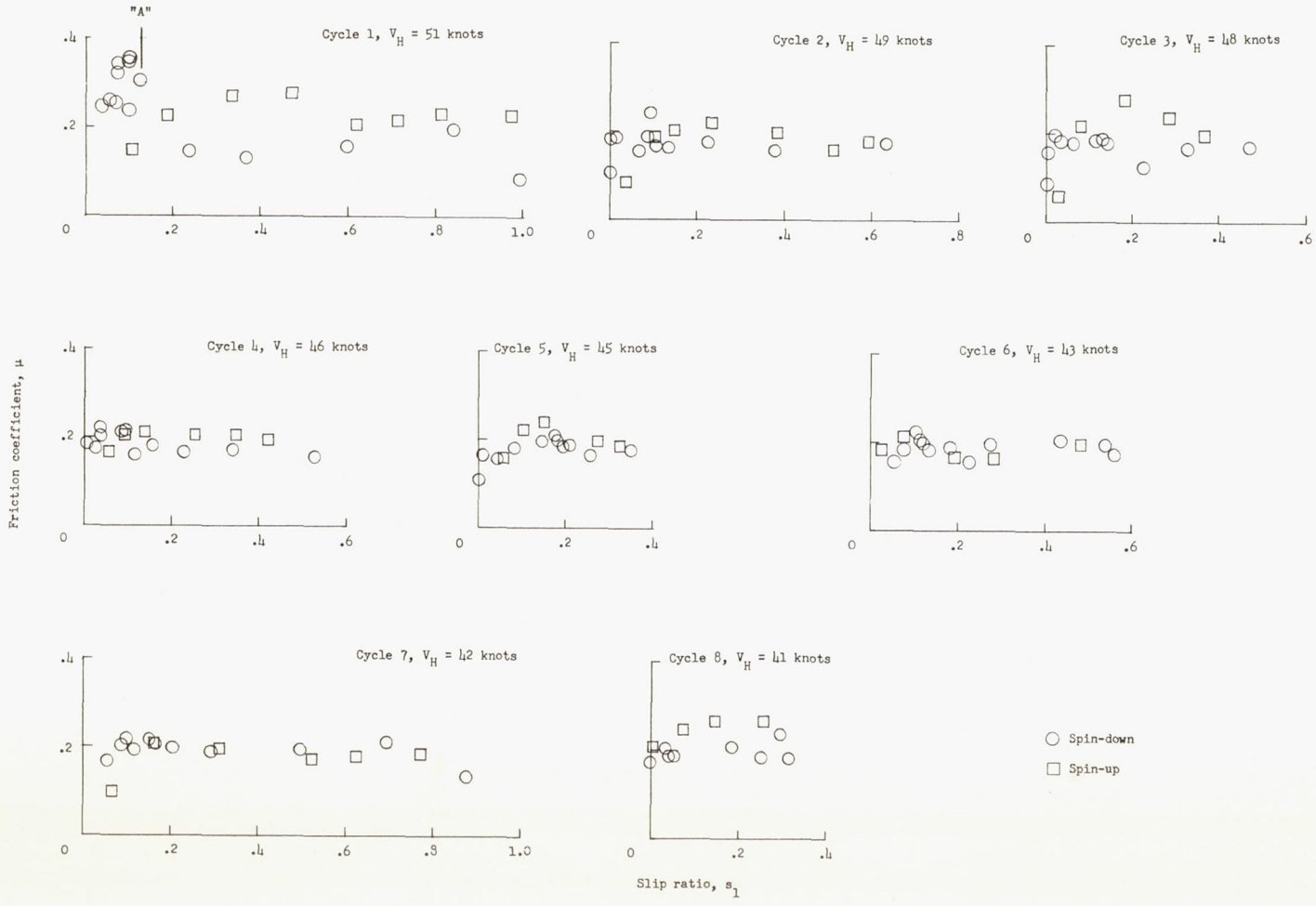

(a) Run 1.

Figure 57.- Tire D5M1, dimple fabric-reinforced tread modified by buffing the tire to remove the dimples. Antiskid unit operating; p = 260 lb/sq in.; d_1 = 0 to 0.3 inch (except where noted); $p_{B,1}$ = 50 lb/sq in.

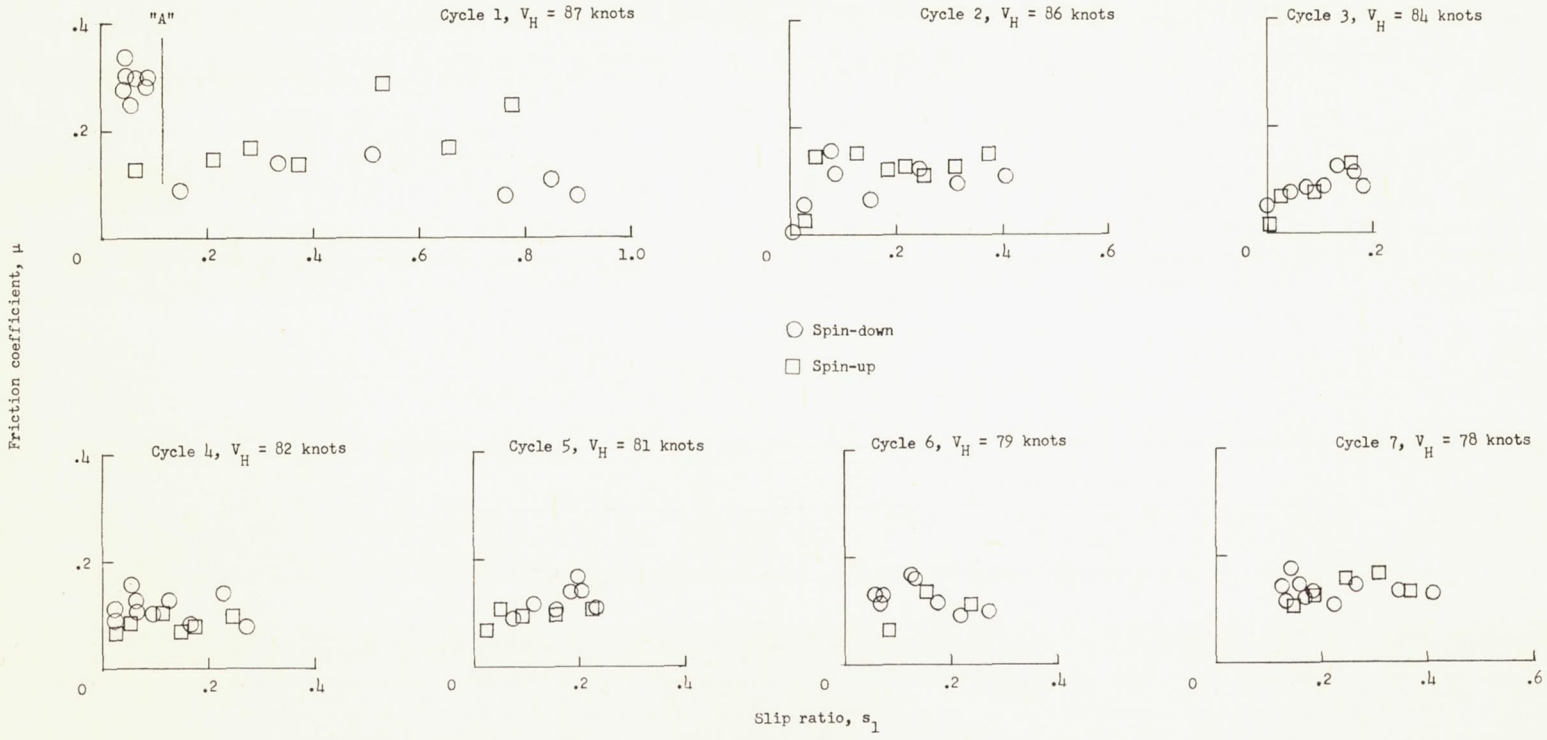

(b) Run 2.

Figure 57.- Concluded.

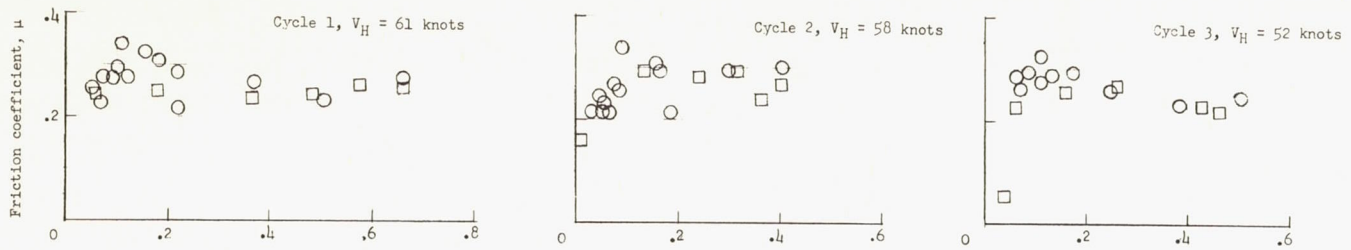

(a) Run 1.

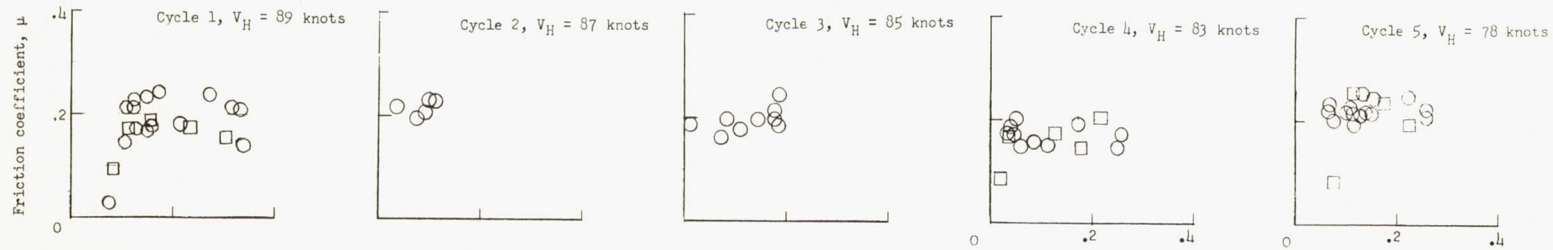

(b) Run 2.

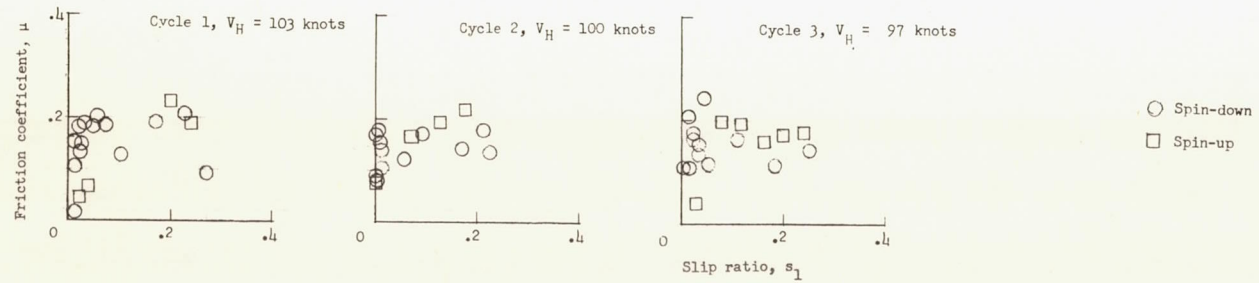

(c) Run 3.

Figure 58.- Tire D6M1, dimple fabric-reinforced tread modified by 5 circumferential grooves. Antiskid unit operating; p = 260 lb/sq in.; d_1 = 0 to 0.3 inch.

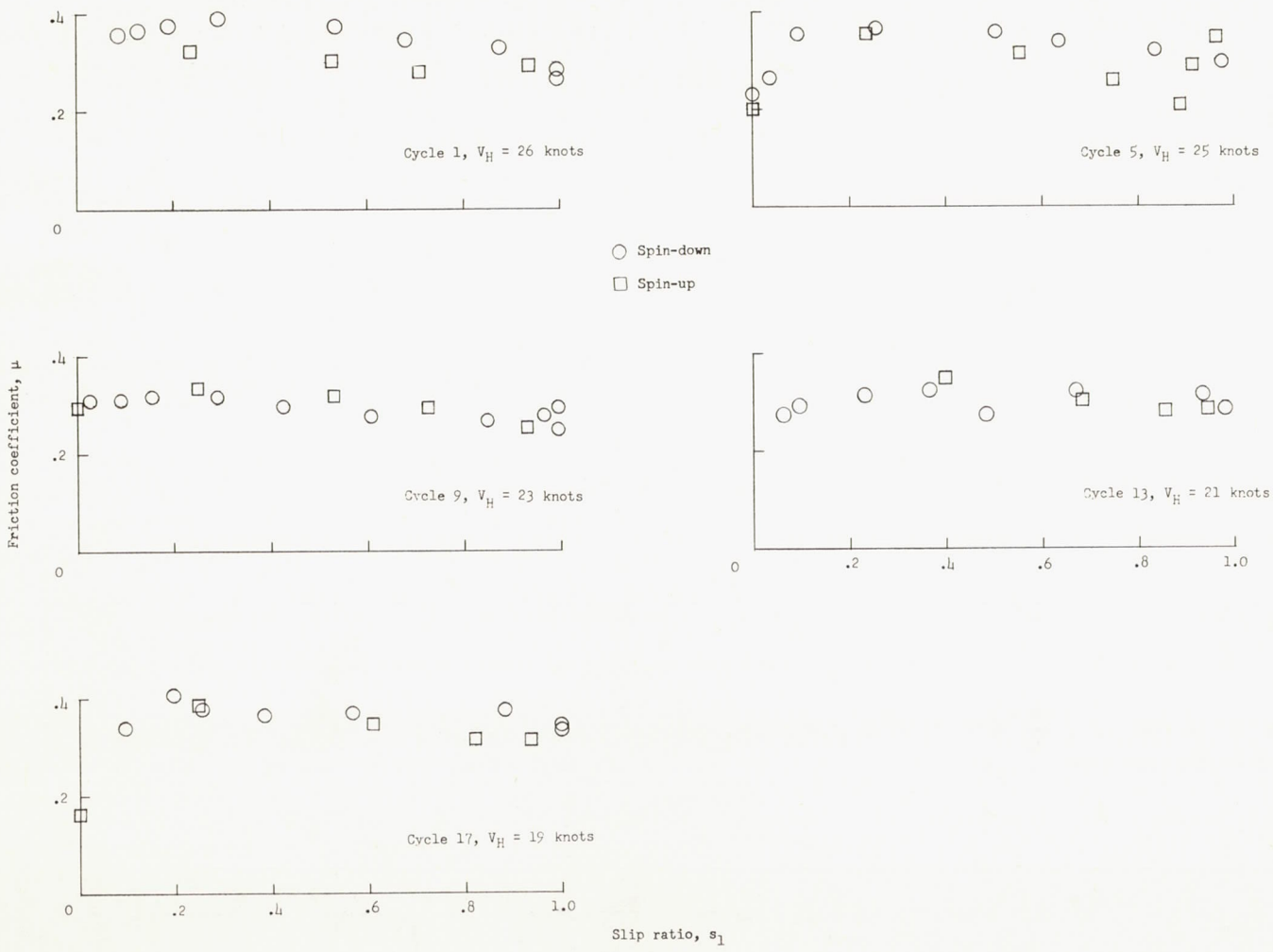

(a) Run 1.

Figure 59.- Tire D7M1, dimple fabric-reinforced tread modified by 37 lateral grooves. Antiskid unit operating; p = 260 lb/sq in.; d_1 = 0 to 0.3 inch.

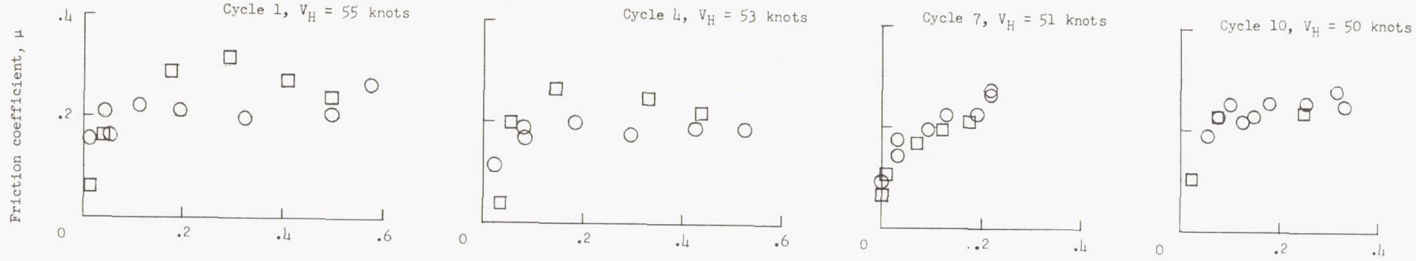

(b) Run 2.

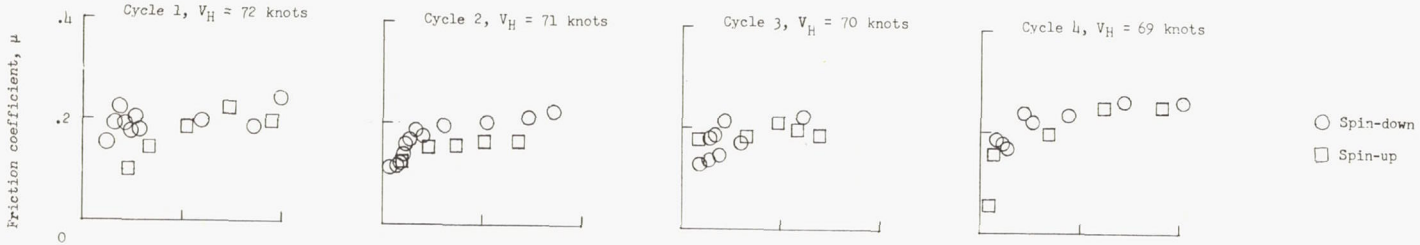

(c) Run 3.

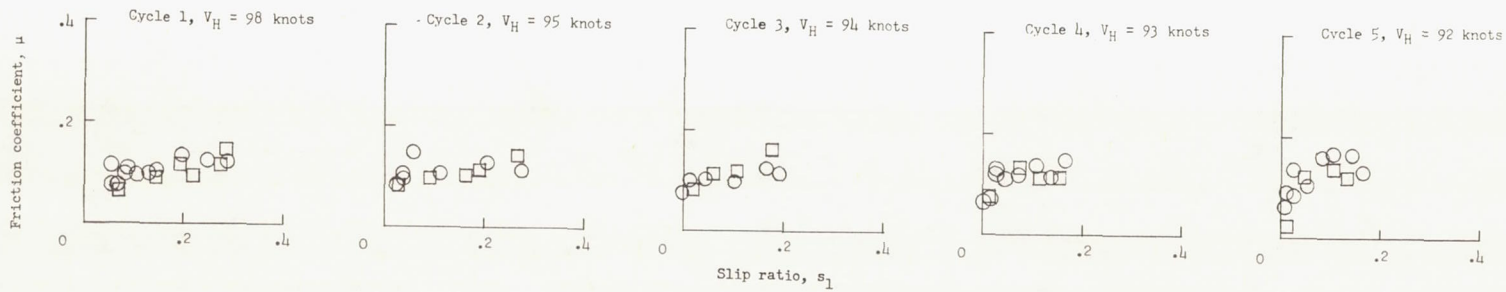

(d) Run 4.

Figure 59.- Concluded.

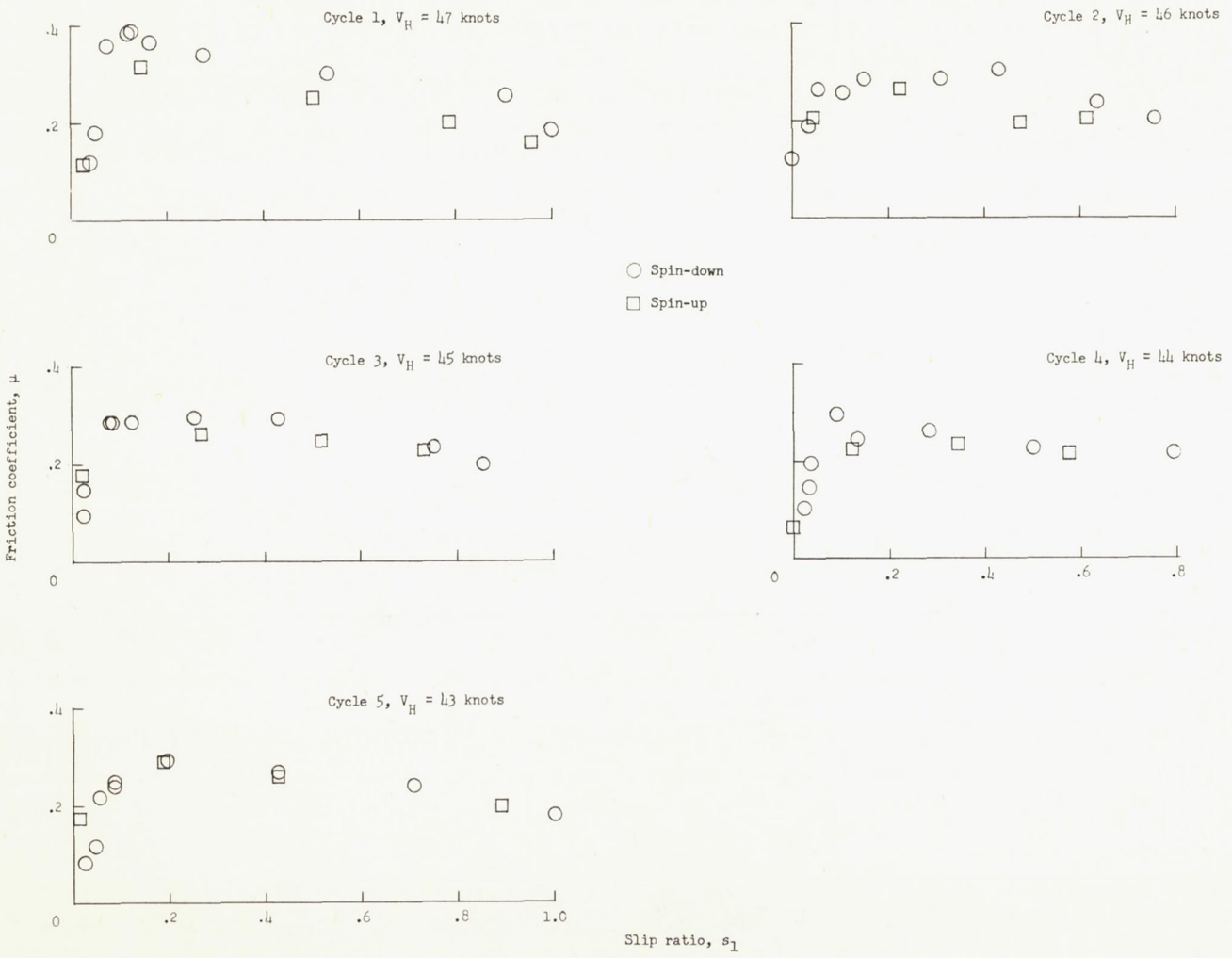

(a) Run 1.

Figure 60.- Tire D8M1, dimple fabric-reinforced tread modified by 2 zigzag circumferential grooves. Antiskid unit operating; p = 260 lb/sq in.; d_1 = 0 to 0.3 inch.

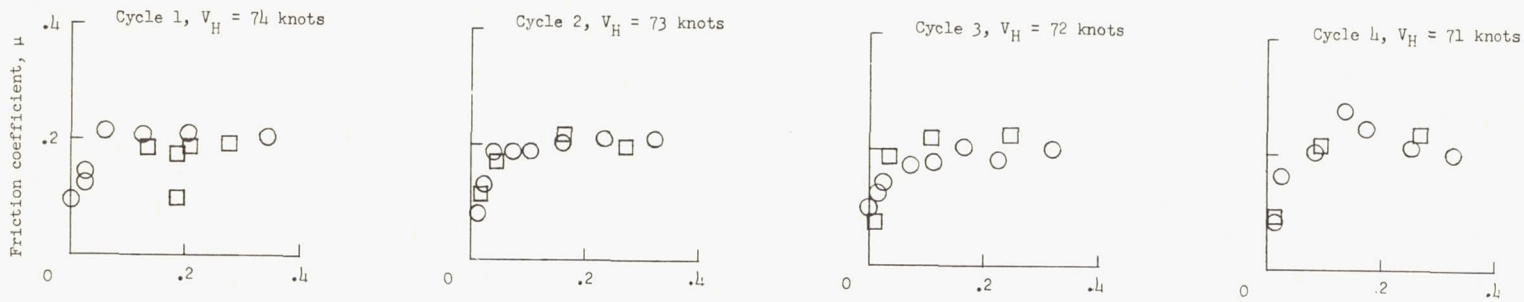

(b) Run 2.

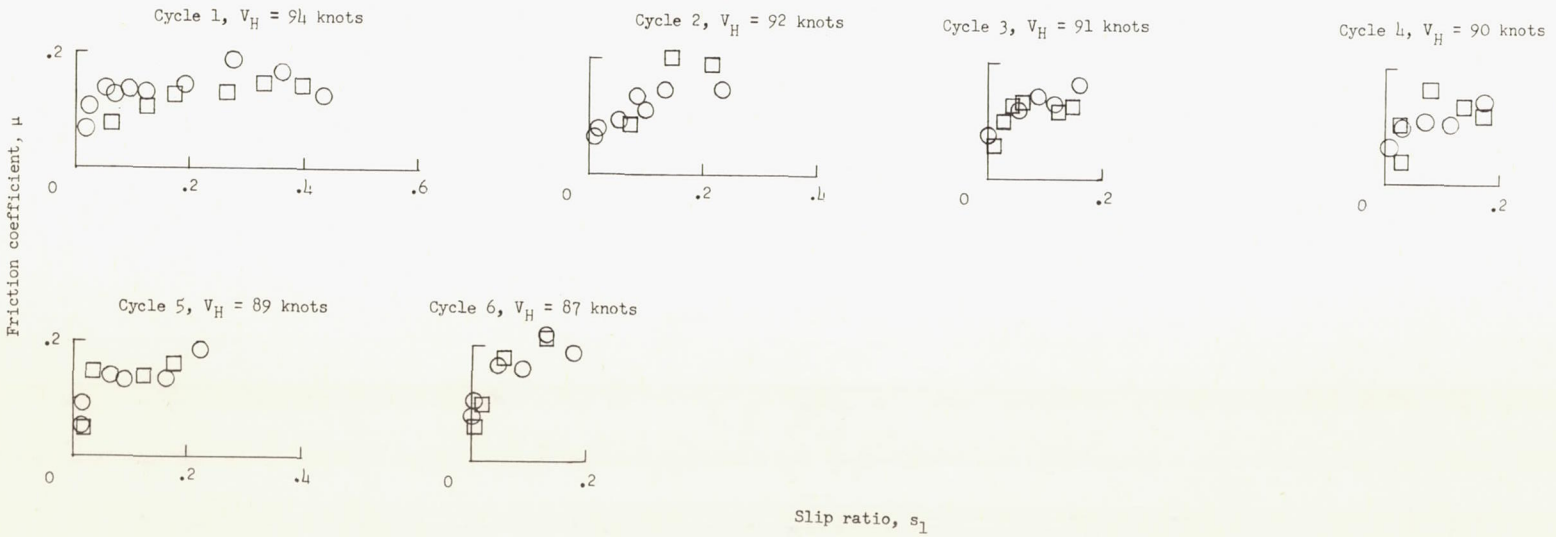

(c) Run 3.

Figure 60.- Concluded.

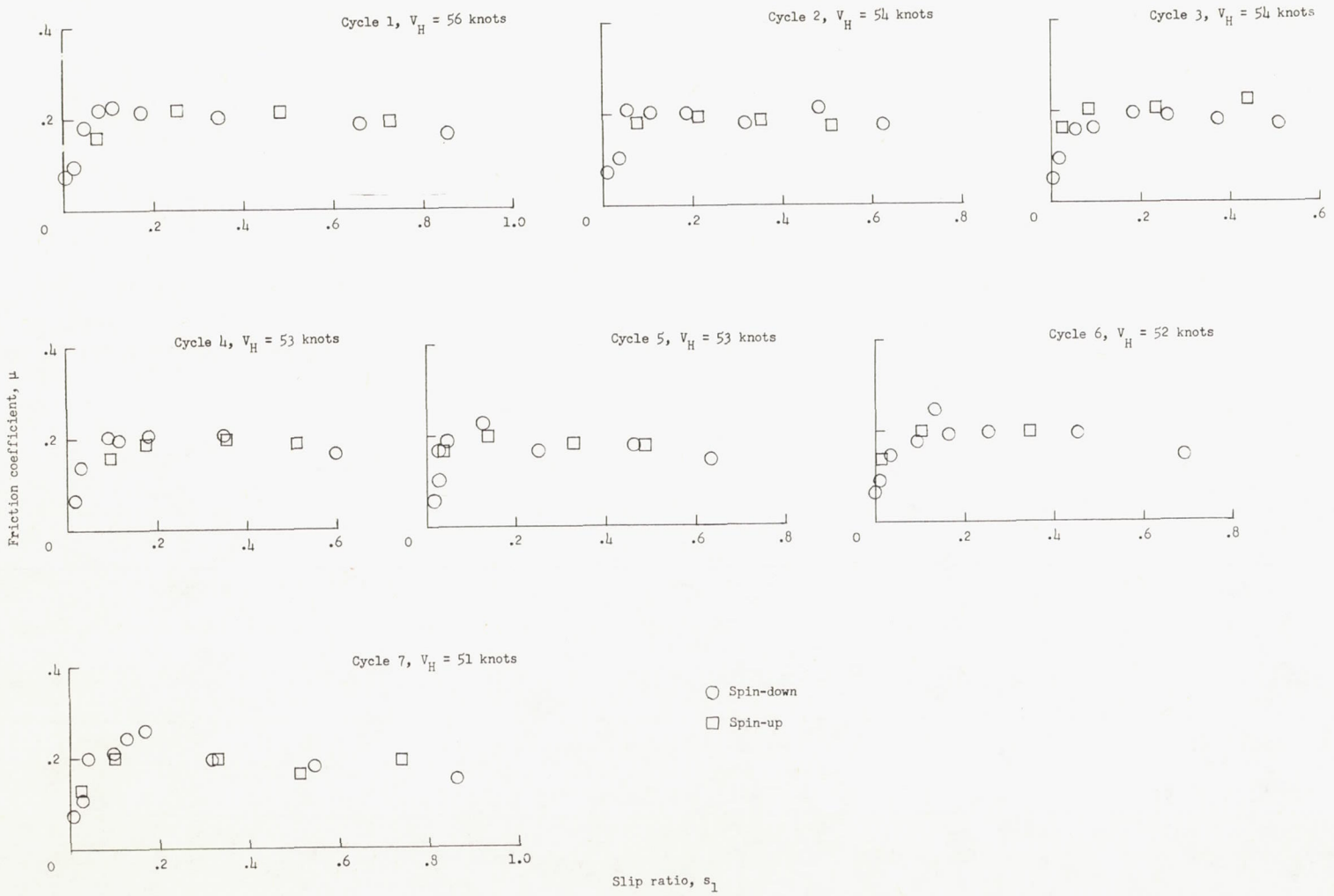

(a) Run 1.

Figure 61.- Tire D8M2, tire D8M1 modified by removing rib between the 2 zigzag grooves. Antiskid unit operating; p = 260 lb/sq in.; d_1 = 0 to 0.3 inch.

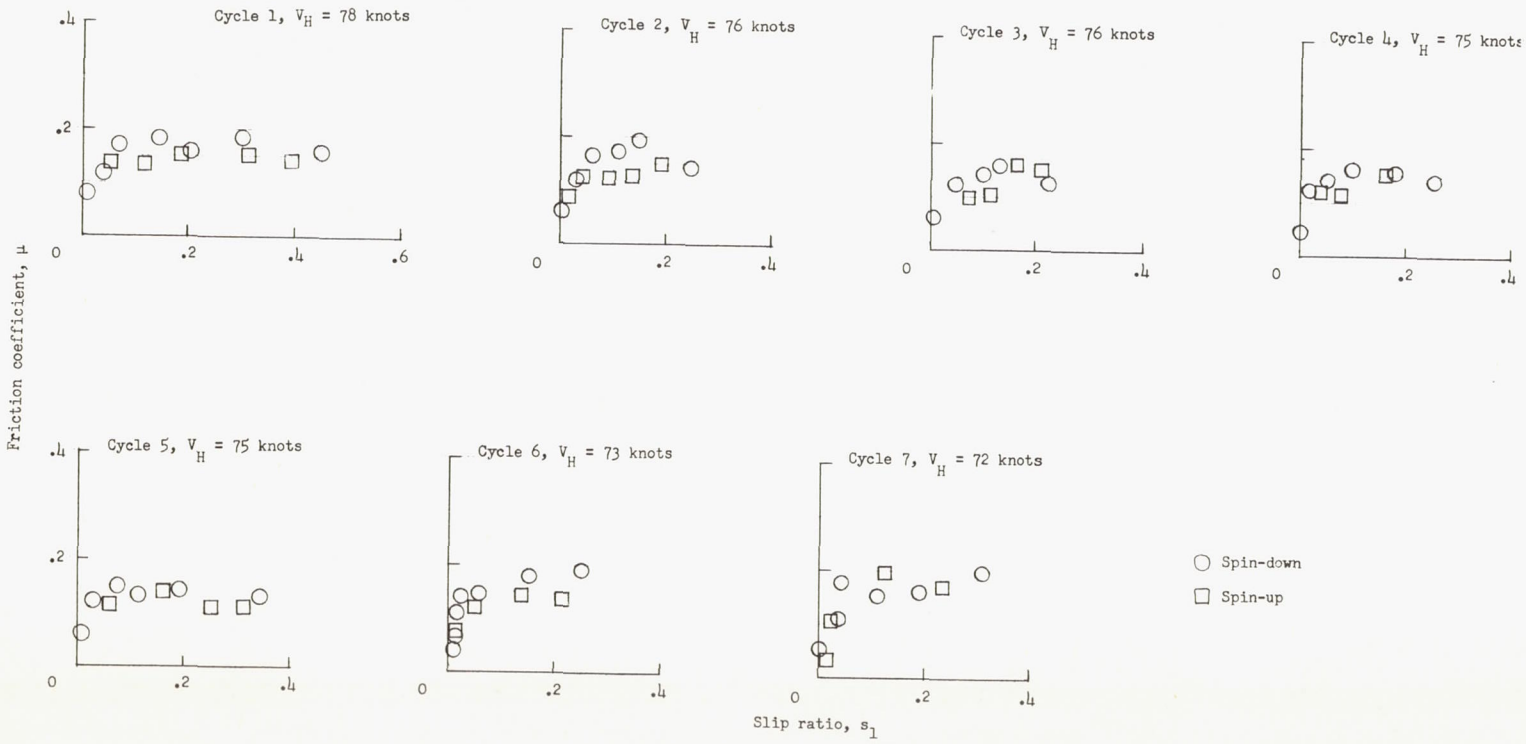

(b) Run 2.

Figure 61.- Concluded.

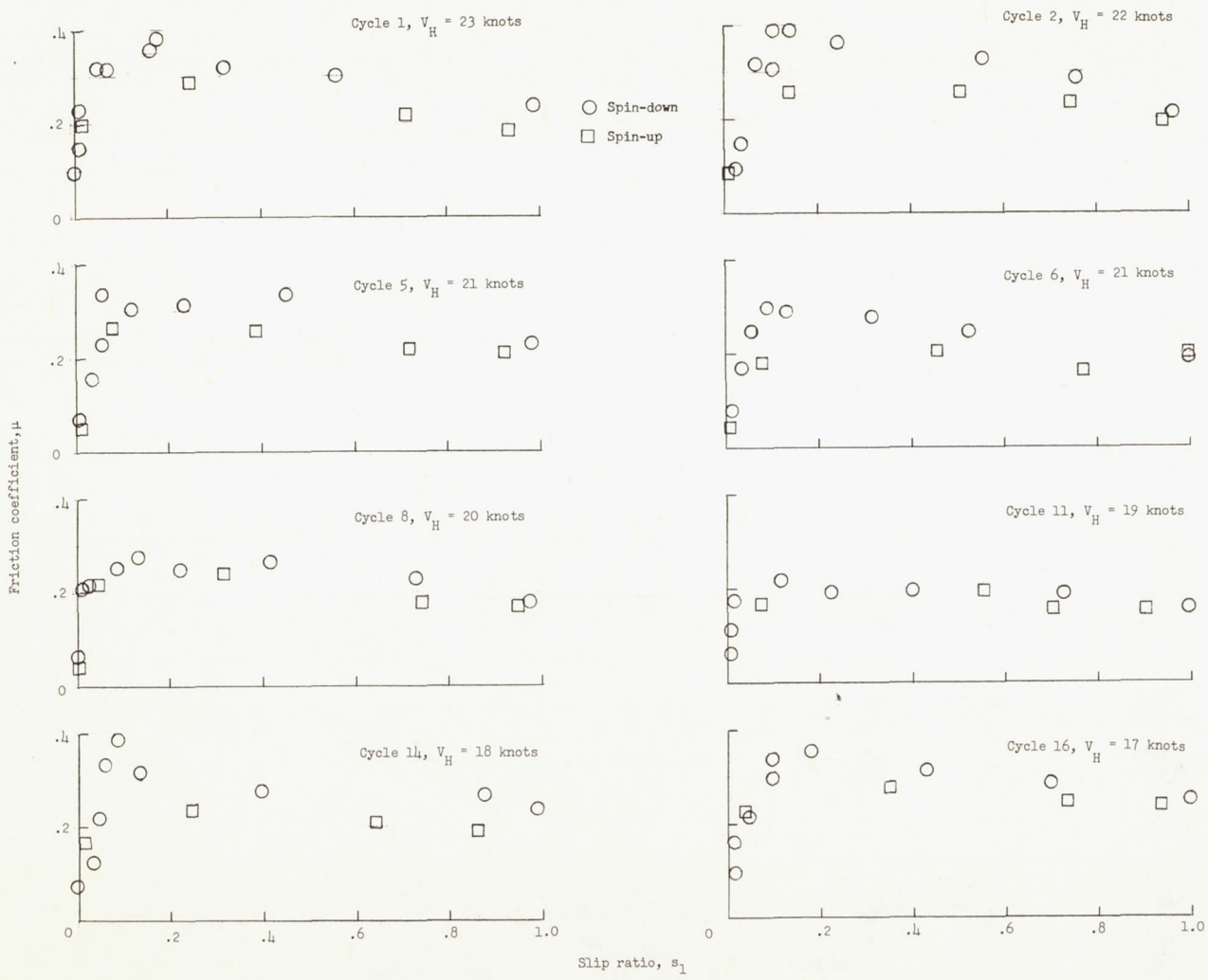

(a) Run 1; p = 260 lb/sq in.

Figure 62.- Tire S1, smooth, all-rubber tread. Antiskid operating; d_1 = 0 to 0.3 inch.

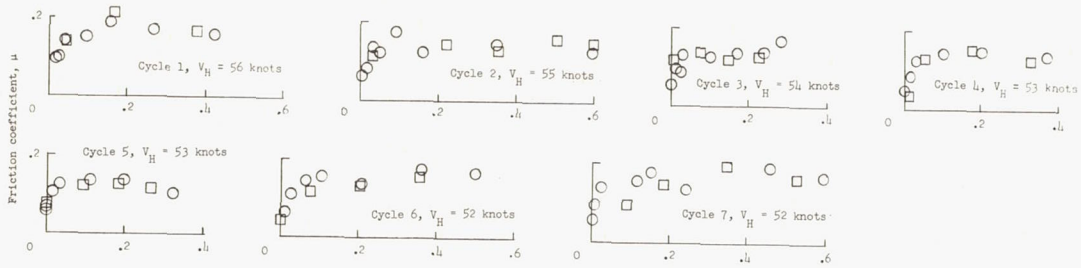

(b) Run 2; p = 260 lb/sq in.

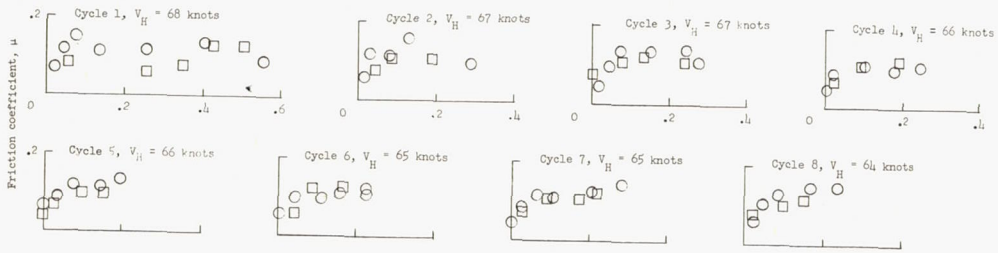

(c) Run 3; p = 260 lb/sq in.

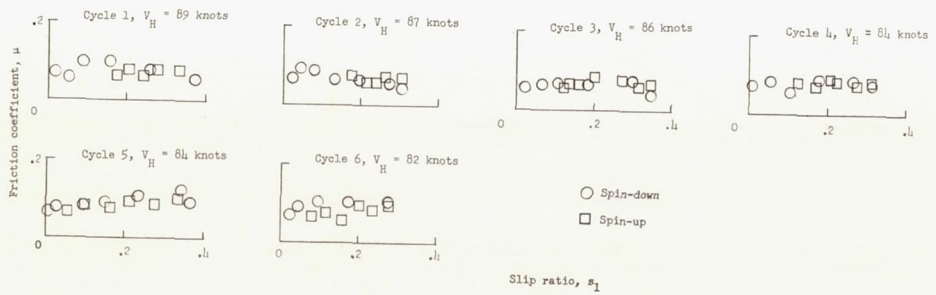

(d) Run 4; p = 260 lb/sq in.

Figure 62.- Continued.

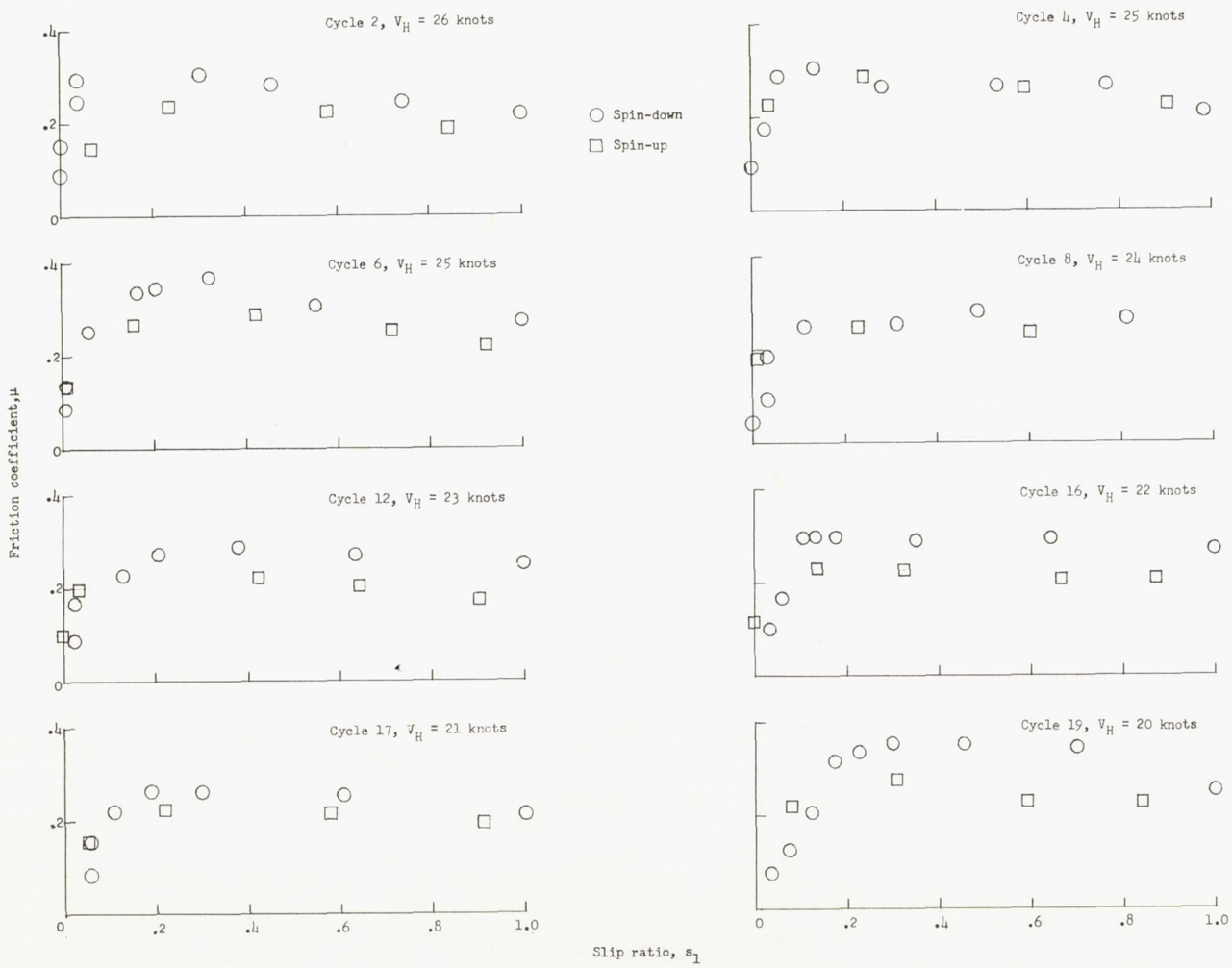

(e) Run 1; p = 120 lb/sq in.

Figure 62.- Continued.

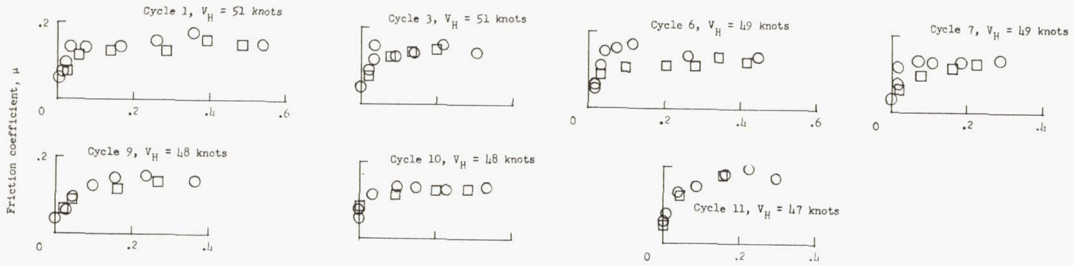

(f) Run 2; p = 120 lb/sq in.

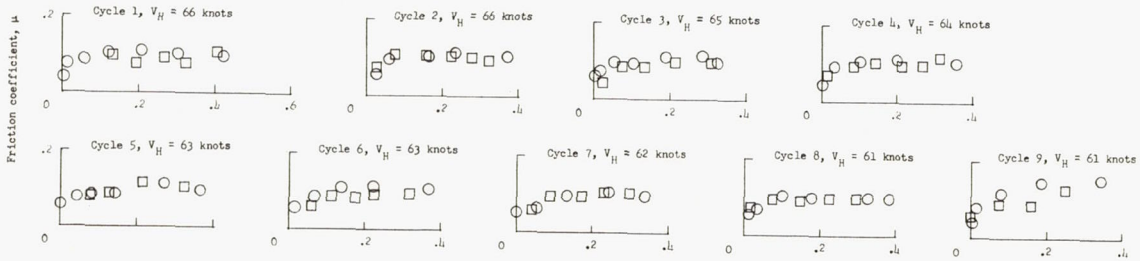

(g) Run 3; p = 120 lb/sq in.

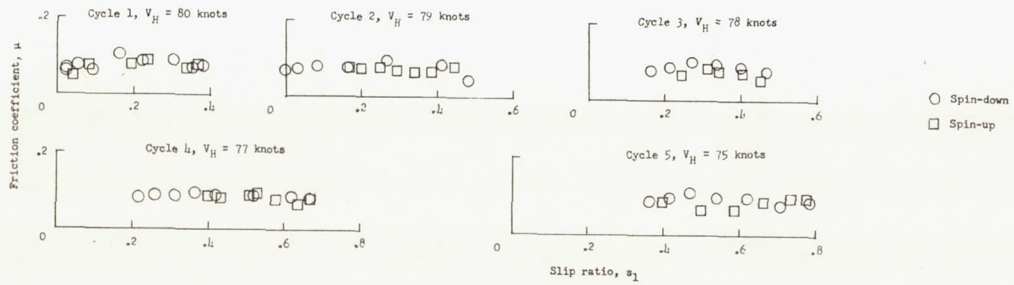

(h) Run 4; p = 120 lb/sq in.

Figure 62.- Continued.

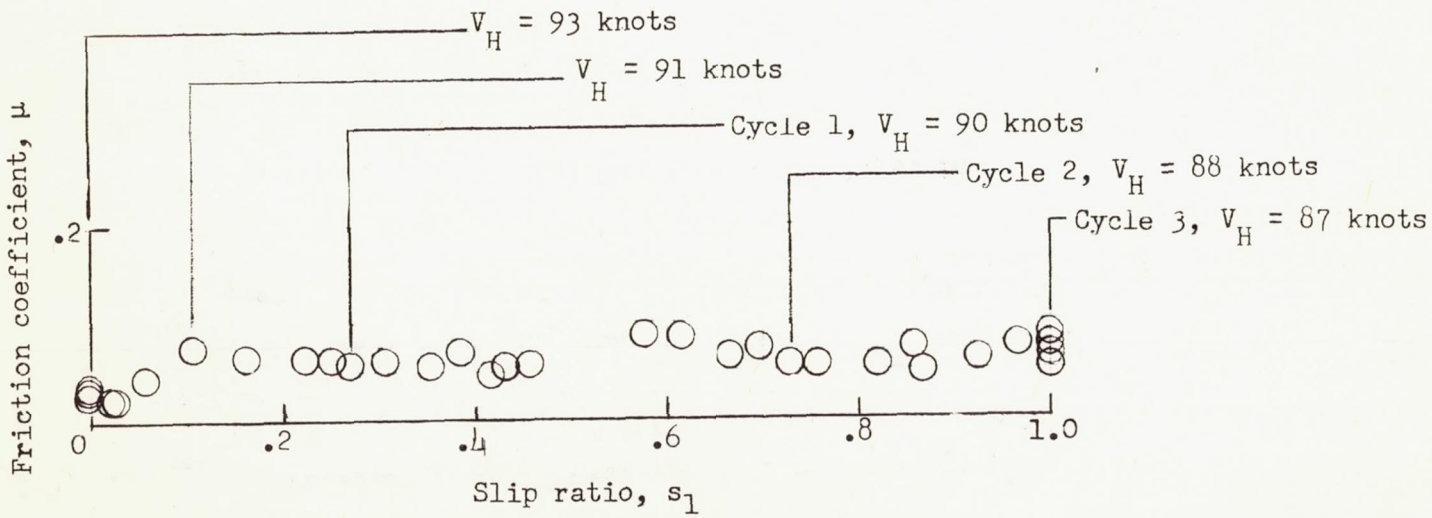

(i) Run 4; p = 120 lb/sq in.

Figure 62.- Concluded.

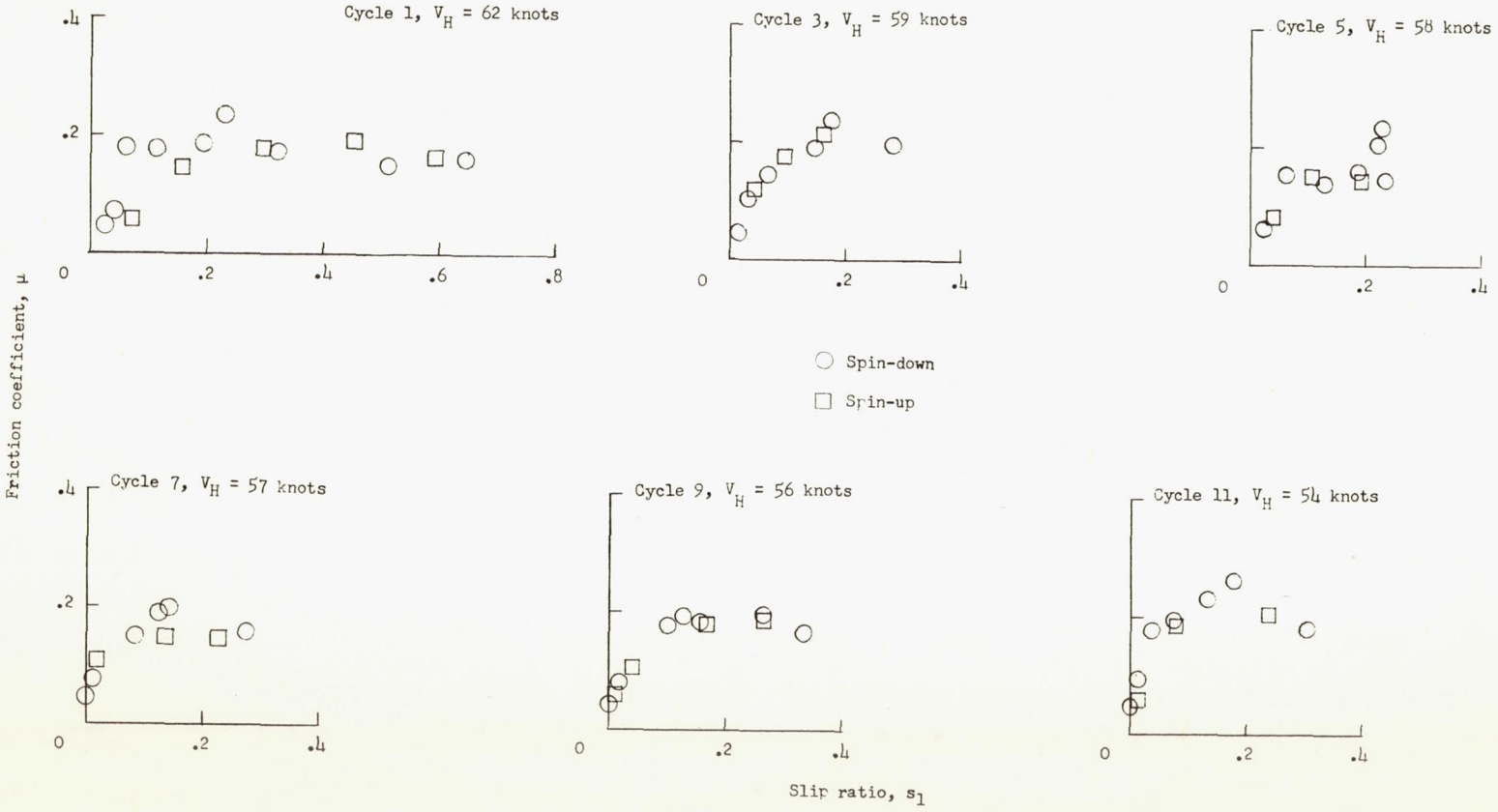

Figure 63.- Tire S1M1, tire S1 modified by 1/2-inch-wide circumferential groove. Run 1; antiskid unit operating; p = 260 lb/sq in.; d_1 = 0 to 0.3 inch.

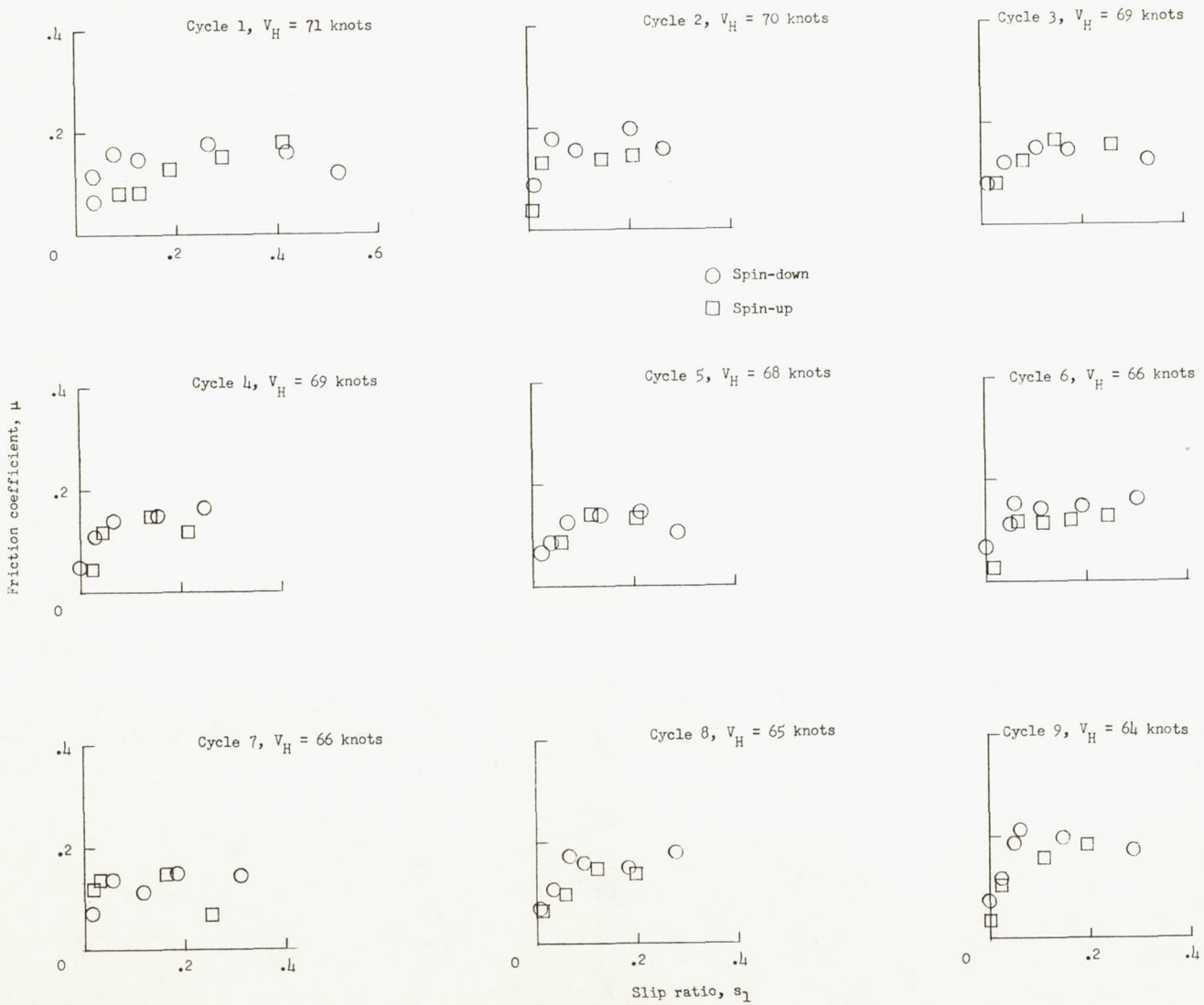

Figure 64.- Tire S1M2, tire S1 modified by 3/4-inch-wide circumferential groove. Run 1; anti-skid unit operating; p = 260 lb/sq in.; d_1 = 0 to 0.3 inch.

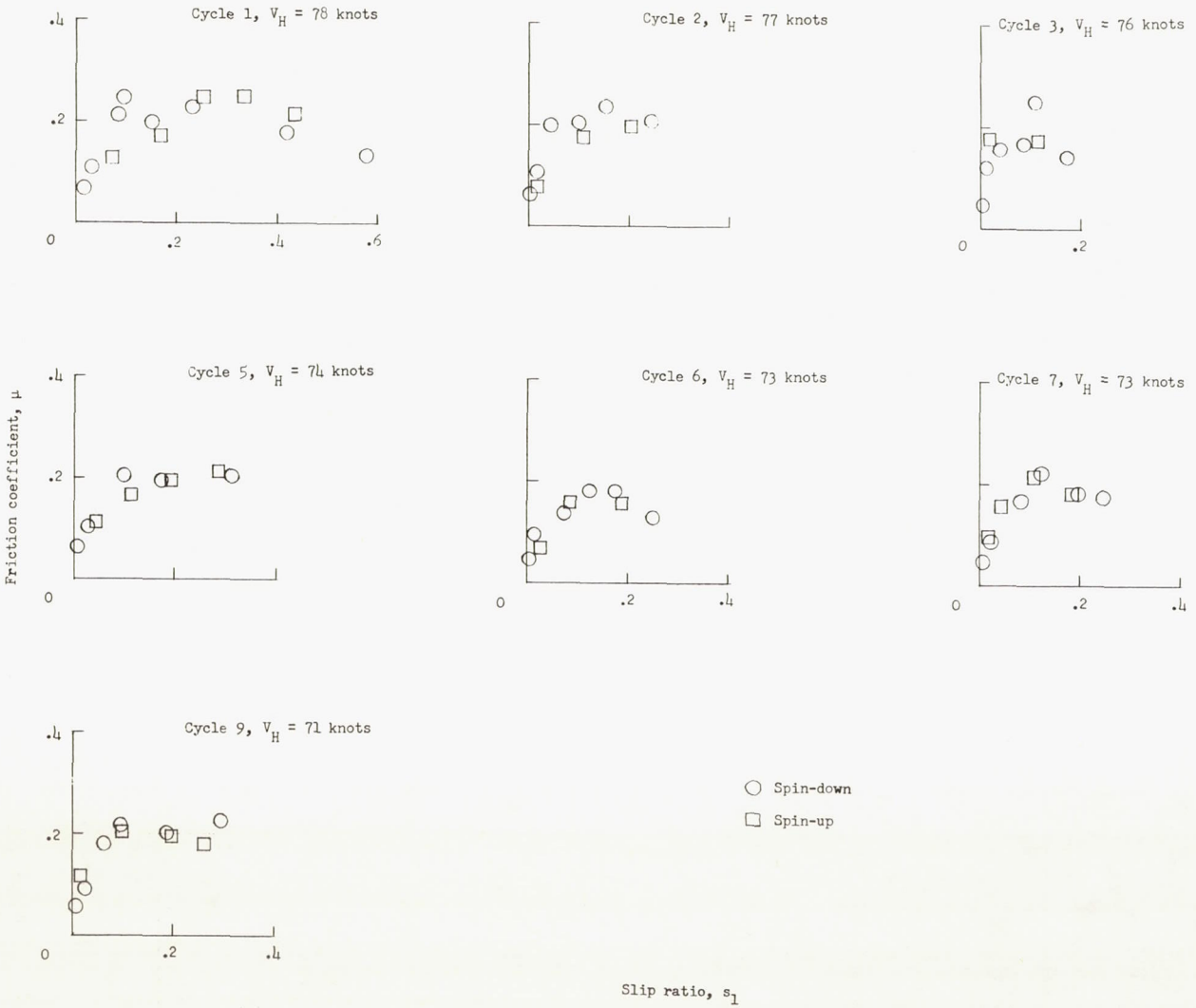

Figure 65.- Tire S1M3, tire S1M2 modified by adding two 3/8-inch-wide circumferential grooves. Run 1; antiskid unit operating; p = 260 lb/sq in.; d_1 = 0 to 0.3 inch.

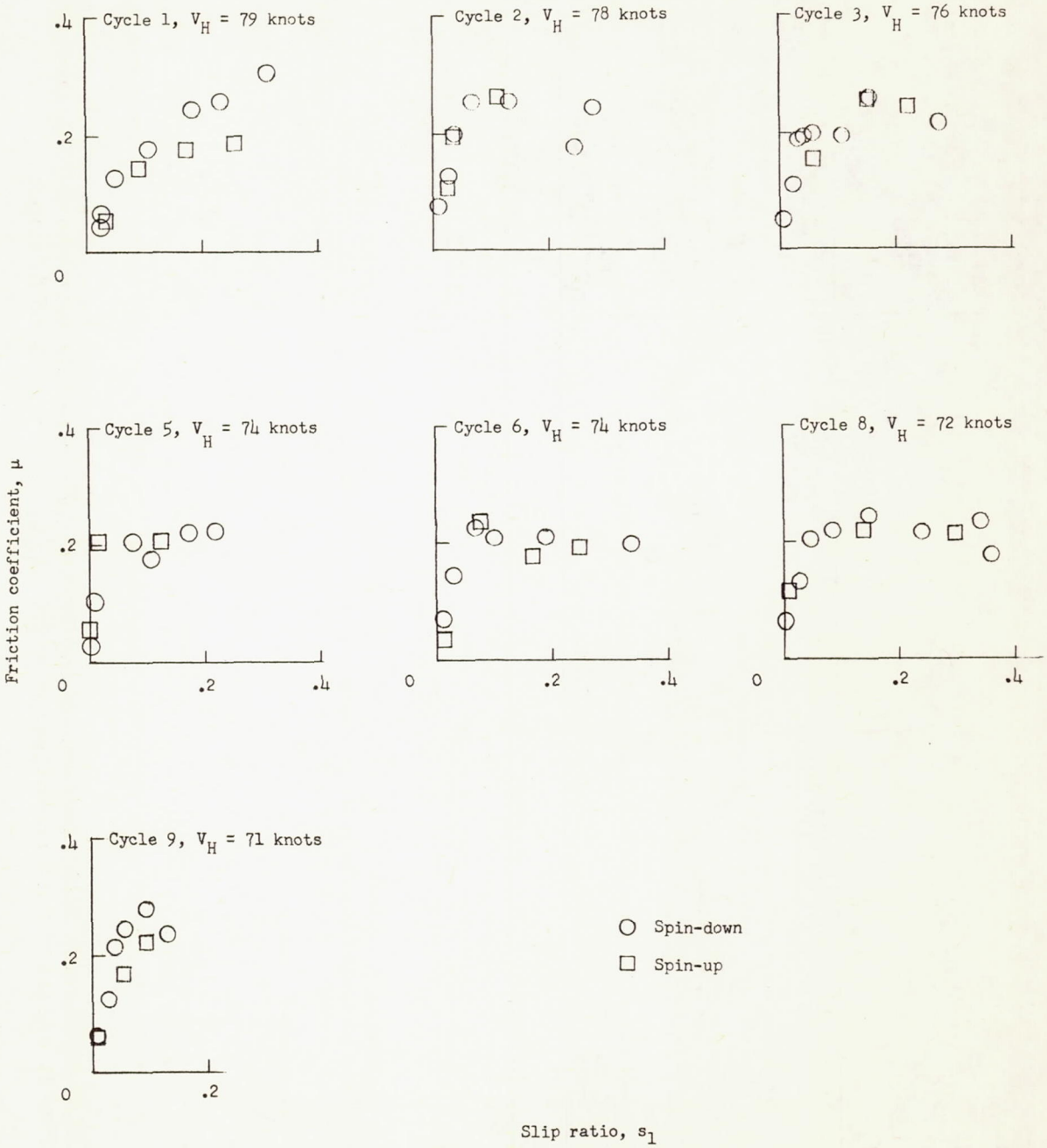

Figure 66.- Tire S1M3. Run 1; antiskid unit operating; p = 260 lb/sq in. For this run, the wet runway was broomed free of water, that is, the runway was left damp with no standing puddles of water; $d_1 \approx 0$.

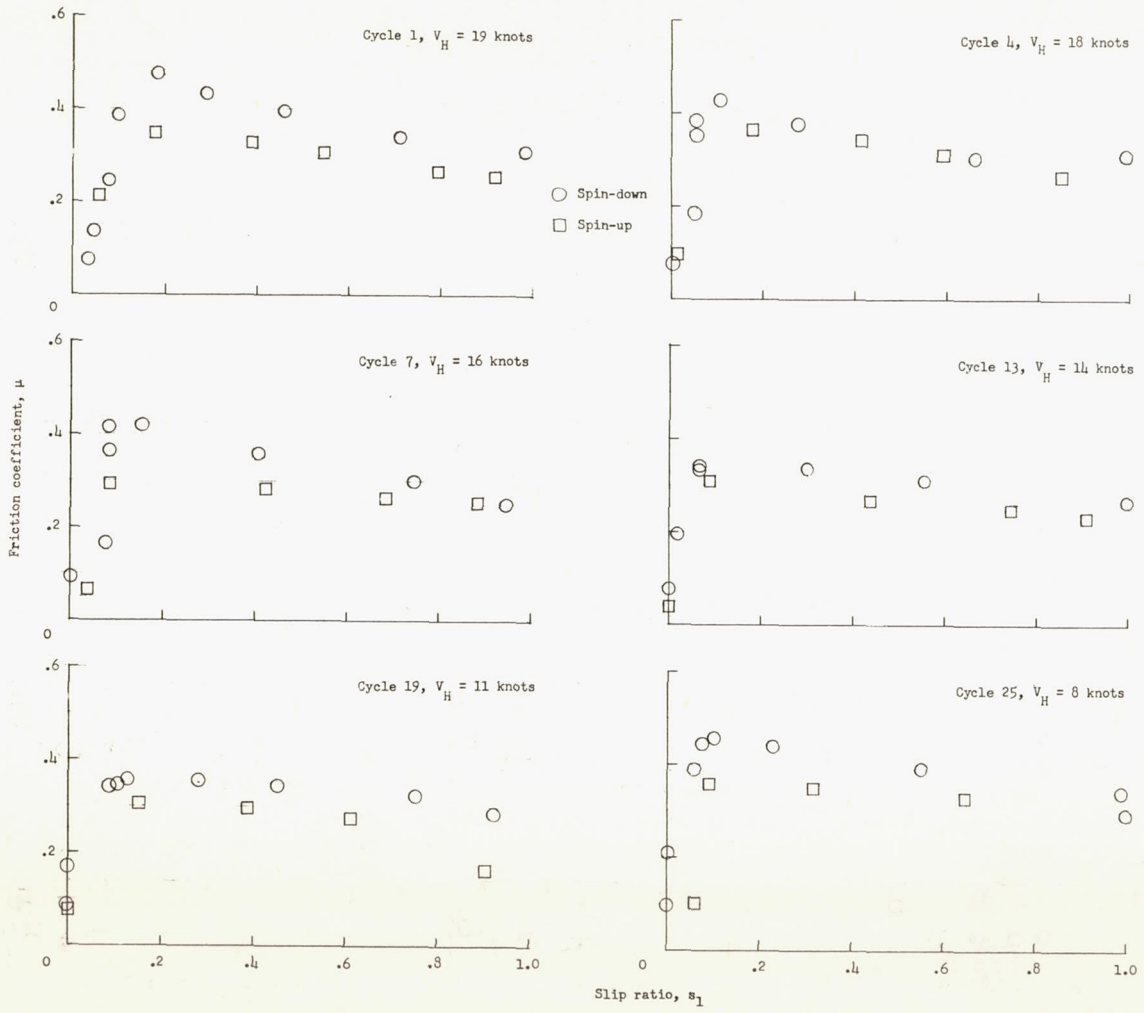

(a) Run 1; p = 260 lb/sq in.

Figure 67.- Tire S2, smooth fabric-reinforced tread, rubber surface. Antiskid unit operating; d_1 = 0 to 0.3 inch.

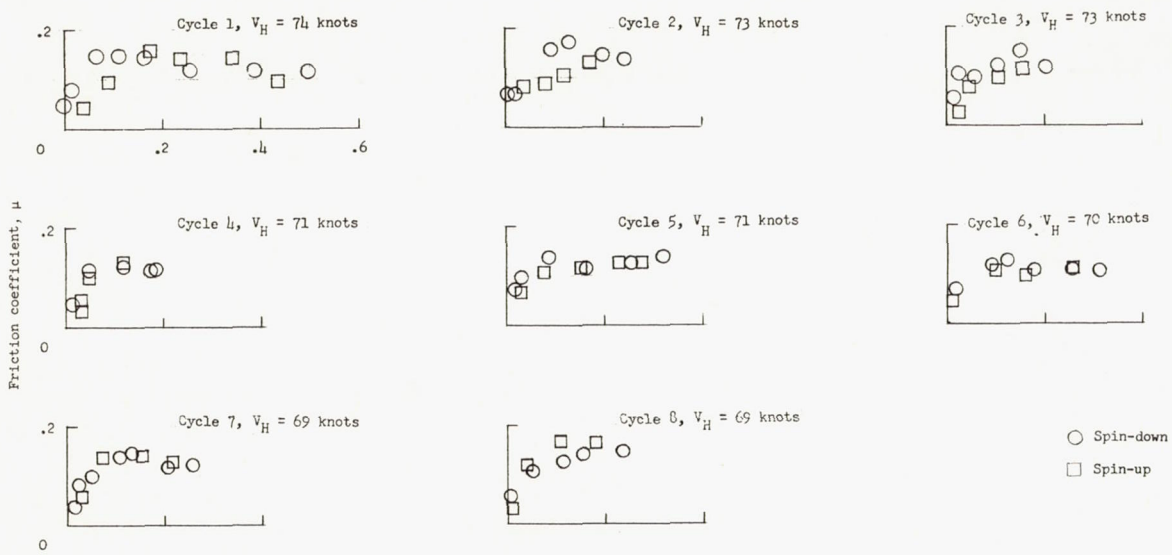

(b) Run 2; p = 260 lb/sq in.

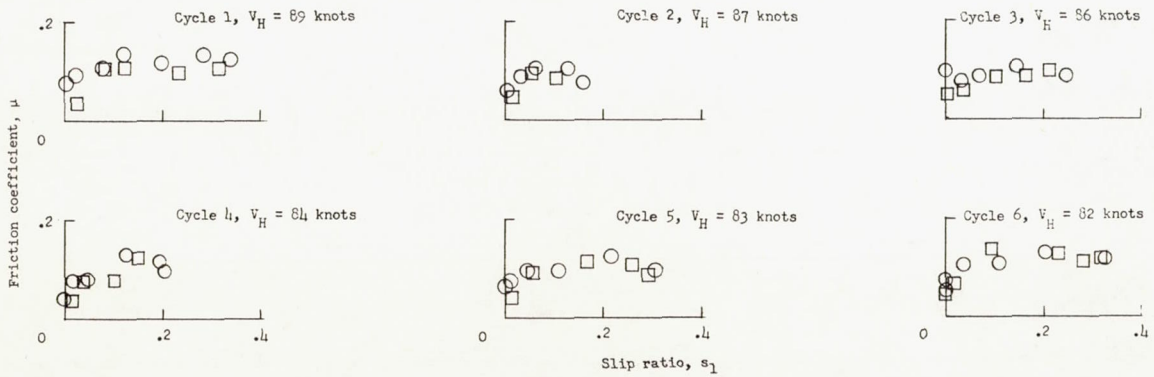

(c) Run 3; p = 260 lb/sq in.

Figure 67.- Continued.

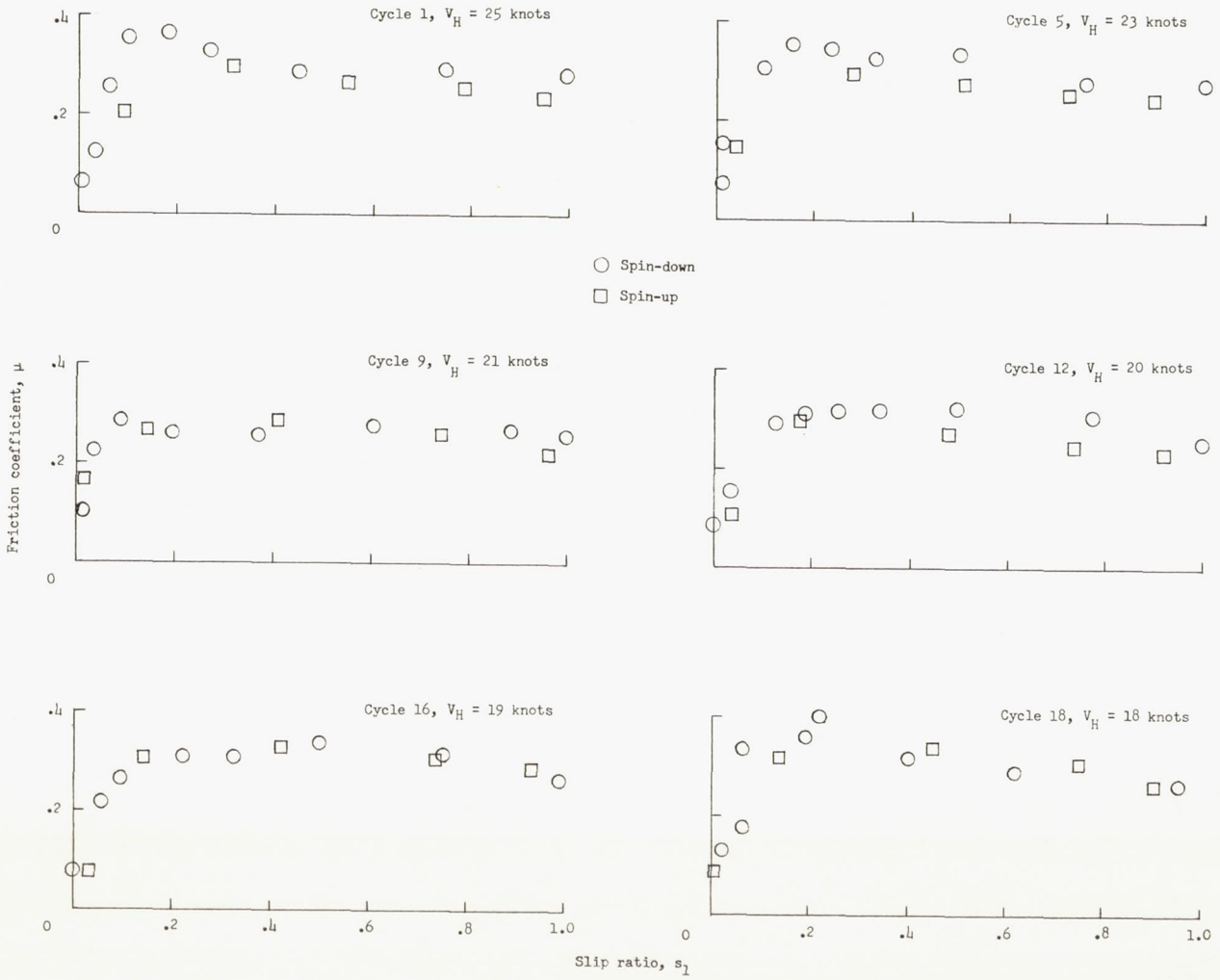

(d) Run 1; p = 120 lb/sq in.

Figure 67.- Continued.

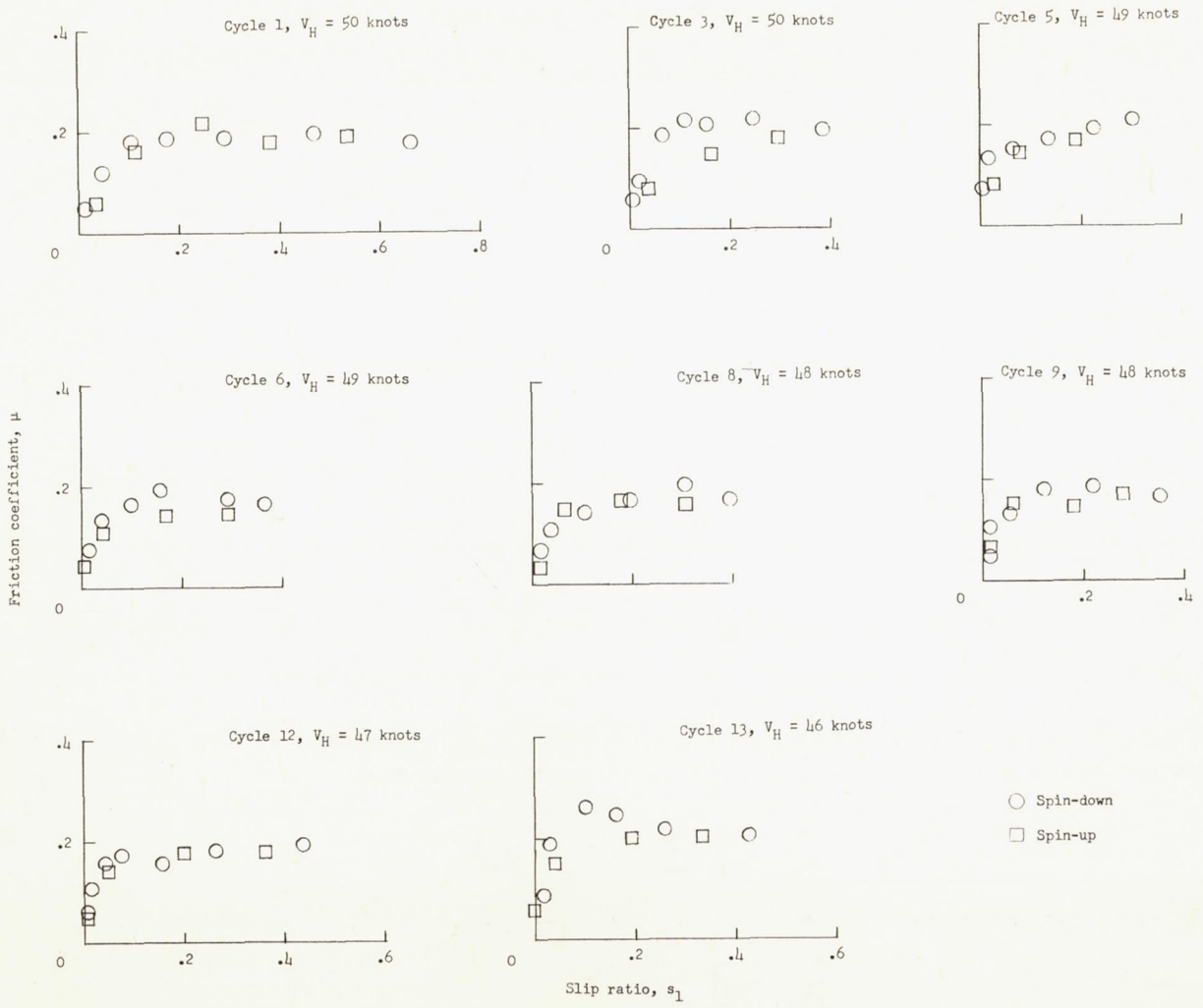

(e) Run 2; p = 120 lb/sq in.

Figure 67.- Continued.

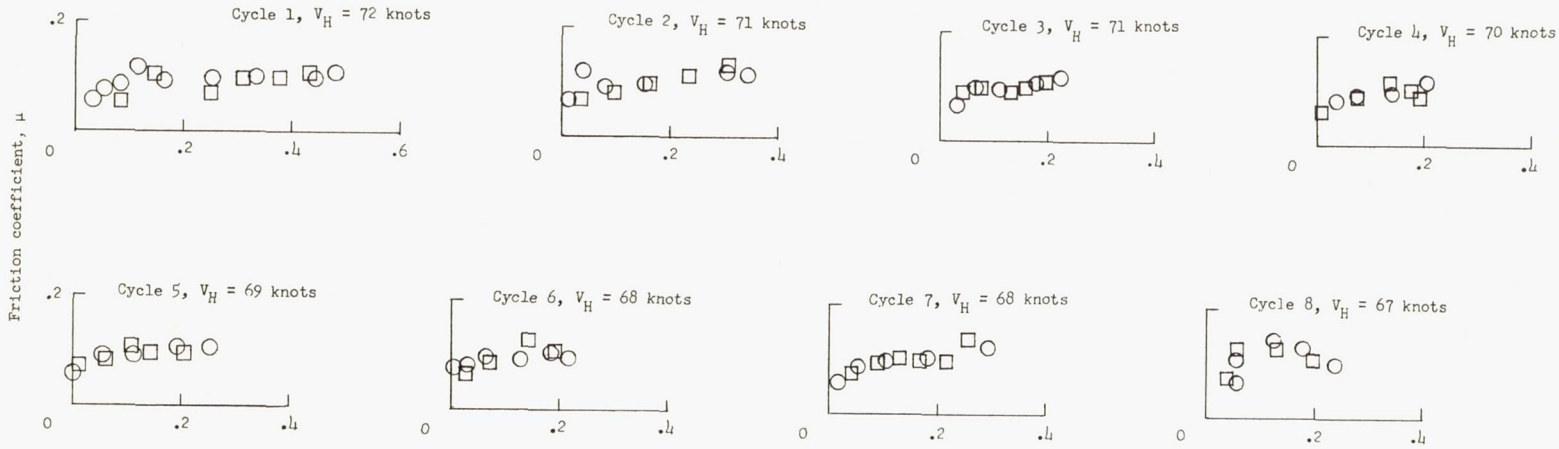

(f) Run 3; p = 120 lb/sq in.

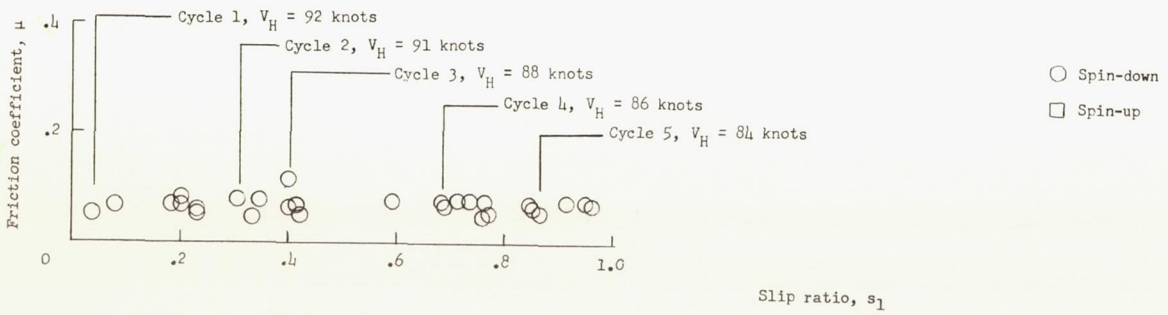

(g) Run 4; p = 120 lb/sq in.

Figure 67.- Concluded.

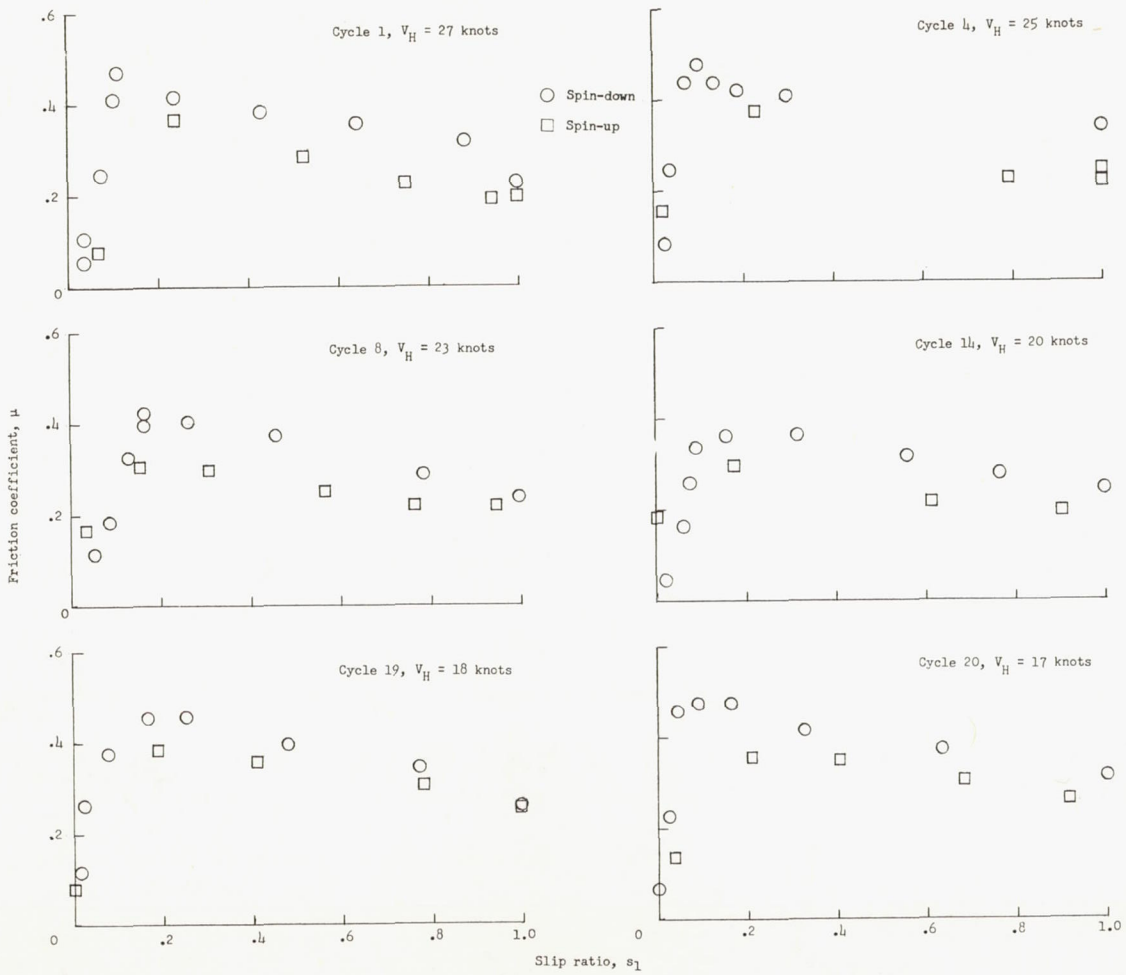

(a) Run 1.

Figure 68.- Tire S2M1, tire S2 modified by adding 4 circumferential grooves. Antiskid unit operating; p = 260 lb/sq in.; d_1 = 0 to 0.3 inch.

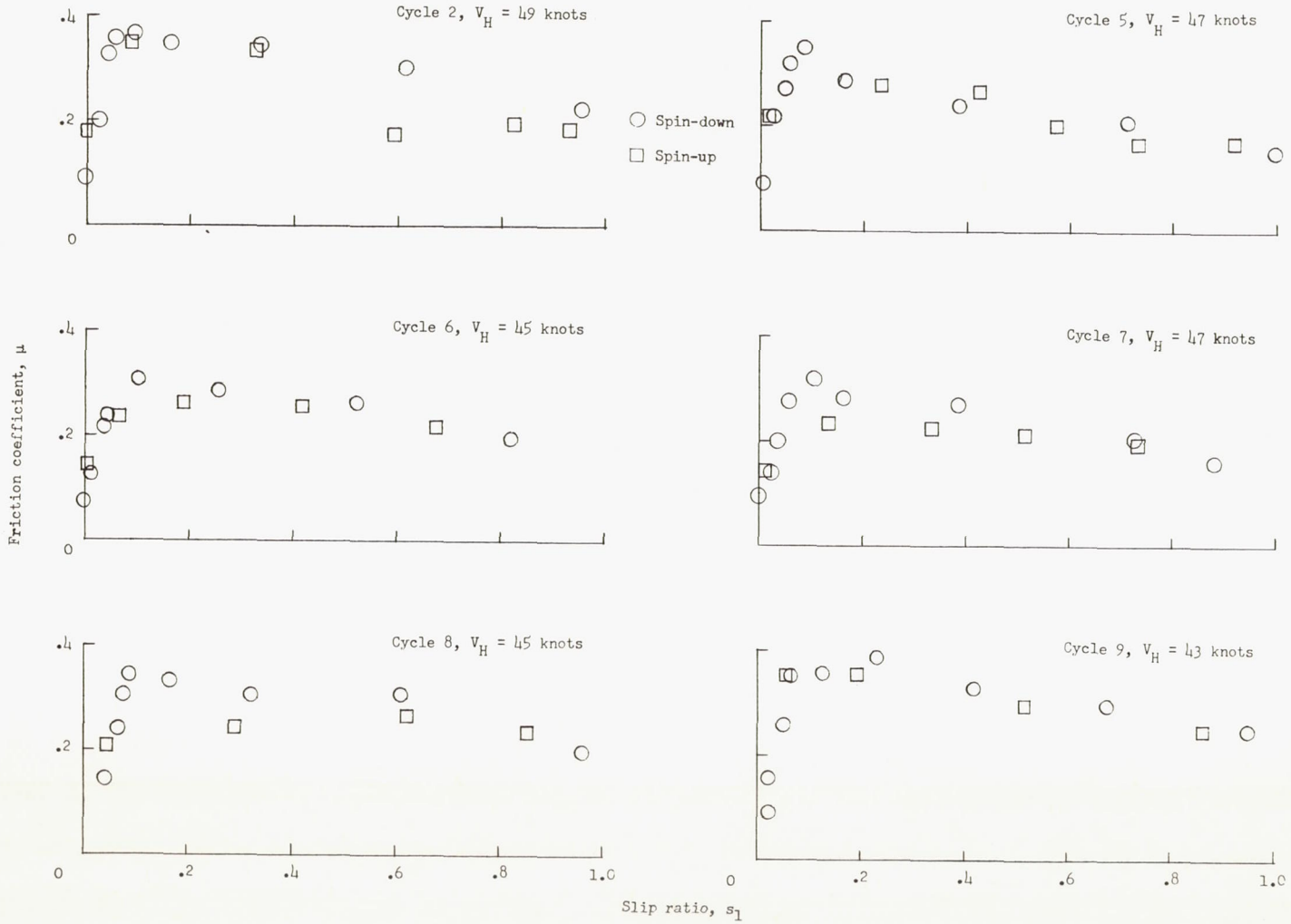

(b) Run 2.

Figure 68.- Continued.

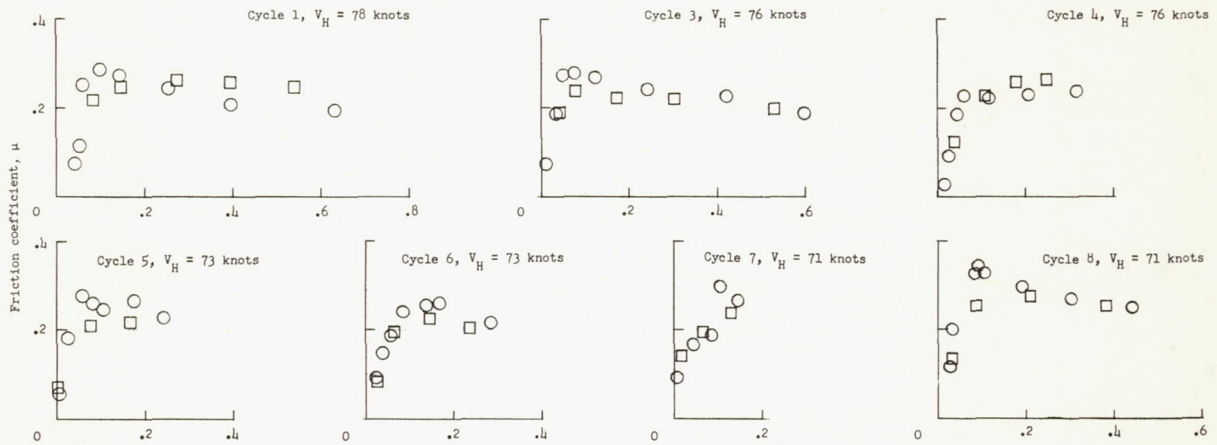

(c) Run 3.

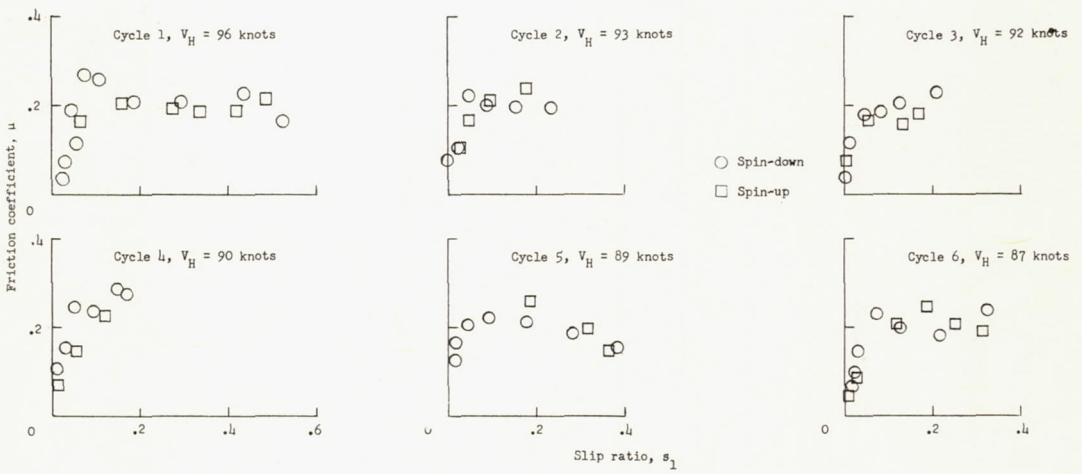

(d) Run 4.

Figure 68.- Concluded.

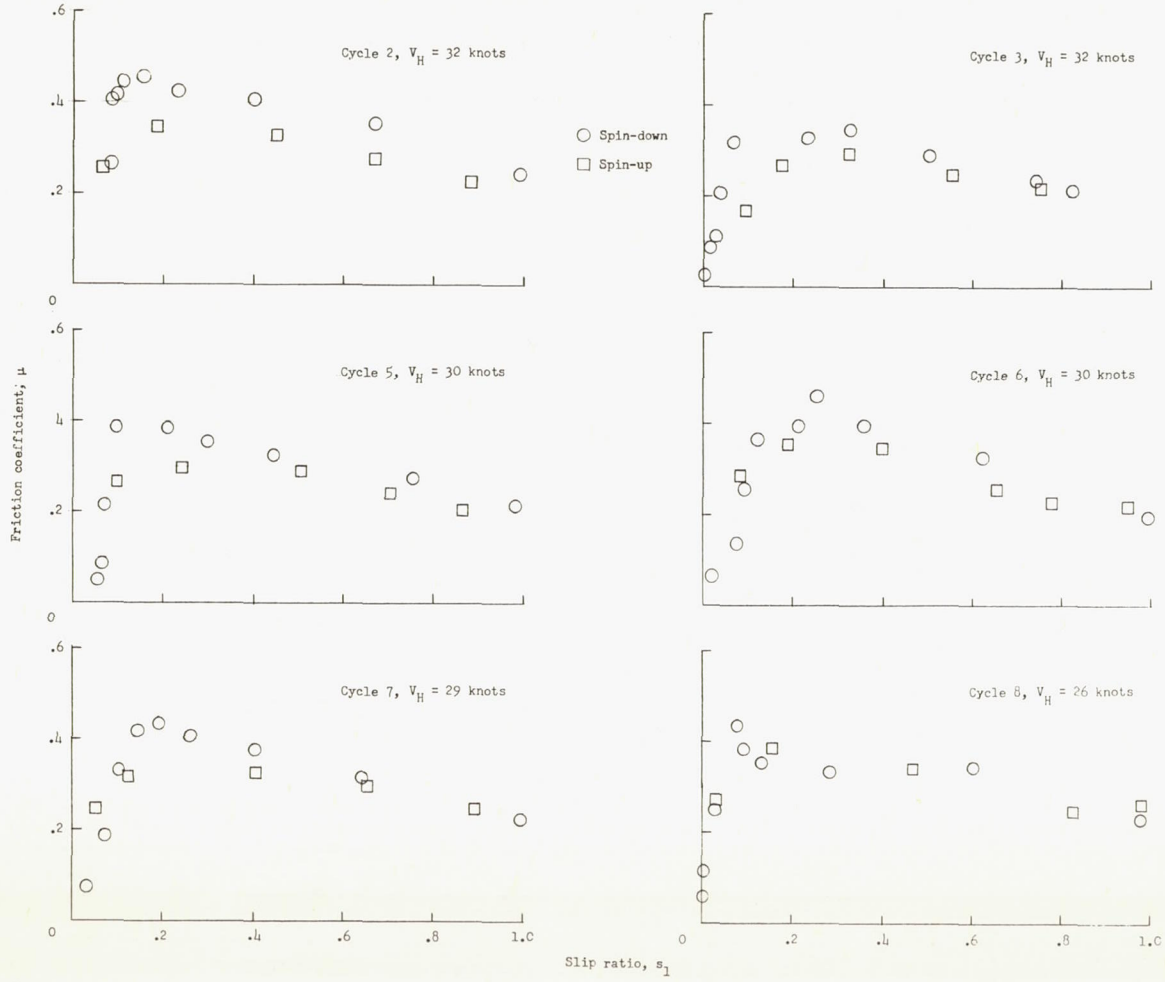

(a) Run 1; p = 260 lb/sq in.

Figure 69.- Tire S2M2, tire S2M1 modified by adding 1 narrow circumferential groove at center line. Antiskid unit operating; d_1 = 0 to 0.3 inch.

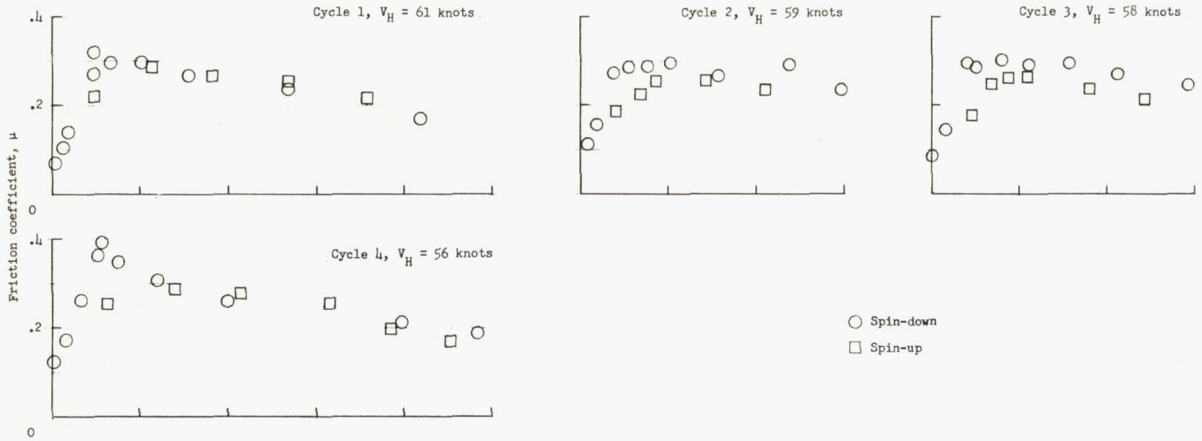

(b) Run 2; p = 260 lb/sq in.

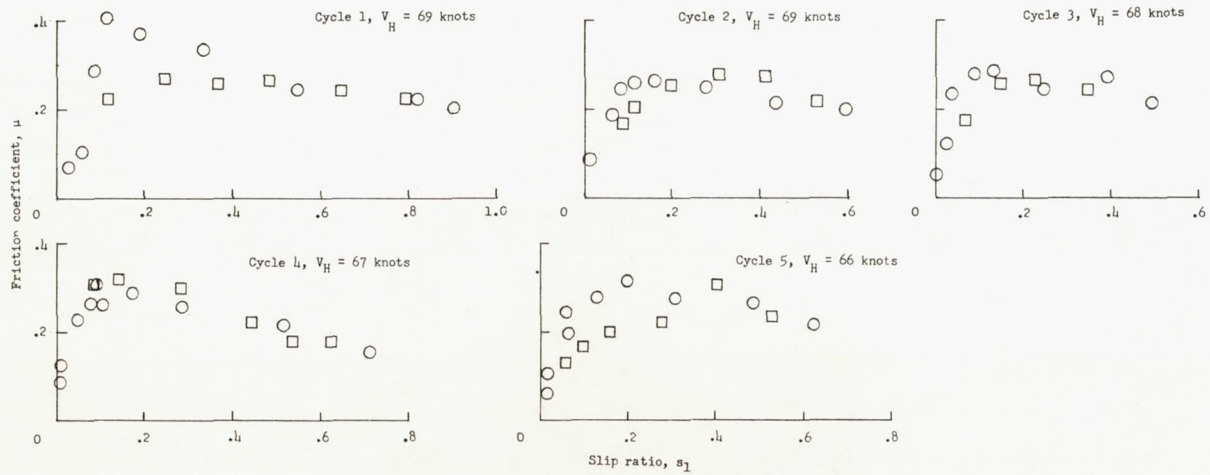

(c) Run 3; p = 260 lb/sq in.

Figure 69.- Continued.

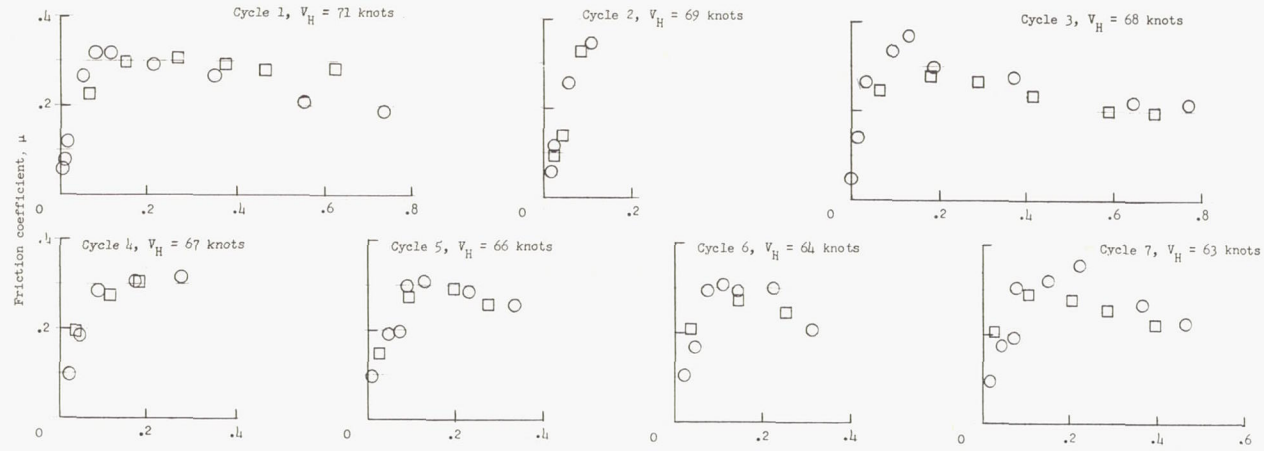

(d) Run 4; p = 260 lb/sq in.

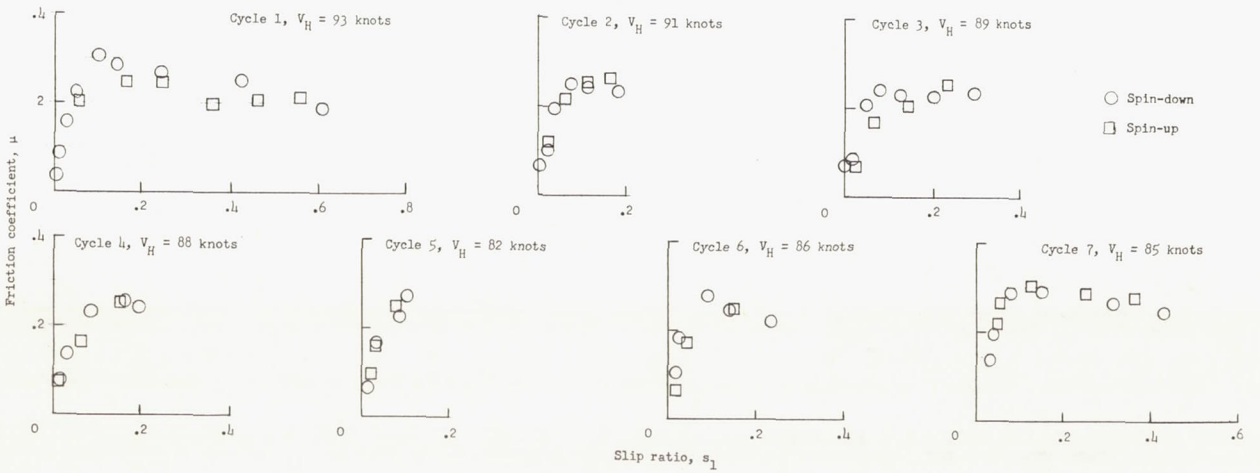

(e) Run 5; p = 260 lb/sq in.

Figure 69.- Continued.

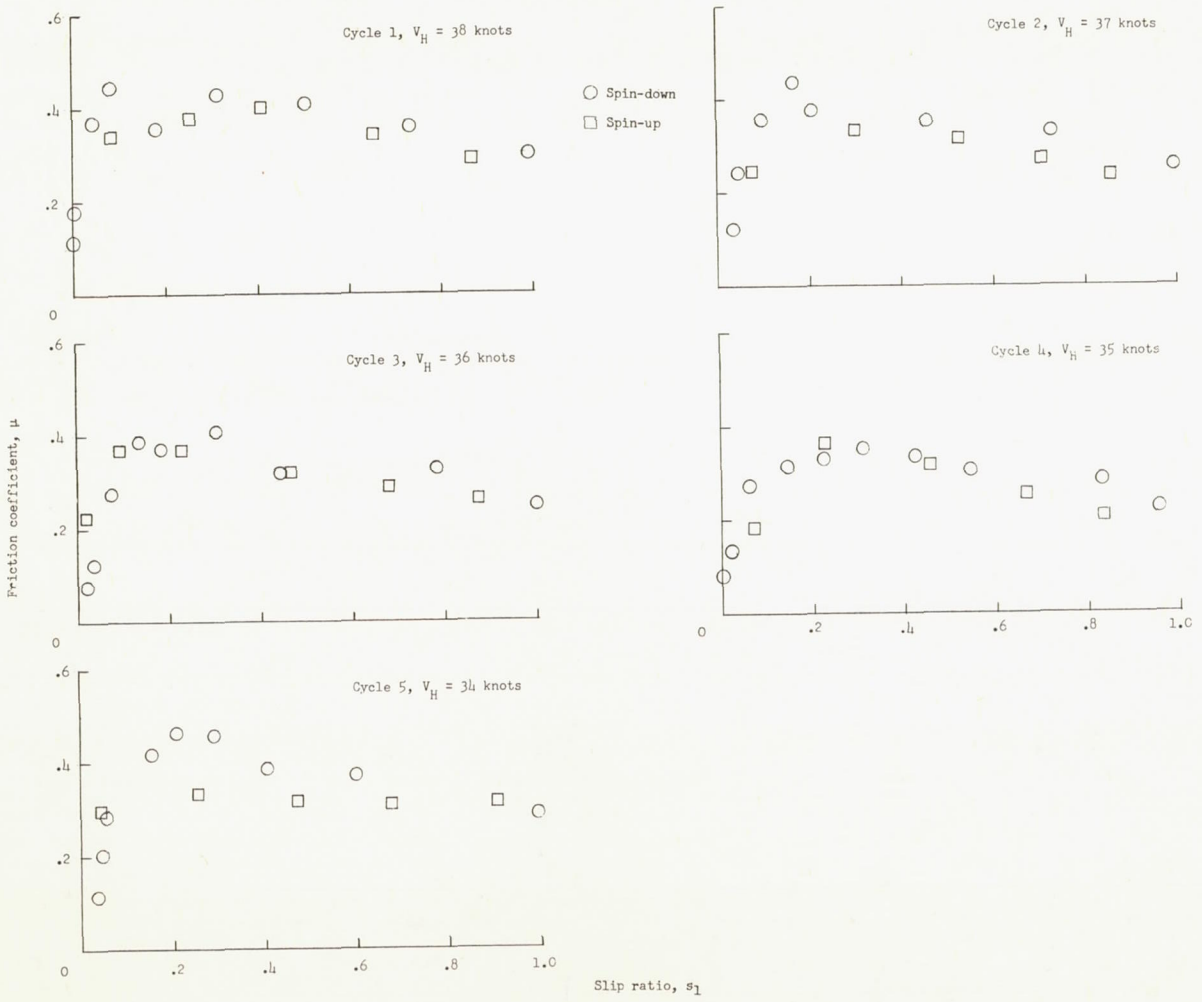

(f) Run 1; p = 120 lb/sq in.

Figure 69.- Continued.

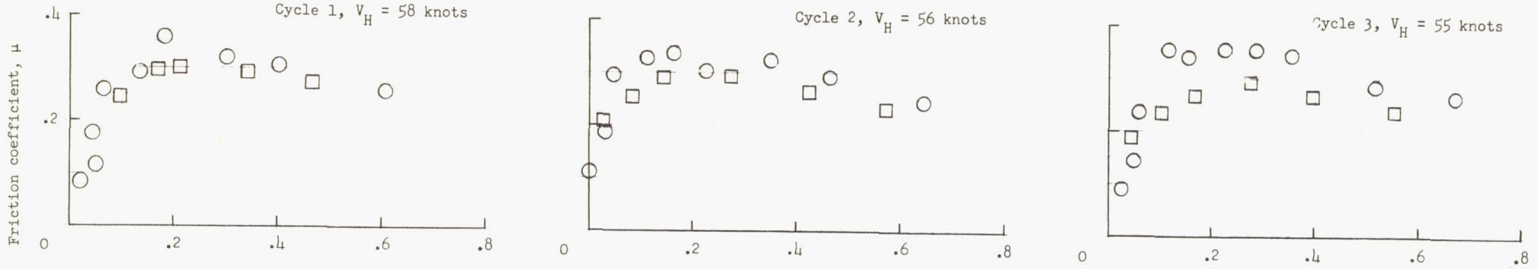

(g) Run 2; p = 120 lb/sq in.

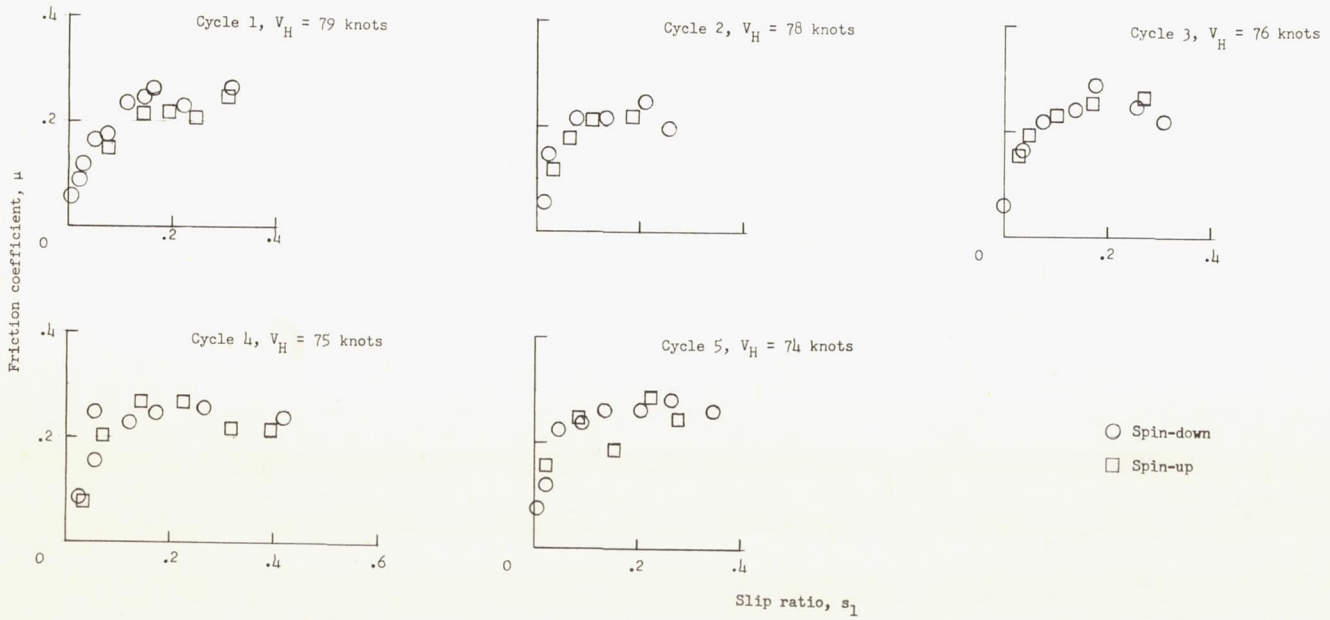

(h) Run 3; p = 120 lb/sq in.

Figure 69.- Concluded.

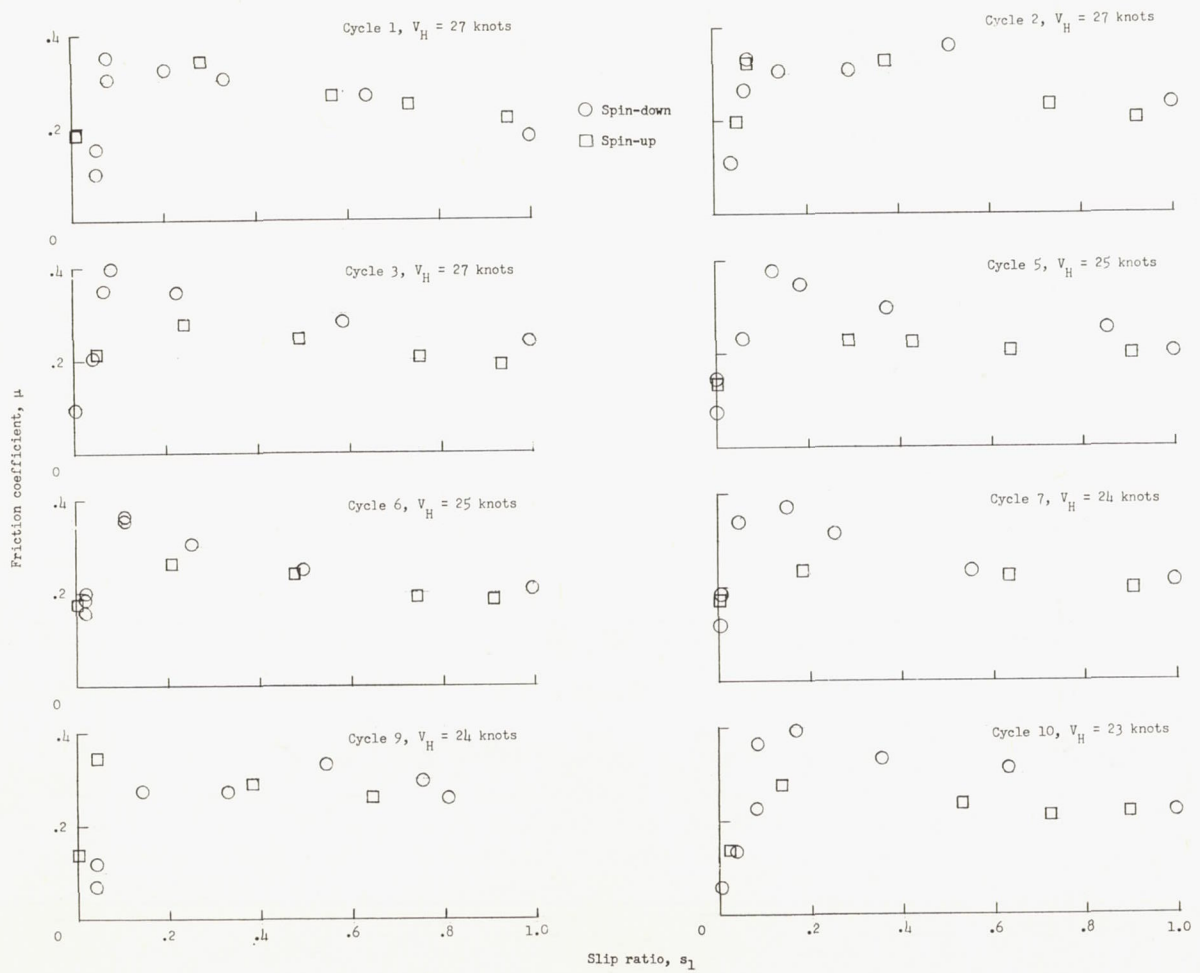

(a) Run 1.

Figure 70.- Tire S3, smooth fabric-reinforced tread, fabric surface. Antiskid unit operating; p = 260 lb/sq in.; d_1 = 0 to 0.3 inch.

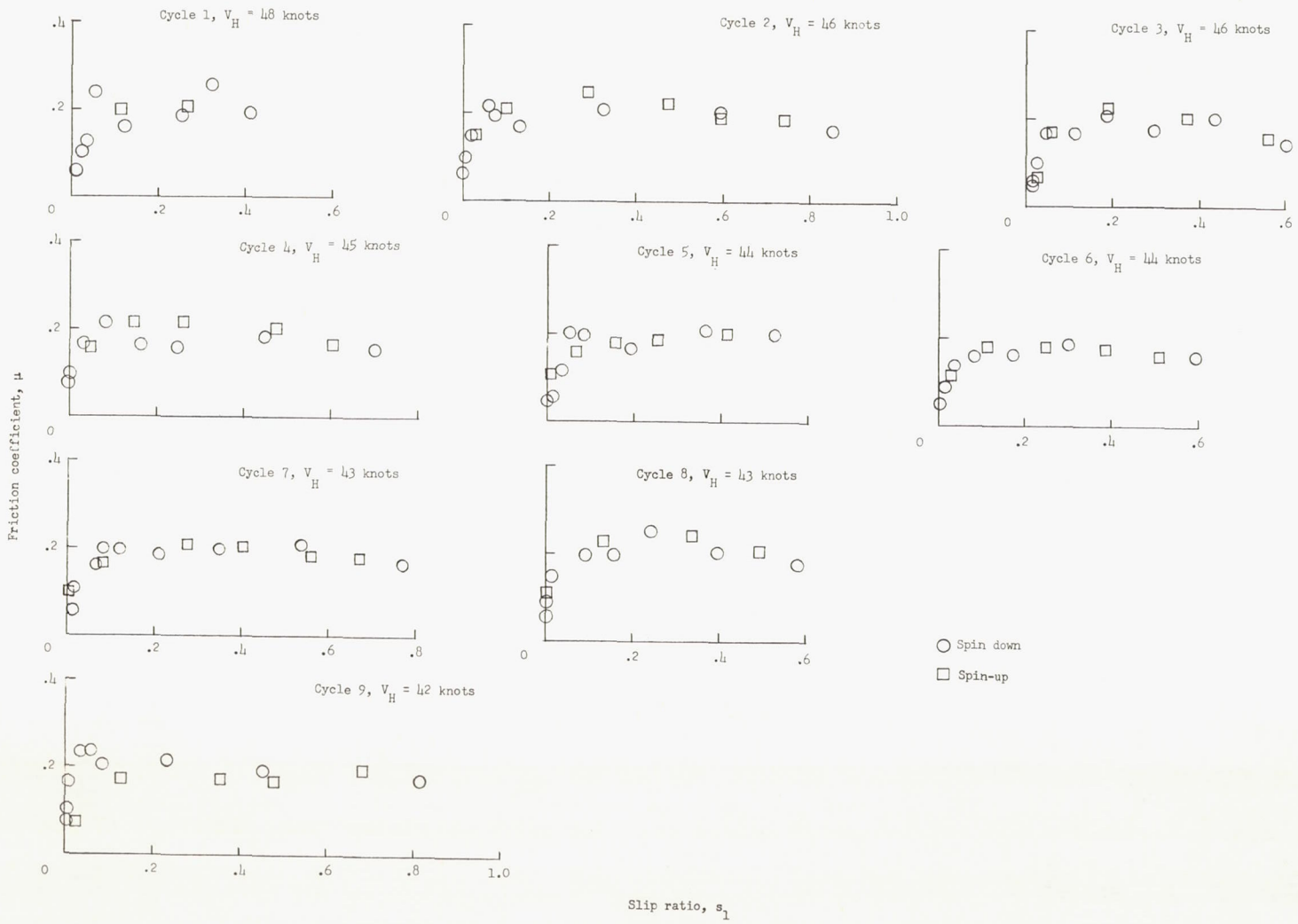

(b) Run 2.

Figure 70.- Continued.

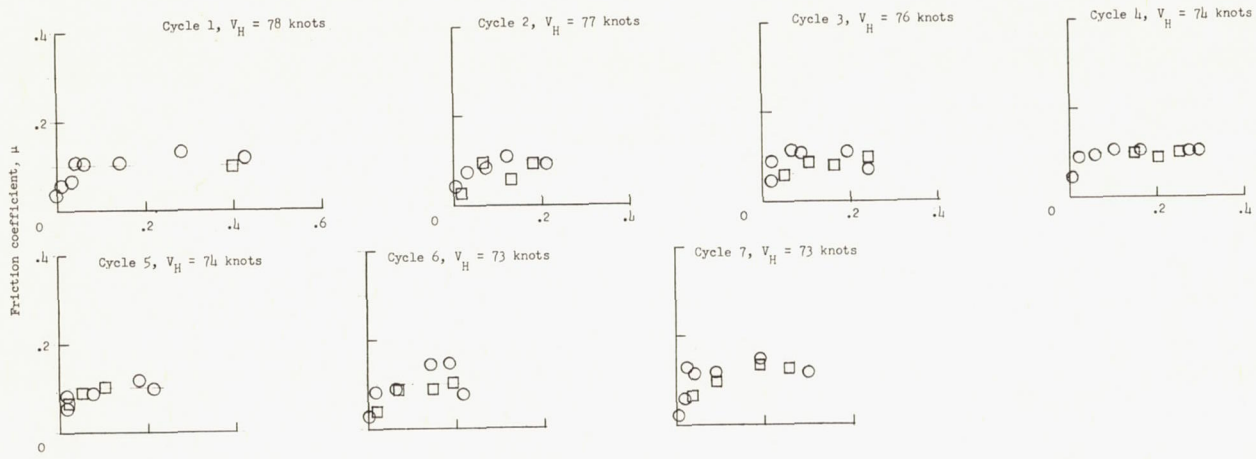

(c) Run 3.

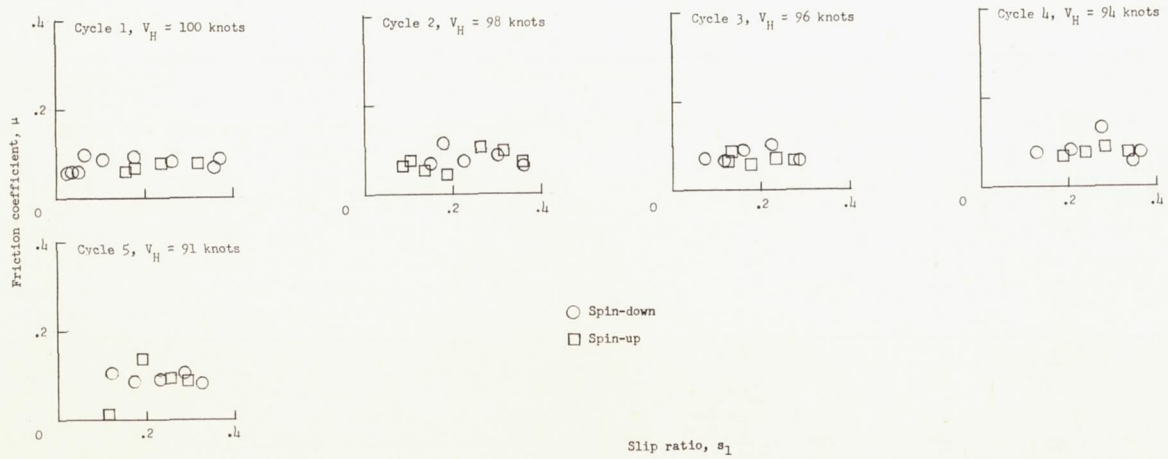

(d) Run 4.

Figure 70.- Concluded.

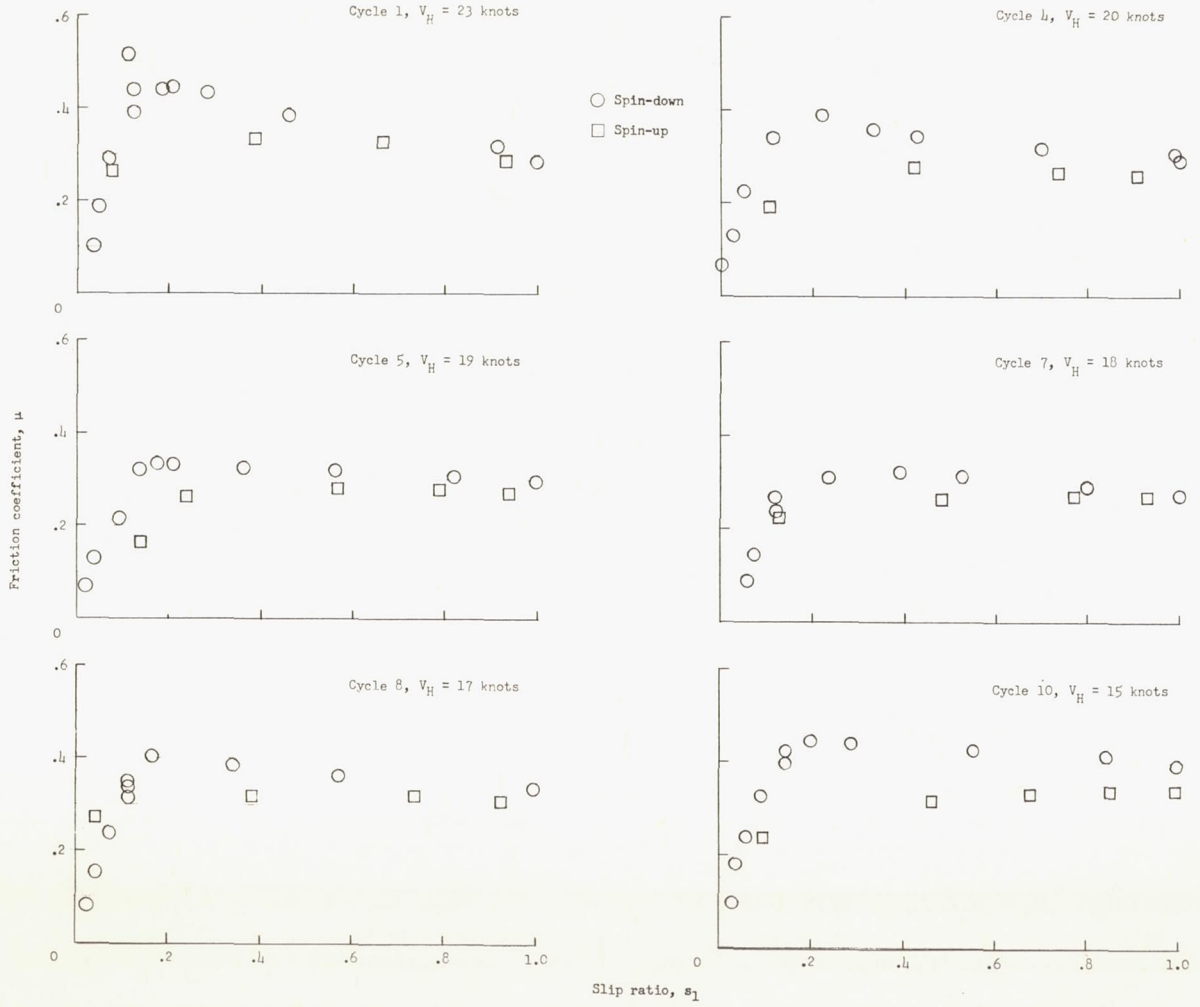

(a) Run 1.

Figure 71.- Tire S4M1, smooth fabric-reinforced tread, rubber surface, modified by adding a large diamond pattern. Antiskid unit operating; p = 260 lb/sq in.; d_1 = 0 to 0.3 inch.

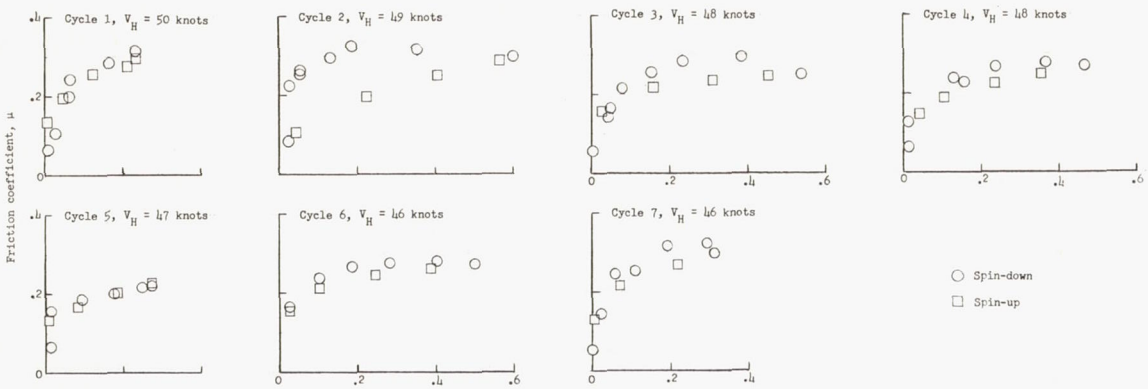

(b) Run 2.

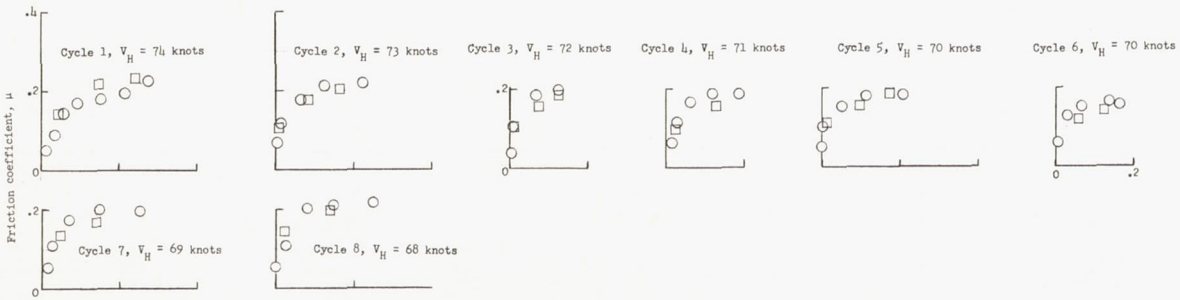

(c) Run 3.

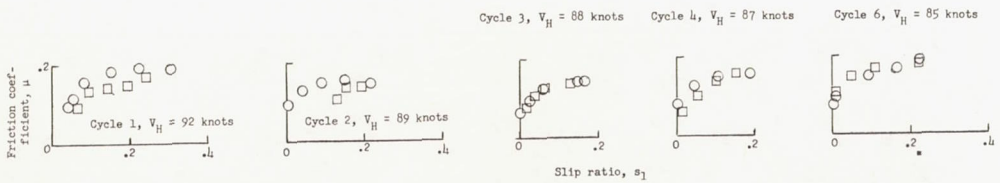

(d) Run 4.

Figure 71.- Concluded.

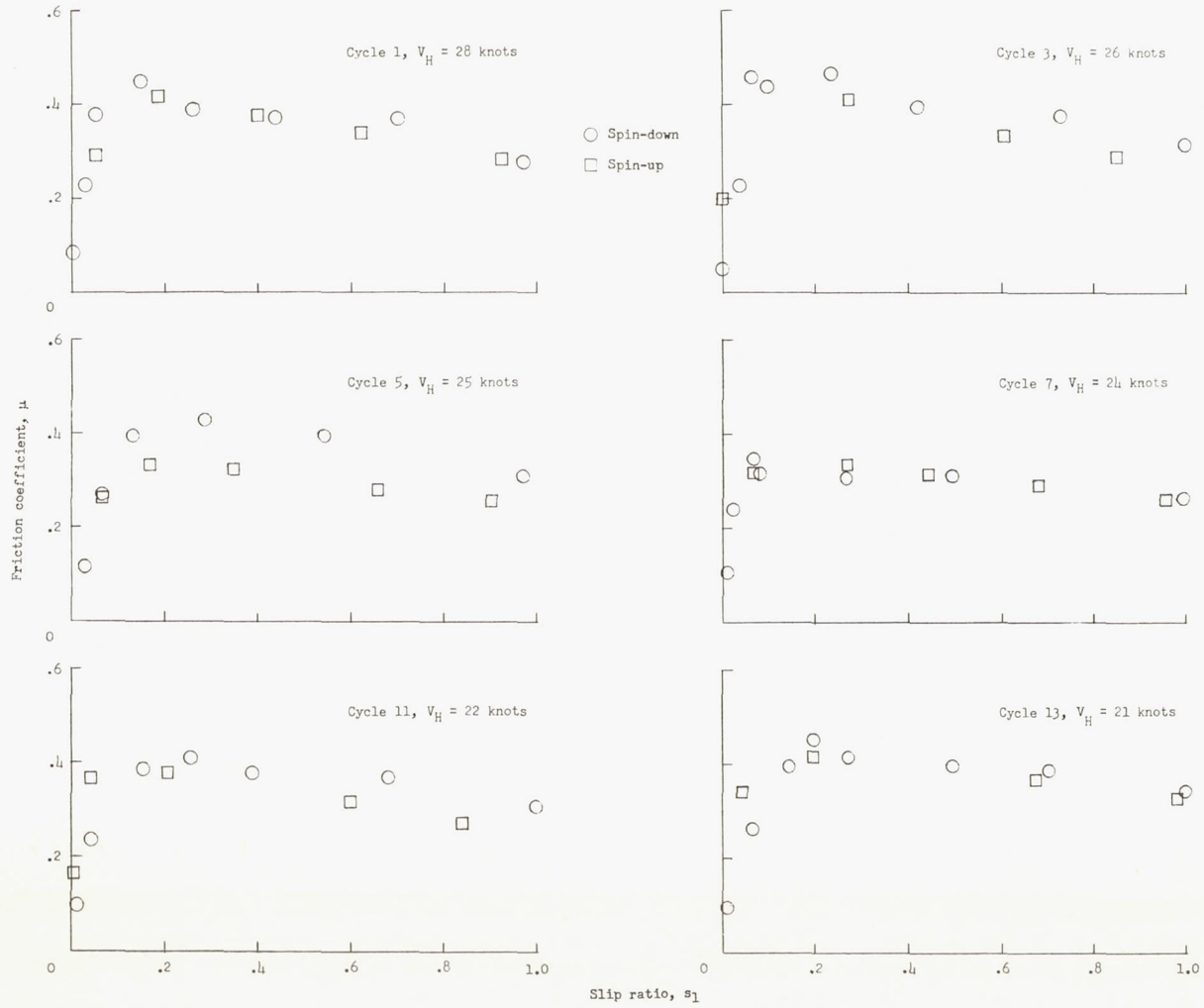

(a) Run 1.

Figure 72.- Tire S5M1, smooth fabric-reinforced tread, rubber surface, modified by adding a small diamond pattern. Antiskid unit operating; p = 260 lb/sq in.; d_1 = 0 to 0.3 inch.

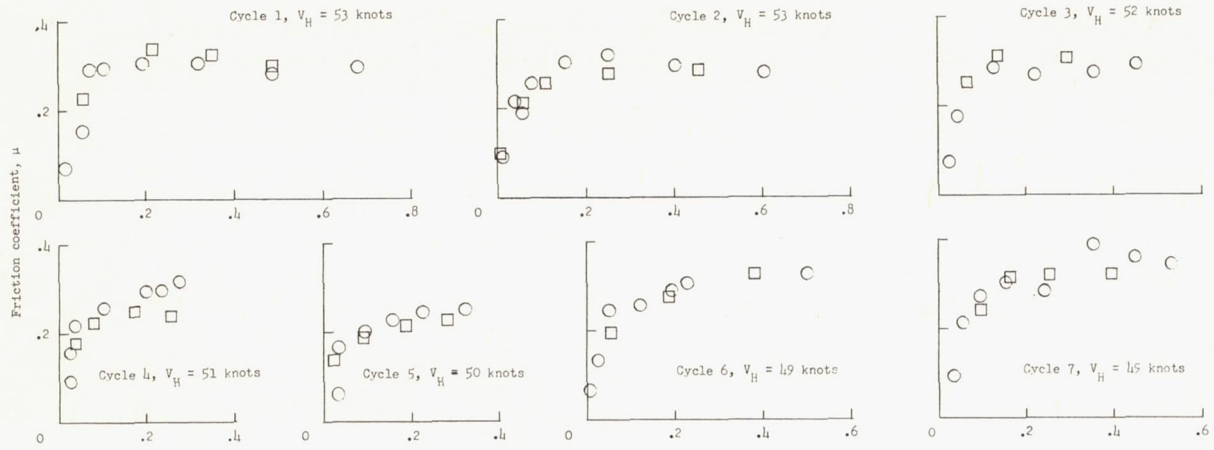

(b) Run 2.

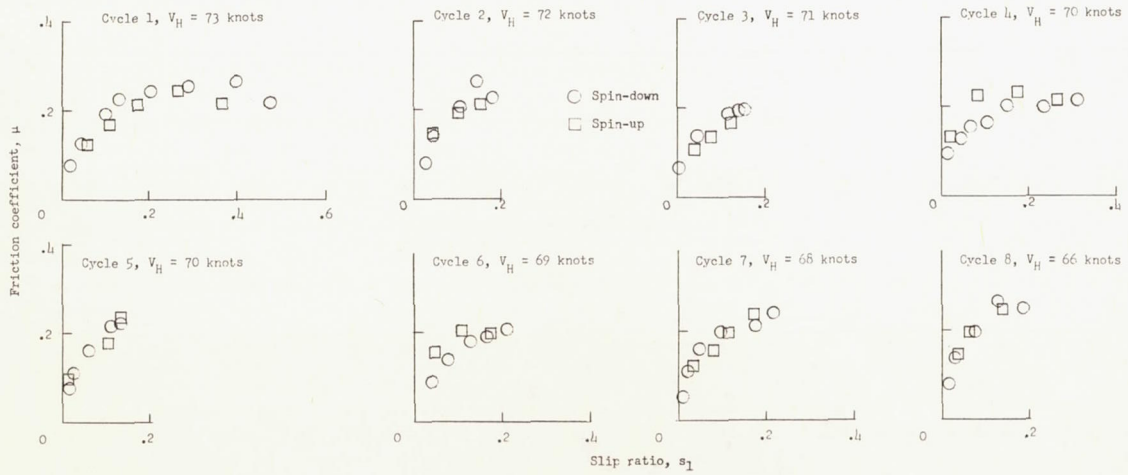

(c) Run 3.

Figure 72.- Continued.

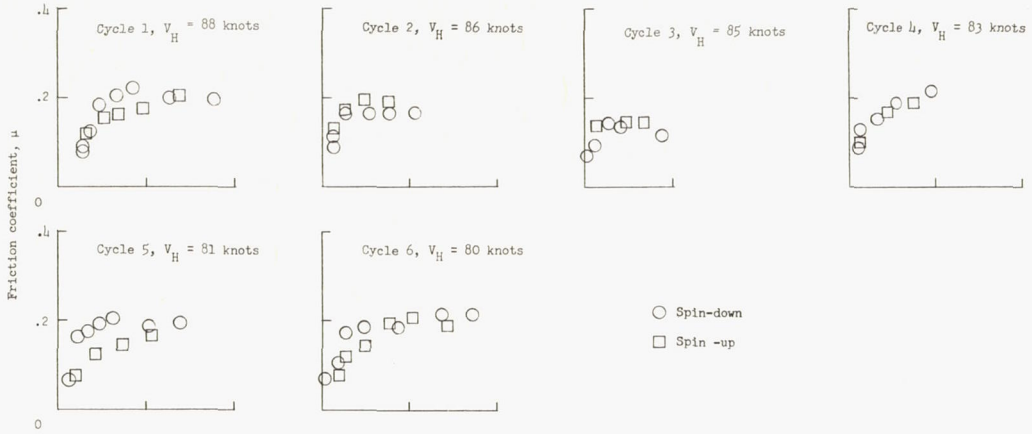

(d) Run 4.

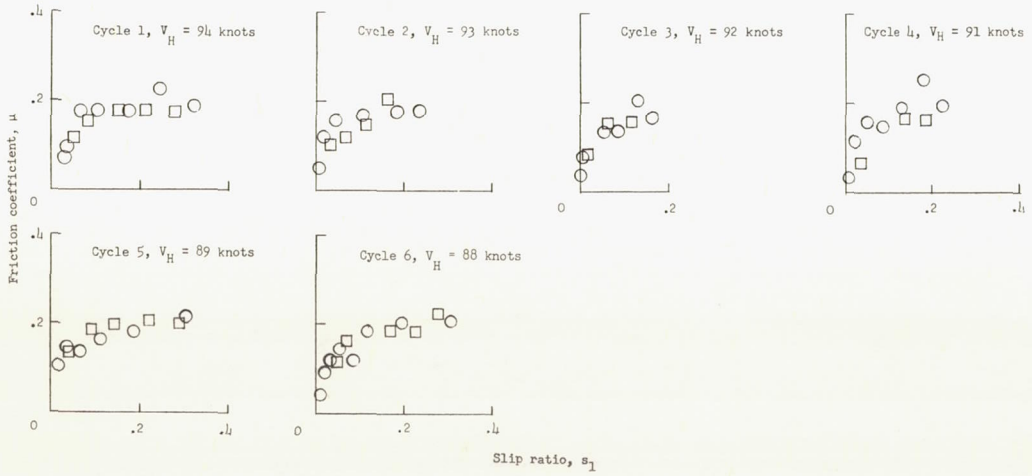

(e) Run 5.

Figure 72.- Concluded.

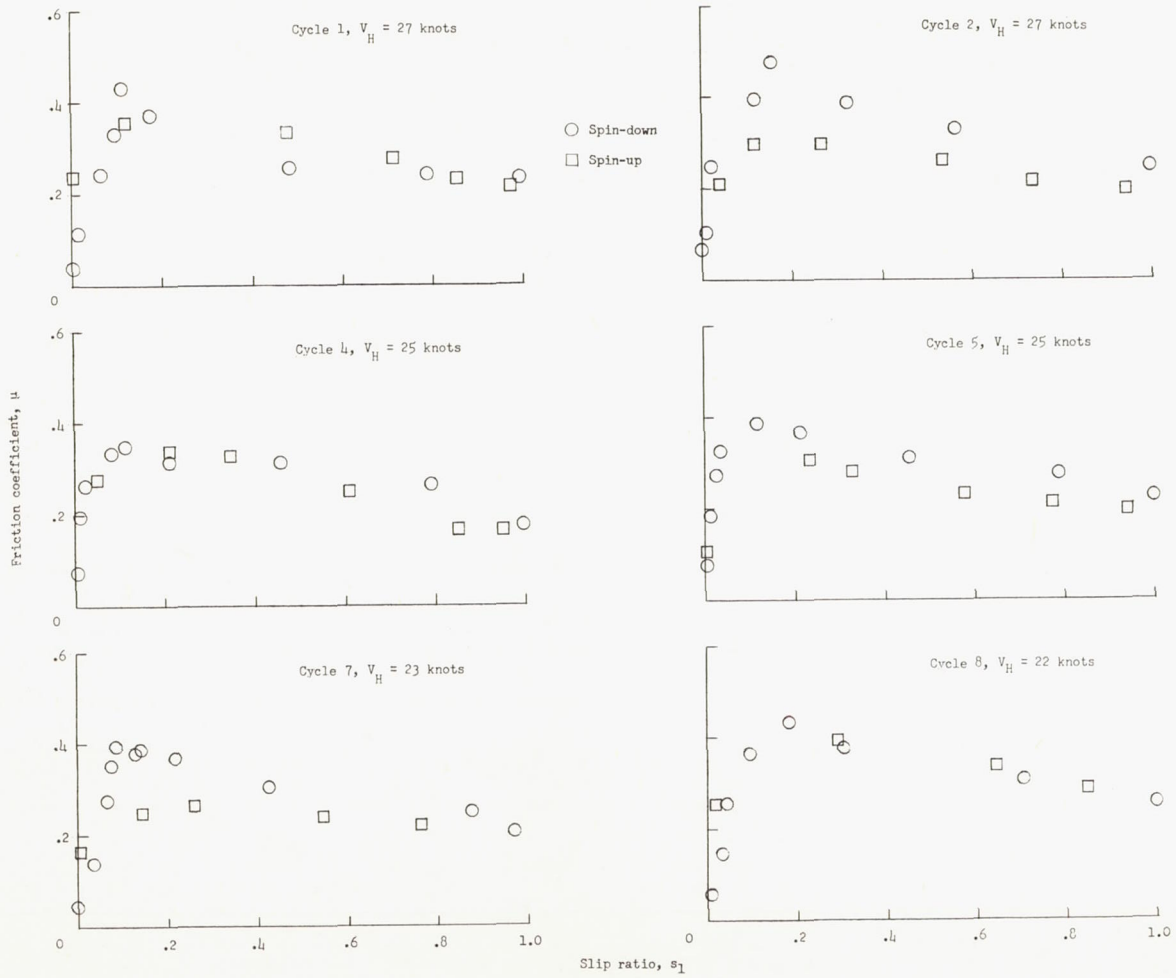

(a) Run 1.

Figure 73.- Tire S6M1, smooth fabric-reinforced tread, rubber surface, modified by adding 7 circumferential grooves (sine-wave cross section). Antiskid unit operating; p = 260 lb/sq in.; d_1 = 0 to 0.3 inch.

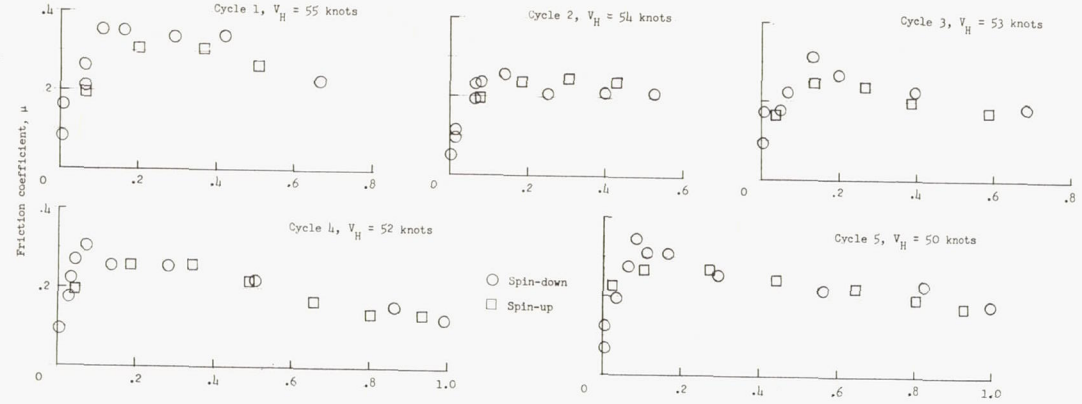

(b) Run 2.

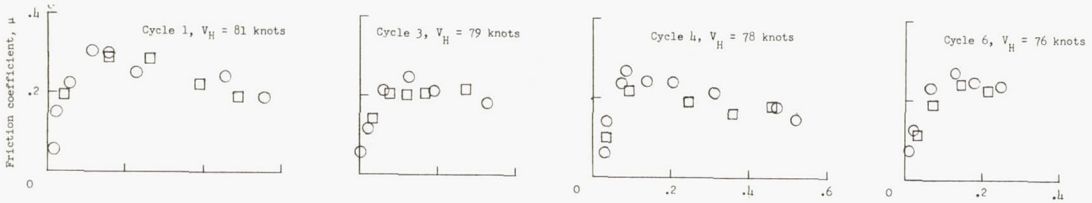

(c) Run 3.

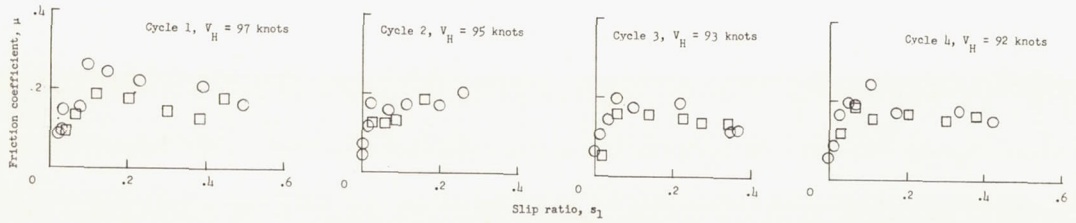

(d) Run 4.

Figure 73.- Concluded.

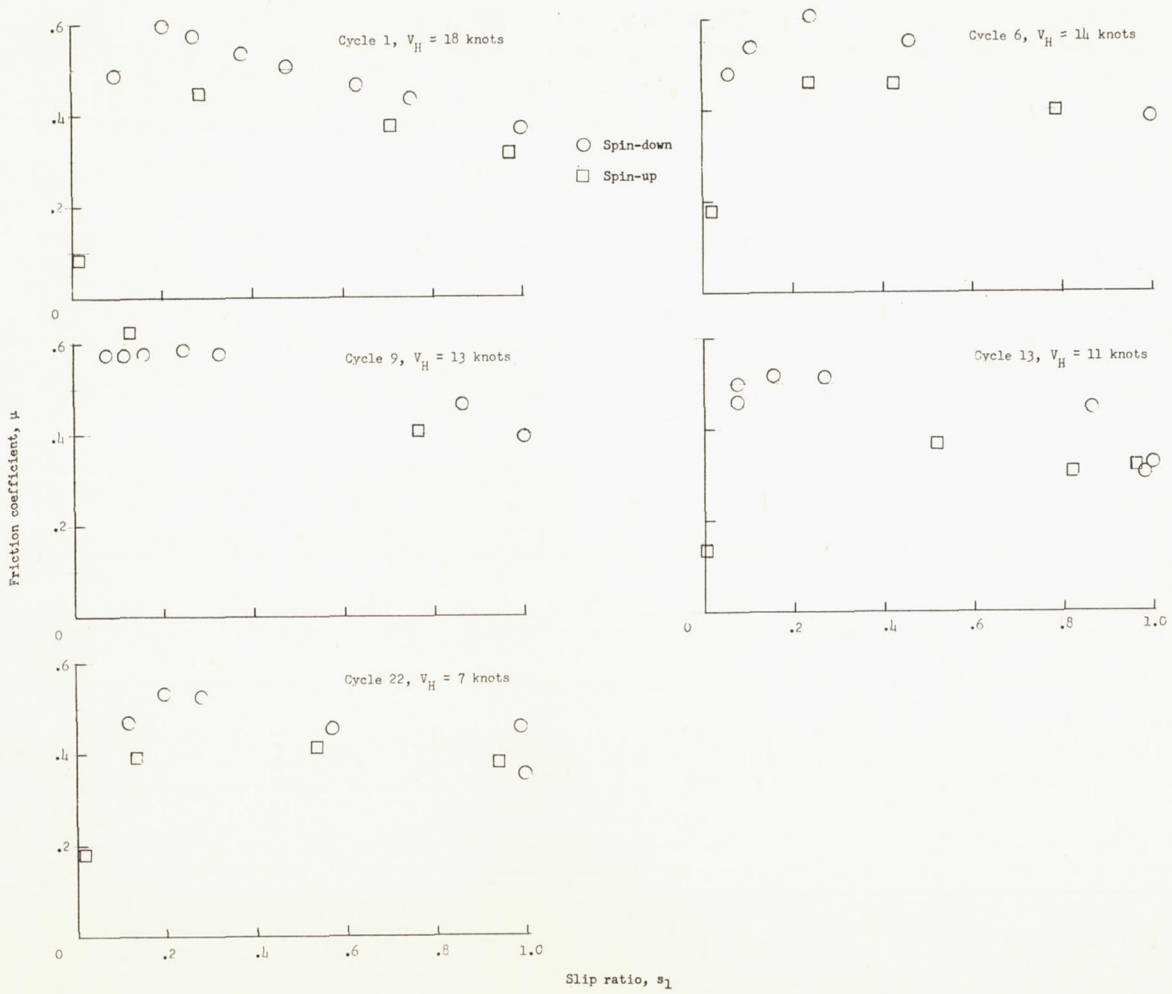

(a) Run 1.

Figure 74.- Tire R1, rib all-rubber tread, 9 grooves. Antiskid unit operating; p = 260 lb/sq in.; d_1 = 0 to 0.3 inch.

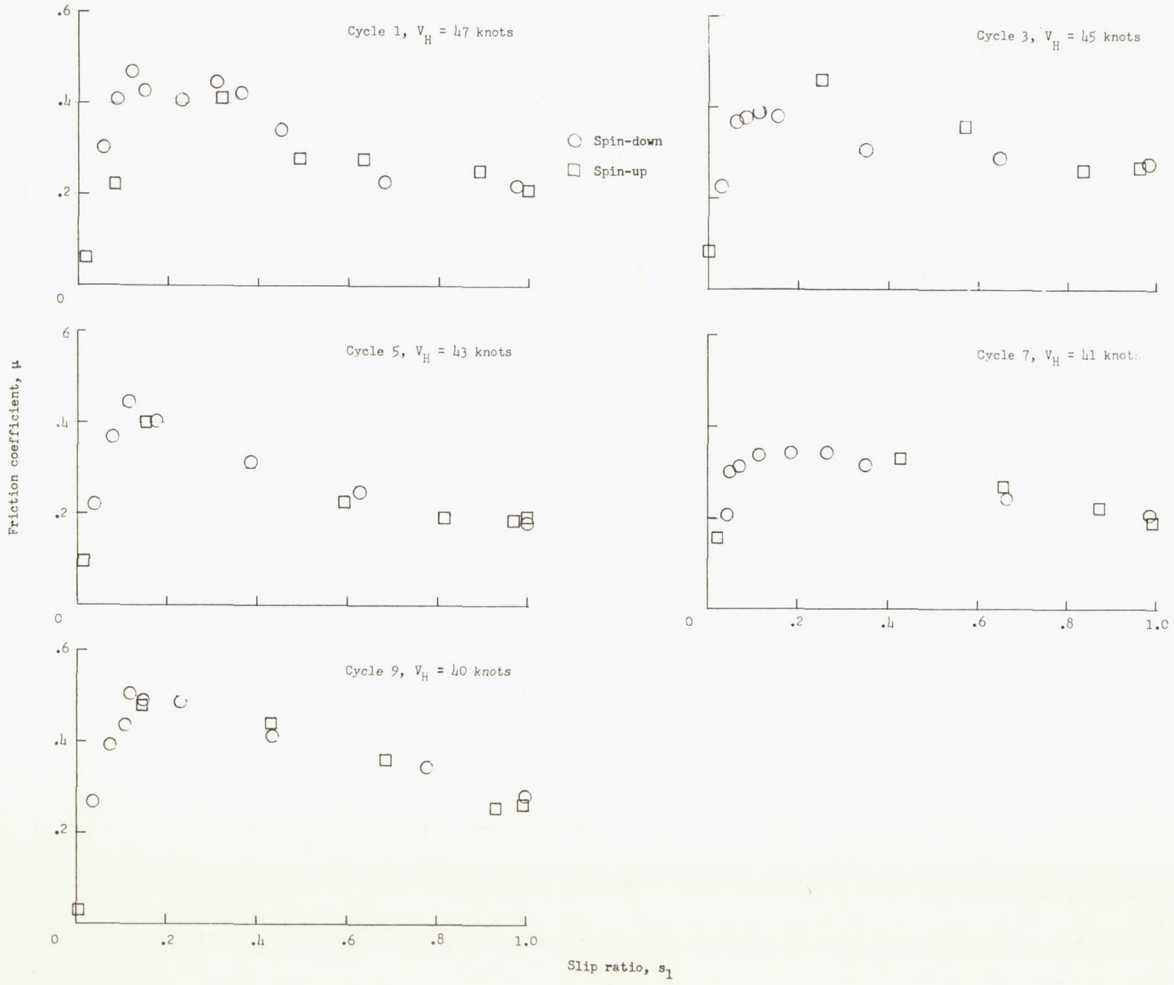

(b) Run 2.

Figure 74.- Continued.

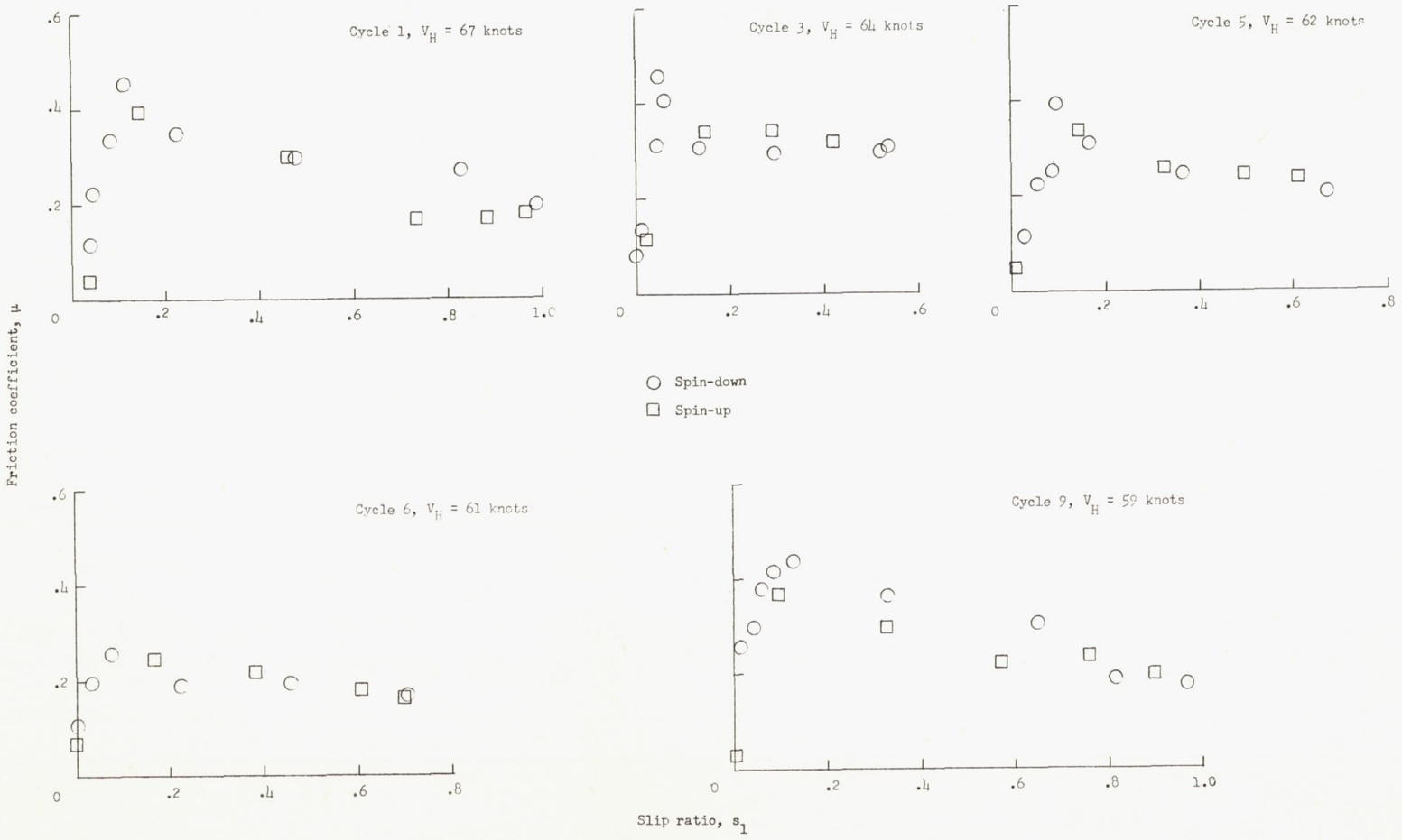

(c) Run 3.

Figure 74.- Continued.

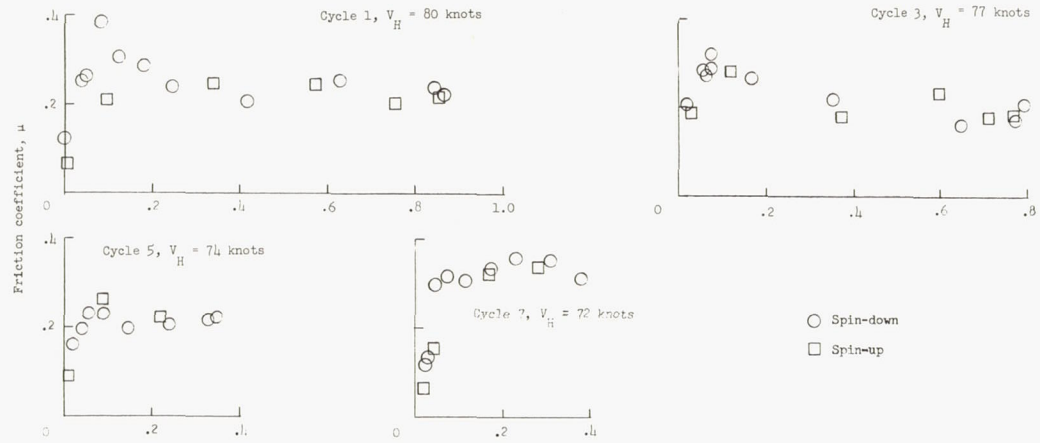

(d) Run 4.

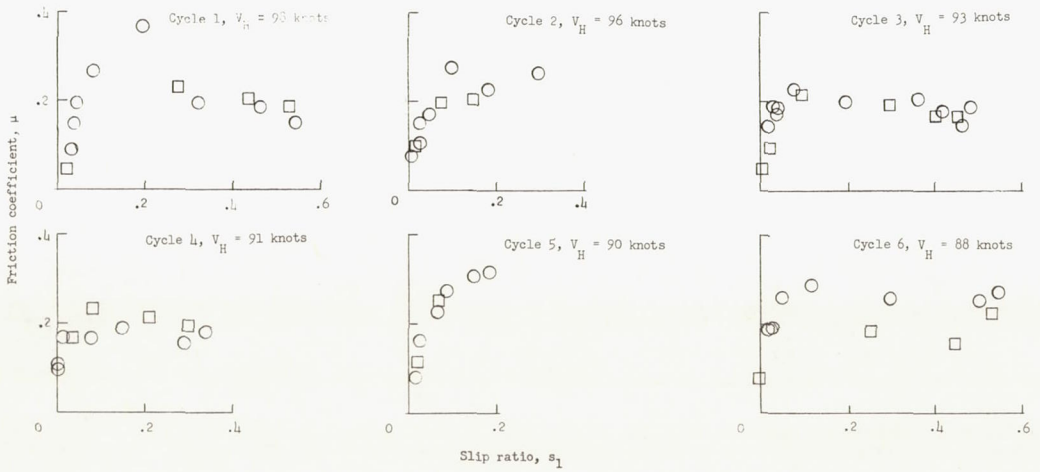

(e) Run 5.

Figure 74.- Concluded.

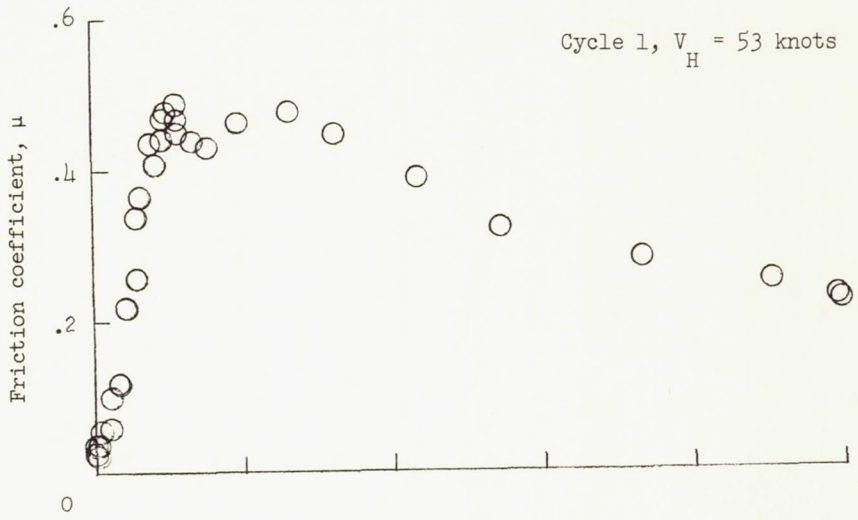

(a) Run 1.

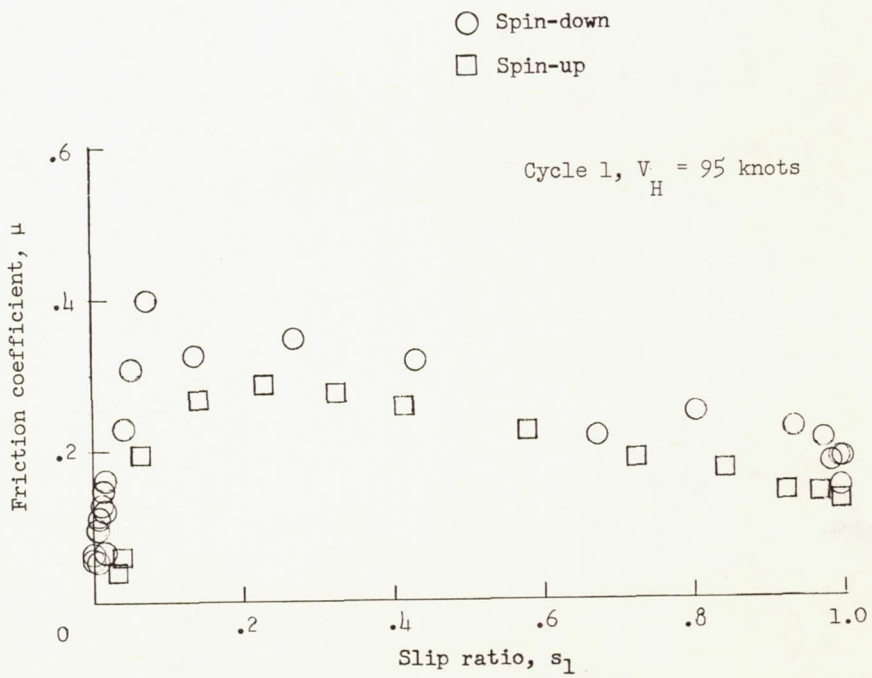

(b) Run 2.

Figure 75.- Tire R2, rib all-rubber tread, 9 grooves. Antiskid unit not operating; p = 260 lb/sq in.; d_1 = 0 to 0.3 inch.

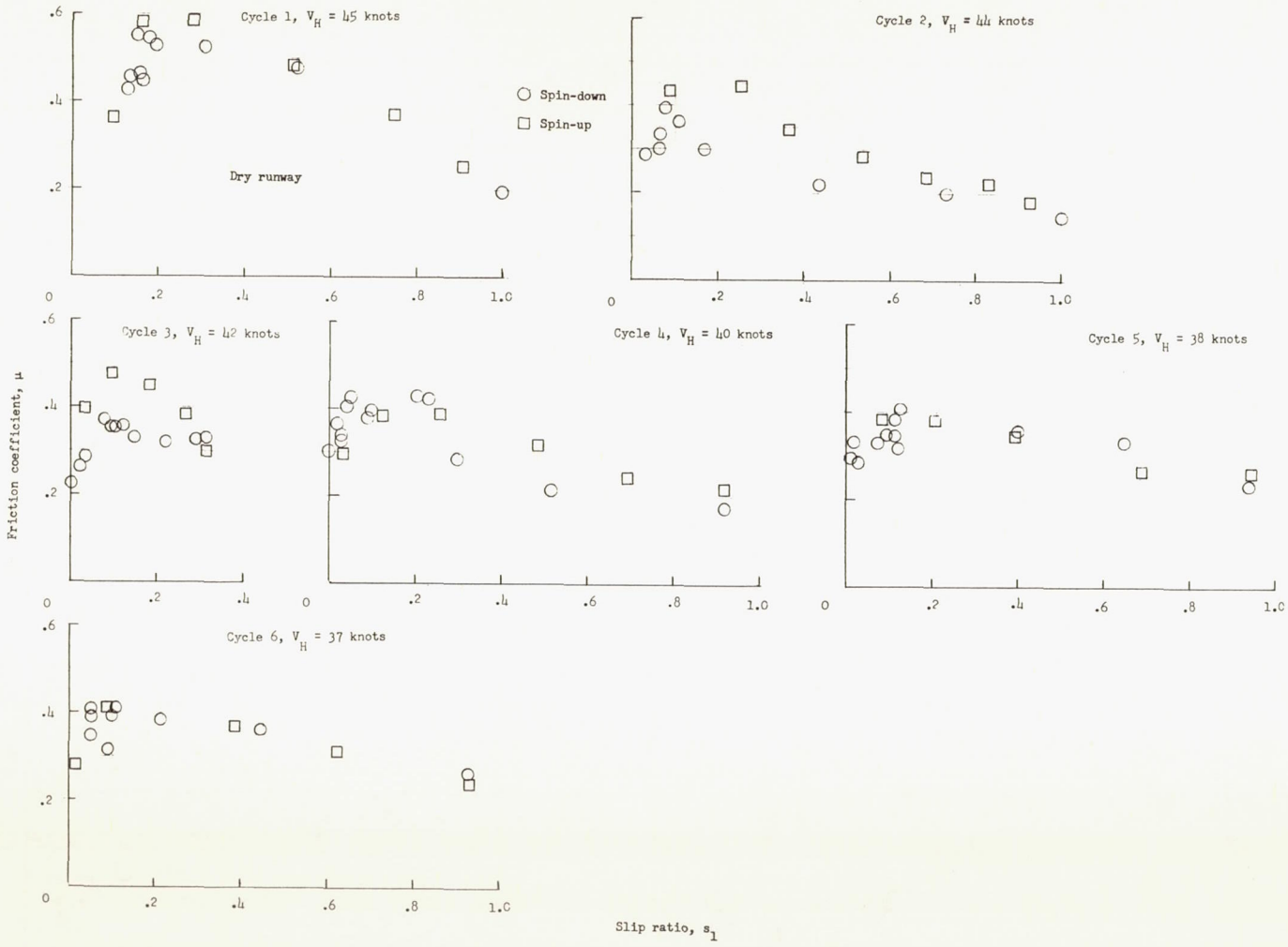

(a) Run 1.

Figure 76.- Tire R4, rib all-rubber tread, 11 grooves. Antiskid unit operating; p = 260 lb/sq in.; $p_{B,1}$ = 50 lb/sq in.; d_1 = 0.2 to 0.5 inch (except where noted).

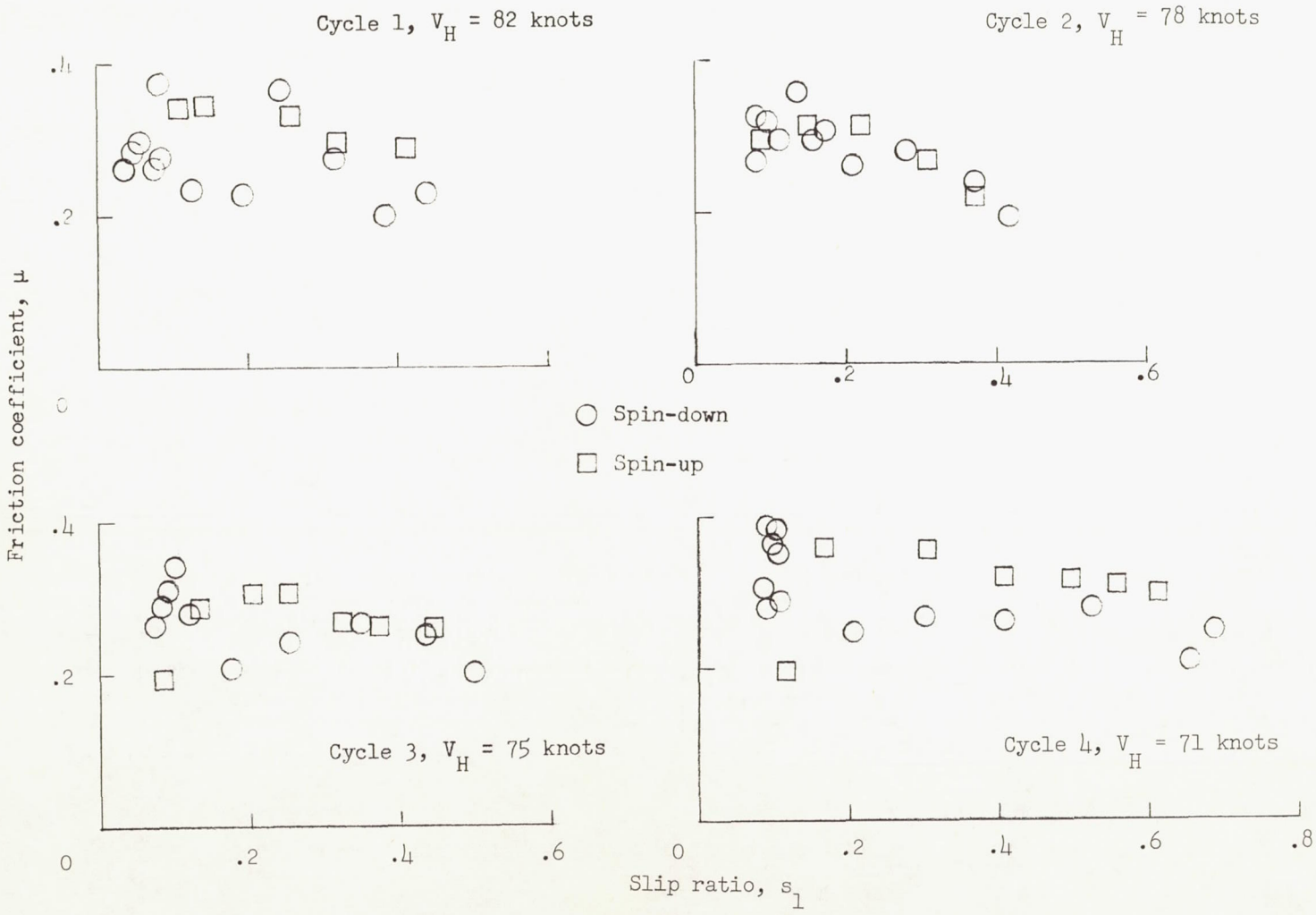

(b) Run 2.

Figure 76.- Concluded.

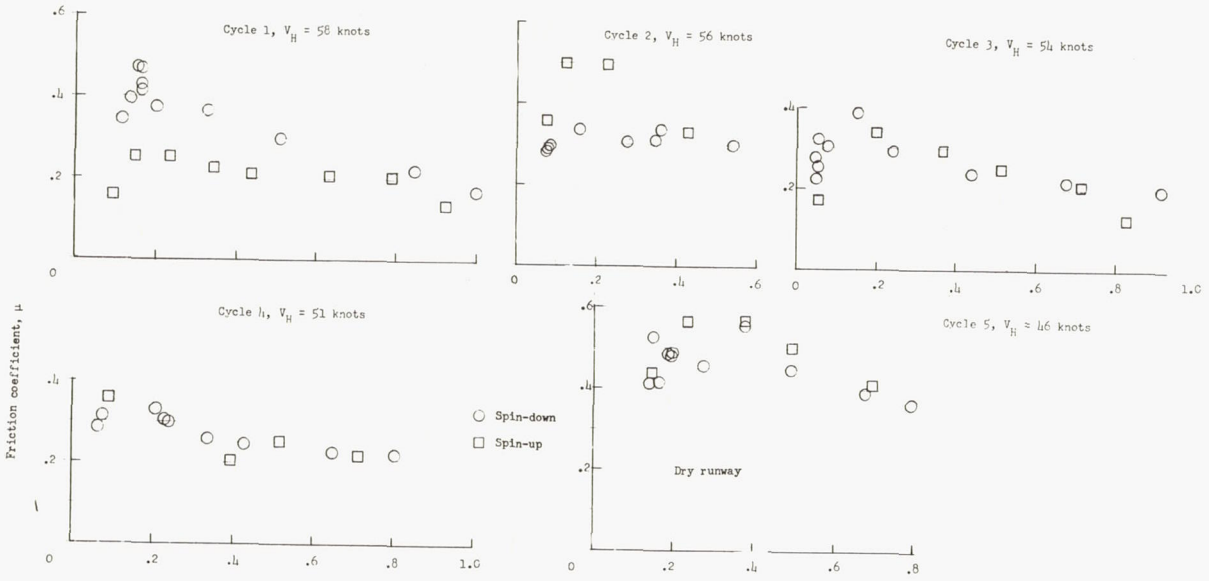

(a) Run 1.

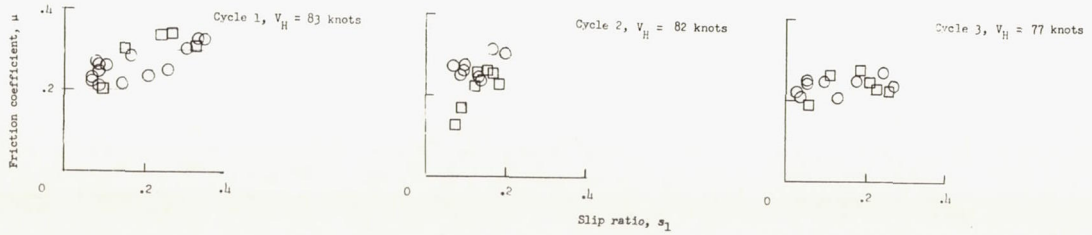

(b) Run 2.

Figure 77.- Tire R4, rib all-rubber tread, 11 grooves. Antiskid unit operating; p = 260 lb/sq in.; $p_{B,1}$ = 50 lb/sq in.; d_1 = 0 to 0.3 inch (except where noted).

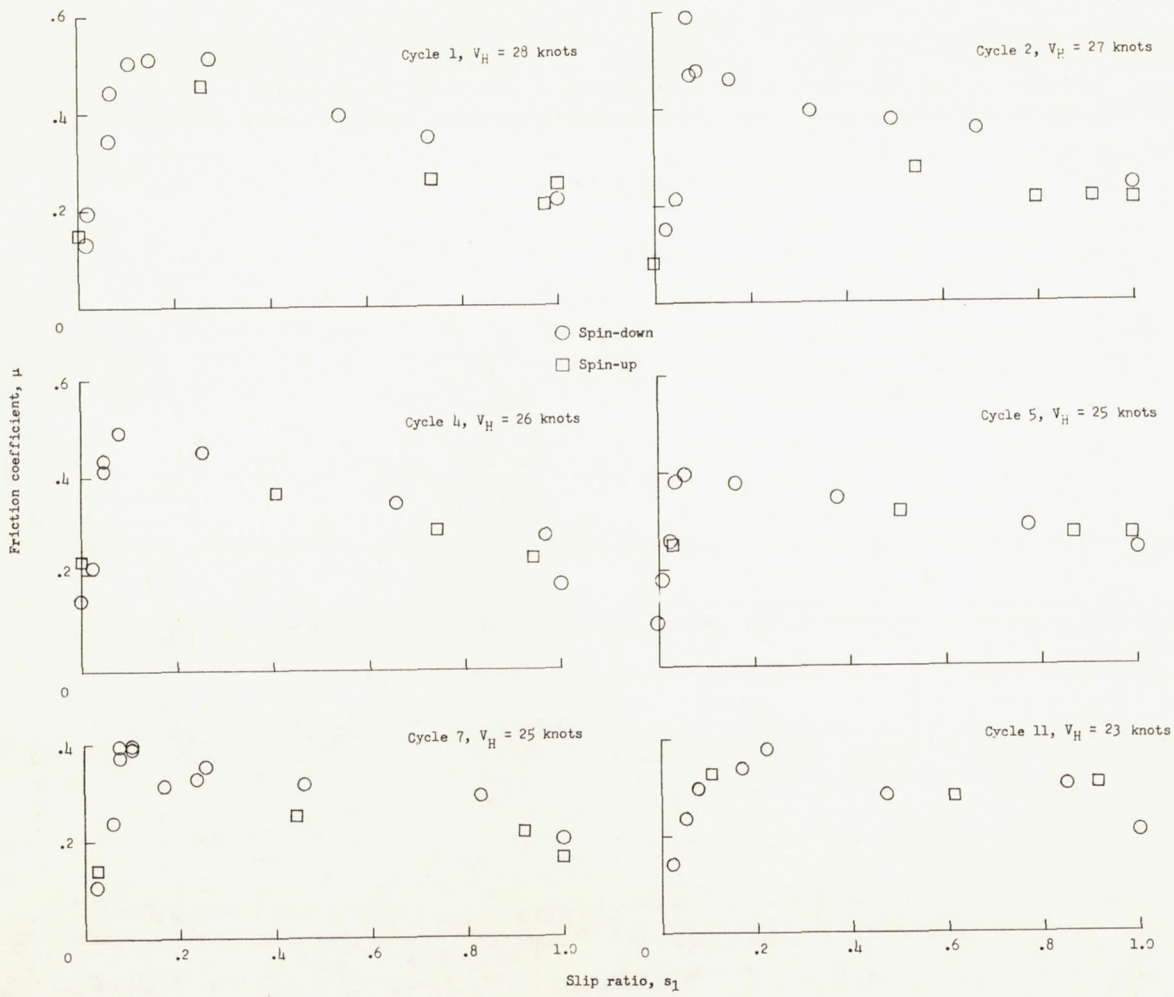

(a) Run 1.

Figure 78.- Tire R5, rib fabric-reinforced tread, 3 grooves. Antiskid unit operating; p = 260 lb/sq in.; d_1 = 0 to 0.3 inch.

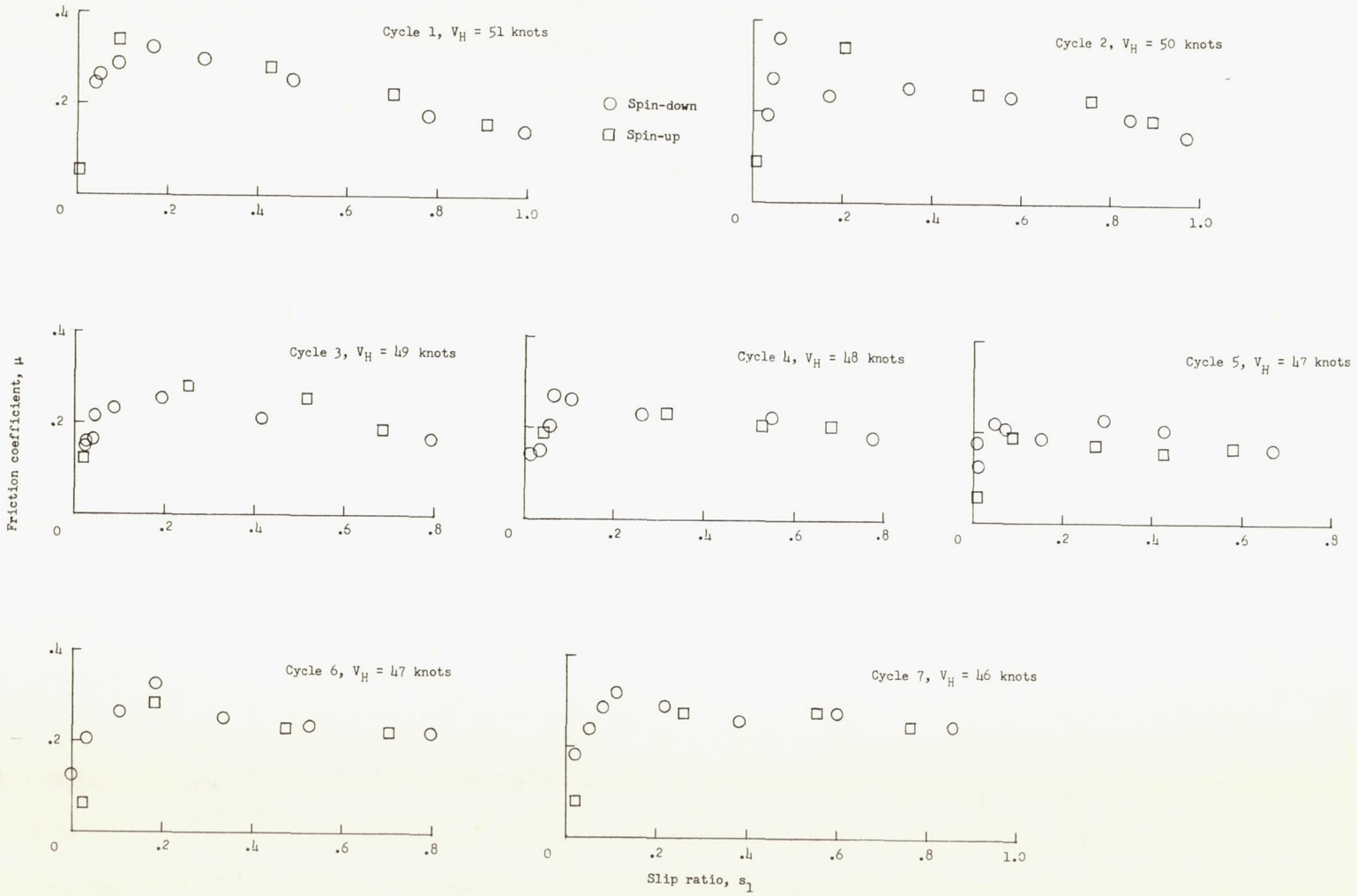

(b) Run 2.

Figure 78.- Continued.

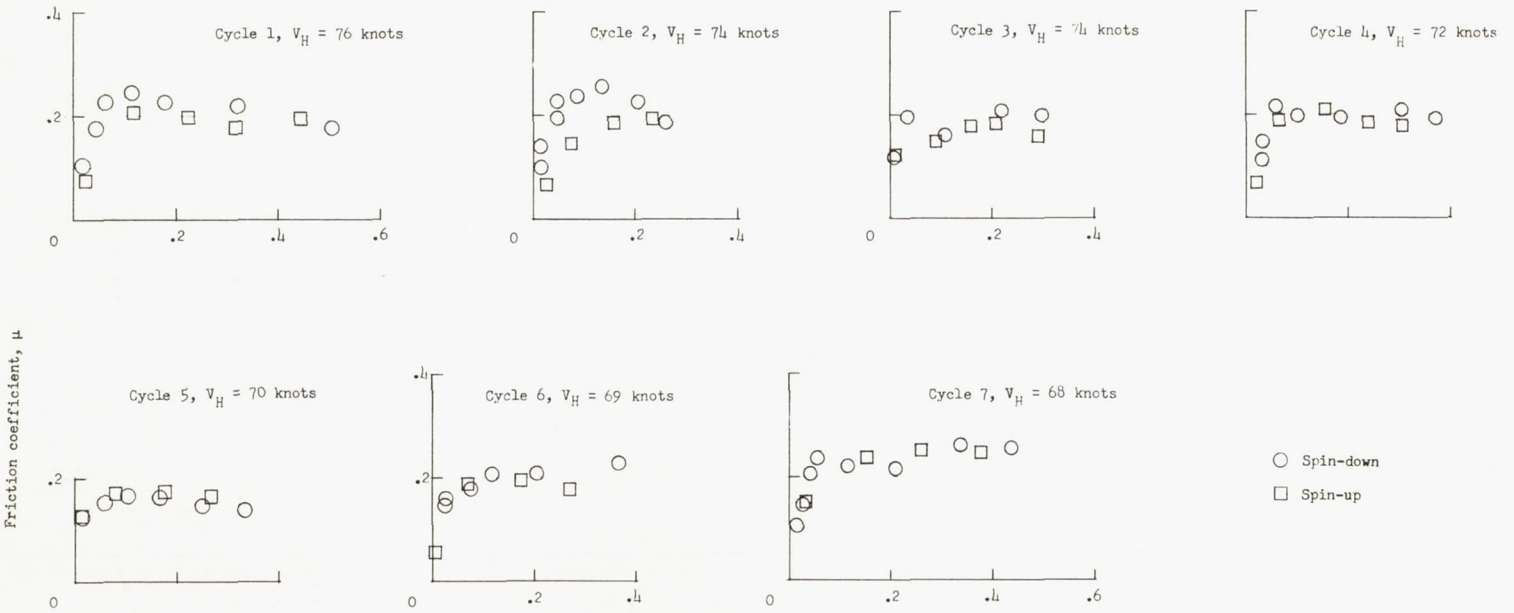

(c) Run 3.

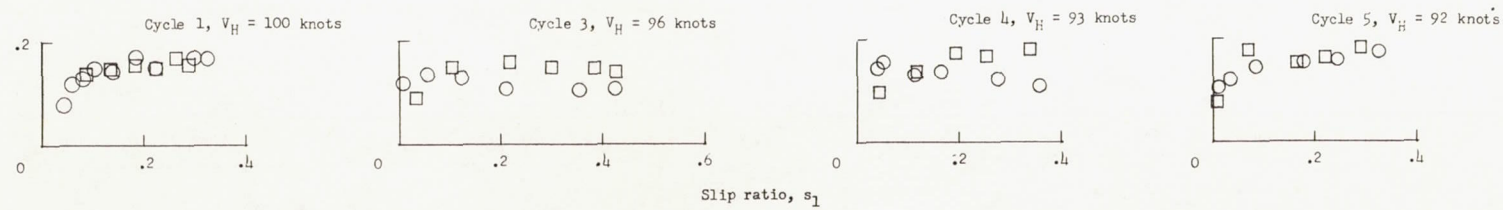

(d) Run 4.

Figure 78.- Concluded.

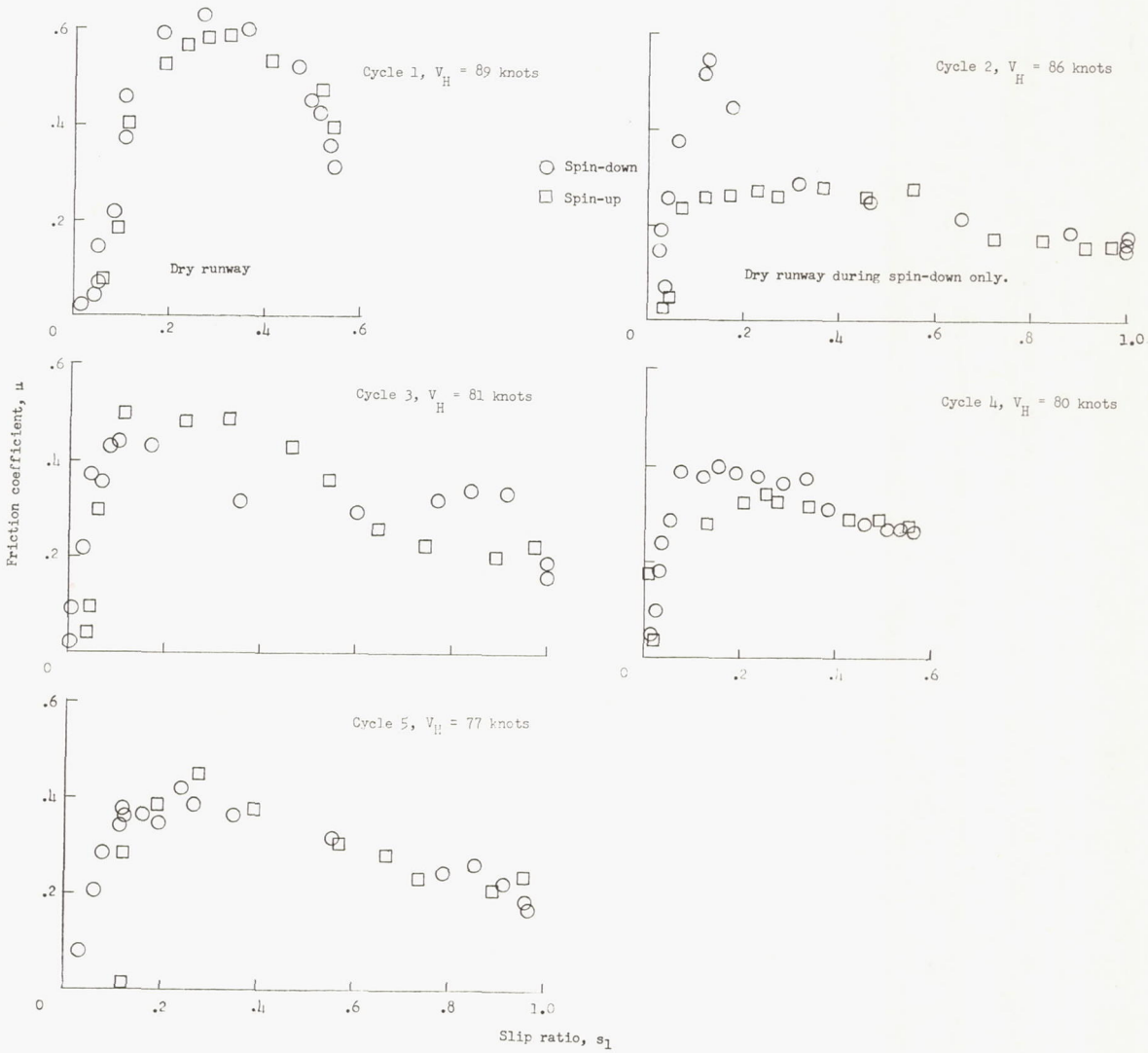

(a) Run 1.

Figure 79.- Tire R3, rib all-rubber tread, 9 grooves. Antiskid unit operating; p = 260 lb/sq in.; d_1 = 0 to 0.3 inch (except where noted). Runs in this figure are arranged chronologically (see appendix).

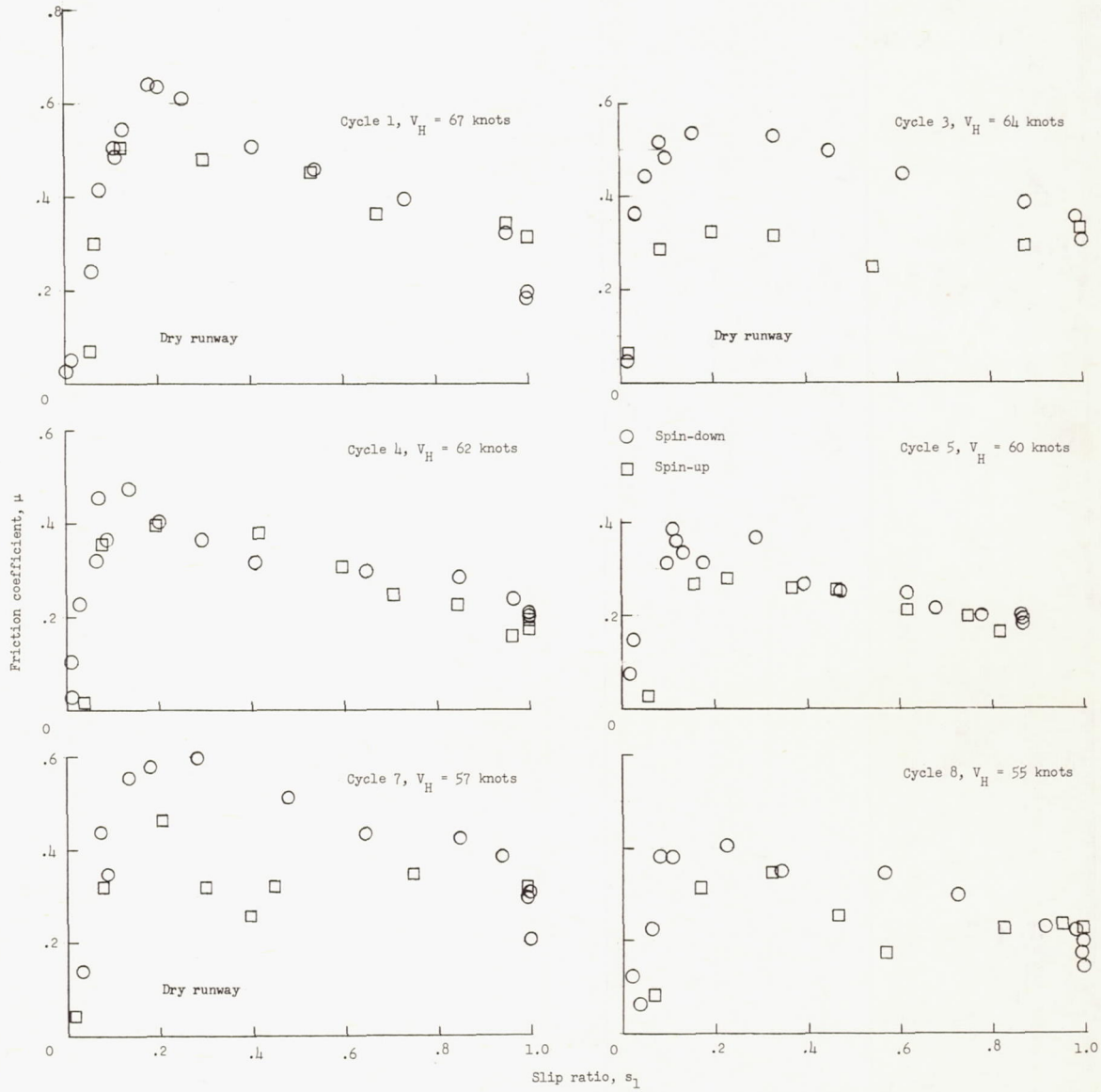

(b) Run 2.

Figure 79.- Continued.

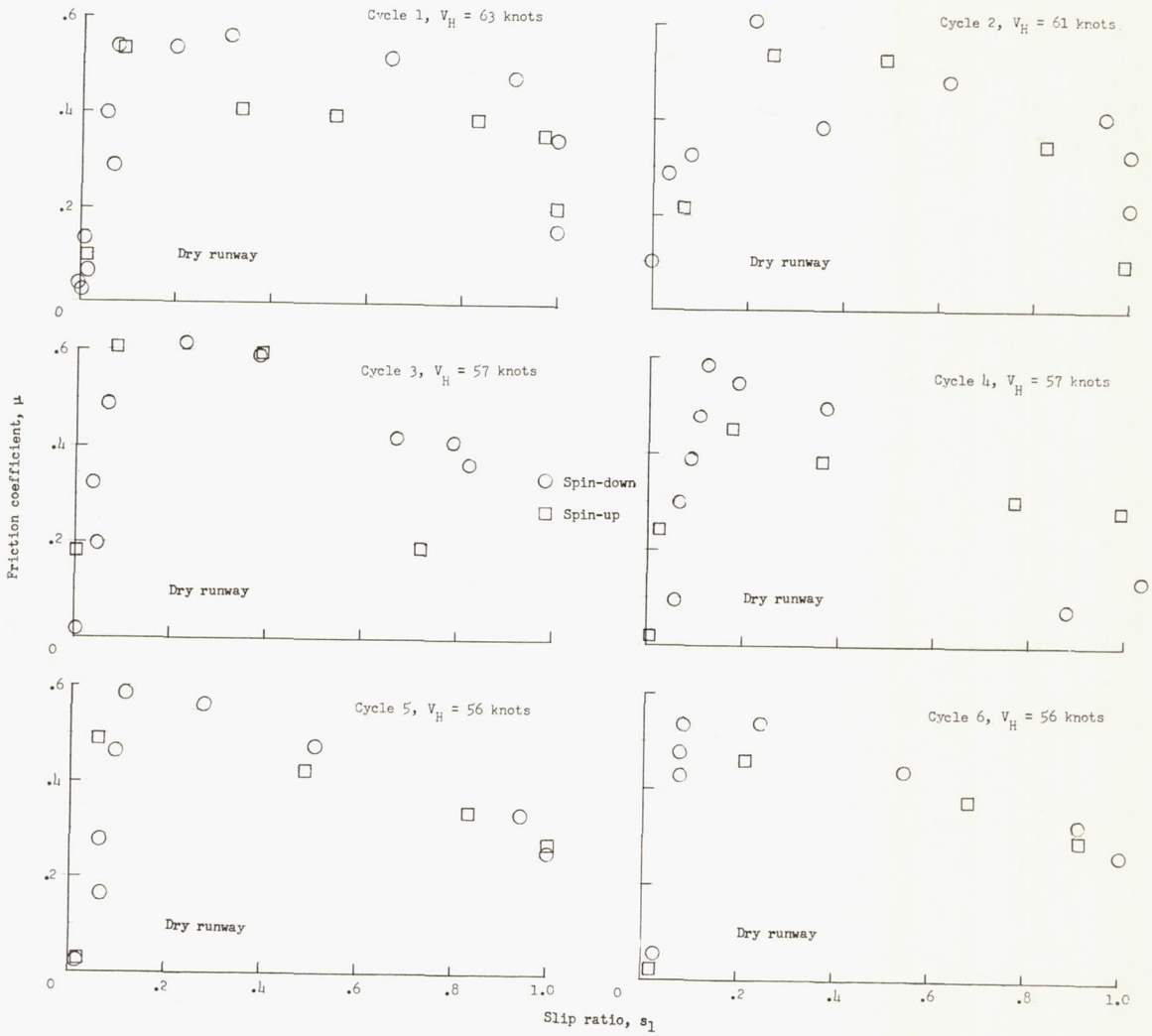

(c) Run 3.

Figure 79.- Continued.

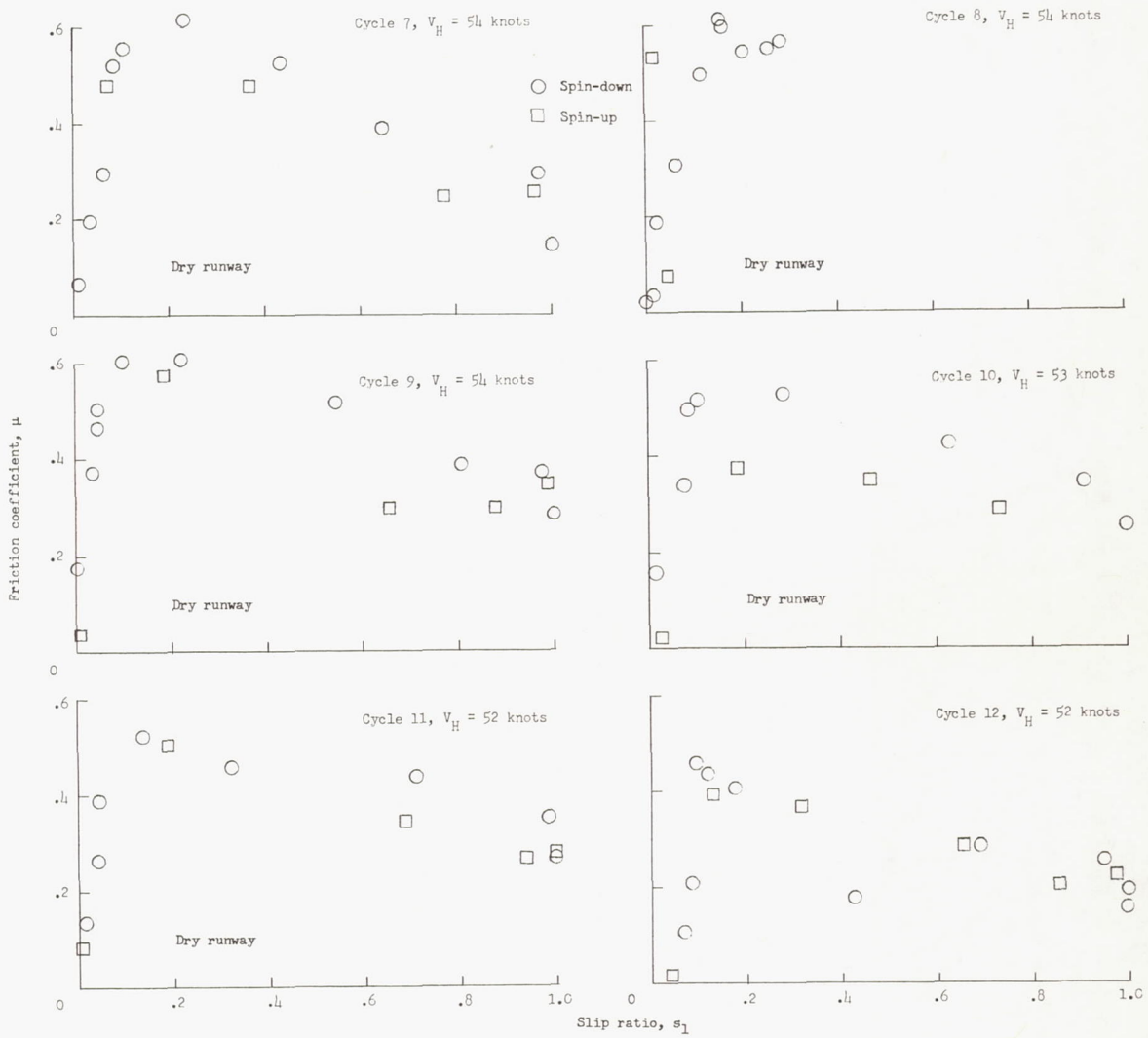

(c) Run 3. Continued.

Figure 79.- Continued.

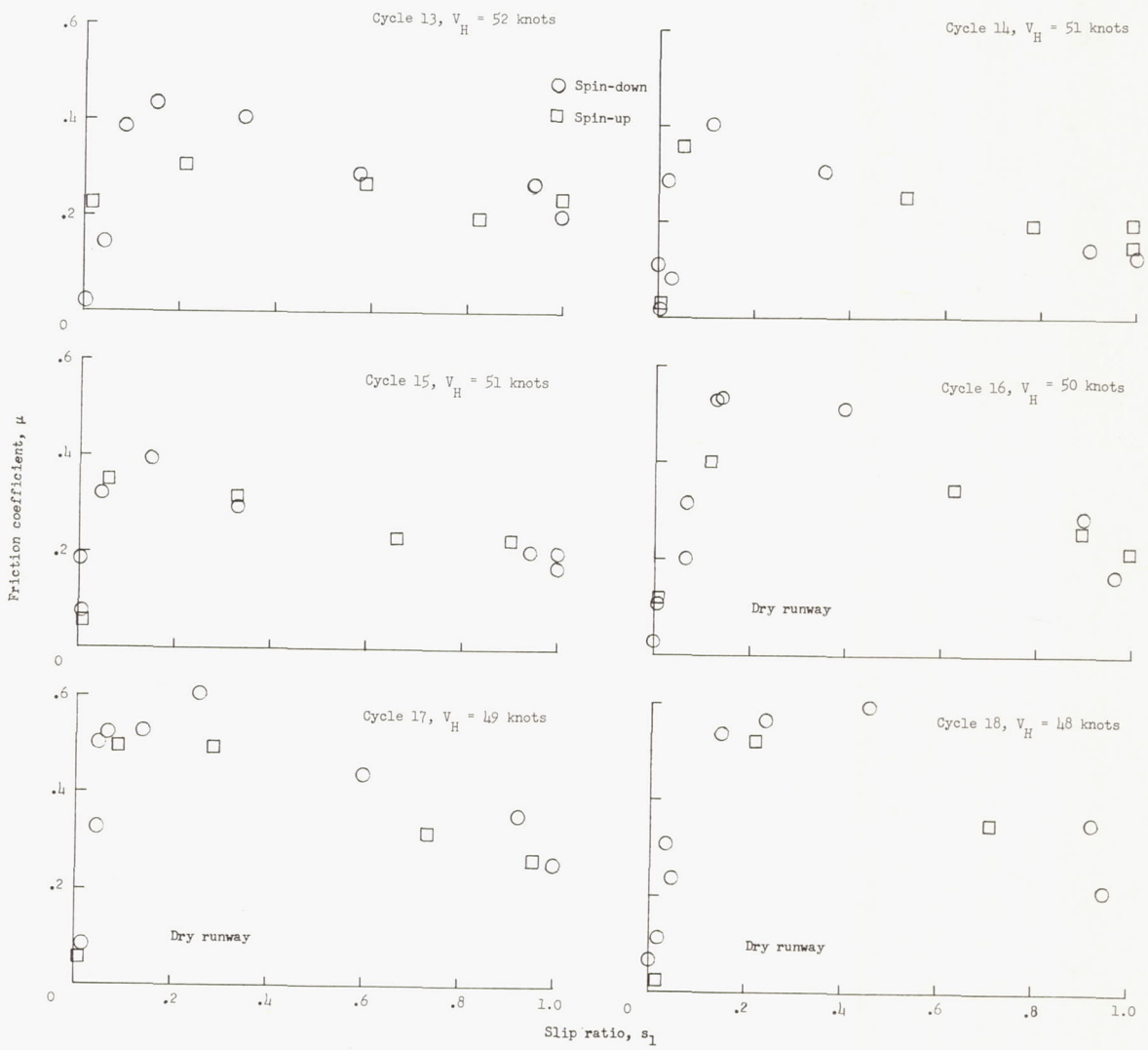

(c) Run 3. Continued.

Figure 79.- Continued.

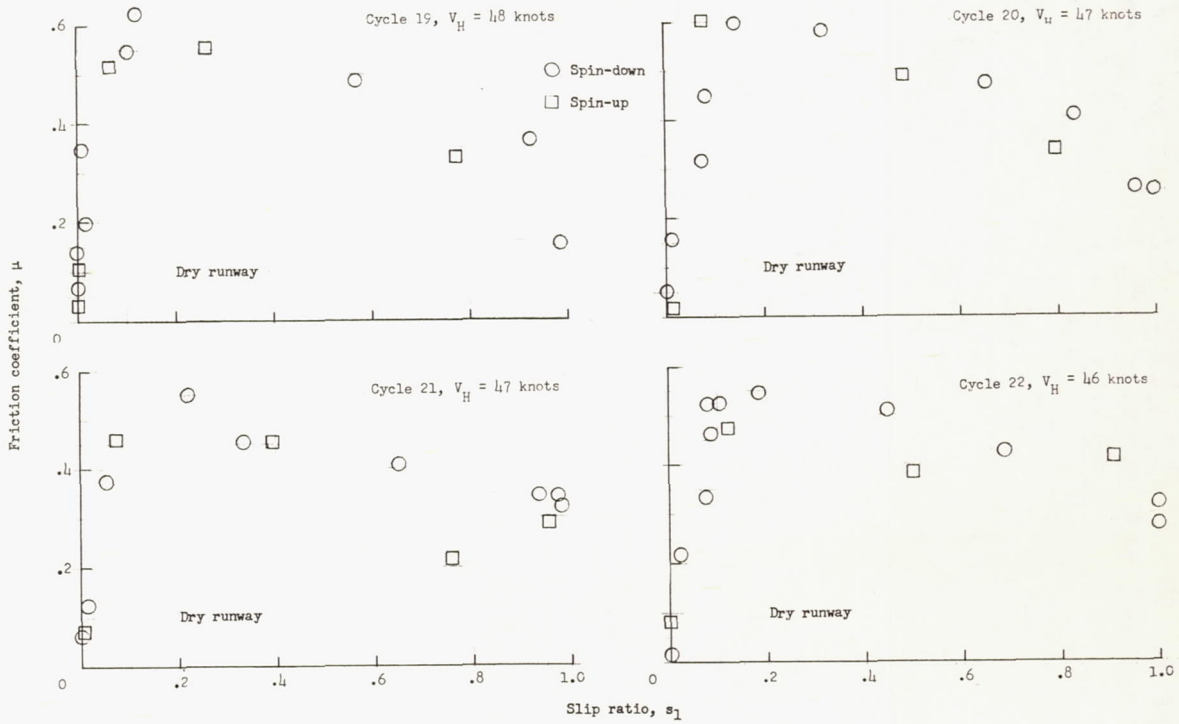

(c) Run 3. Concluded.

Figure 79.- Continued.

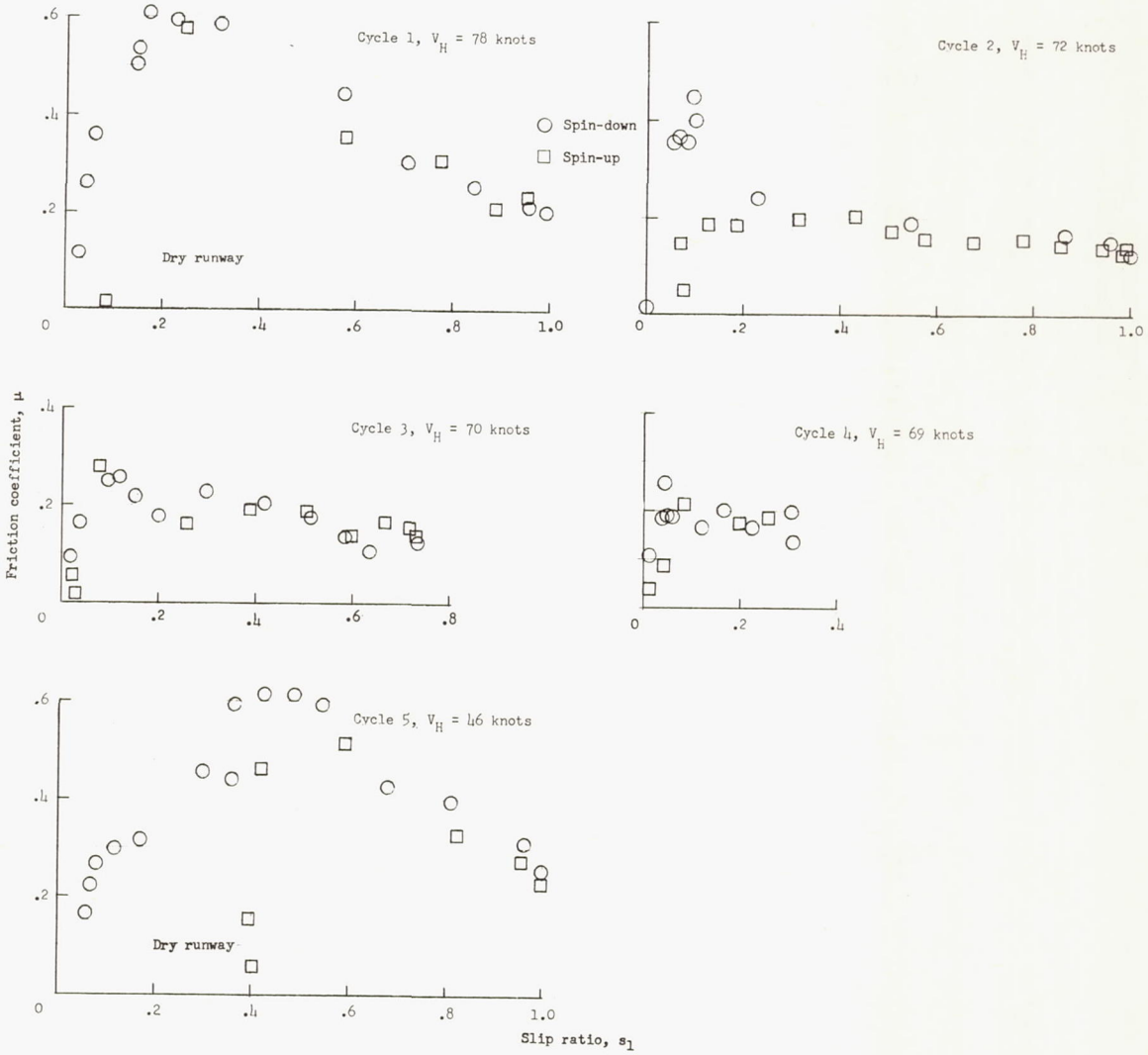

(d) Run 4.

Figure 79.- Continued.

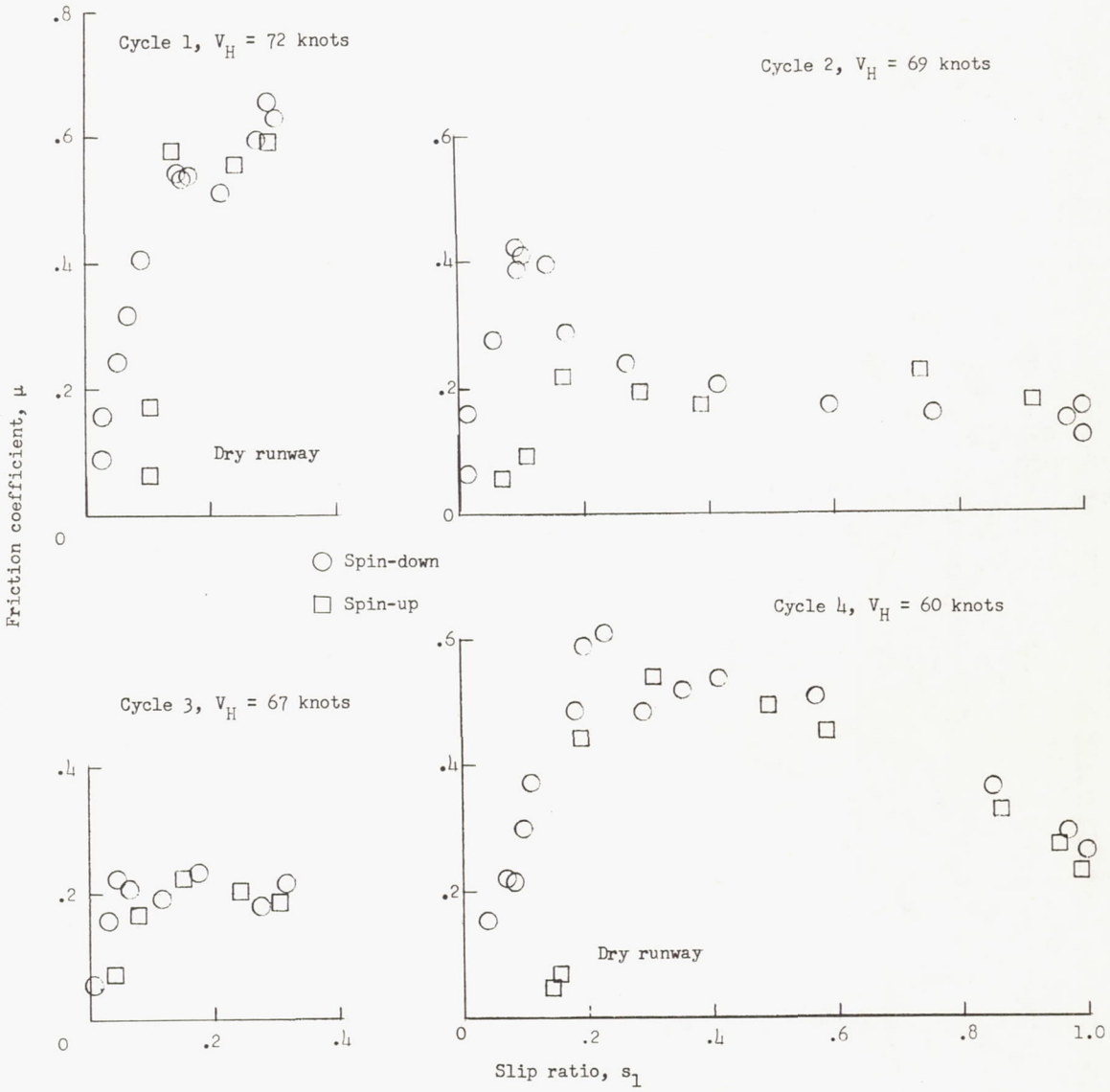

(e) Run 5.

Figure 79.- Concluded.